REPORT
54

GOVERNMENT OF
WESTERN AUSTRALIA

GEOLOGY AND MINERAL RESOURCES OF THE RAVENSTHORPE AND COCANARUP 1:100 000 SHEETS

by W. K. Witt

GEOLOGICAL SURVEY OF WESTERN AUSTRALIA

DEPARTMENT OF MINERALS AND ENERGY

GEOLOGICAL SURVEY OF WESTERN AUSTRALIA

REPORT 54

GEOLOGY AND MINERAL RESOURCES OF THE RAVENSTHORPE AND COCANARUP 1:100 000 SHEETS

by
W. K. Witt

Perth 1998

Copy editor: J. F. Johnston

REFERENCE
The recommended reference for this publication is:
WITT, W. K., 1998, Geology and mineral resources of the Ravensthorpe and Cocanarup 1:100 000 sheets: Western Australia Geological Survey, Report 54, 152p.

National Library of Australia
Cataloguing-in-publication entry

Witt, W. K.
Geology and mineral resources of the Ravensthorpe and Cocanarup 1:100 000 sheets.

Bibliography.
ISBN 0 7309 6606 2

1. Geology — Western Australia — Ravensthorpe Region.
2. Geology — Western Australia — Ravensthorpe Region — Maps.
3. Ravensthorpe Region (W.A.) — Maps.
I. Geological Survey of Western Australia.
II. Title. (Series: Report (Geological Survey of Western Australia); 54).

559.412

ISSN 0508–4741

Cover photograph:
Gently south-dipping (to right of photograph) Mesoproterozoic Kundip Quartzite (of the Mount Barren Group) overlies Archaean Manyutup Tonalite (poorly exposed beneath bush at left), near Kundip. This poorly exposed contact between the Archaean and Mesoproterozoic has generally been interpreted as an unconformity, but evidence is presented herein for a tectonic contact between the two

Contents

Chapter 5 Archaean metamorphism

Chapter 6 Geology of the Proterozoic rocks

Chapter 7 Structure of the Mesoproterozoic Mount Barren Group

Chapter 8 Proterozoic metamorphism

Chapter 9 Economic geology

Chapter 10 Summary and conclusions

Plate

Appendices

Figures

Tables

Geology and mineral resources of the Ravensthorpe and Cocanarup 1:100 000 sheets

by

W. K. Witt

Abstract

The Archaean greenstone belt at Ravensthorpe contains three distinct tectonostratigraphic terranes. In the east, the Carlingup Terrane (c. 2960 Ma) contains metamorphosed komatiite, basalt, sedimentary rocks (including banded iron-formation), and minor acid volcanic rocks. The Ravensthorpe Terrane (c. 2990 to 2970 Ma) occupies the central part of the greenstone belt and consists of tonalite and a volcanic association dominated by andesitic volcaniclastic rocks. The Cocanarup greenstones comprise a strongly deformed belt of predominantly metasedimentary rocks, with fewer ultramafic and mafic rocks, lying along the western margin of the greenstone belt. The Ravensthorpe Terrane and the Cocanarup greenstones were thrust eastward over the Carlingup Terrane. The accreted terranes were subsequently deformed to produce a large-scale, south-plunging synform that defines the overall shape of the greenstone belt. Following formation of the Beulah synform, there was a change in the regional tectonics and subsequent Archaean deformation was in response to north–south compression.

Metamorphic mineral assemblages indicate conditions that vary from <400°C to >600°C, at about 2.5 kb. Metamorphic assemblages grew before and during tectonic emplacement of the Ravensthorpe Terrane and the Cocanarup greenstones over the Carlingup Terrane, but final metamorphic equilibration followed the main phase of accretion-related deformation. Thermal gradients during metamorphism were controlled largely by contemporaneous emplacement of granitoid sheets below the greenstones.

The Archaean basement is structurally overlain by the Mesoproterozoic Mount Barren Group. The mainly metasedimentary rocks of the Mount Barren Group have traditionally been regarded as lying unconformably on the Archaean Yilgarn Craton. However, there is no compelling evidence for derivation of the precursor sediments from the Yilgarn, and the Mount Barren Group may be entirely allocthonous. During the Albany–Fraser Orogeny the Mount Barren Group was deformed by several phases of folding and faulting, at c. 1300 Ma. The metamorphic grade of the Mount Barren Group increases southward, discontinuously, from the contact with Archaean rocks. Kyanite-bearing metapelitic schists exposed on the coast west of Hopetoun equilibrated at P >6kb and T >600°C. These high-pressure metamorphic rocks were uplifted south of secondary splays related to the Jerdacuttup Fault. High-grade Archaean (Munglinup) orthogneiss located south of the Jerdacuttup Fault was deformed during the Albany–Fraser Orogeny, and subsequently uplifted.

The Archaean greenstones host a diverse range of mineral deposits. Submarine, synvolcanic Cu–Au and Cu–Zn mineralization occurs at several localities in the Ravensthorpe Terrane. Nickel sulfide deposits and massive to bedded pyrite are found in the Carlingup Terrane. During accretion of the terranes, tourmaline-rich pegmatites were intruded into active thrust faults. The more fractionated of these contain Ta–Nb ore minerals and subeconomic concentrations of spodumene. Some base- and precious-metal mineralization in the Ravensthorpe Terrane may have been remobilized at this stage. During the Tertiary, nickel laterites formed over ultramafic rocks and magnesite deposits formed at the base of the Pallinup Siltstone from magnesium that was remobilized from the underlying ultramafic rocks. Manganese-rich sedimentary rocks are known in the Mount Barren Group but relatively little mineralization has been identified in Proterozoic rocks. The recent discovery of base- and precious-metal mineralization in Mount Barren Group metasedimentary rocks at Trilogy has changed the long-held perception that these rocks are not prospective.

KEYWORDS: Archaean, Yilgarn Craton, Ravensthorpe greenstone belt, tectonics, metamorphism, mineralization, Albany–Fraser Orogeny, Ravensthorpe 1:100 000 sheet, Cocanarup 1:100 000 sheet

Chapter 1

Introduction

Location, access, physiography and vegetation

The RAVENSTHORPE* and COCANARUP 1:100 000 sheets (Fig. 1) are located on the south coast of Western Australia, in the southwest corner of the RAVENSTHORPE 1:250 000 sheet, and in the southeast corner of the NEWDEGATE 1:250 000 sheet, respectively. The towns of Ravensthorpe and Hopetoun lie within the Shire of Ravensthorpe (population 1374). Ravensthorpe, on the South Coast Highway, is approximately midway between Albany and Esperance, situated on RAVENSTHORPE, adjoining the map boundary with COCANARUP. Hopetoun, on the coast, is connected to Ravensthorpe by sealed road and has a small fishing harbour. COCANARUP contains a large part of the Fitzgerald River National Park. The main commercial activities in the Ravensthorpe–Hopetoun area are agriculture, fishing and tourism.

RAVENSTHORPE and COCANARUP lie south of the Jarrahwood Axis (Cope, 1975), which separates northward drainage toward inland (mostly saline) lakes from southward-directed drainage systems such as the Jerdacuttup and Phillips Rivers. Except for two major physiographic anomalies, the land surface rises gradually from sea level to about 200 m near the northern boundaries of the sheets. The highest peaks, rising to >400 m, are in the Ravensthorpe Range, north and east of Ravensthorpe. The Fitzgerald River National Park includes peaks of around 300 m that rise abruptly from sea level.

Much of the area covered by RAVENSTHORPE and COCANARUP is under cultivation. Eucalypt woodland in the Ravensthorpe Range and around Cocanarup is accompanied by a thick understorey on windward (west- and south-facing) slopes, but is relatively open on leeward slopes. Within about 25 km of the coast, dense native heath covers flat and undulating country. Steeper slopes support a dense growth of thin eucalypts. The rugged topography of the Fitzgerald River National Park supports a diverse flora representing one of three nodes of high species diversity in southwest Western Australia (CALM, 1991).

* Capitalized names refer to standard map sheets. More detailed geology is shown on RAVENSTHORPE and COCANARUP (Witt, 1996a,b), which should be used in conjunction with Plate 1 of this report.

Regional geological setting

RAVENSTHORPE and COCANARUP contain three major Precambrian tectonic units (Plate 1*, Fig. 1). The northern parts of the sheets cover the southern margin of the Archaean Yilgarn Craton, including the Ravensthorpe greenstone belt (Griffin, 1990). Recent geochronological data indicate ages of 2950–3000 Ma for these greenstones (Nelson, 1995; Savage et al., 1995). The Ravensthorpe granite–greenstone association has traditionally been regarded as forming part of the Southern Cross Province (Gee et al., 1981). More recent interpretations (Myers, 1993, 1995a) place the Ravensthorpe greenstone belt within the Central Yilgarn or Southern Cross Superterrane of the Yilgarn Craton. Northern RAVENSTHORPE and COCANARUP also fall within the northern foreland of the Albany–Fraser Orogen (Myers, 1990a) or the Northern Domain of the Albany Mobile Belt (Beeson et al., 1988).

To the south, the Archaean granite–greenstone association is overlain by metasedimentary rocks of the Mesoproterozoic Mount Barren Group. The age of these rocks is uncertain but is probably somewhere in the range 1700–1300 Ma (Myers, 1995b). The Mount Barren Group was accreted to the northern foreland (Yilgarn Craton) during the Albany–Fraser Orogeny between about 1300 Ma and 1100 Ma (Nelson et al., 1995; Myers, 1995b).

Munglinup Gneiss, which underlies much of southeast RAVENSTHORPE, is part of the Biranup Complex. The Biranup Complex is the northern of two major tectonic components of the Albany–Fraser Orogen (Myers, 1990a). The northeast-trending Jerdacuttup Fault separates Munglinup Gneiss from the Mount Barren Group and Archaean granite–greenstones. The gneiss, which has been dated at about 2630 Ma, was deformed and metamorphosed at granulite facies during the Albany–Fraser Orogeny, prior to uplift south of the Jerdacuttup Fault (Nelson et al., 1995; Myers, 1995b).

* Note that on Plate 1, Zone 51 of the Australian Map Grid (AMG) has been extended westward from longitude 120°E to encompass the whole of the plate. AMGs for the western (COCANARUP) part of Plate 1 thus need to be read from the COCANARUP sheet itself (see Witt, 1996b)

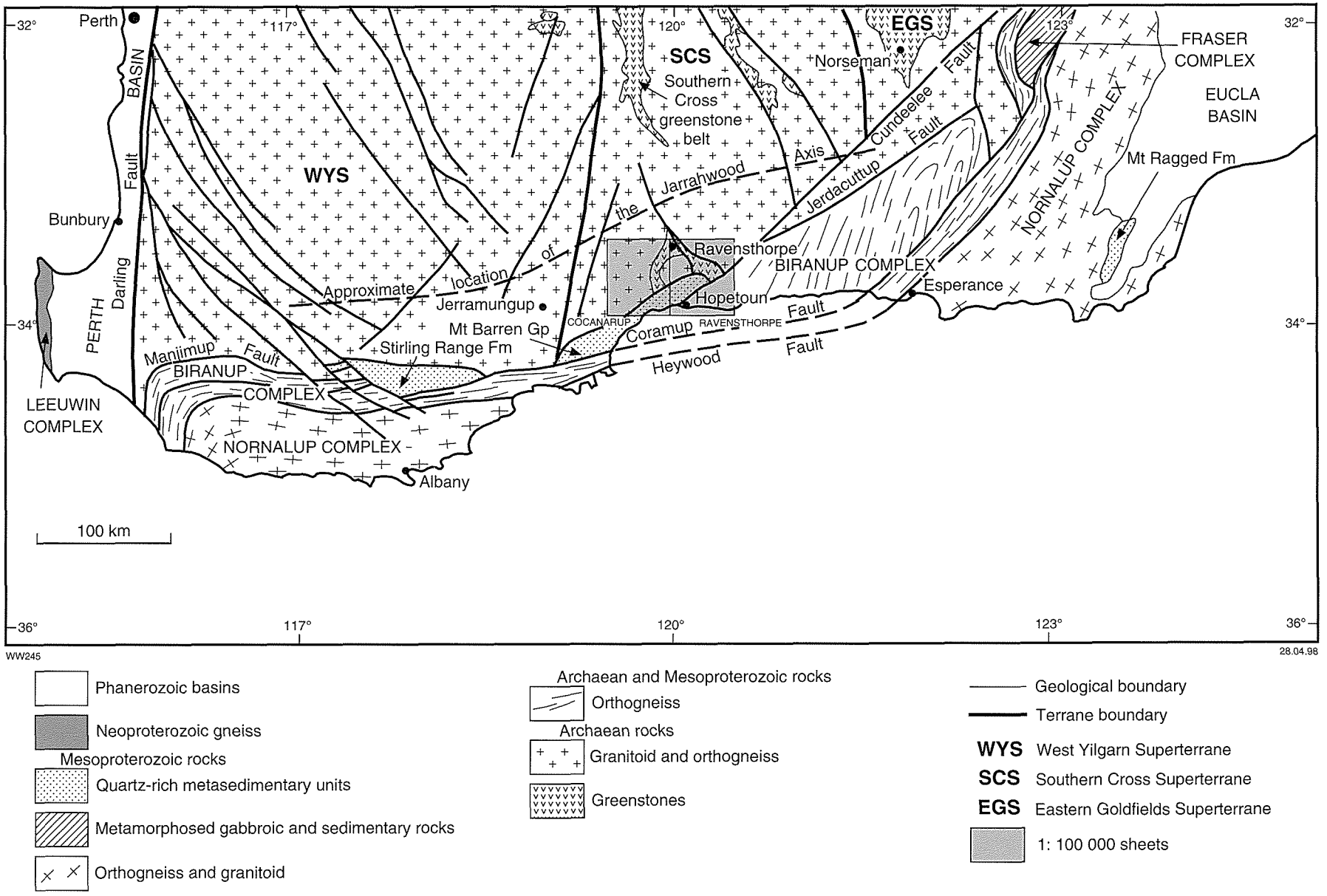

Figure 1. Geological map of the southwestern part of Western Australia showing the boundaries of COCANARUP and RAVENSTHORPE. Geology adapted from Myers and Hocking (1988) and Myers (1993)

Previous studies

The first detailed description of the geology and mineral deposits in the Ravensthorpe–Hopetoun area was published by Sofoulis (1958). The geology of RAVENSTHORPE and COCANARUP is shown on the RAVENSTHORPE and NEWDEGATE 1:250 000 geological map sheets, respectively, and is described in the relevant Explanatory Notes (Thom et al., 1977, 1984). Davy and Leonard (1989) carried out an orientation geochemical survey of the Fitzgerald National Park and adjoining areas to assist in the determination of economic mineral potential in the park area. RAVENSTHORPE and COCANARUP are accompanied by a relatively brief description of the geology in Witt (1997). These two sheets lie on ESPERANCE and ALBANY 1:1 000 000 sheets respectively. The geology of ESPERANCE has been described by Myers (1995b). Mineral occurrences on ALBANY were described by Townsend (1994).

Several recent research projects have been carried out in the area in support of university degrees. Savage (1992) described Cu–Au mineralization in the Kundip and Mount Chester areas of the Ravensthorpe greenstone belt, and is continuing to work on this topic for an MSc thesis. Structural mapping of the Mount Barren Group was carried out as part of a PhD study by C. Brown, in the 1980s. However, the PhD has not yet been completed and the data remain unpublished. G. Blackburn commenced a sedimentological study of the Mount Barren Group, but this work has not been completed. S. Wetherly is currently studying the structural and metamorphic history of the Mount Barren Group in support of a PhD. Preliminary results were published in Wetherley et al. (1994) and Wetherley (1995).

The main rock types exposed on RAVENSTHORPE and COCANARUP are described in Witt (1997), along with a short summary of the deformation and metamorphic history of the Archaean and Proterozoic rocks and the geology of the Cainozoic rocks. This report describes the Precambrian geological history and economic geology of the area covered by the two sheets in greater detail. The Cainozoic geological history is not described in this report, except in the summary (Chapter 10) where the Precambrian history is placed in a broader context.

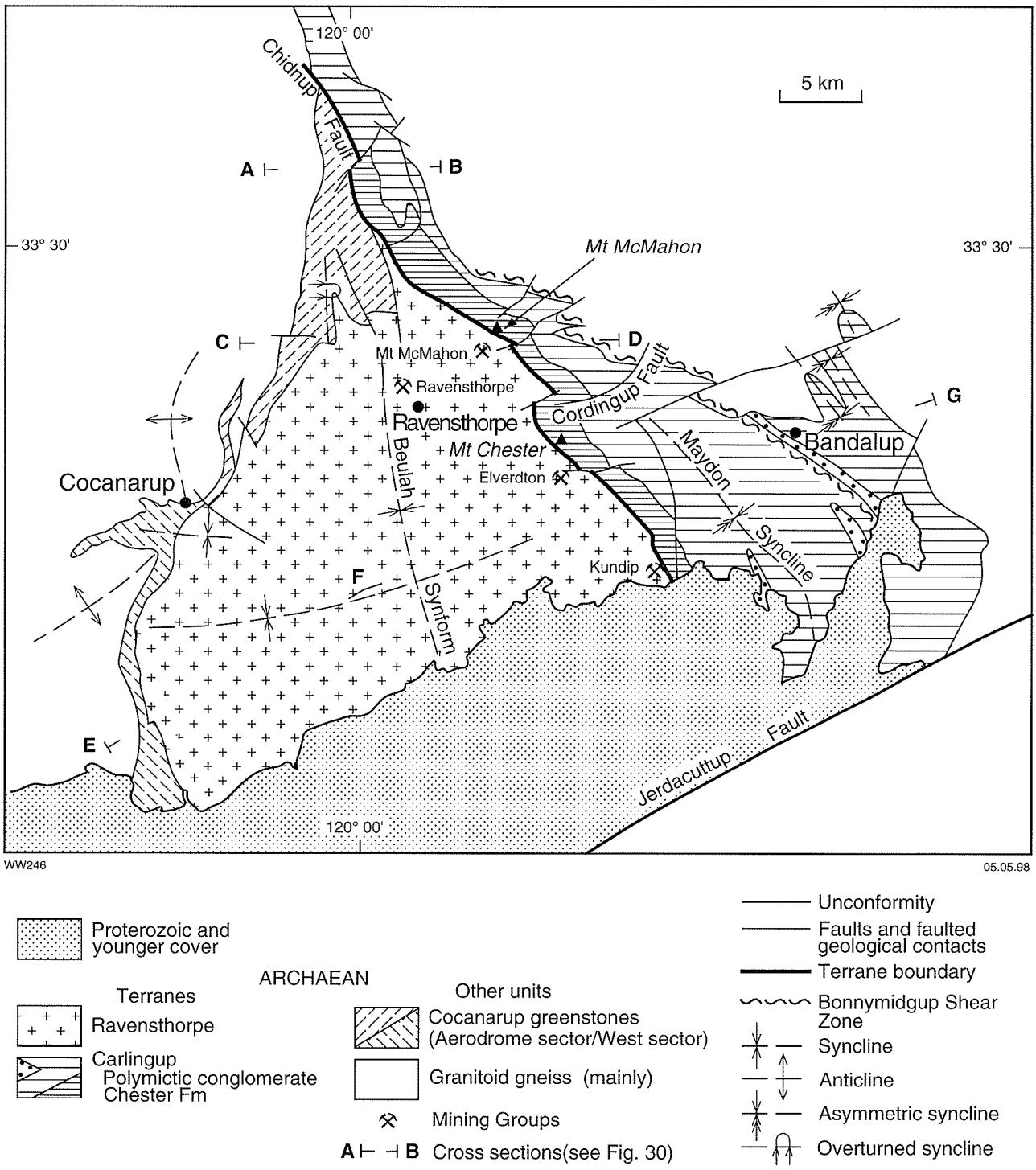

Figure 2. Geological map showing main tectonostratigraphic subdivisions and some of the main structures of the Archaean Ravensthorpe greenstone belt

Chapter 2

Geology of the Archaean rocks

Description of the terranes

Stratigraphic reconstruction is difficult in areas of strong deformation, particularly those involving low-angle thrust repetition. As described in the following section, low-angle thrusts are an important component in the structural history of the Ravensthorpe greenstone belt. A common approach in complexly deformed greenstone belts (Swager et al., 1992; Myers, 1992, 1995), and one followed in this chapter, is the definition of terranes as fault-bound rock packages that can be distinguished from adjacent terranes on the basis of lithological associations and deformation history. It is important to note that this approach conveniently subdivides greenstone belts into distinct, fault-bound entities as a preliminary step to interpreting the geological history of an area. It does not necessarily imply that the entities so defined are 'suspect' terranes (i.e. microcontinental plates that have travelled large distances over oceanic crust before accreting with one another, e.g. Monger et al., 1972).

In this report, three Archaean, fault-bounded tectonic units are recognized (Fig. 2):

1. Carlingup Terrane;
2. Ravensthorpe Terrane; and
3. Cocanarup greenstones.

Petrographic descriptions of the rock units that define these tectonic units can be found in Witt (1997).

Carlingup Terrane

The Carlingup Terrane comprises metamorphosed mafic and ultramafic rocks, together with metasedimentary rocks, including banded iron-formation, and minor felsic metavolcanic (dacitic to rhyolitic) rocks. A provisional stratigraphy is proposed (Fig. 3), based on the least-deformed portion of the terrane — in the Maydon farm area on the southwest limb of the Maydon Syncline. The stratigraphic units of the Carlingup Terrane are formally defined in Witt (1997). The contact between the Chester Formation and the Bandalup Ultramafics is strongly deformed and is interpreted as a low-angle thrust fault across which the upper part of the greenstone sequence was tectonically emplaced over the Chester Formation. Contacts between other units are poorly exposed.

Chester Formation

The Chester Formation comprises mainly metamorphosed sedimentary rocks with minor felsic volcanic rocks. The unit is at least 750 m thick, but structural complexity precludes a more accurate determination. The metasedimentary rock package contains predominantly pelitic rocks with subordinate psammites and minor rudites. Metamorphic assemblages (see below) indicate the presence of interbedded low-Al and high-Al pelites. Individual beds of pelitic and psammitic material are well sorted. The clastic rocks are interbedded with several thin units of chert and massive to bedded limonite. Aeromagnetic data suggest that some of the chert units are surface expressions of banded iron-formation, and deep drilling beneath limonitic units has intersected massive pyrite (Gray and Gleeson, 1951a). Several lenses of andesitic to dacitic volcanic and volcaniclastic rock are found locally within the metasedimentary rock package associated with metamorphosed banded iron-formation and iron-rich pelites.

Thinly and evenly interbedded, pelitic and fine-grained psammitic metasedimentary rocks display little evidence of graded bedding. Low-angle cross-bedding, flame and dewatering structures, rip-up clasts and intraformational breccia have been observed locally but are uncommon. The lithological association and sedimentary structures of the Chester Formation suggest a low-energy (below storm-wave base), marine depositional environment with limited introduction of coarser grained clastic material. Chemical sedimentary units (chert, banded iron-formation, pyrite) formed during quiescent periods when the marine basin was starved of clastic detritus. Local deposits of volcaniclastic material may have been locally derived or introduced from distal volcanic centres. Unequivocal volcanic deposits have not been identified but high heat-flow is implied by the local association of volcaniclastic units with silicate-facies banded iron-formation and iron-rich pelites.

Bandalup Ultramafics

The Bandalup Ultramafics is a 1500 m-thick sequence of metamorphosed komatiitic volcanic rocks with minor high-Mg basalt and gabbro. Several thin units of metamorphosed banded iron-formation form interflow sedimentary horizons or may have been tectonically

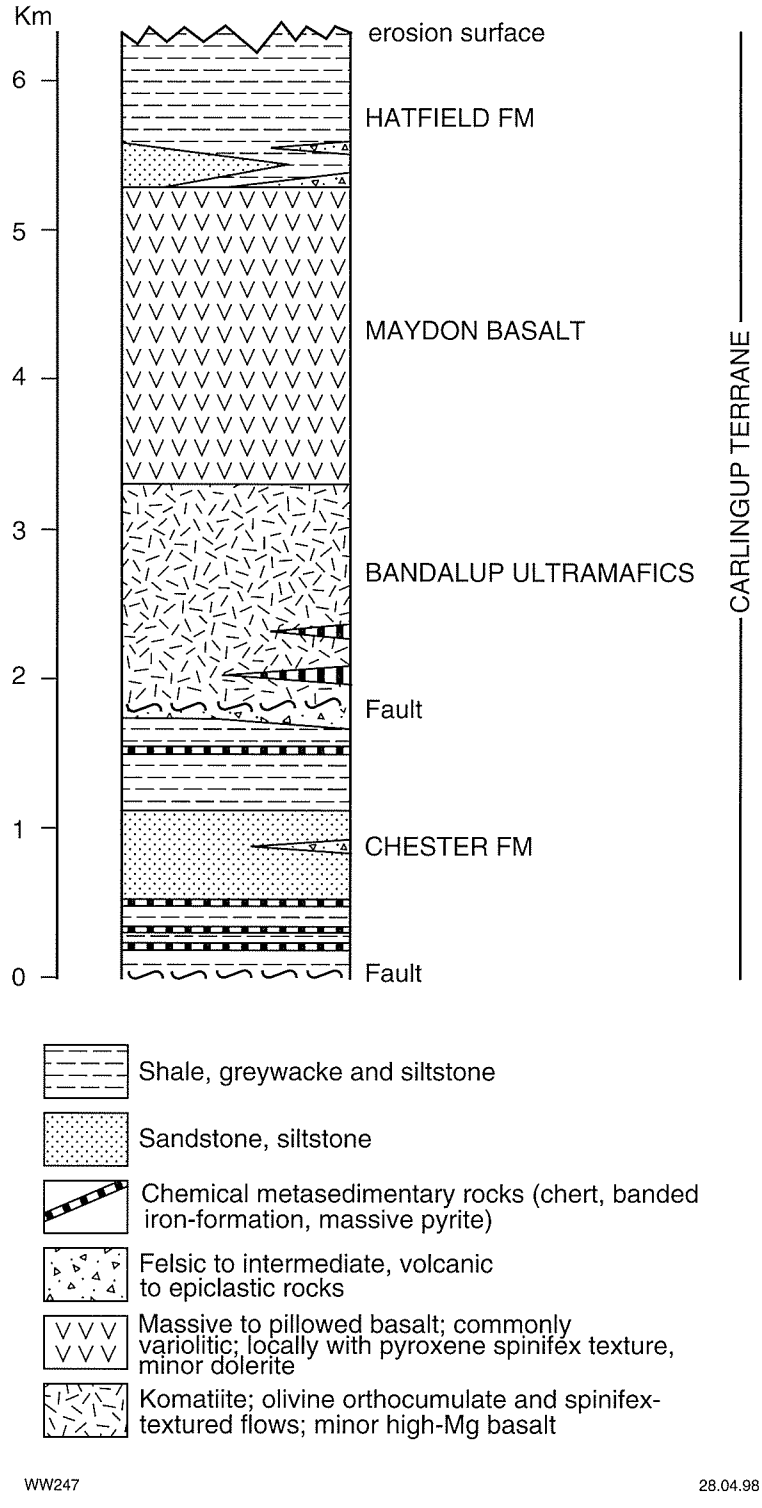

Figure 3. Stratigraphy of the Carlingup Terrane

emplaced. The komatiitic flows have the typical zoned structure described by Arndt et al. (1977), in which olivine spinifex-textured komatiite overlies olivine orthocumulate rocks. Serpentinized, adcumulate dunite is a relatively minor component of the ultramafic unit and occurs mainly in the strongly deformed northeastern part of the Ravensthorpe greenstone belt where banded iron-formation interflow units are uncommon. Hopper-shaped olivine, harrisitic-textured olivine and linked parallel-growth crystals of olivine (Fig. 4) also occur locally. The various olivine morphologies, including those in adcumulate dunite, have been linked to nucleation and growth rates and reflect crystallization under a range of supercooling conditions (Donaldson,

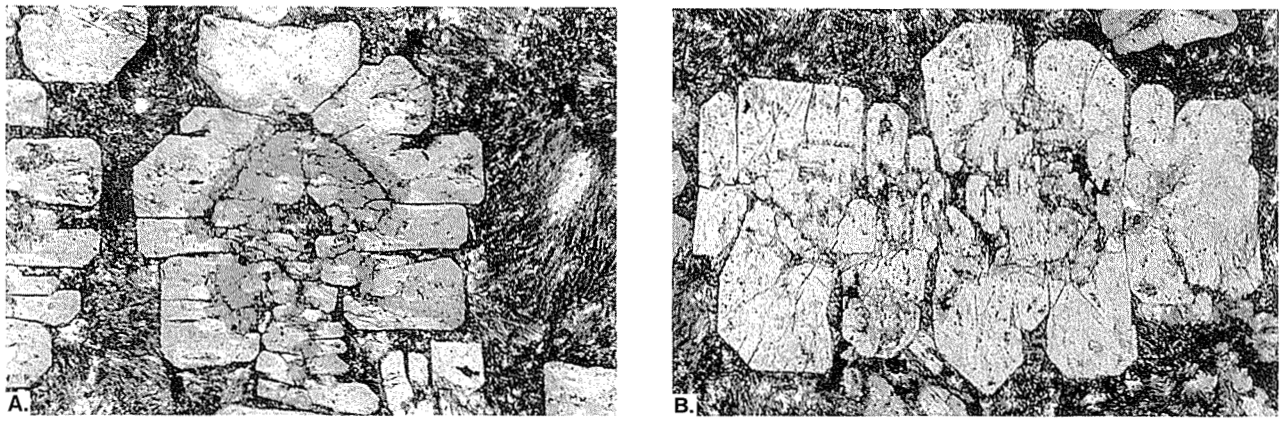

Figure 4. Olivine phenocrysts displaying linked parallel-growth crystal forms (Donaldson, 1976), Bandalup Ultramafics komatiite. GSWA sample no. 110263, plane-polarized light, 50X. A: Section cut normal to c-axis; B: Section cut parallel to c-axis

1976; Hill et al., 1987). There is no evidence for an intrusive origin for any of the komatiitic rocks. There is one published whole-rock analysis of a low-Al_2O_3 komatiite from the Bandalup Ultramafics (Table 1).

Maydon Basalt

The Maydon Basalt is a 2 km-thick sequence of metamorphosed to pillowed basalt with minor metamorphosed dolerite and rare interflow metasedimentary units. Pillows are up to 1.5 m across. Variolitic texture and acicular amphibole pseudomorphs after skeletal pyroxene are common. Varioles are 2–5 mm in diameter and increase in size toward pillow centres where they coalesce and form 80–90% of the basalt. Variolitic zones are separated from pillow margins by a 1–2 cm thick, devitrified, glassy rim. Some pillow margins are vesicular (RAVENSTHORPE AMGs 417752 and 453727). Zones of pillow breccia and hyaloclastite containing angular to subrounded clasts of massive to variolitic basalt, up to several metres in diameter, are exposed at RAVENSTHORPE AMG 428739. Although the basalt is generally aphyric, tabular phenocrysts of plagioclase were noted in the Bandalup area.

The stratigraphy and volcanology of the Maydon Basalt suggest rapid, submarine effusion of high-magnesian basalt lava and, less commonly, phreatomagmatic eruption and deposition of hyaloclastite. Redman and Keayes (1985) described the Maydon Basalt as siliceous high-Mg basalt (Table 1) and interpreted it as forming by melting of an enriched mantle source. More recent interpretations of mafic volcanic rocks with the chemical characteristics of siliceous high-Mg basalt invoke contamination of komatiitic magma with continental crust (Barley et al., 1986; Morris, 1993).

Hatfield Formation

The Hatfield Formation comprises a minimum thickness of one km of metamorphosed, fine-grained clastic sedimentary rocks with minor dacitic volcanic and volcaniclastic rocks and thin, limonitic units after massive to bedded pyrite. Minor coarser grained clastic units are interbedded with pelitic rocks near Bandalup Pools. Lithological associations and sedimentary structures in the Hatfield Formation are similar to those in the Chester Formation although the Hatfield Formation includes unequivocal dacitic volcanic rocks. A similar depositional environment for the two stratigraphic units is inferred.

Unassigned units

Other rock types that form part of the Carlingup Terrane cannot readily be assigned to any of the stratigraphic units. These are felsic volcanic rocks (dacite, rhyolite) east of Kundip and southeast of Bandalup, and coarse, poorly sorted sedimentary rocks, mainly on the northeast limb of the Maydon Syncline.

Felsic volcanic rocks

Metamorphosed, fine-grained, rhyolitic pyroclastic flow deposits are exposed southeast of Bandalup, and their strongly deformed equivalents can be recognized north of Bandalup. Minor quartz-poor amphibole–plagioclase rock (metamorphosed ?andesite) is also present. This unit occurs within a structurally complex area and is not associated with metasedimentary rocks so it cannot readily be correlated with felsic volcanic rocks in the Hatfield or Chester Formations. A sample of rhyolite from southeast of Bandalup yielded a SHRIMP* U–Pb zircon age of 2958 ± 4 Ma (Nelson, 1995).

Poorly sorted, felsic volcaniclastic rocks east of Kundip are in fault-bound contact with Bandalup Ultramafics. These rocks have undergone a strong, pervasive episode of hydrothermal alteration.

* SHRIMP: Sensitive High-Resolution Ion MicroProbe

Table 1. Geochemical analyses of ultramafic and mafic rocks in the Carlingup Terrane

	Komatiite 331/347	*Siliceous high-Mg basalt 27*	*Siliceous high-Mg basalt 28*
		Percentage	
SiO_2	47.88	54.7	52.7
TiO_2	0.53	0.70	0.60
Al_2O_3	5.75	14.2	12.28
Fe_2O_3	14.50	8.69	10.38
MnO	0.23	0.20	0.19
MgO	24.00	5.53	9.97
CaO	7.55	12.62	11.17
Na_2O	0.25	2.01	1.66
K_2O	0.02	0.11	0.27
P_2O_5	0.06	0.08	0.06
LOI	5.39	nd	1.72
H_2O	nd	nd	1.34
CO_2	nd	nd	0.57
Total	**106.16**	**98.84**	**99.28**
		Parts per million	
Sc	nd	37	37
V	nd	212	208
Cr	nd	311	978
Co	nd	52	59
Ni	nd	135	222
Cu	nd	72	113
Zn	nd	63	76
S	nd	77	81
Rb	nd	nd	9
Sr	nd	155	85
Zr	nd	62	42
Y	nd	19	16

NOTE: nd: not determined

REFERENCES: Komatiite 331/347 — Sun and Nesbitt (1978); Siliceous high-Mg basalts 27,28 — Redman and Keays (1985)

Metamorphosed polymictic conglomerate

Metamorphosed, poorly sorted, polymictic conglomerate and greywacke occur as fault-bounded lenses within mafic and ultramafic volcanic rocks of the Carlingup Terrane. Clasts are dominated by tonalite and basaltic to dacitic volcanic rocks. Clasts of banded iron-formation and komatiite are rare or absent. Sandstone and grit display widespread low-angle cross-bedding. Strongly deformed equivalents of this unit are exposed as medium- to coarse-grained quartz–plagioclase–amphibole(–biotite) schist and gneiss near the northeast margin of the Ravensthorpe greenstone belt. The conglomerate and sandstone are interpreted as alluvial or very shallow marine deposits.

Metamorphosed sandstone and oligomictic conglomerate

Metamorphosed, poorly bedded, quartz-rich sandstone, and oligomictic conglomerate that contains clasts of chert or quartzite, are found between Bandalup Creek and the Bandalup magnesite pits. Although these occurrences are shown as Archaean deposits on RAVENSTHORPE, the quartz-rich conglomerates and relatively pure orthoquartzite contrast with the finely bedded, opaque-rich, muddy sandstone and siltstone of the Chester and Hatfield Formations and the polymictic conglomerate. Similar quartzites have not been observed elsewhere in the Archaean greenstones. It is possible that the Bandalup quartzite and oligomictic conglomerate are part of an originally more extensive, tectonically emplaced slice of the Mesoproterozoic Mount Barren Group.

Ravensthorpe Terrane

The main component of the Ravensthorpe Terrane is a calc-alkaline complex that can be subdivided into the Annabelle Volcanics and the Manyutup Tonalite. The intimate spatial association of tonalite, tonalite porphyry dykes and calc-alkaline volcanic rocks suggests a co-magmatic relationship between all three, and this conclusion is supported by geochemical data (Chapter 3). The age of the calc-alkaline complex has been determined by SHRIMP U–Pb in zircon geochronology as c. 2.97–2.99 Ga (Savage et al., 1995). The geochemistry of these units is described and discussed in Chapter 3.

Annabelle Volcanics

The Annabelle Volcanics is a stratigraphically complex sequence of metamorphosed, calc-alkaline volcanic rocks. The sequence is dominated by volcaniclastic rocks that are associated with minor lava flows. Visual, field-based estimates, supported by petrographic observations and some geochemical data, suggest that the relative proportions of rock types are approximately 10–20% basalt, 50–70% andesite and 20–30% dacite. Quartz-phyric rocks are rare, but minor rhyolite has been tentatively identified. The proportion of dacite increases from near Ravensthorpe southeast toward Kundip, and southwest toward West River. Dolerite is a minor component of the Annabelle Volcanics, perhaps comprising 5% of the unit.

Volcaniclastic rocks are massive to coarsely bedded, metamorphosed andesitic and dacitic agglomerate and tuff or their resedimented equivalents (Fig. 5). Clast-supported and matrix-supported, mafic to intermediate agglomerate is widespread, although matrix-supported varieties appear to be dominant. Angular to subrounded clasts of basalt, andesite and dacite are enclosed by a fine- to medium-grained mafic to intermediate matrix. Coarse-scale bedding (>1 m) is defined by variable clast size and population and variable matrix composition. Clasts within individual beds are poorly sorted, and are mostly less than 20 cm, although there are rare clasts up to one metre across. Dacitic rocks, predominantly lapilli tuff, tend to be less coarsely fragmental than more mafic varieties. Clasts in dacitic rocks are commonly mafic, possibly reflecting pre-metamorphic chloritization of dacitic fragments. Locally preserved, flattened clast shapes may represent fiammé.

In addition to volcanogenic clasts, there are fewer clasts of quartz–amphibole schist, tonalite and coarse

vein quartz. The first probably represent metamorphosed epiclastic sedimentary rocks derived from the intermediate volcanic suite. Tonalitic clasts were probably derived from bodies similar to the adjacent Manyutup Tonalite. In the Phillips River, around COCANARUP AMG 704732, subrounded clasts of intensely epidotized rock are locally present. The source and precursor for these epidotized clasts are unknown, but the clasts were probably derived from within the calc-alkaline volcanic suite as there are no other 'exotic' clasts in the volcaniclastic rocks.

Finer grained, well-bedded tuffs range in composition from andesitic to dacitic. The tuffs are widespread but less common than agglomerate and lapilli tuff. Massive to weakly bedded hornblende–plagioclase porphyry, which occurs as a 2–3 m-thick bed or lens within andesitic agglomerate near the Maori Queen mine, may represent a metamorphosed dacitic ash-flow tuff.

Basaltic to andesitic lavas are uncommon but have been identified in drillcore from the Kundip area. Elsewhere, vesicles are locally common, and possible hyaloclastite has been observed, in low-strain domains around and south of COCANARUP AMG 700710. Xenoliths of amygdaloidal basalt with possible pillow margins have been observed in tonalite east of the old Ravensthorpe smelter (RAVENSTHORPE AMG 307803).

The Annabelle Volcanics becomes increasingly strongly deformed south of Cocanarup where it is exposed as fine- to medium-grained quartz–plagioclase–amphibole(–biotite) gneiss. Stretched clasts, indicative of an original fragmental structure, can be recognized in relatively low-strain domains within the gneiss.

Quartz-rich, garnet- and cordierite-bearing volcaniclastic rock and schist occur locally north and northeast of Ravensthorpe. These rocks may have originated as either epiclastic sedimentary rocks or altered volcaniclastic rocks. A large (2.5 × 0.5 km) area of cordierite–orthoamphibole rock near West River is interpreted as the metamorphosed equivalent of andesitic and dacitic rocks that have been modified by sea-floor alteration (cf. Vallance, 1967; Yardley, 1989).

The abundance of poorly sorted agglomerate, the poorly developed bedding, the rapid lateral and vertical facies variations, and the absence of non-volcanogenic sedimentary interbeds combine to suggest a proximal volcanic environment, with rapid deposition from mass debris flows (mass flows of pyroclastic debris or mass flows of volcaniclastic debris or both; following the terminology of Stix, 1991). Although submarine mass flows can transport debris long distances from a volcanic source, the Annabelle Volcanics is intruded by compositionally similar (co-genetic) tonalitic rocks that suggests they have not been transported large distances from the magmatic centre. The evidence for sea-floor alteration, particularly that near West River, implies a submarine depositional environment. The deposits are typical of those associated with mass wastage of emergent, calc-alkaline volcanic cones (Cas and Wright, 1987).

Manyutup Tonalite Complex

The Manyutup Tonalite Complex occupies the central part of the Ravensthorpe greenstone belt and is included in the Ravensthorpe Terrane. There is slight modal variation and considerable textural variation within the Manyutup Tonalite (Fig. 6), but these variations are difficult to recognize in the field, and only major areas of finer grained tonalite (*Aytm*) are shown on RAVENSTHORPE and COCANARUP. Estimated modal compositions vary from diorite to granodiorite but the intrusion is mainly tonalite, after the classification of Streckeisen (1976).

The most widespread phase of the Manyutup Tonalite is a coarse-grained, equigranular biotite–hornblende tonalite, similar to that shown in Figures 6A–C. Igneous banding (Fig. 6D), defined by oriented biotite and amphibole, and weak to strong, mm-scale mineral layering, is found locally. Its orientation is variable, generally between west and northwest. Ferromagnesian minerals comprise 5–15% of the rock; K-feldspar is absent or a very minor component; and accessory minerals are magnetite, ilmenite, apatite, zircon and, rarely, allanite. Variation in ferromagnesian content and amphibole:biotite ratio, shown in Figure 7, suggests that both parameters decrease inward from the northwest margin of the intrusive complex, but vary irregularly from west to east, probably as a result of thrust faulting.

Intrusive contacts between coarse-grained tonalite and volcanic country rocks (Annabelle Volcanics) are sharp but very irregular. Good exposures of contact features can be seen by walking upstream from the pegmatite locality in Cattlin Creek (Fig. 8). Pluton margins are characterized by abundant volcanic xenoliths, and extensive textural and modal variation for up to about 100 m from the contacts. The main modal variations involve ferromagnesian silicate mineral content. Textural variations mainly involve grainsize but include magmatic banding at some localities. Variants include coarse-grained quartz diorite, bimodal grainsize microtonalite, tonalite porphyry, hornblendite and anorthositic gabbro. Dolerite forms a contact phase between Stevenson Creek and Cocanarup and also intrudes the overlying volcanic unit (Annabelle Volcanics). Fine-grained tonalite and tonalite porphyry in texturally variable contact zones are compositionally similar to the volcanic country rocks and the two can be difficult to distinguish in these exposures. Xenoliths of rock types other than those that are present in the Annabelle Volcanics have not been observed, even southeast of the Mount McMahon mining group where the Annabelle Volcanics unit is very thin or absent.

Medium-grained tonalite forms relatively small plutons within the coarse-grained tonalite and adjacent volcanics, particularly along the northwest margin of the intrusion. Most of these bodies have a high proportion of ferromagnesian minerals (20–30%; Fig. 6H), whereas some are relatively leucocratic (e.g. Fig. 6I). In the more melanocratic plutons, amphibole is dominant over biotite and commonly is the only ferromagnesian silicate mineral. As with the coarse-grained tonalite, there is widespread textural and modal variation (including

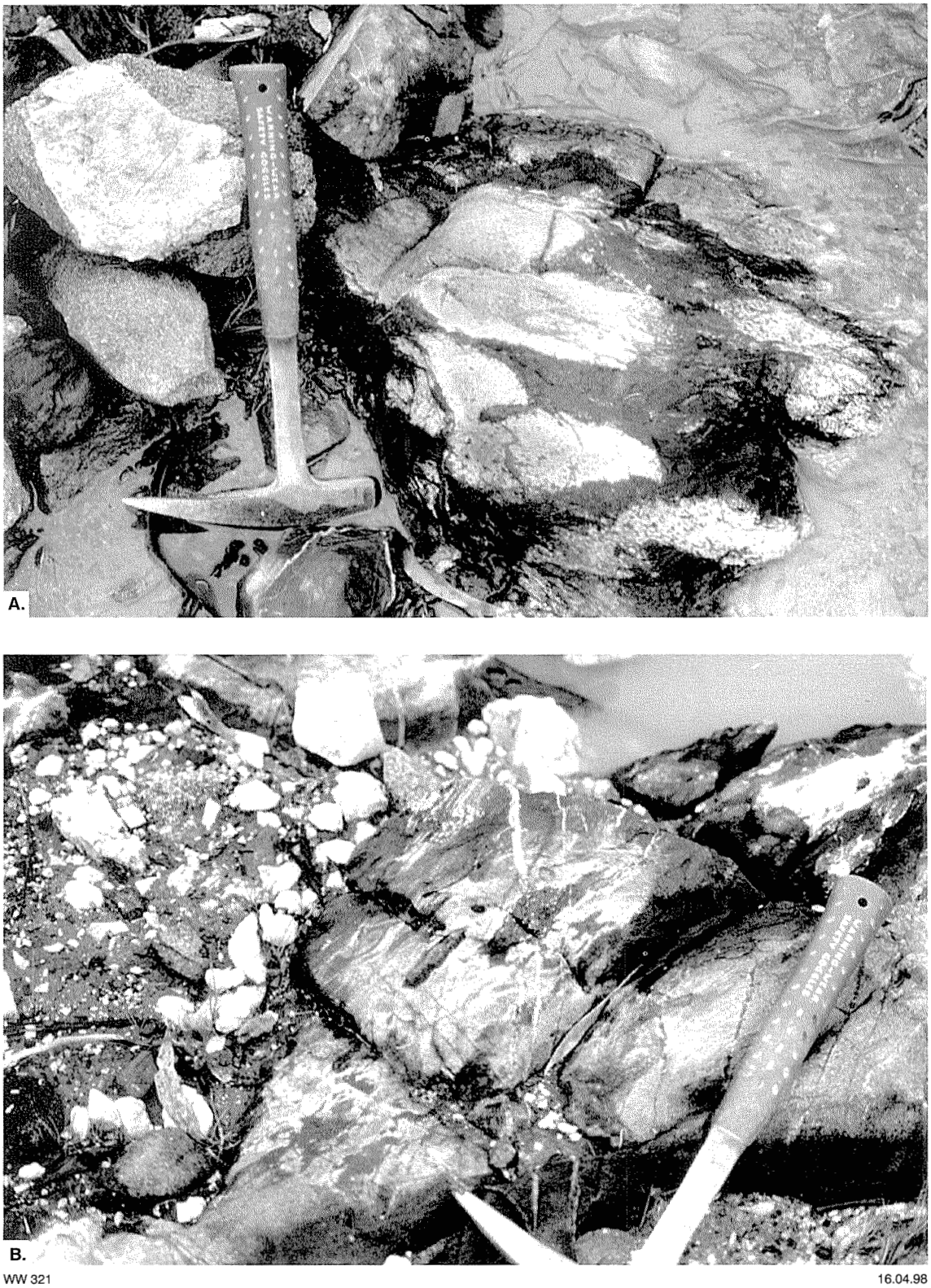

Figure 5. **Andesitic agglomerate, Annabelle Volcanics, exposed in a small creek around AMG 263843, on RAVENSTHORPE. A: Clasts of dacite in an andesitic matrix. B: Metre-scale layering defined by colour index with mafic clasts in more leucocratic (dacitic) matrix. Note late-stage veining, including amphibole-rich veinlets, near handle of hammer**

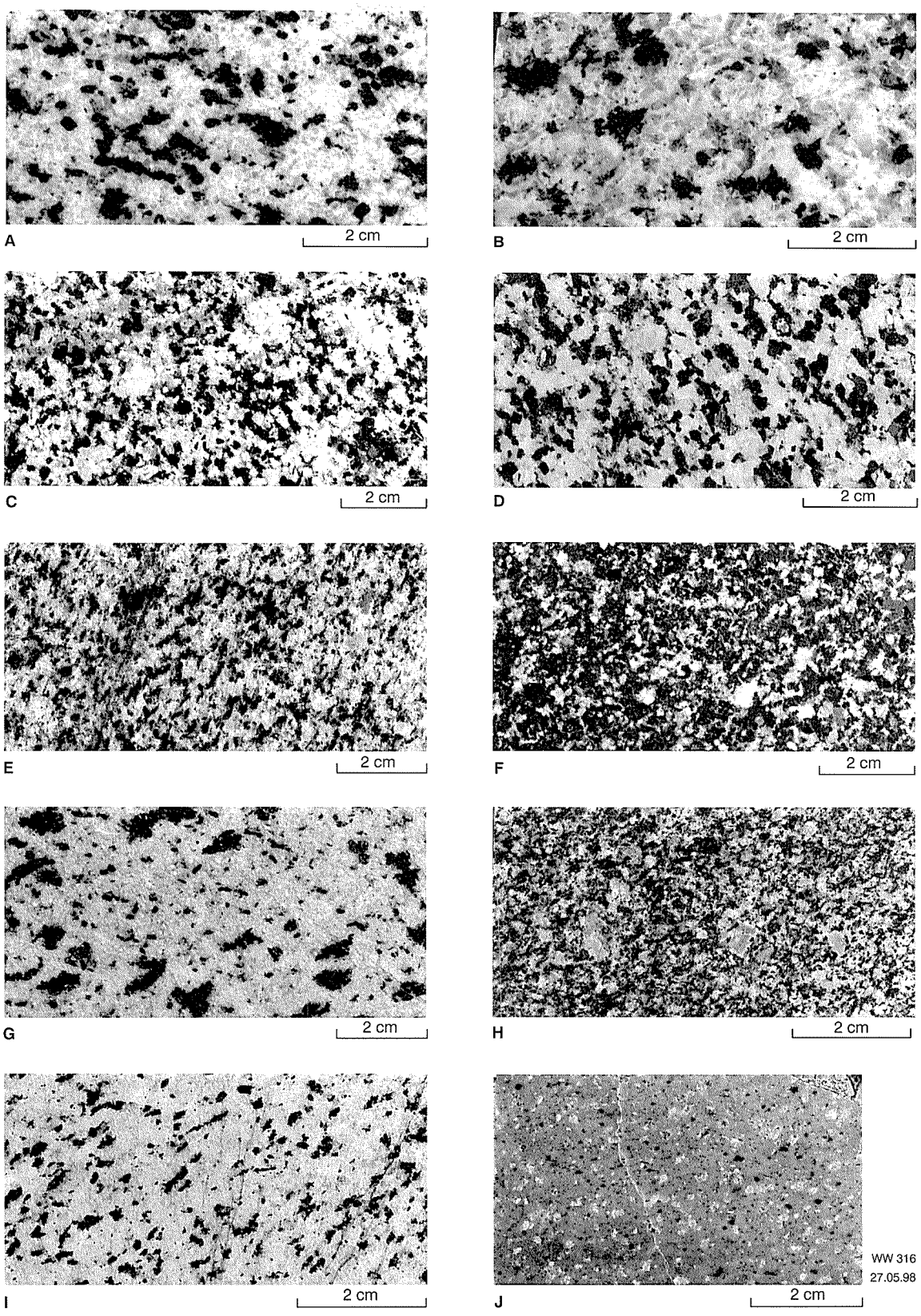

Figure 6. Variable textures and colour indices of Manyutup Tonalite and related rock types. A–D show the main textural variants that comprise the bulk of the pluton. Note the magmatic layering in Figure 6D. Figures 6E and 6H are strongly recrystallized tonalites from the southwestern part of the intrusive complex. Figure 6F is a relatively melanocratic quartz diorite that forms a minor component of the intrusive complex. Figures 6G and 6I are medium-grained dykes and pluton. Figure 6J is a late cross-cutting dacite porphyry dyke. Note the epidote veining in the top left corner of Figure 6C, and other fine-scale veinlets and fractures in Figures 6E, I and J. Locations are shown on Figure 7 — A: 119916; B: 119914; C: 119948; D: 119929; E: 119926; F: 119920; G: 119908; H: 119930; I: 119912; J: 119917. All numbers are GSWA sample numbers

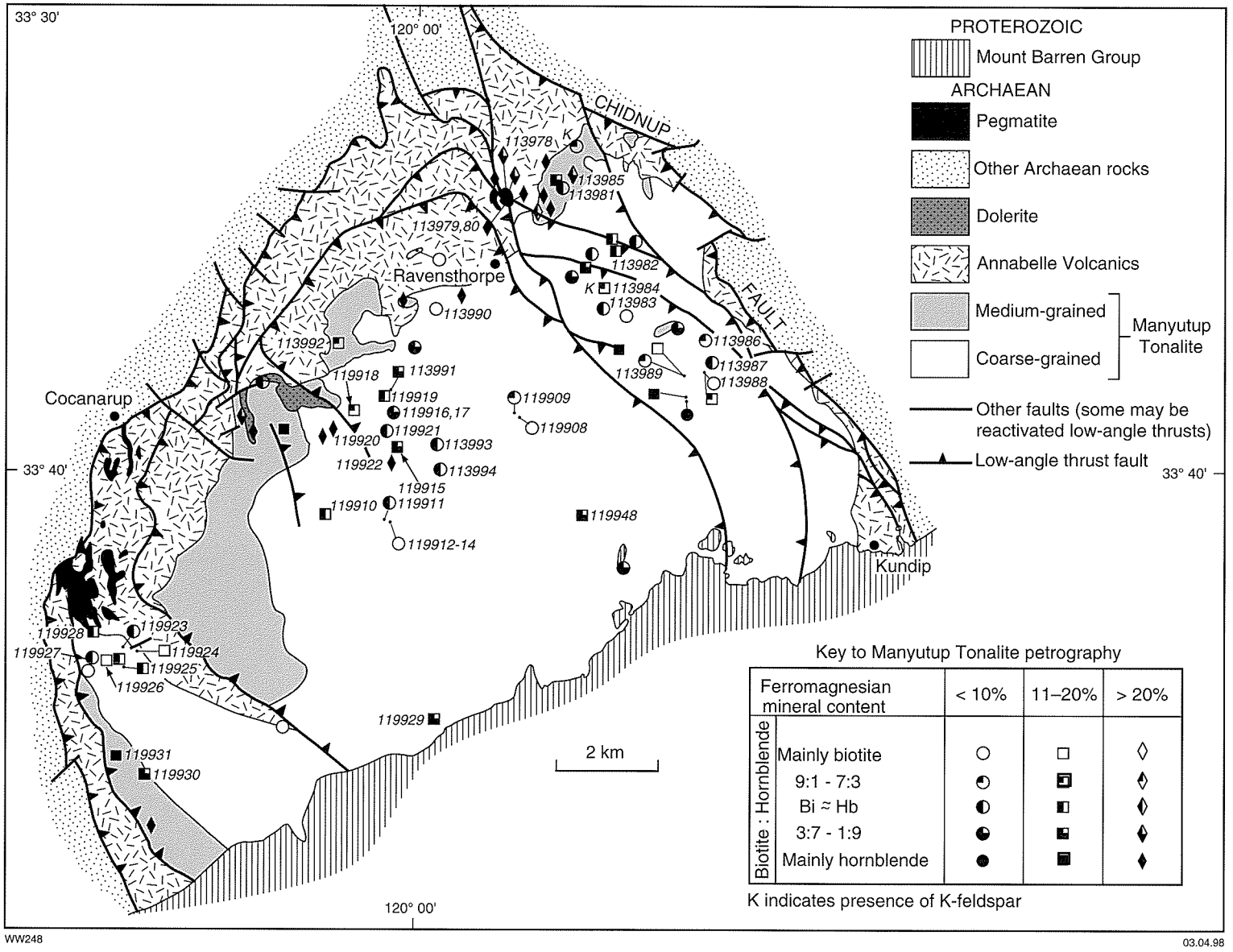

Figure 7. Whole-rock geochemistry samples from the Ravensthorpe Terrane showing variations in ferromagnesian mineral content and relative biotite:amphibole ratios in Manyutup Tonalite

WW 322 10.03.98

Figure 8. Irregular contact between Manyutup Tonalite (light) and Annabelle Volcanics (dark), exposed in Cattlin Creek (RAVENSTHORPE AMG 248827). Xenoliths of Annabelle Volcanics lie in Manyutup Tonalite

mm-scale magmatic banding), especially in marginal zones of the plutons. Intrusive contacts between medium-grained tonalite and volcanic rocks are exposed in Stevenson Creek. Contact relations between medium-grained tonalite plutons and coarse-grained tonalite have not been observed but are probably sharp to gradational over tens of metres (based on rock-float distribution).

Medium-grained, amphibole-rich tonalite also exists as a marginal phase (up to several kilometres wide) to coarse-grained tonalite along the west and southwest contacts of the Manyutup Tonalite. Contacts between medium-grained and coarse-grained phases in this area are broadly gradational (over several hundred metres). The medium-grained tonalite lacks xenoliths and is moderately to strongly recrystallized (Fig. 6E). Some samples display a distinct tectonic foliation, defined by closely spaced, anastomosing zones of intense recrystallization and granoblastic fabric. The foliation is generally oriented subparallel to lithological contacts. This contact unit is interpreted to result from tectonic recrystallization and is probably not genetically equivalent to the medium-grained tonalite plutons described above.

Numerous dykes of fine-grained tonalite and tonalite porphyry intrude medium- and coarse-grained tonalite and volcanic country rocks along the northwest and eastern contact zones. They are also found, but are less common, in the interior of the Manyutup Tonalite. Contacts between the dykes and coarse-grained equigranular tonalite and other compositional/textural variants are sharp and irregular, or sharply transitional (over one or two centimetres).

Between Manyutup Creek and the Phillips River, the Manyutup Tonalite is cut by a swarm of northwest-trending, fine-grained, leucocratic feldspar porphyry dykes (Fig. 6J). The dykes are of unknown age, but are deemed to be related to the Archaean tonalite. The dykes are difficult to distinguish from the dacitic component of the Annabelle Volcanics but have been observed within volcanic rocks near Stevenson Creek (COCANARUP AMG 735758). They have not been recognized in units outside the Ravensthorpe Terrane.

The Manyutup Tonalite is interpreted as having crystallized from a subvolcanic magma chamber that is geochemically equivalent to calc-alkaline lavas and pyroclastic rocks of the Annabelle Volcanics. Textural and modal variations suggest a dynamic magmatic environment that may have been fed by several sequential pulses of dioritic to tonalitic magma while crystallization took place in the magma chamber. Microtonalitic dykes, rooted in the main body of Manyutup Tonalite, represent feeder channels into the overlying volcanic pile. During construction of the volcanic edifice, the mainly tonalitic magma chamber rose up into the volcanic pile that it intruded by piecemeal stoping at the contacts.

Cocanarup greenstones

The Cocanarup greenstones are composed mainly of metasedimentary rocks, but do contain metamorphosed mafic and ultramafic rocks. The package of rocks is strongly deformed and has been metamorphosed at amphibolite facies conditions. Primary depositional features are rarely preserved in the greenstones of the belt but spinifex-textured komatiite has been recognized in the Aerodrome sector. Correlation between metasedimentary rocks of the Cocanarup greenstones and the Chester Formation is uncertain, as described below. The Cocanarup greenstones are subdivided into the Aerodrome sector in the north and the West sector in the south (Fig. 2), reflecting changes in the nature of the metasedimentary rocks and associated units across a northwest-trending fault near Cocanarup.

The Aerodrome sector: The Aerodrome sector comprises micaceous quartzite, quartz–muscovite schist and quartz–feldspar–biotite–andalusite schist, interleaved with metamorphosed ultramafic rocks, minor amphibolite and mafic gneiss. Although this association is similar to that in the Carlingup Terrane, a major difference is the abrupt decrease in the amount of banded iron-formation. Banded iron-formation has been identified, but is extremely rare, in the Aerodrome sector. Furthermore, metasedimentary rocks of the Aerodrome sector differ from the mainly metapelitic rocks and quartz-rich metasedimentary rocks of the Chester Formation. The tourmaline-rich, predominantly quartzofeldspathic rocks in the Aerodrome sector suggest an immature sedimentary protolith with a felsic igneous provenance.

The West sector: Para-amphibolite and quartz–plagioclase–mica–garnet schist are the main components of the West sector. These metasedimentary rocks contain higher Ca, Fe and Mg than those of the Aerodrome sector and are, in that respect, more similar to rocks of the Chester Formation. Para-amphibolite has not been identified outside the West sector on RAVENSTHORPE or COCANARUP. Ultramafic rocks are much less common here than in the Aerodrome sector. Although the lithological associations in the Aerodrome and West sectors are reasonably distinctive, quartz–feldspar–biotite(–garnet–aluminosilicate) schist is found north and south of the fault separating the two sectors and may represent a transitional sedimentary facies between quartzofeldspathic metasedimentary rocks of the Aerodrome sector and metapelites of the West sector. Minor banded iron-formation is present in the Copper King – Last Venture mines area (Perring, 1991).

Intrusive rocks

Granitoid gneiss

Extensive areas of granitoid gneiss lie northwest and northeast of the Archaean greenstones. The contacts with greenstones are highly strained and the gross trends of gneissic banding, contacts, and lithological units within the greenstones, are all more or less parallel with one another.

The predominantly leucocratic gneiss ranges in composition from trondhjemite to syenogranite but monzogranitic and granodioritic varieties are most abundant. In the Cocanarup area, a predominantly mesocratic, tonalitic to dioritic gneiss, commonly associated with mafic gneiss, occurs as bands and lenses up to 2 km wide, within the leucocratic gneiss and the Cocanarup greenstones. The tonalitic gneiss bands are parallel to the gneiss–greenstone contacts, and contacts between leucocratic and mesocratic gneiss, exposed in the Phillips River, are gradational over 50 to 100 m. Some of the mesocratic gneiss bands appear to lie along strike from mafic gneiss units of the Cocanarup greenstones.

Granitoid gneiss, predominantly leucocratic, is well-exposed along the West River, where relationships between the various components of the gneiss can be interpreted with reasonable confidence. The earliest phase is mesocratic, medium- to coarse-grained granodiorite to diorite (10–30% biotite) with well-developed gneissic banding. This phase is not necessarily equated with the predominantly mesocratic granitoid gneiss near Cocanarup that contains a significant amphibole component. Coarser grained leucocratic (mostly <5% biotite) monzogranite and granodiorite intrude the earlier phase. Intrusion was mostly subparallel to gneissic banding in the granodiorite to diorite gneiss but was locally discordant. This later phase is recrystallized but has only a weak gneissic banding. Medium- to coarse-grained tonalitic dykes cut across the gneissic banding at low to moderate angles but are themselves foliated and boudinaged. The granitoid gneiss complex is intruded by equigranular, locally garnet-bearing, biotite monzogranite, syenogranite and granitic pegmatite, which, in turn, have been variably deformed. This latest intrusive phase is commonly transgressive across gneissic banding, with bodies ranging up to pluton size, although intermittent exposure and difficult access prevent definition of most such plutons.

Granitoid gneiss north and east of the Carlingup Terrane displays features that are mostly consistent with the history described for the West River gneisses. However, there are some minor compositional differences between the two gneiss complexes. Biotite is the main ferromagnesian silicate phase in gneiss west of the Cocanarup greenstones, whereas north and east of the Carlingup Terrane the gneiss contains amphibole and biotite. As well, titanite is a more abundant accessory mineral in gneiss to the north and east of the Carlingup Terrane.

The Munglinup Gneiss, lying to the south of the Jerdacuttup Fault, is exposed along the southern coastline, east of Hopetoun. It is petrographically similar to the West River gneiss but has undergone a further period of deformation related to the Albany–Fraser Orogeny (Myers, 1995b). U–Pb in zircon (SHRIMP) dating of three Munglinup Gneiss samples from the RAVENSTHORPE 1:250 000 sheet has yielded ages, interpreted as emplacement ages of the granitoid protoliths, of 2588 ± 12 Ma, 2632 ± 37 Ma and 2649 ± 6 Ma (Nelson, 1995; Nelson et al., 1995).

Several small plutons of undeformed, equigranular biotite monzogranite and biotite granodiorite were emplaced near the northeast contact of the Carlingup Terrane. A larger body of biotite monzogranite with K-feldspar megacrysts has been identified northwest of Cocanarup. This pluton contains biotite schlieren and xenolithic blocks of granitoid gneiss and is probably equivalent to the late intrusive phase in granitoid gneiss exposed along the West River, described above.

Chapter 3

Mineralogy and whole-rock chemistry of the Ravensthorpe Terrane rocks

Mineralogy of the Manyutup Tonalite

Selected analyses of plagioclase, amphibole and biotite, and secondary chlorite from the Manyutup Tonalite are given in Appendix 1. Analyses were carried out using a JEOL 6400 scanning electron microscope at the Centre for Electron Microscopy, University of Western Australia. Analytical conditions are described in Appendix 1.

The main rock-forming minerals are quartz, plagioclase, biotite and amphibole. A few samples contain minor K-feldspar. Accessory minerals are magnetite, ilmenite, zircon and apatite. In addition, secondary minerals define widespread propylitic alteration. Two magmatic suites are distinguished on the basis of whole-rock chemical composition: a low-SiO_2 suite and a high-SiO_2 suite. These are discussed more fully below.

Plagioclase

Subhedral tabular grains of plagioclase in medium- and coarse-grained tonalite display strong normal to oscillatory zoning. Irregular calcic cores are common in coarse-grained tonalite. Compositions of plagioclase in several samples of Manyutup Tonalite are summarized in Figure 9. The composition is very variable from sample to sample (Fig. 10).

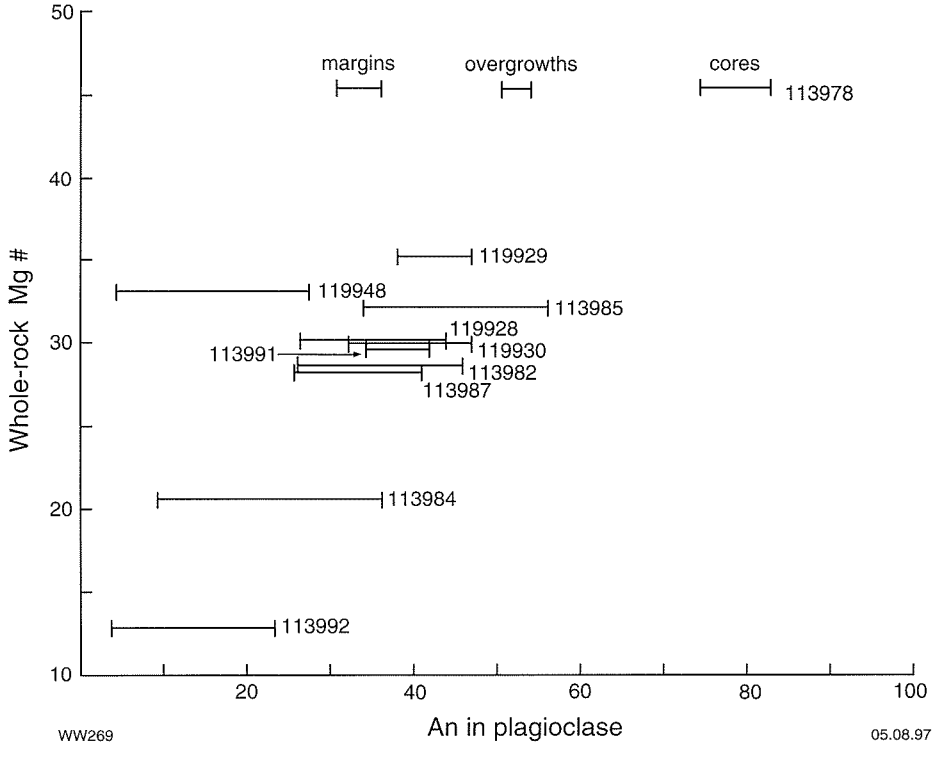

Figure 9. Compositional variation of plagioclase, and comparison with whole-rock Mg#, in selected samples of Manyutup Tonalite. Three distinct generations of plagioclase were recognized in GSWA 113978. Other samples contained zoned plagioclase but distinct generations could not be recognized

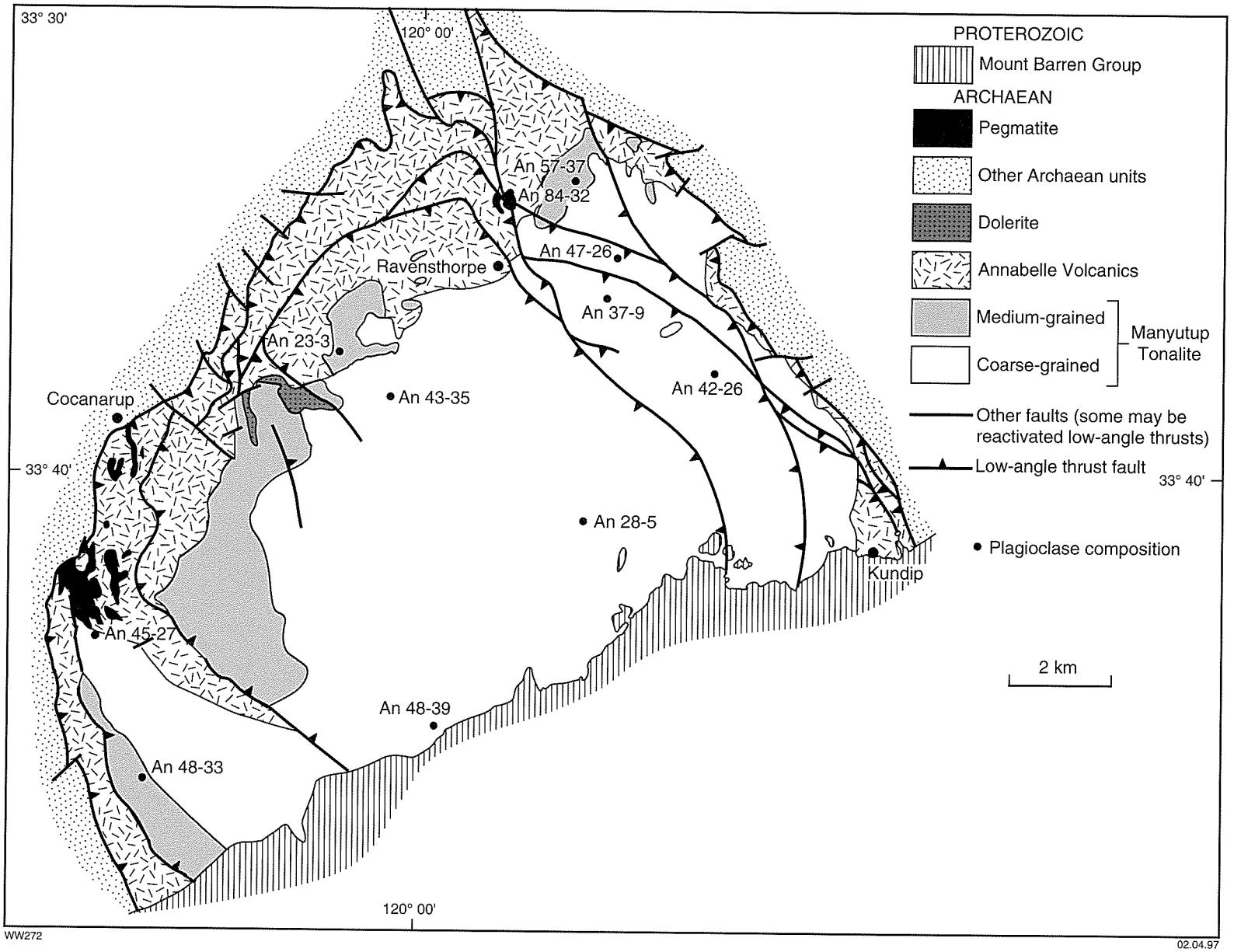

Figure 10. Variation in plagioclase compositions in samples from Manyutup Tonalite, by locality

Fine-grained, secondary sericite is common in most samples and selectively replaces cores and relatively calcic zones. A later generation of coarser grained, secondary chlorite and epidote occurs as irregular, patchy and veinlet-controlled alteration of plagioclase (Fig. 11A). Secondary chlorite and epidote are commonly associated with lesser amounts of quartz and muscovite and, more rarely, secondary carbonate, biotite and amphibole and disseminated sulfides (Fig. 11B). Some plagioclase grains in tonalite of the high-SiO_2 suite contain fine-grained (<50 μ) inclusions of opaque minerals (Fig. 11C). Opaque inclusions in most samples are magnetite and/or ilmenite although only relatively coarse-grained inclusions can be identified with any confidence. In a few samples, sulfide inclusions are present instead of, or in addition to, magnetite and ilmenite. Sulfide inclusions are mostly chalcopyrite, but pyrite and pyrrhotite may also be present. In some samples, the fine-grained oxide and sulfide inclusions are apparently unrelated to fractures and other secondary minerals and may be magmatic inclusions. However, coarser grained sulfide disseminations, associated with secondary chlorite and epidote, are also present in many of the samples (Fig. 11D). Samples containing plagioclase with sulfide inclusions, although uncommon, are not confined to any specific area of the Manyutup Tonalite. However, they have not been observed in samples from the eastern margin of the Manyutup Tonalite Complex, between Ravensthorpe and Kundip, where most of the copper sulfide mineralization occurs. All samples containing sulfide inclusions are relatively unfractionated samples (<68% SiO_2) of the high-SiO_2 suite.

Amphibole

Subhedral prismatic amphibole is commonly zoned from brown-green cores to green or blue-green margins (Fig. 11E). The cores are presumed to be igneous amphibole, whereas the margins have probably equilibrated with hydrothermal (possibly regional metamorphic) fluids at subsolidus temperatures. Amphibole analytical data is summarized in Figures 12 and 13. The brown-green cores generally have a higher Mg number (Mg/Mg + Fe) and Si:Al than green to blue-green margins. Although amphibole cores have high Si:Al, the proportion of aluminium in octahedral co-ordination is lower than in the blue-green amphibole margins. Brown-green amphibole cores are magnesio-hornblende whereas the green to blue-green margins are tschermakitic hornblende. Relict clinopyroxene cores were observed in only one sample, a coarse-grained tonalite (113979) of the low-SiO_2 suite from Cattlin Creek.

Brown-green cores of many amphibole grains contain dusty to fine-grained (<50 μ) inclusions of biotite and opaque minerals. These inclusions are commonly crystallographically oriented within the cleavage planes of the amphibole host (Fig. 11F). Apatite and fluid inclusions are less common. Although these minerals appear to be magmatic inclusions in the amphibole grains, in some samples they are associated with irregularly distributed disseminations of coarser grained, secondary biotite and opaque minerals. Opaque inclusions exist in samples of both the low-SiO_2 and high-SiO_2 suites. Inclusions in the samples from the low-SiO_2 suite are ilmenite, which, in sample 119920 (a primitive quartz diorite), is accompanied by chalcopyrite. Inclusions in samples from the high-SiO_2 suite are also ilmenite. Chalcopyrite inclusions accompany ilmenite in sample 113984 (one of the most fractionated samples).

Amphibole in most samples displays minor alteration to secondary biotite and chlorite.

Biotite

Biotite forms irregular books and aggregates that display minor to moderate alteration to chlorite and epidote or muscovite. Altered biotite contains inclusions of ilmenite, titanite and rutile as irregular disseminations or oriented inclusions within cleavage planes. The range of biotite Mg# extends between 40 and 65. Note that several samples of chlorite after biotite (Appendix 1, Table 1.5) display the optical properties of biotite. Thus petrographic examination has under-estimated the amount of chlorite in at least some samples.

Opaque oxide minerals

The main opaque oxide minerals in the Manyutup Tonalite are magnetite, ilmenite and titanomagnetite (subsolidus processes have converted titanomagnetite to an intergrowth of ilmenite and hematite). The tonalite belongs to the magnetite series granites of Ishihara (1977). Ilmenite is dominant in the granitoids from the low-SiO_2 suite and in the more primitive samples of the high-SiO_2 suite. Magnetite is dominant in the more fractionated members of the high-SiO_2 suite.

Pervasive alteration of the Manyutup Tonalite

Most samples of Manyutup Tonalite examined in thin section show evidence of interaction with a hydrothermal fluid. Secondary mineral assemblages can be assigned to either of two main alteration styles (propylitic alteration or potassic alteration) that are more or less pervasively distributed through the Manyutup Tonalite. No meaningful distribution patterns could be distinguished for either alteration style. The intensity of alteration appears unrelated to lithology, chemical suite or geographic location. However, a more thorough study of a larger number of samples, to accurately determine the modal abundances of secondary minerals, may reveal some meaningful correlations.

Propylitic alteration

Propylitic alteration is evidenced by disseminations, aggregates and discontinuous veinlets of chlorite and epidote(–muscovite–quartz–carbonate) in plagioclase

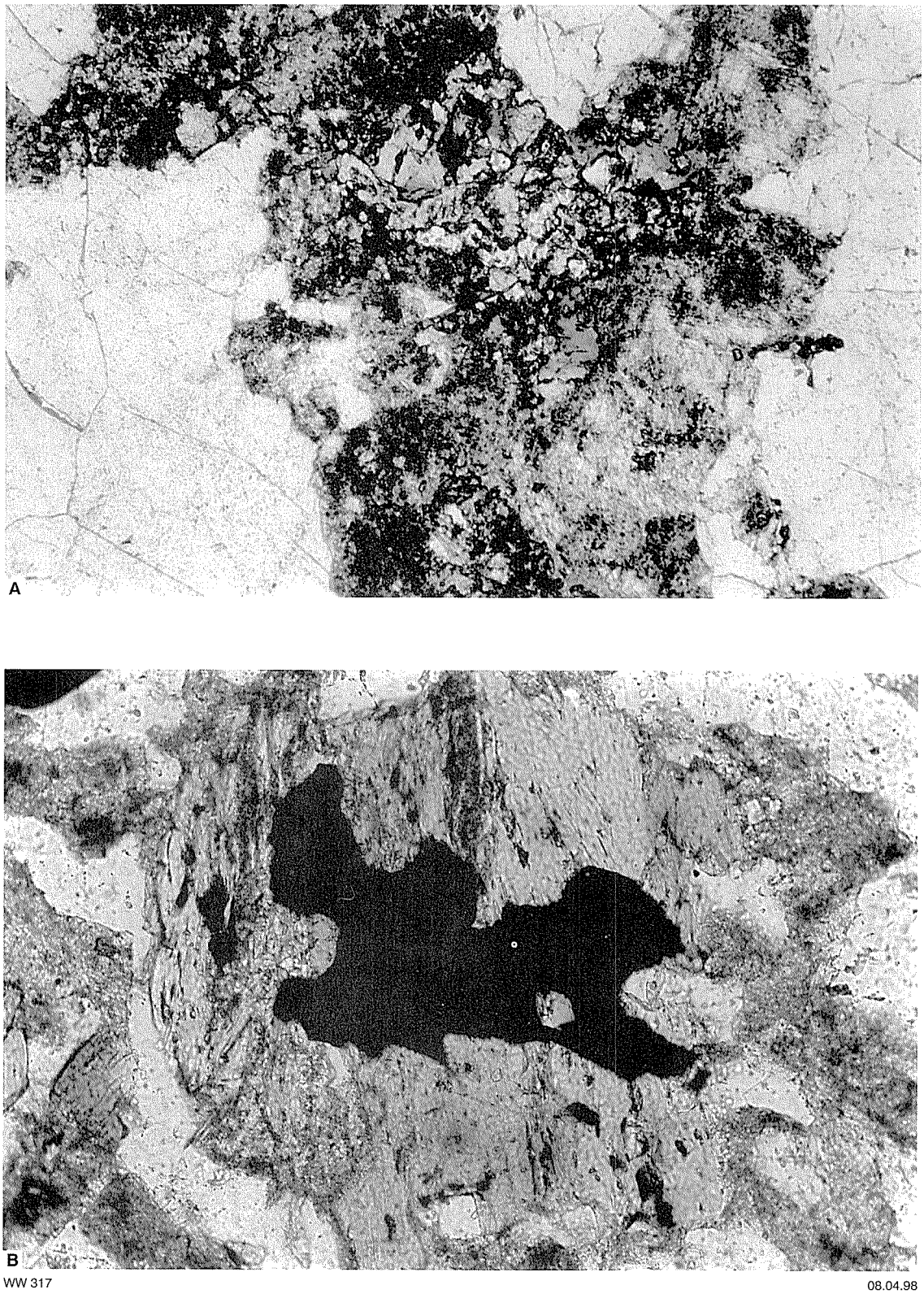

Figure 11. Photomicrographs from the Manyutup Tonalite

A: Secondary epidote and chlorite (propylitic alteration) in plagioclase. GSWA 113988, plane-polarized light, width of view approximately 3 mm (50X)
B: Disseminated chalcopyrite associated with chloritized biotite. GSWA 113985, plane-polarized light, width of view approximately 1 mm (150X)

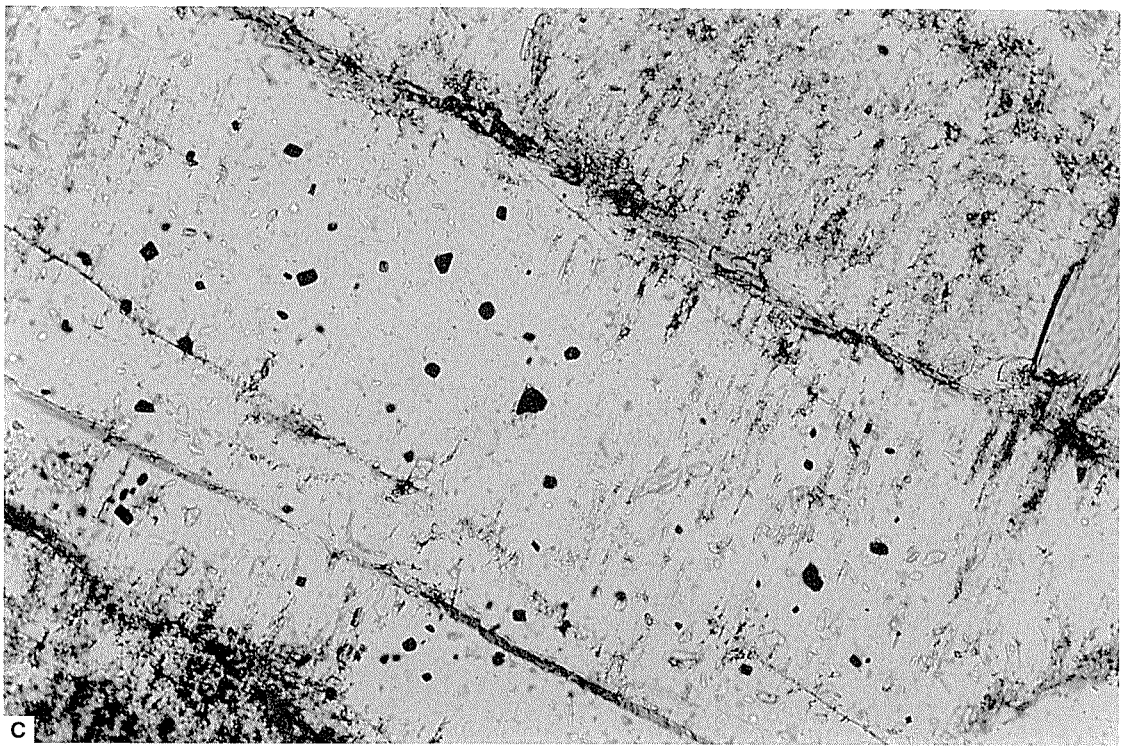

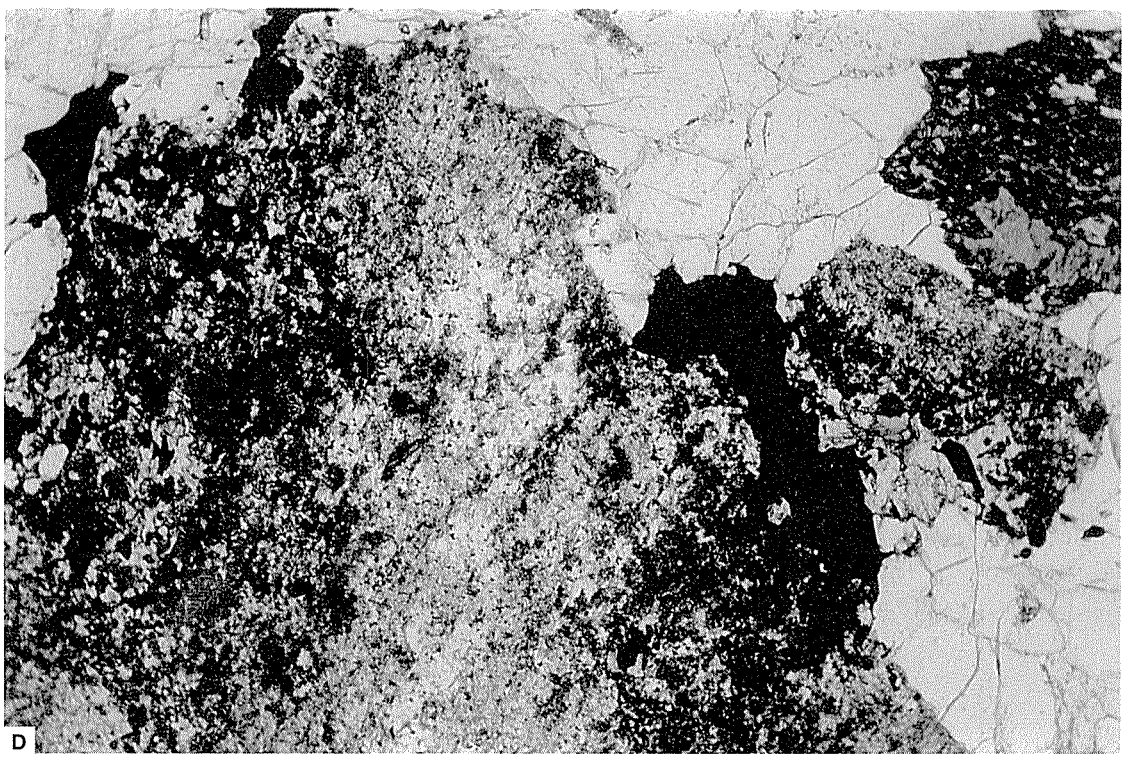

C: Small inclusions of magnetite in core of plagioclase grain. GSWA 113994, plane-polarized light, width of view approximately 1 mm (150X)
D: Secondary, disseminated chalcopyrite associated with propylitic alteration of plagioclase. GSWA 119910, plane-polarized light, width of view approximately 3 mm (50X)

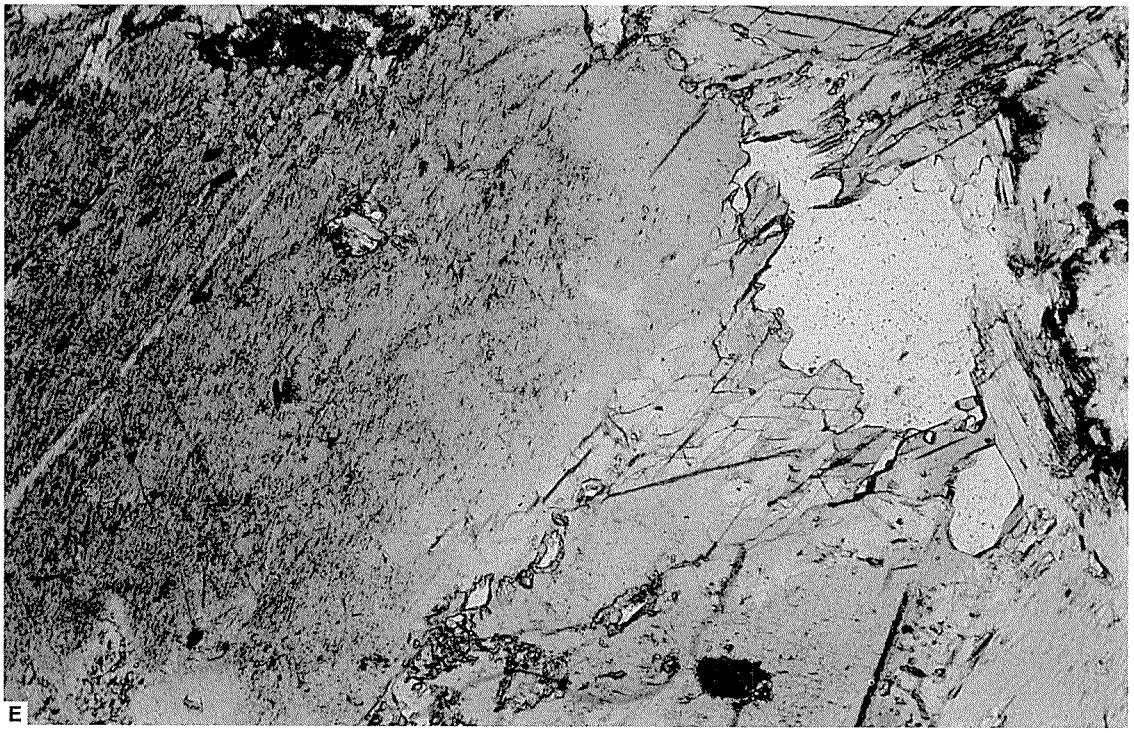

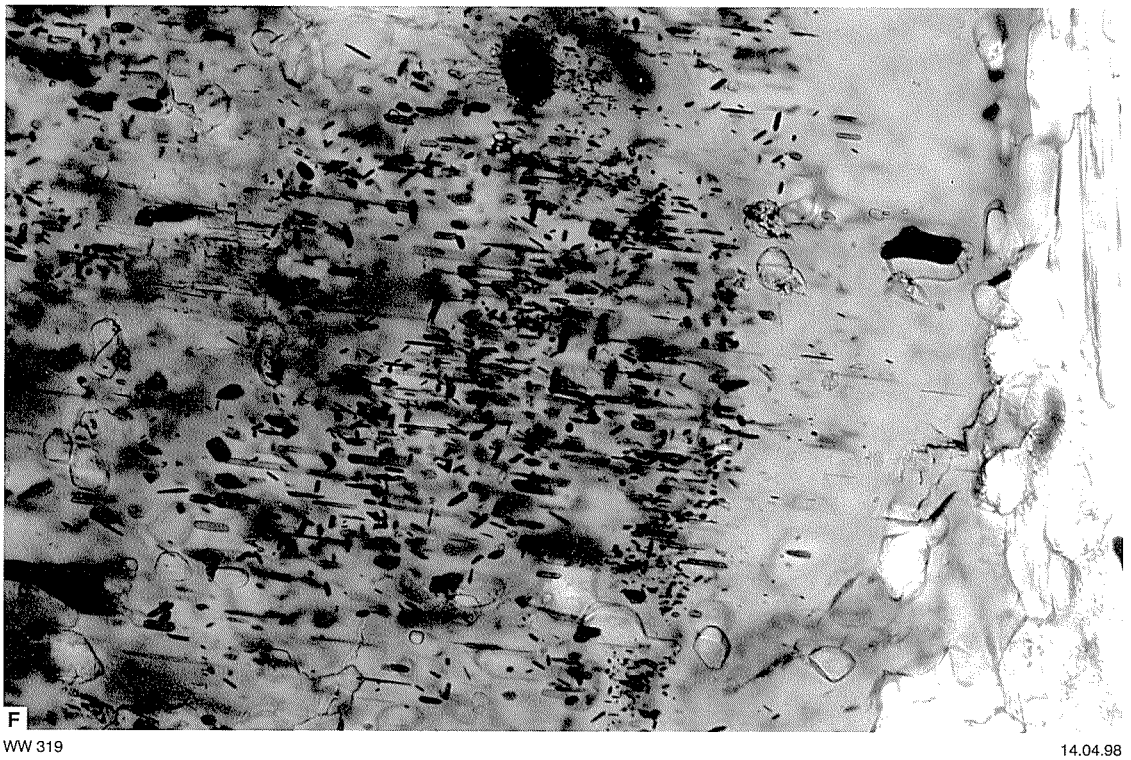

WW 319

14.04.98

E: Igneous (dark, inclusions common, toward centre of grain) and metamorphic (paler coloured, inclusions rare, at margin of grain) amphibole. GSWA 119920, plane-polarized light, width of view approximately 3 mm (50X)

F: Small inclusions of ilmenite and biotite in amphibole. Note absence of inclusions in the metamorphic amphibole margin. GSWA 113992, plane-polarized light, width of view approximately 3 mm (50X)

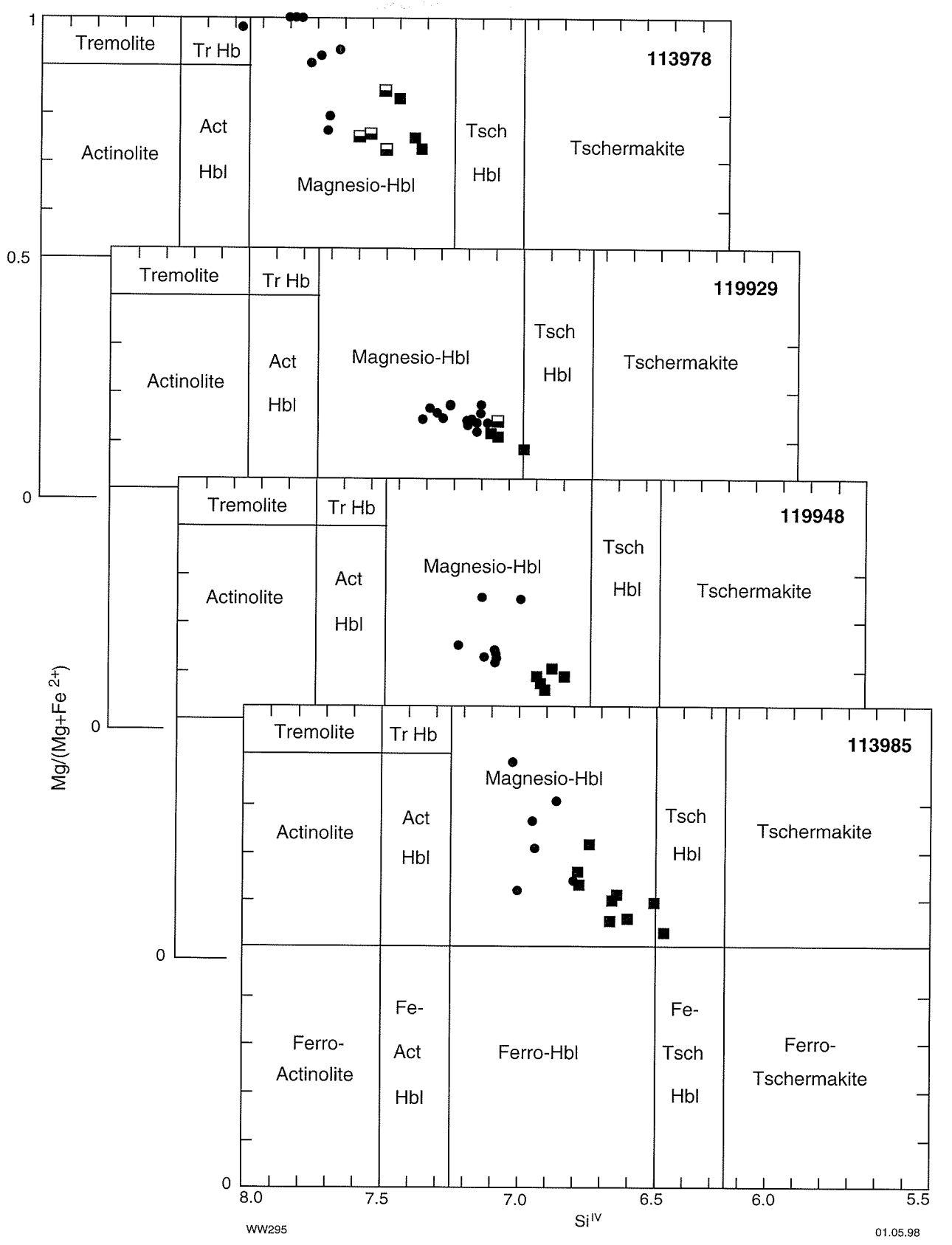

Figure 12. Compositions of amphiboles from selected samples of Manyutup Tonalite. Circles: igneous amphibole; half squares: transitional amphibole; squares: metamorphic amphibole

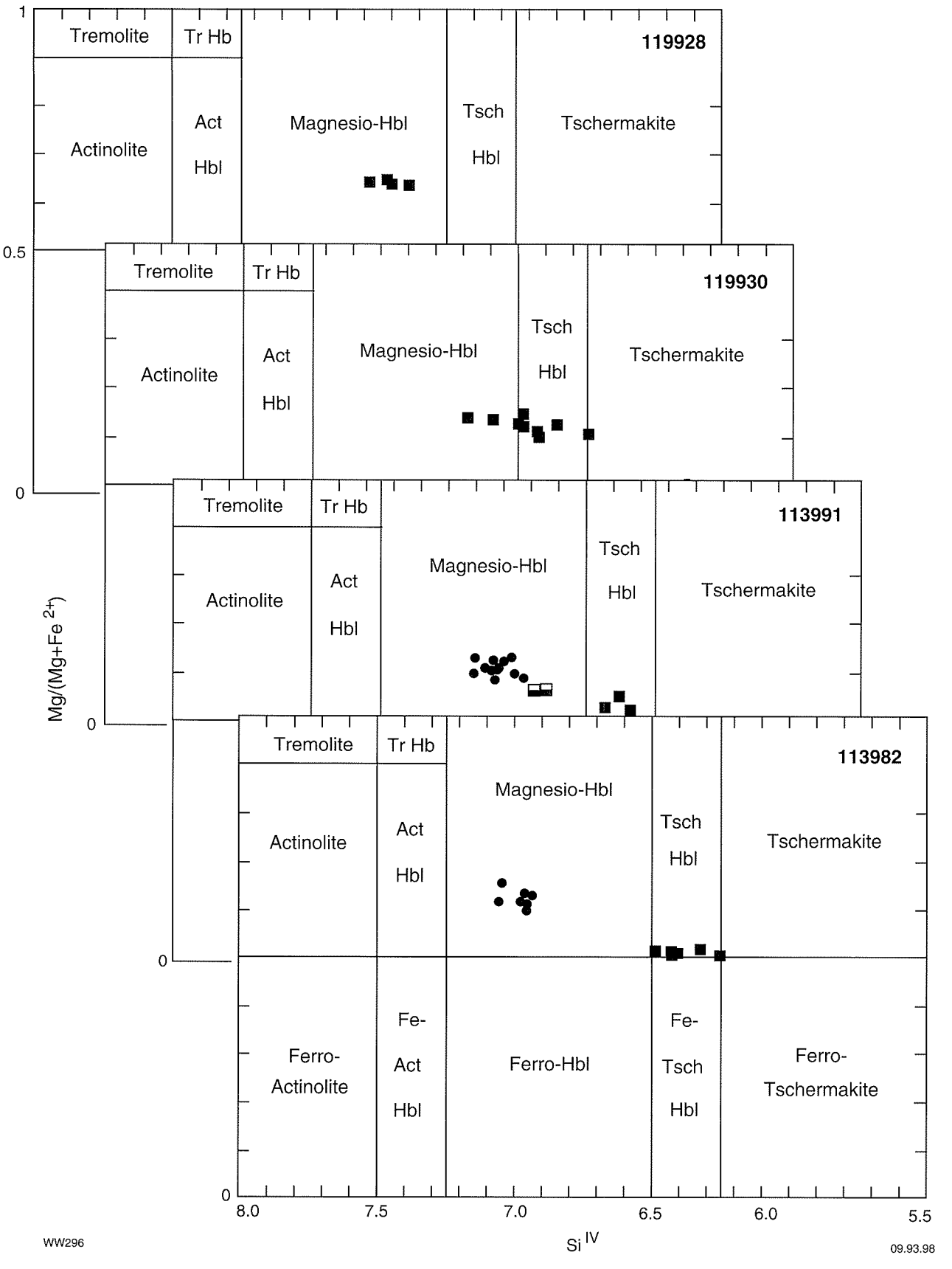
1
0.5
0
Tremolite
Tr Hb
Actinolite
Act
Hbl
Magnesio-Hbl
Tsch
Hbl
Tschermakite
119928
119930
113991
113982
Mg/(Mg+Fe 2+)
Ferro-
Actinolite
Fe-
Act
Hbl
Ferro-Hbl
Fe-
Tsch
Hbl
Ferro-
Tschermakite
8.0
7.5
7.0
6.5
6.0
5.5
Si IV
WW296
09.93.98

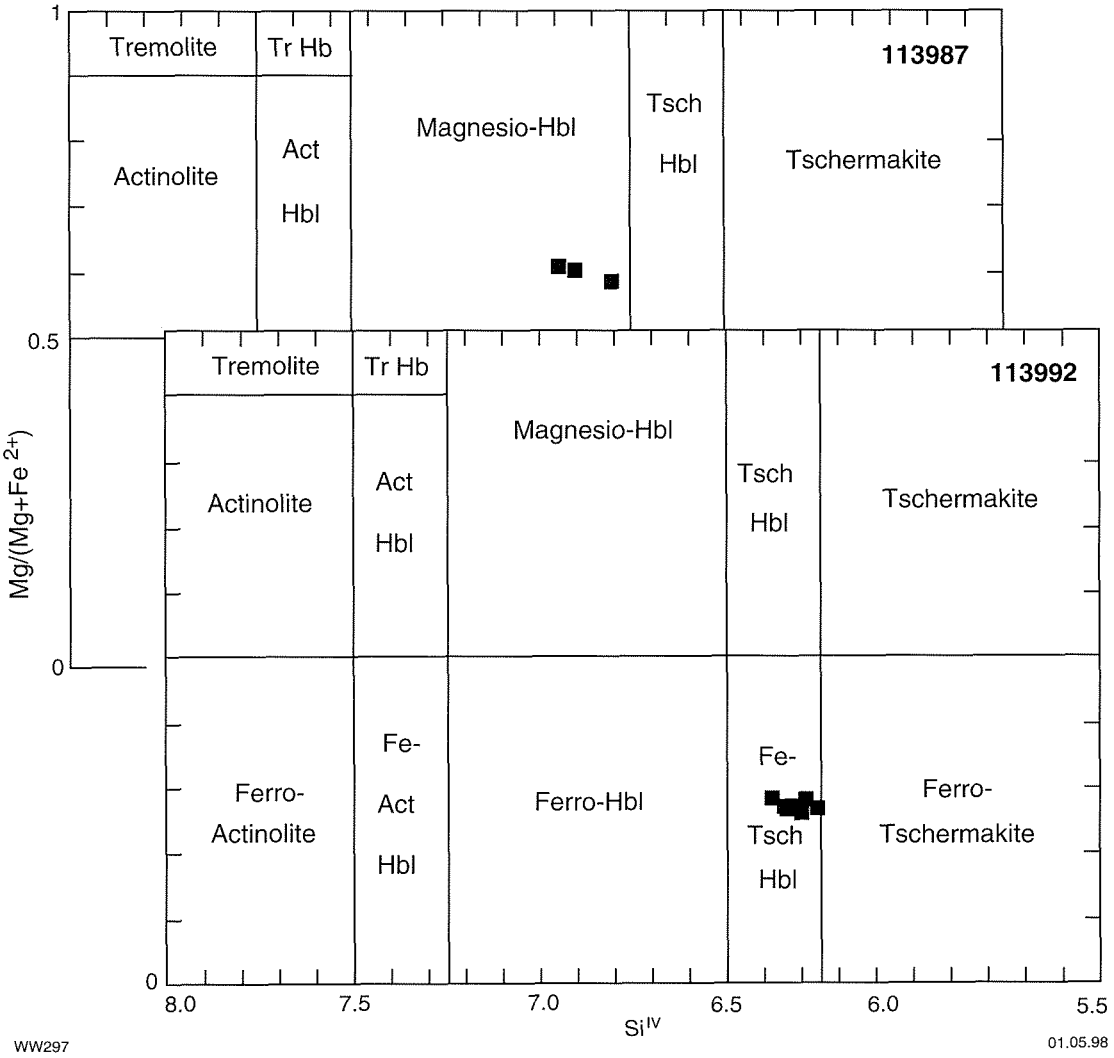

(Fig. 11A) and alteration of amphibole and biotite to epidote, chlorite and muscovite. The green to blue-green margins of amphibole grains may also have formed during the propylitic alteration event. In some samples, these secondary mineral assemblages are spatially associated with disseminated pyrite and chalcopyrite (Figs 11B, D). Most samples that contain disseminated sulfides came from the eastern margin of the Manyutup Tonalite Complex, between Ravensthorpe and Kundip. The distribution of secondary, disseminated sulfides is therefore antithetic to that of sufide inclusions in plagioclase (see above).

Potassic alteration

Potassic alteration is less consistently developed than propylitic alteration and, where present, is a less volumetrically significant style of alteration. Potassic alteration produced disseminated biotite and irregular, discontinuous veinlets of biotite (PHOTO 113992, Figure 11F). Irregular inclusions of K-feldspar in plagioclase, noted in some samples, may also be related to potassic alteration.

Copper analyses of minerals in the Manyutup Tonalite

Reconnaissance analyses for copper from two samples of Manyutup Tonalite are presented in Appendix 1 (Table 1.7). Sample 119929 is a coarse-grained tonalite, and sample 113985 is a medium-grained tonalite. Both samples belong to the low-SiO_2 suite. Although of a reconnaissance nature, the analyses indicate generally low levels (below or close to a lower level of detection equal to 6 ppm Cu) of copper in most minerals. It is notable, however, that higher copper contents (>10 ppm) are confined to samples of metamorphic and/or propylitic hornblende and chlorite after biotite.

Whole-rock chemistry

Whole-rock geochemical data for the Manyutup Tonalite are presented in Appendix 2 (Table 2.1), together with analyses of some samples of the Annabelle Volcanics that were collected from core recovered from the Kundip area. The locations of Manyutup Tonalite whole-rock samples

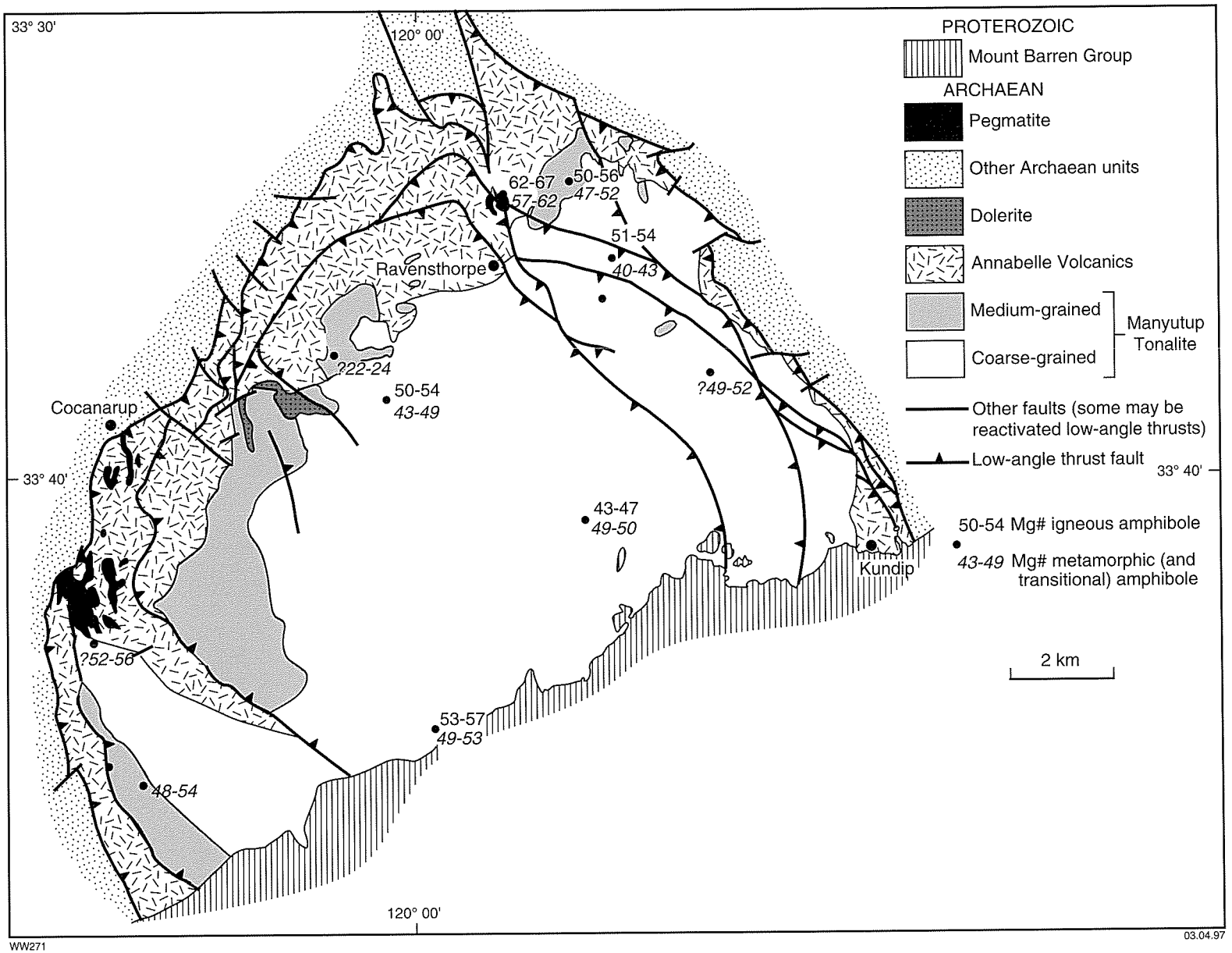

Figure 13. Variation in ranges of Mg# for igneous and metamorphic amphibole in samples of Manyutup Tonalite, by locality

are shown in Figure 7. Sample collection and analytical methods are described in Appendix 2. Despite petrographic evidence for propylitic and potassic alteration, most whole-rock analyses of Manyutup Tonalite and Annabelle Volcanics collectively define coherent trends that are reasonably interpreted in terms of magmatic processes. The following discussion relates to 'unaltered samples' only. These include samples with pervasive styles of alteration but exclude intensely altered samples associated with mineralization at Kundip. Three 'unaltered samples' from Kundip drillcore have low Ca and high Cu compared to other 'unaltered samples'. These three samples display a very intense propylitic alteration that is common to all microtonalite samples from the Kundip area, but is nevertheless distinct from the stronger, vein- and shear-related alteration more intimately associated with mineralization.

Normative quartz–alkali feldspar–plagioclase diagrams (Le Maitre, 1989) are consistent with estimates of modal compositions that classify most samples as tonalite with a few samples of quartz diorite and granodiorite (Fig. 14). The samples define a calc-alkaline trend on an AFM diagram (Fig. 15).

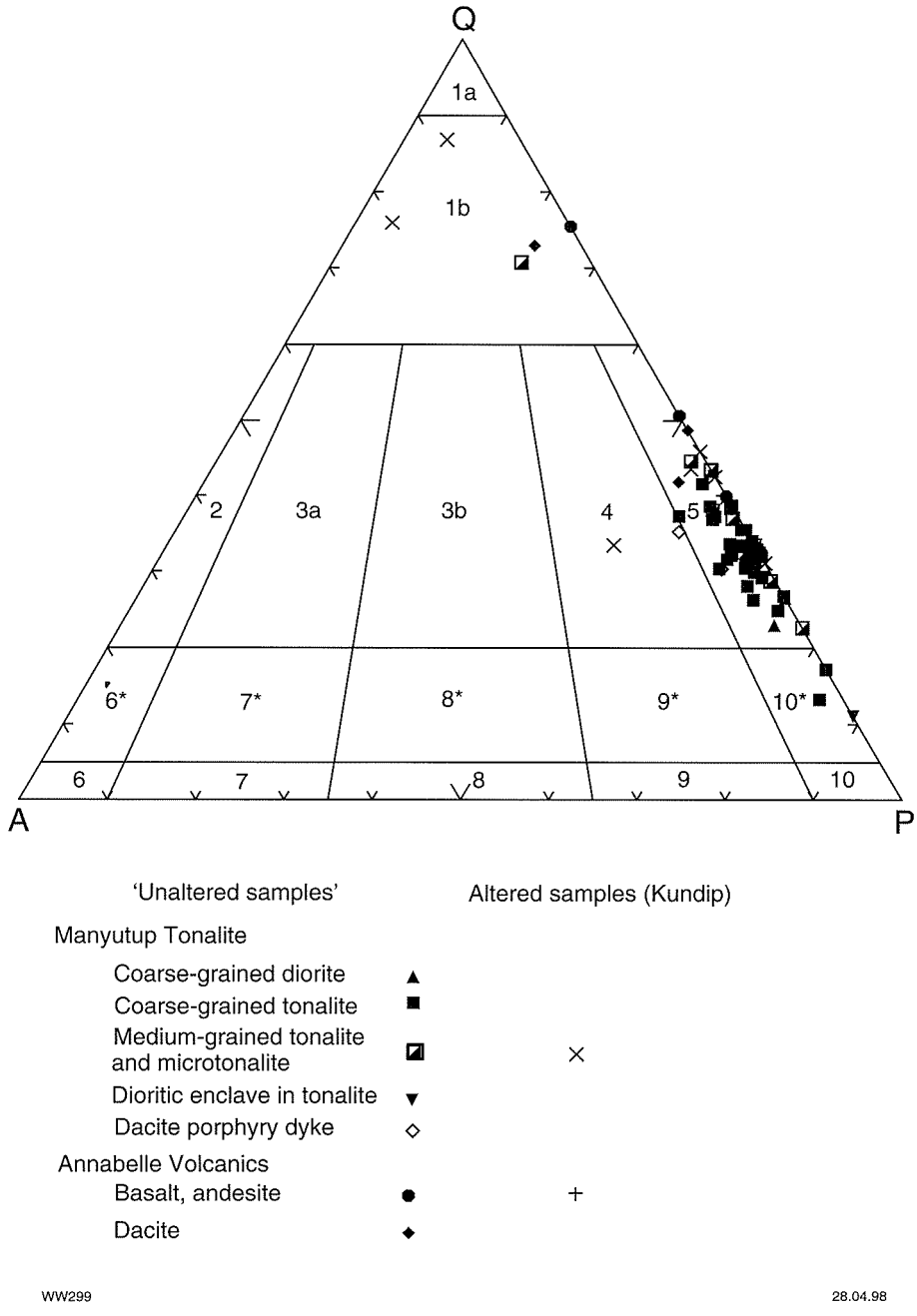

Figure 14. Whole-rock composition of Manyutup Tonalite and Annabelle Volcanics (and altered equivalents) on a normative quartz–alkali feldspar–plagioclase diagram (after Le Maitre, 1989). Most samples plot in the tonalite field (5)

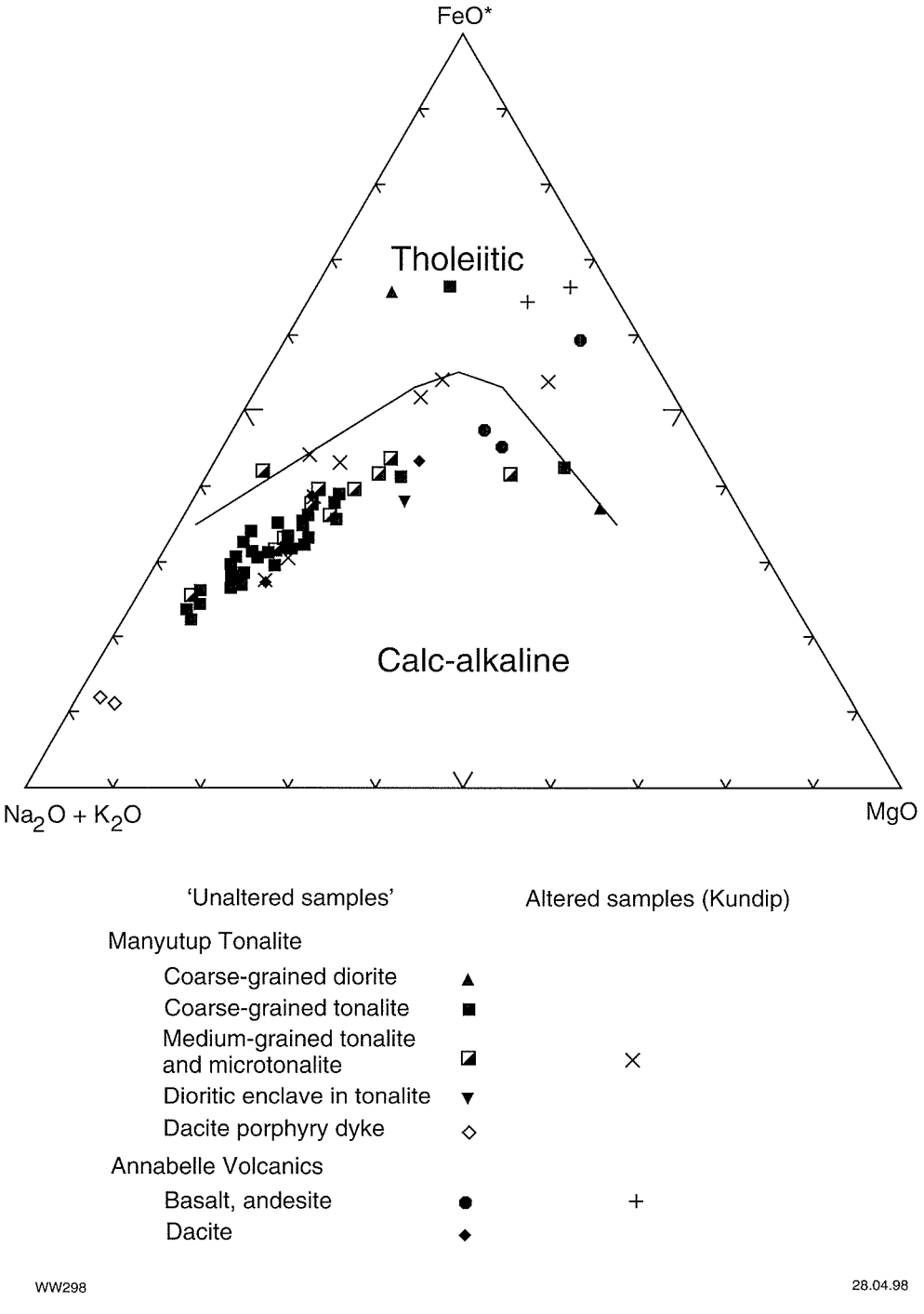

Figure 15. Whole-rock composition of Manyutup Tonalite and Annabelle Volcanics (and altered equivalents) on an AFM diagram (after Irvine and Baragar, 1979). Most samples display a calc-alkaline trend

Figure 16 shows that the whole-rock data for Manyutup Tonalite and Annabelle Volcanics fall within the field of island-arc suites, defined by Titley and Beane (1981). In terms of a Na_2O–K_2O–CaO triangular diagram (Fig. 17), they plot in a similar field to those defined by Pacific and Caribbean island arcs (Hine and Mason, 1978; Beane and Titley, 1981). The samples define a low-K series trend on a K_2O versus SiO_2 diagram (Wilson, 1989).

Two igneous suites are recognized: a low-SiO_2 suite and a high-SiO_2 suite. The low-SiO_2 suite extends from 49.4% SiO_2 to 58.10% SiO_2 (approximately 61% SiO_2 anhydrous, Figs 19, 20). This suite comprises basalt and andesite from Kundip, two quartz diorite samples (119920 and 119922) from the northwestern part of the Manyutup Tonalite, two coarse-grained tonalite samples (113979 and 113980) and one medium-grained tonalite sample from the Cattlin Creek area near Ravensthorpe

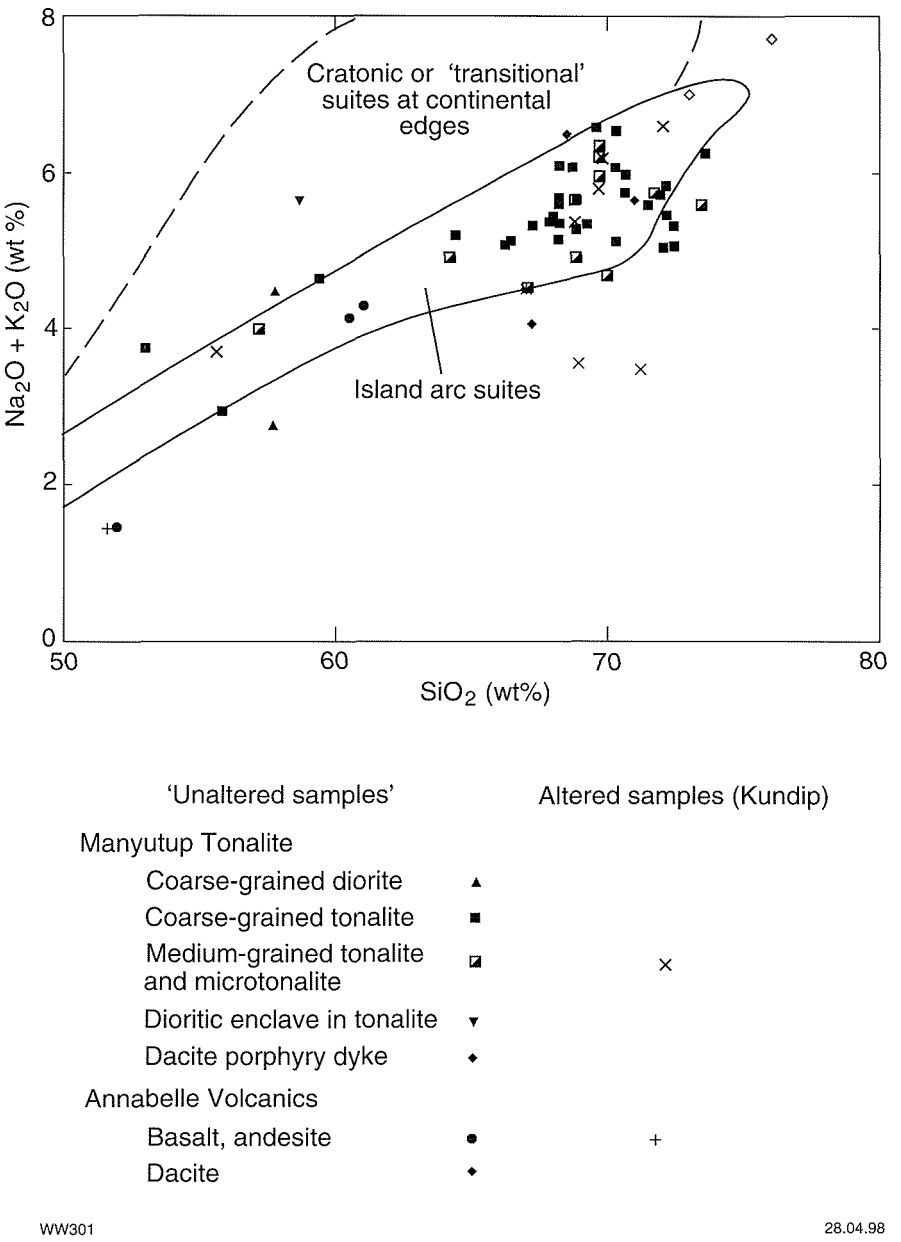

Figure 16. Whole-rock composition of Manyutup Tonalite and Annabelle Volcanics (and altered equivalents) on a $Na_2O + K_2O$ versus SiO_2 diagram. Fields for island-arc suites and cratonic or 'transitional' suites at continental edges are from Titley and Beane (1981)

(113978), and a sample from the southern part of the exposed intrusive complex (119929). All are amphibole-rich samples.

The remaining samples comprise the high-SiO_2 suite that includes samples with up to 76.0% SiO_2. This suite comprises most of the coarse-grained and medium-grained tonalite samples, two dacite porphyry dykes and two drillcore samples of dacitic volcanic rock from Kundip.

Some calc-alkaline plutons in younger geological terranes display more or less regular variations in chemical composition from the margins to the interior that are interpreted to reflect magmatic differentiation from the margins inward (e.g. Bateman and Chappell, 1978) or successive pulses of intrusive magma (Fridrich and Mahood, 1984). There appears to be no such systematic variation of Mg# ($MgO/(MgO + \Sigma FeO)$) with geographical location within the Manyutup Tonalite (Fig. 18). Anorthite ranges in plagioclase and Mg# for amphiboles are similarly erratic but vary sympathetically with the whole-rock Mg#.

Selected Harker variation diagrams for low-SiO_2 and high-SiO_2 suite samples are shown in Figures 19 and 20. Most high-SiO_2 suite tonalites and related rocks have Mg# between approximately 45 and 30, and there is an

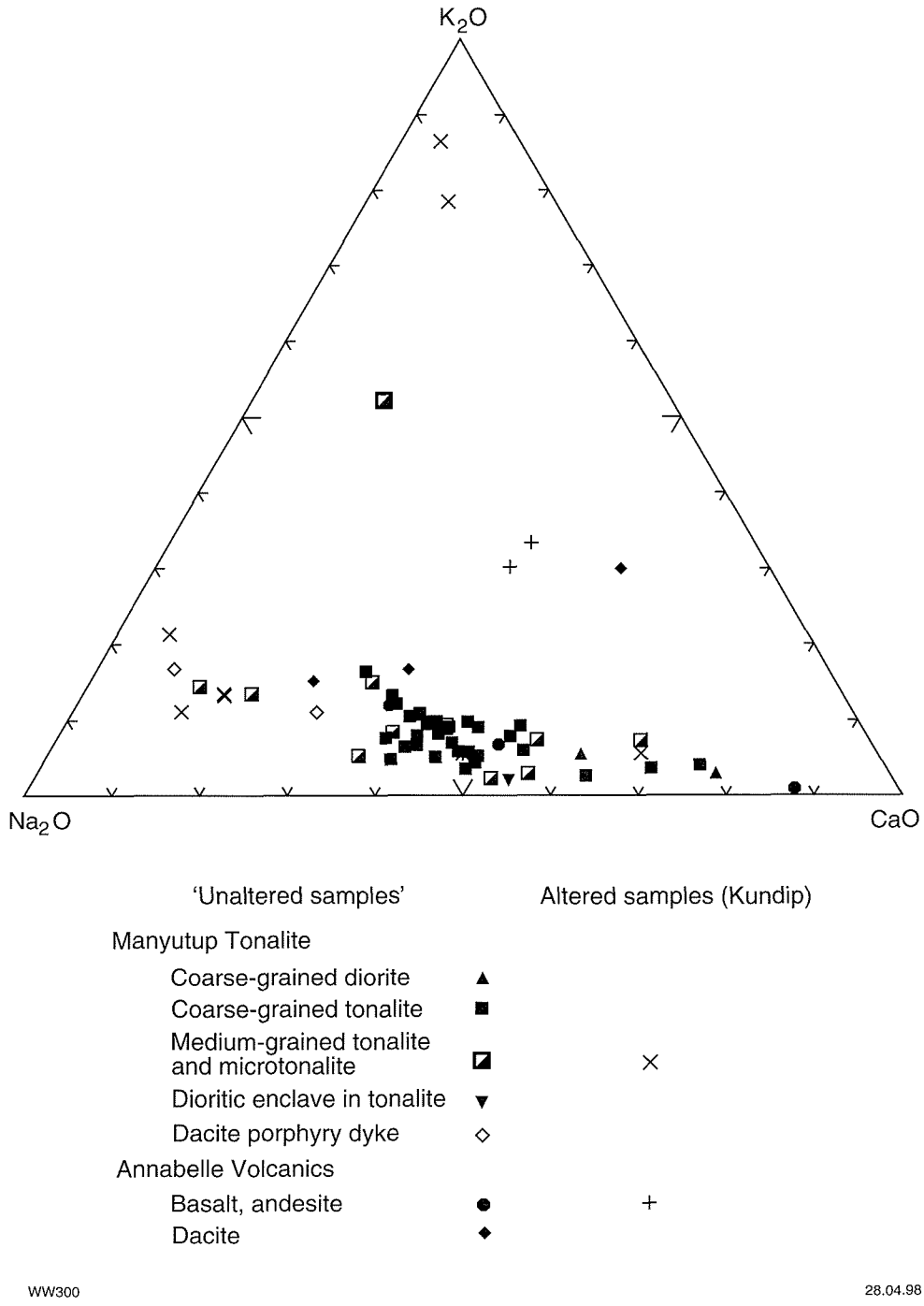

Figure 17. Whole-rock composition of Manyutup Tonalite and Annabelle Volcanics (and altered equivalents) on a Na_2O–K_2O–CaO triangular diagram

inverse correlation between Mg# and SiO_2 (Fig. 19A). Low-SiO_2 suite intrusive and volcanic rocks exhibit a greater range of Mg#s. Mg#s are greater than 50 and inversely correlated with SiO_2 for most of the suite, but three samples are anomalously low and two have Mg# <30.

In the high-SiO_2 suite, several major and trace elements, including TiO_2, Al_2O_3, FeO* (FeO + 0.9Fe_2O_3), CaO, P_2O_5, Cr, Ni, V, Cu and Co, decrease more or less regularly with increasing SiO_2. As with Mg#, patterns are more erratic in the low-SiO_2 suite. Harker variation diagrams for other elements display erratic patterns for both low-SiO_2 and high-SiO_2 suites. Those involving K_2O, Na_2O, Rb, Ba and Sr may have been influenced by subsolidus processes, including metamorphism and hydrothermal (propylitic and potassic) alteration. However, other trace elements that are normally considered immobile during metamorphic and most hydrothermal processes (Zr, Y, Th) also display erratic

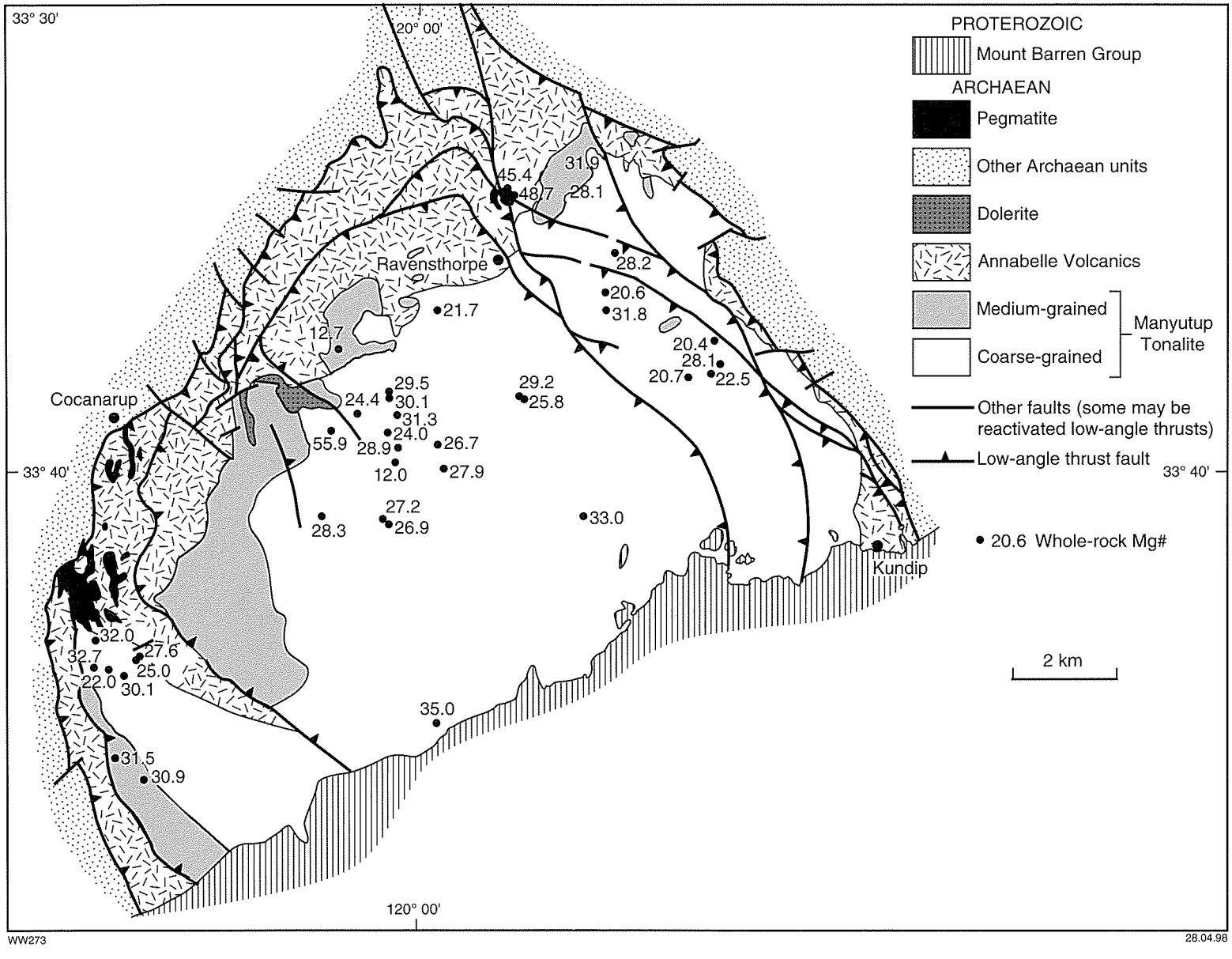

Figure 18. Location of samples showing variations in whole-rock Mg# in Manyutup Tonalite

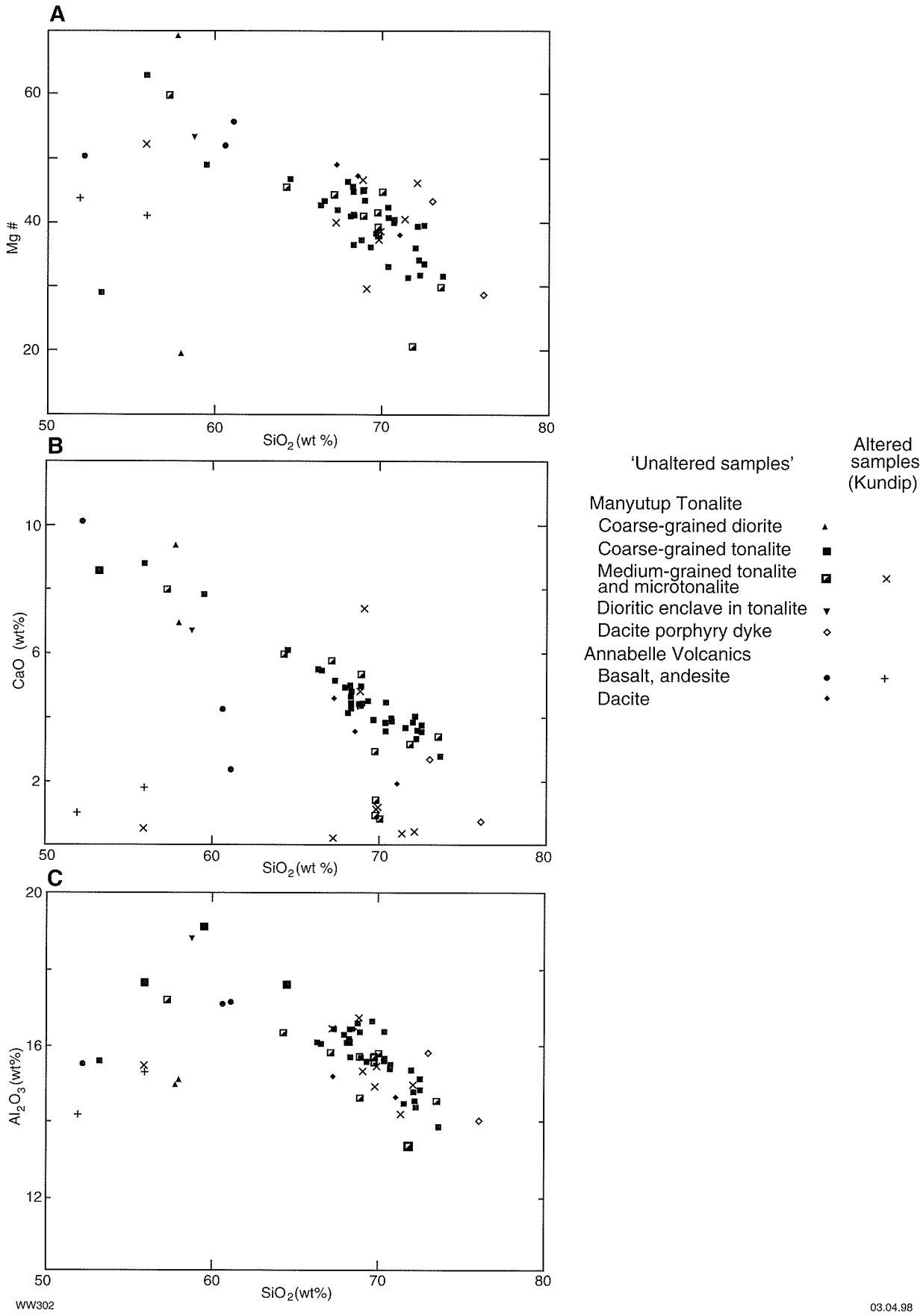

Figure 19. Harker variation diagrams for Manyutup Tonalite and Annabelle Volcanics (and their altered equivalents). A: Mg#; B: CaO; C: Al_2O_3; D: FeO* (FeO + 0.9Fe_2O_3); E: Na_2O; F: K_2O

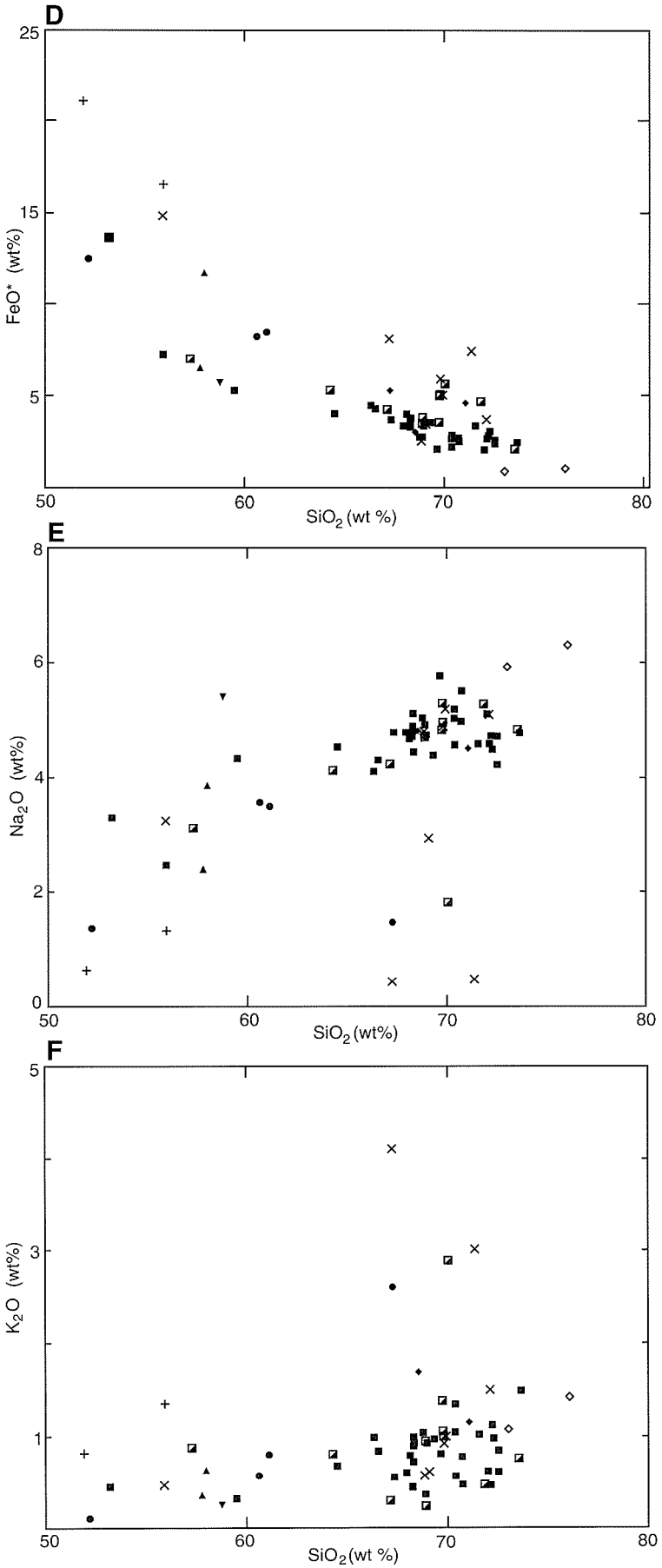
D
25
15
5
FeO* (wt%)
50
60
70
80
SiO2 (wt %)
E
8
6
4
2
0
Na2O (wt%)
50
60
70
80
SiO2 (wt%)
F
5
3
1
K2O (wt%)
50
60
70
80
SiO2 (wt %)
'Unaltered samples'
Altered samples (Kundip)
Manyutup Tonalite
Coarse-grained diorite
Coarse-grained tonalite
Medium-grained tonalite and microtonalite
Dioritic enclave in tonalite
Dacite porphyry dyke
Annabelle Volcanics
Basalt, andesite
Dacite
WW302a
29.04.98

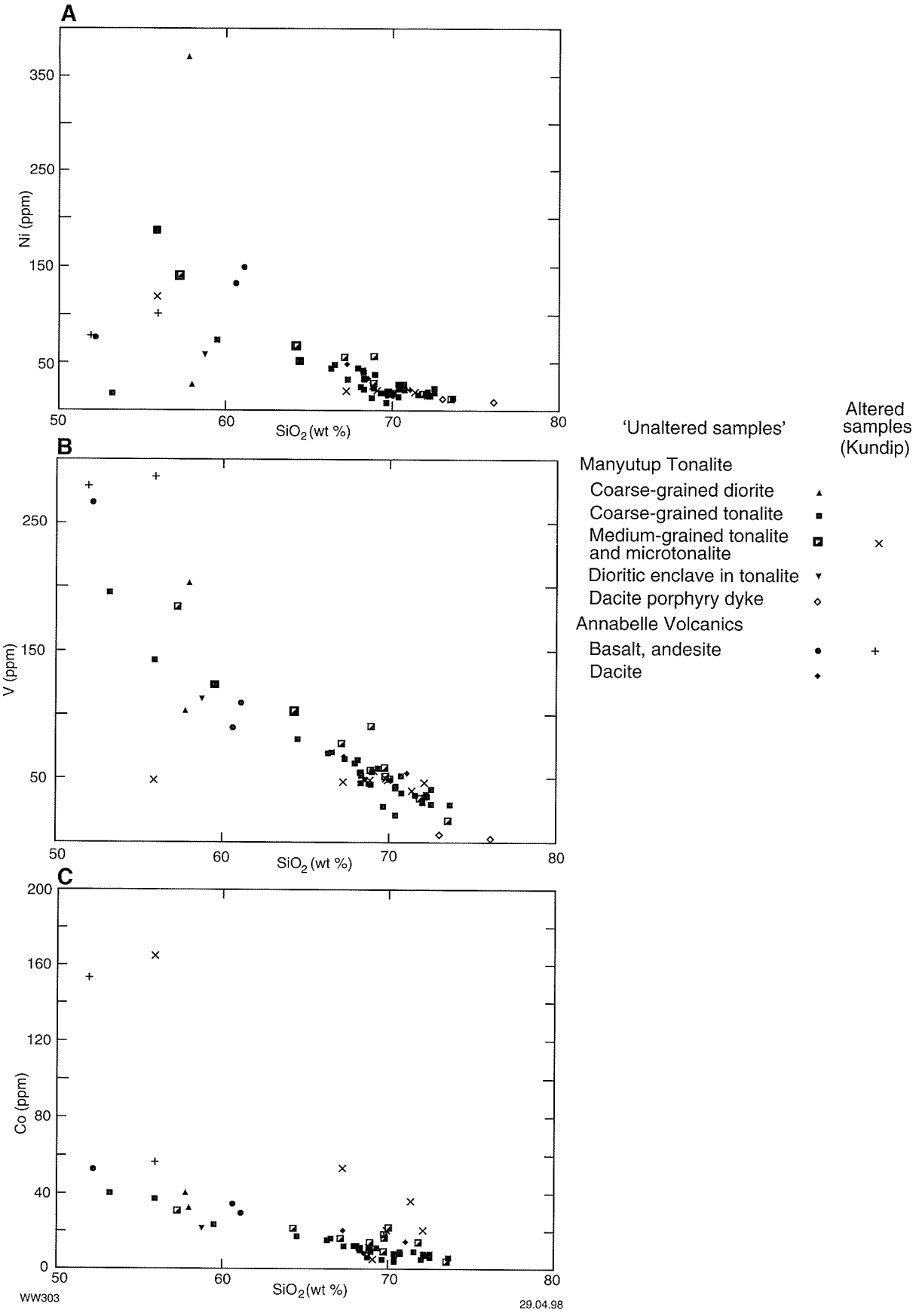

Figure 20. **Harker variation diagrams for Manyutup Tonalite and Annabelle Volcanics (and their altered equivalents). A: Ni; B: V; C: Co; D: Cu; E: Ba; F: Y; G: Zr; H: Th**

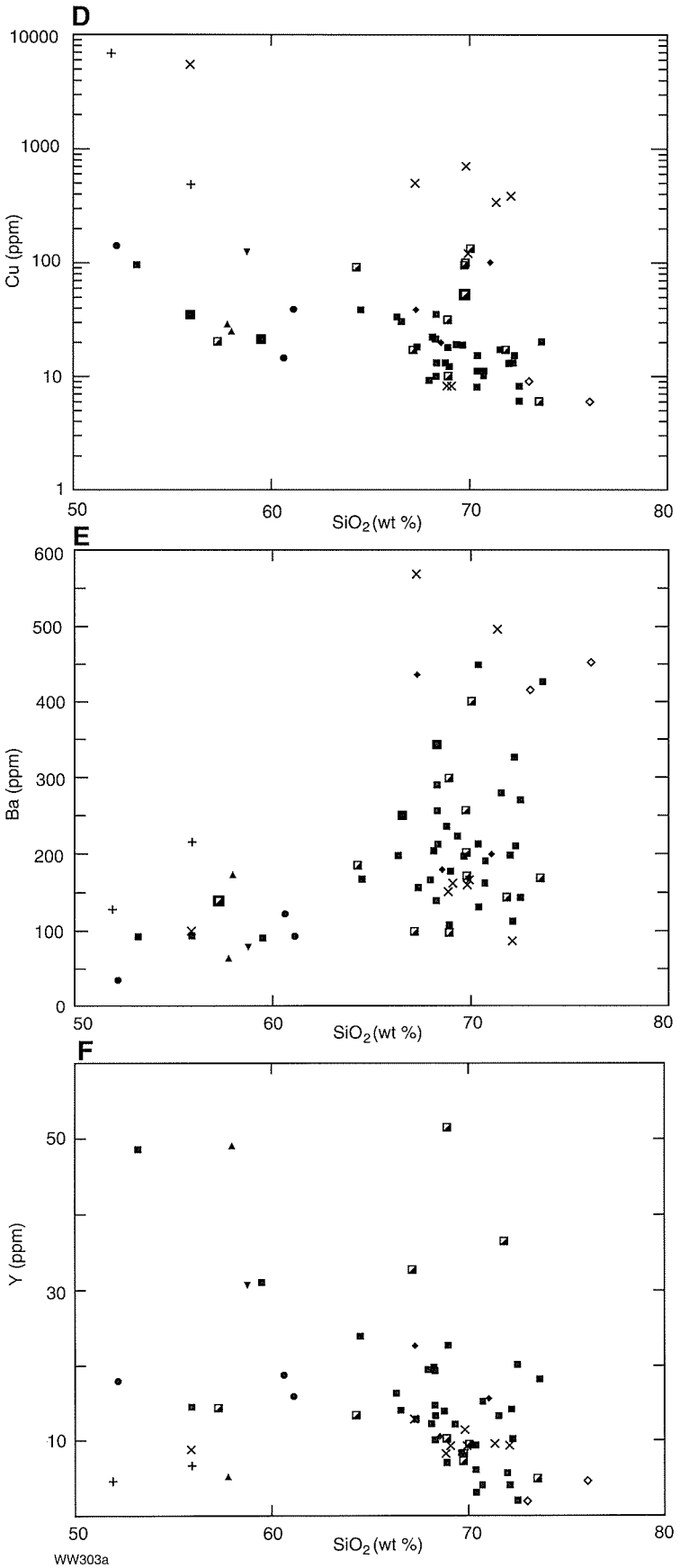

'Unaltered samples'

Manyutup Tonalite
- Coarse-grained diorite
- Coarse-grained tonalite
- Medium-grained tonalite and microtonalite
- Dioritic enclave in tonalite
- Dacite porphyry dyke

Annabelle Volcanics
- Basalt, andesite
- Dacite

Altered samples (Kundip)

29.04.98

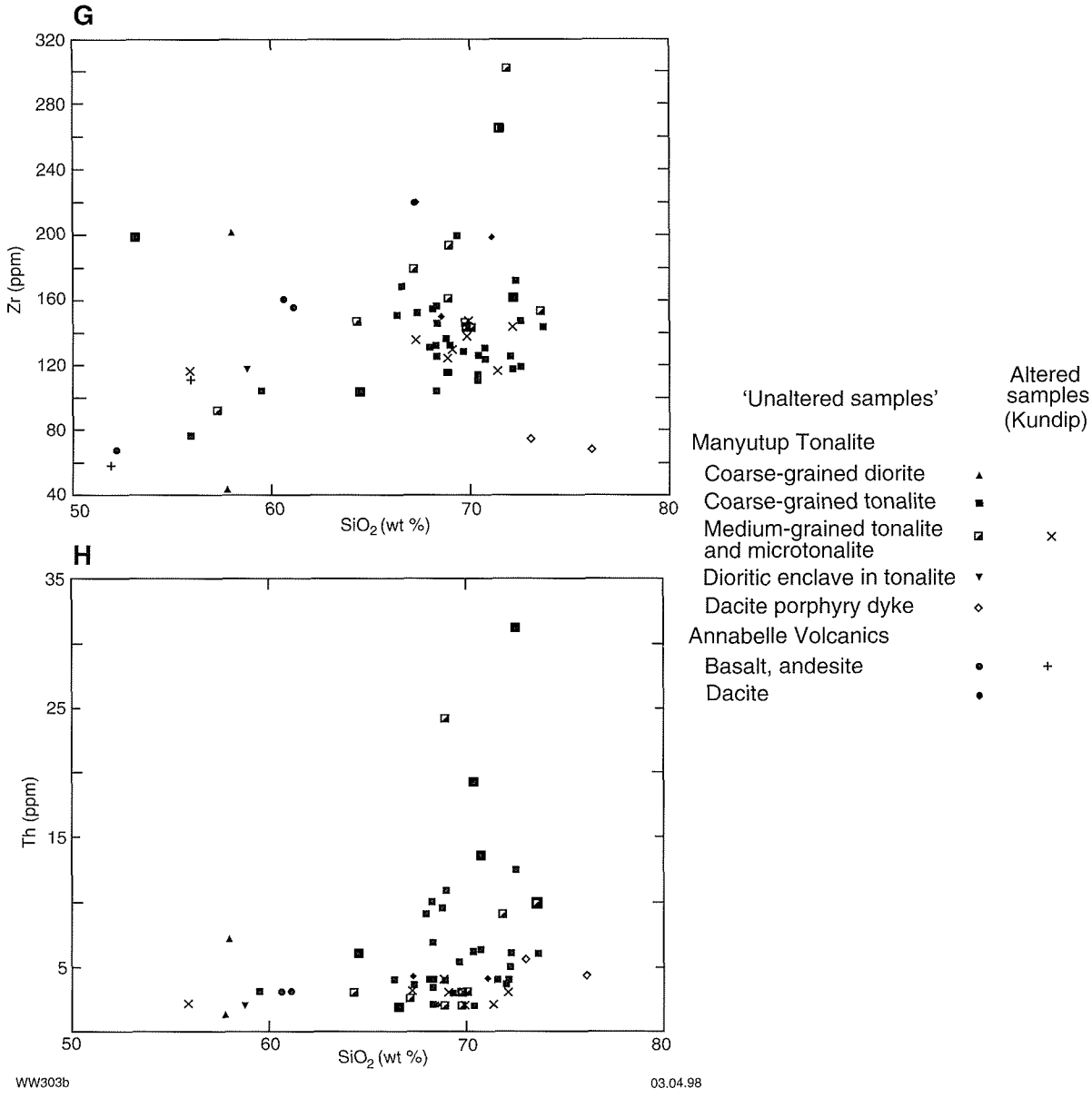

patterns on Harker variation diagrams. The immobility of these elements in the Ravensthorpe Terrane rocks is illustrated by the lack of separation of unaltered and strongly altered samples on the relevant Harker variation diagrams. Interpretation of these scattered patterns is difficult because samples that are enriched in one element are not necessarily enriched in the other elements.

Rare-earth element (REE) data is summarized in Figure 21. As a group, samples from the Ravensthorpe Terrane display weakly to moderately fractionated REE curves. Negative and positive Eu anomalies are absent or very weak. Positive Eu anomalies (e.g. in quartz diorite sample 119922) may be due to a component of plagioclase accumulation. There is no distinction between low-SiO_2 and high-SiO_2 suites on the basis of REE contents or the shapes of REE curves. REE curves for samples from the low-SiO_2 suite lie above (sample 119920) and below (sample 119922) the high-SiO_2 suite group of curves. The patterns are more fractionated, with higher LREE and total REE contents than those of primitive, oceanic island-arc tonalites (Whalen, 1985), but less fractionated than those of subduction-related volcanic arcs on thin continental crust, such as the Sierra Nevada batholith (Gromet and Silver, 1987). They are most similar to the tonalites and granodiorites of the western Sierra Nevada batholith. The petrogenesis of the western tonalites and granodiorites involved a lesser role for continental crust than did the petrogenesis of the eastern tonalites of the Sierra Nevada batholith (Gromet and Silver, 1987).

Interpretation of geochemical data

The inverse relationship between SiO_2 and Mg# for the high-SiO_2 suite is interpreted as resulting mainly from

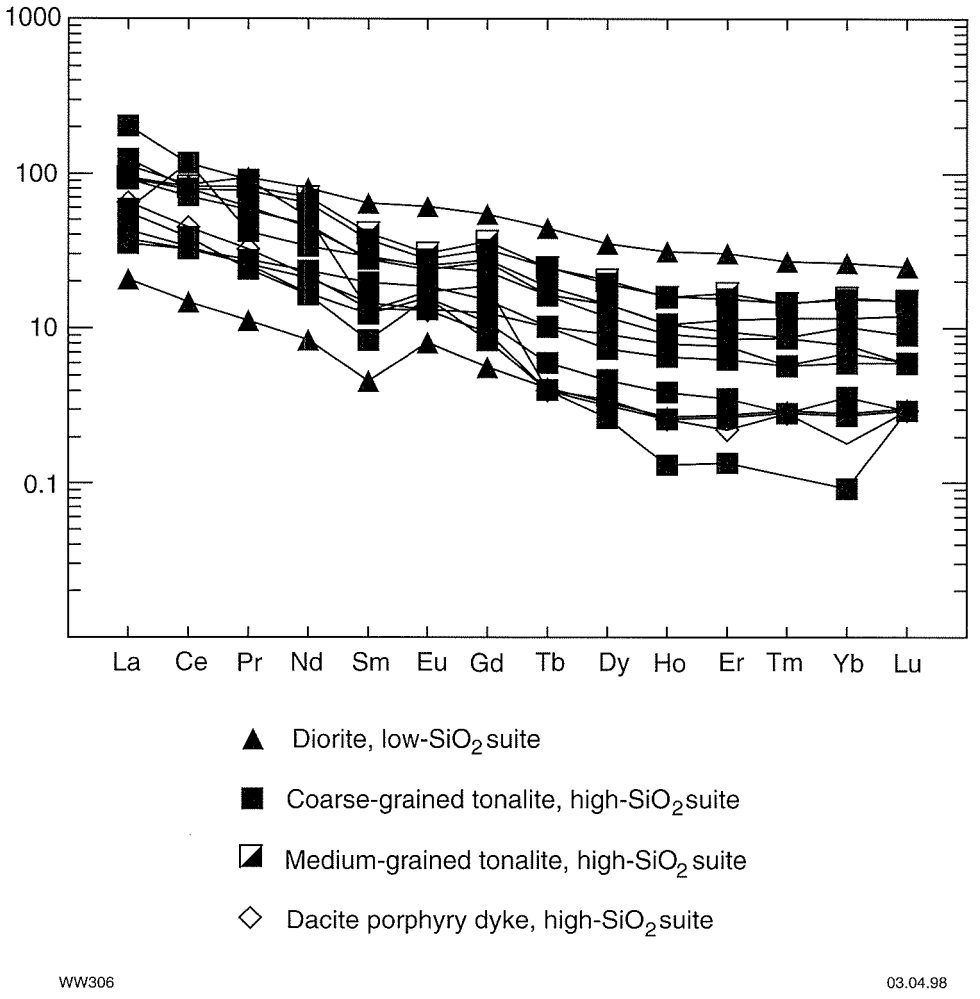

Figure 21. Chondrite-normalized REE plots (normalizing values after Taylor and McLennan, 1985) for Manyutup Tonalite

fractional crystallization of their respective parent magmas. The more erratic distribution of data for the low-SiO_2 suite probably requires a range of genetic processes including two or more of: multiple source rocks; variable volume partial melting; fractional crystallization; and crustal contamination. The close spatial and temporal association of the low-SiO_2 and high-SiO_2 suites suggests that both suites were derived by partial melting of the same source region. This source region may have been a subducted oceanic plate or metasomatized aesthenospheric mantle (Wilson, 1989). The weakly to moderately fractionated REE curves imply an absence of garnet in the source rocks.

Within each suite, there is no systematic correlation of grain size with degree of fractionation. That is, fractionated samples include coarse-grained tonalite as well as subvolcanic and volcanic rocks. Fractional crystallization of amphibole, biotite, Fe–Ti oxides, apatite and possibly pyroxene extracted TiO_2, FeO + Fe_2O_3, CaO, P_2O_5, Cr, Ni, V and Co from magmas of the high-SiO_2 suite, producing the inverse correlations between SiO_2 and these elements on Harker variation diagrams. Depletion of Cu may imply early crystallization of sulfides from the Manyutup Tonalite magma and this would be consistent with the interpretation of small sulfide inclusions in plagioclase as magmatic inclusions. Although the partition coefficient for Cu in Fe–Ti oxide minerals is not well-established, it is generally believed that magmatic sequestration of Cu requires the involvement of a sulfide phase (Candela and Holland, 1986; Wyborn and Sun, 1994). The role of plagioclase as a fractionating phase is uncertain. Although negative Eu anomalies are not well-developed on REE curves, plagioclase is an early crystallizing phase in all samples. Extraction of Eu in plagioclase may have been balanced by amphibole fractionation as the partition coefficient for amphibole is lower for Eu than for other REE (Arth and Barker, 1976).

In most magmatic systems, incompatible trace elements such as Th and Zr display geometric increases in abundance with progressive fractional crystallization (Hanson, 1978). The scatter of Th, Zr and Y on Harker variation diagrams for the high-SiO_2 suite indicates that some other process has contributed to the composition of these rocks. If the scatter in incompatible elements is

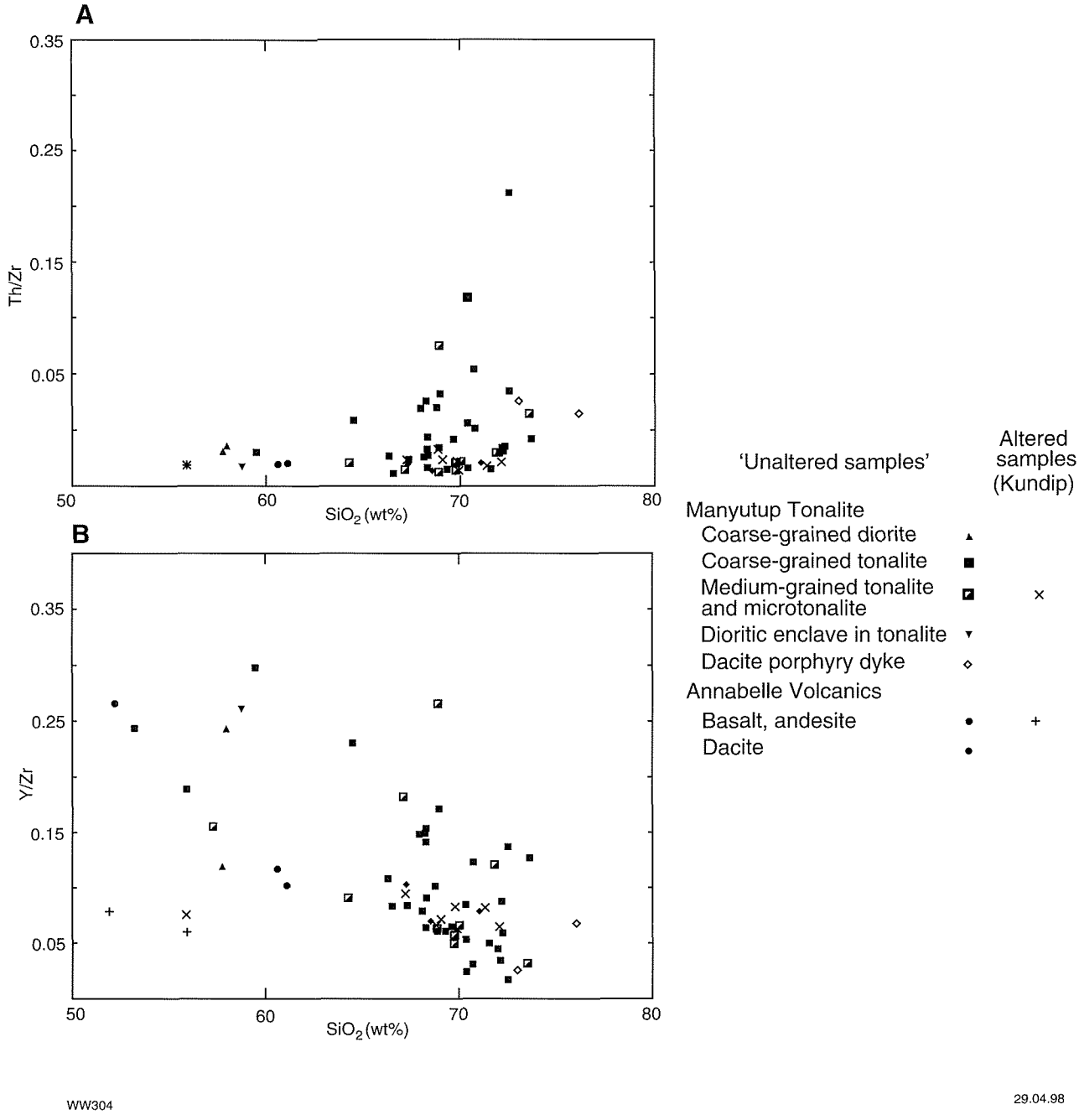

Figure 22. A: Th/Zr versus SiO_2; B: Y/Zr versus SiO_2 for Manyutup Tonalite and Annabelle Volcanics (and their altered equivalents)

due to variations in the proportion of cumulus crystals and intercumulus melt, incompatible element ratios should remain constant. The considerable scatter on plots involving Y/Zr and Th/Zr (Fig. 22) indicate that cumulus processes are an inadequate explanation for the variation of Th, Zr and Y. The most likely explanation for this variation is crustal contamination.

Although isotopic data are required to demonstrate a role for crustal contamination, some trace element data are consistent with compositional variation within the high-SiO_2 suite being due to a combination of crustal assimilation and fractional crystallization. Zr is an incompatible element and should be enriched by fractional crystallization. On the other hand, Y is extracted from most felsic melts and should decrease during differentiation. Therefore, a plot of Zr versus Zr/Y (Fig. 23A) should produce a positive correlation between the two parameters. Approximately half of the high-SiO_2 data fit this predicted fractional crystallization trend but the remainder are variably enriched in Zr (or depleted in Y). Zr is much more abundant in sialic crust than in low-K tonalite and andesite so the data are consistent with a component of crustal contamination acting upon batches of magma that are related but variably fractionated.

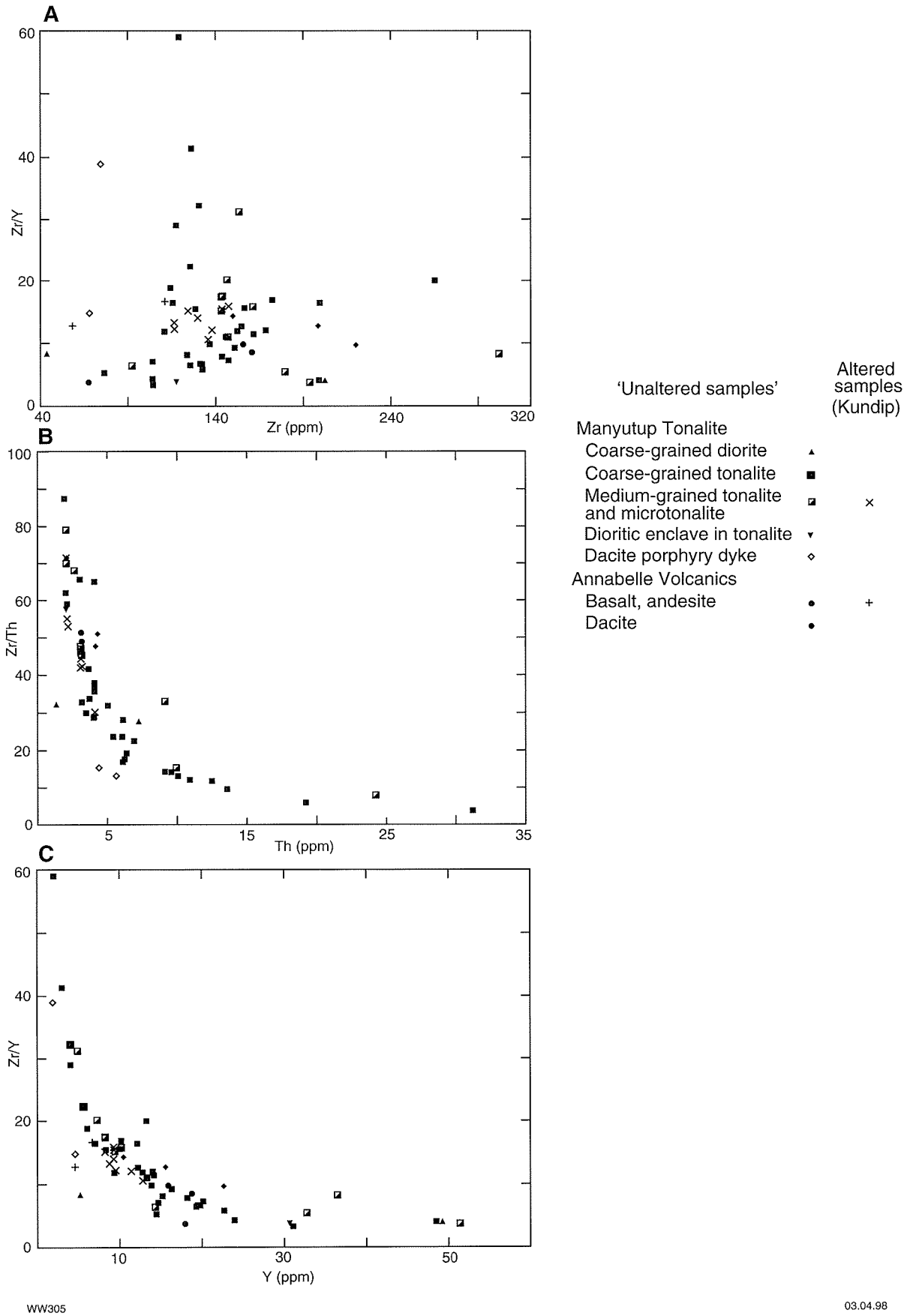

Figure 23. A: Zr/Y versus Zr; B: Zr/Th versus Th; C: Zr/Y versus Y for Manyutup Tonalite and Annabelle Volcanics (and altered equivalents)

On Th versus Zr/Th and Y versus Zr/Y plots (Figs 23B, C) the same data display more coherent trends defining asymptotic curves consistent with fractional crystallization and crustal contamination. As Y decreases with fractionation, addition of crustal Zr becomes increasingly significant, generating a steep rise in the Zr/Y ratio. The Zr/Th ratio decreases rapidly with fractional crystallization because Th is more incompatible than Zr. As fractionation proceeds, Zr/Th decreases less rapidly because Zr is being added as a result of crustal contamination.

Chapter 4

Structural history of Archaean granitoid gneiss and greenstones

The Ravensthorpe greenstone belt forms a wedge-shaped greenstone enclave within a much broader expanse of granitoid gneiss. Thom et al. (1984) interpreted the greenstone enclave as broadly antiformal, with the Manyutup Tonalite forming the core of a structural dome. This interpretation is fundamentally different (Fig. 2). In the northeast part of the Ravensthorpe greenstone belt, the primary layering, the contact between the granitoid gneiss and the greenstone, and the main tectonic fabric all dip at between 30 and 60° southwest. Along the western margin, these same planar structures dip between 50 and 70° east, implying an overall synformal configuration for the greenstone enclave (the Beulah synform).

The Archaean structural history of the Ravensthorpe greenstone belt is summarized in Table 2. The Beulah synform incorporates the Carlingup and Ravensthorpe Terranes and the Cocanarup greenstones and so must have post-dated amalgamation of all three tectonostratigraphic components. However, the structural configuration of greenstones within this broad synform is far from simple. The Carlingup Terrane, the Ravensthorpe Terrane and the Cocanarup greenstones are all fault-bounded tectonostratigraphic units within the Beulah synform. From the following observations, in addition to the deformed contacts, it is clear that the Ravensthorpe Terrane does not have a simple, conformable relationship with adjacent units (the Carlingup Terrane and the Cocanarup greenstones).

1. It is evident from gross outcrop relationships that the Annabelle Volcanics has not been folded around the Maydon Syncline.

2. Xenoliths of Annabelle Volcanics are locally abundant in Manyutup Tonalite but xenoliths of metasedimentary and other rock types have not been observed, even where they are in contact (e.g. east of Ravensthorpe), thus rendering an intrusive relationship between Manyutup Tonalite and the Chester Formation unlikely.

3. The contact of the Annabelle Volcanics is grossly discordant, with tight folds defined by metasedimentary and ultramafic rocks in the Aerodrome sector of the Cocanarup greenstones, north of Beulah farmhouse. At this same locality, the configuration of the contact with respect to drainage suggests the base of the Annabelle Volcanics may lie, at a relatively flat attitude, over the more steeply dipping units of the Cocanarup greenstones.

In this report, the structural histories of the different tectonostratigraphic units are described individually, and are then discussed in terms of possible correlations. The structural histories of the tectonostratigraphic units cannot be fully understood unless the effects of the Beulah synform are discounted and the contacts between granitoid gneiss and greenstones restored to their original subhorizontal attitude.

Pre- to syn-amalgamation deformation histories of the tectonostratigraphic units

Structure of the Carlingup Terrane

D_1 deformation

There are several lines of evidence for an early period of low-angle faulting and recumbent folding (D_1) in the Carlingup Terrane that pre-dated formation of the Maydon Syncline.

1. An early fold closure within Maydon Basalt, on the northeastern limb of the Maydon Syncline, is suggested by opposing younging directions in pillowed basalt, east of the Maydon airstrip.

2. On the southwestern limb of the Maydon Syncline, west of Maydon farmhouse, a fold closure is defined by the contact between olivine orthocumulates and spinifex-textured komatiite. This fold closure is truncated by the contact with Chester Formation metasedimentary rocks to the west. The truncated annular shape of this fold closure suggests sheath fold formation during an early period of highly ductile strain.

3. Mesoscopic, tight to isoclinal (F_1) folds, commonly with sheared limbs, are widespread in the Chester Formation. Refolding of mesoscopic F_1 folds in the Chester Formation by F_2 can be seen at RAVENSTHORPE AMG 401738 and at RAVENSTHORPE AMG 413729. On a macroscopic scale, the symmetrical arrangement of

Table 2. Correlation of deformation events in Archaean tectonostratigraphic units

Cocanarup greenstones	*Ravensthorpe Terrane*	*Carlingup Terrane*
D_1, D_2 (north–south and northeast–southwest compression) * Poorly understood but indicated by subhorizontal lineations and moderately south-plunging boudins on granitoid gneiss–greenstone contact * ?Tight to isoclinal folds	D_1 * Poorly understood but indicated by steep bedding attitudes in Ravensthorpe–Elstree Farm area	D_1 (subhorizontal, ?south to north movement) * Tight to isoclinal folds, especially in metasedimentary units, including banded iron-formation * Irregular and interleaving of units and low-angle faults * Early fabric preserved in porphyroblasts and low-strain domains in Chester Formation metasedimentary rocks
D_3 (east to west transport) * Down-dip lineations on granitoid gneiss–greenstone contact * ?Tight to isoclinal folds	D_2 * Zones of deformation on contacts of Manyutup association rocks, and contact-parallel deformation within the Ravensthorpe Terrane rocks	D_2 (west to east transport) * Maydon Syncline and related structures; asymmetric, overturned (to ?recumbent), vergence to east, sheared out anticlines * Mesoscopic, reclined folds in Chester Formation * Dominant northwest-trending foliation * Simple shear on greenstone–granitoid gneiss contact, on northeast limb of Maydon Syncline
	Amalgamation of Ravensthorpe and Carlingup Terranes	
D_4 (east–west compression) * Beulah synform and north–south antiformal axis, near Cocanarup D_5 (north–south) * Easterly trending folds in Cocanarup area	D_3 (east–west compression) * Beulah synform D_4 (north–south) compression * Basinal structure of Manyutup association; uplift of tonalite in southern part of Beulah synform	D_3 (east–west compression) * Rotation of all structures and granitoid gneiss–greenstone contact to form Beulah synform D_4 (north–south compression) * Reverse movement on Bonnymidgup Shear Zone * Small-scale, open folds with steep easterly trending planes

sandstone and siltstone between metapelitic units in the Chester Formation, between Kundip and Mount McMahon, may also reflect F_1 folding, although this geometry could, alternatively, simply reflect primary depositional facies variations. Mesoscopic isoclinal folds are also common in banded iron-formation on the southwest limb of the Maydon Syncline and in Hatfield Formation metasedimentary rocks.

4. In the Jerdacuttup River area, south of Maydon farmhouse, thin, discontinuous slices and lenses of talc–carbonate schist (after ultramafic rocks) are interleaved with, and occur as pods within, mafic rocks, and vice versa. Outcrop patterns for the ultramafic units are very irregular and, in places, suggest F_2 fold closures. These relationships suggest interleaving of mafic and ultramafic units prior to D_2.

5. The dominant, pervasive foliation in Chester Formation and Hatfield Formation metasedimentary rocks, and a more irregularly developed foliation in mafic to ultramafic rocks, is broadly parallel to both lithological layering and the axis of the Maydon Syncline. It is probably mainly an S_2 fabric or a composite S_1–S_2 fabric. In Chester Formation metasedimentary rocks, relicts of an earlier foliation (S_1) have been locally preserved in porphyroblasts and in low-strain micro-domains between spaced S_2 foliations and in pressure shadows adjacent to some porphyroblasts (Fig. 24). Additionally, mesoscopic foliation planes at a high angle to the F_2 axial planar orientation have been observed at several localities and in all units of the Carlingup Terrane. Some of these anomalous foliations may be related to later fault movements but others are probably S_1 fabrics that were rotated during D_2.

6. Mesoscopic evidence for low-angle thrusting was observed in Hatfield Formation metasedimentary rocks at Bandalup Pools (RAVENSTHORPE AMG 490699) and around RAVENSTHORPE AMG 475709 (Fig. 25A).

Significance of D_1 for stratigraphy of the Carlingup Terrane

Recognition of recumbent folds, sheath folds and low-angle thrust faults in the Carlingup Terrane raises the possibility of correlation between the Chester and Hatfield Formations. It is possible that the two sedimentary formations were deposited as one unit but that the Hatfield Formation, with the underlying Maydon Basalt and Bandalup Ultramafics, was thrust over the Chester Formation during D_1. The contact between the Chester Formation and the Bandalup Ultramafics is a zone of intense deformation and metasomatism. Talc–carbonate schist and massive to schistose, tremolite-rich ultramafic rocks lie adjacent to the contact. Abundant coarse, unoriented tremolite in these rocks formed by metamorphic recrystallization of talc(–chlorite)–carbonate schist. Carbonate porphyroblasts also occur in metasedimentary rocks of the Chester Formation adjacent to this contact. The deformed contact is well-exposed in a tributary of the Jerdacuttup River, at RAVENSTHORPE AMG 404744, where several hundred metres of talc–chlorite(–carbonate–tremolite) schist abuts Chester Formation metasedimentary rocks. Similarly, interleaving of chert units and ultramafic rocks north of Mount McMahon (around RAVENSTHORPE AMG 315856) suggests a tectonic contact between Bandalup Ultramafics and the Chester Formation. The direction of D_1 transport is not known. Linear fabrics are not preserved on the contact between Chester Formation and Bandalup Ultramafics. The shape of the truncated sheath fold on the southwest limb of the Maydon Syncline is consistent with an east–west transport vector though the direction of transport cannot be determined.

Maydon Syncline and related folds (F_2)

The main fold structure in the Carlingup Terrane is an asymmetric, upright to slightly overturned syncline referred to as the Maydon Syncline. Younging directions are provided by pillows in Maydon Basalt; zoned

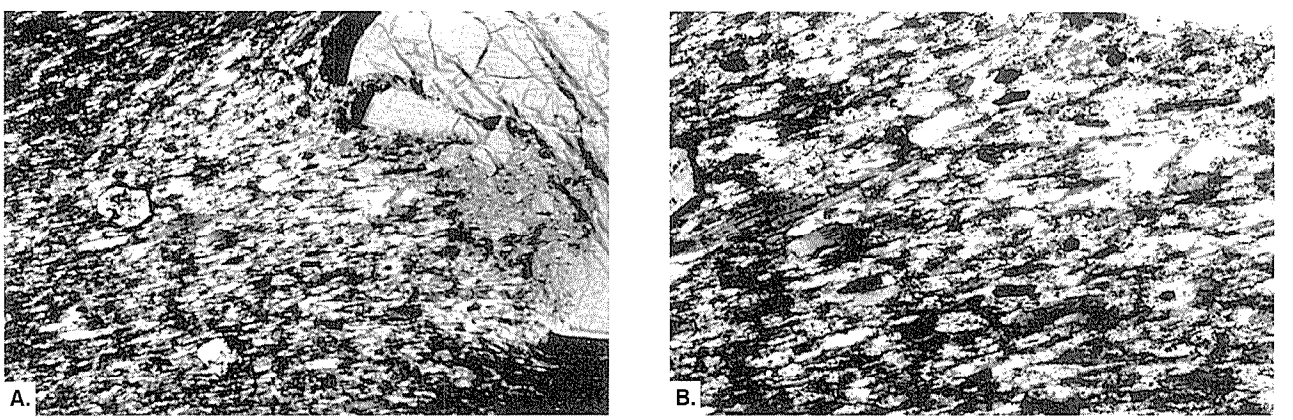

Figure 24. Early quartz–plagioclase–biotite fabric (S_1) preserved in pressure shadow of andalusite porphyroblast, Chester Formation metasedimentary rocks. A: GSWA 113929, plane-polarized light, field of view is approximately 1 mm (50X). B: Shows close-up view of part of A, plane-polarized light, field of view is approximately 0.5 mm (100X)

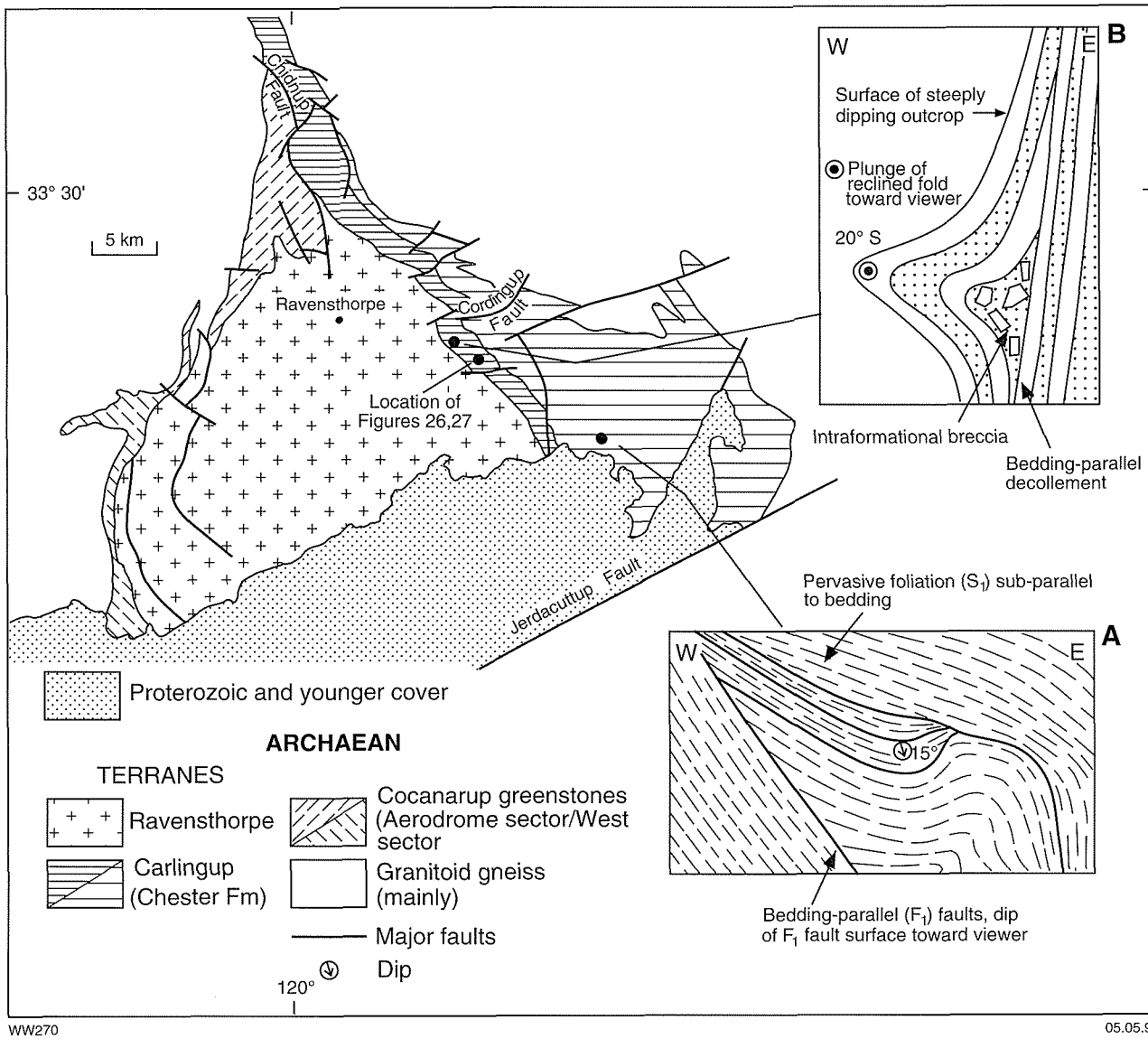

Figure 25. Mesoscopic structures in Chester Formation metasedimentary rocks. Location of Figures 26 and 27 also shown. A: Bedding-parallel faults; B: Reclined fold overlying a bedding-parallel decollement

komatiite flows in the Bandalup Ultramafics; and cross-bedding, flame structures and scour-and-fill structures in metasedimentary rocks of the Chester and Hatfield Formations. The axial plane of this syncline dips about 70° southwest. Fold closure to the northwest indicates a southeast plunge for the Maydon Syncline. Mesoscopic folds with similar form and geometry in the Chester Formation plunge 30–40° southeast (Fig. 26). Good examples of these folds can be observed in a tributary of the Jerdacuttup River (RAVENSTHORPE AMG 401738). Aeromagnetic data indicate the presence of further F_2 folds that are outlined by the contact between ultramafic rocks and granitoid gneiss, north of Bandalup. The anticlinal zones between F_2 synclines are sheared out and the anticline to the west of the Maydon Syncline has been tectonically removed at the present erosion level. When the contact between the Carlingup Terrane greenstones and granitoid gneiss is restored to its original subhorizontal orientation, it becomes evident that the F_2 folds formed as inclined to recumbent folds with eastward vergence (Fig. 27). Overprinting relationships described above indicate that the Maydon Syncline and related folds formed after D_1 thrusting and recumbent folding and this folding event is assigned to D_2.

Mesoscopic, reclined folds associated with small-scale, bedding-parallel decollements have been noted within Chester Formation metasedimentary rocks at several localities (Fig. 25B), but not in other stratigraphic units. Timing relationships between reclined folds and other fold structures in the Carlingup Terrane are not clear but the orientation of the reclined folds and their location near the terrane contact are consistent with formation as part of the D_2, west to east transport of the Carlingup Terrane greenstones.

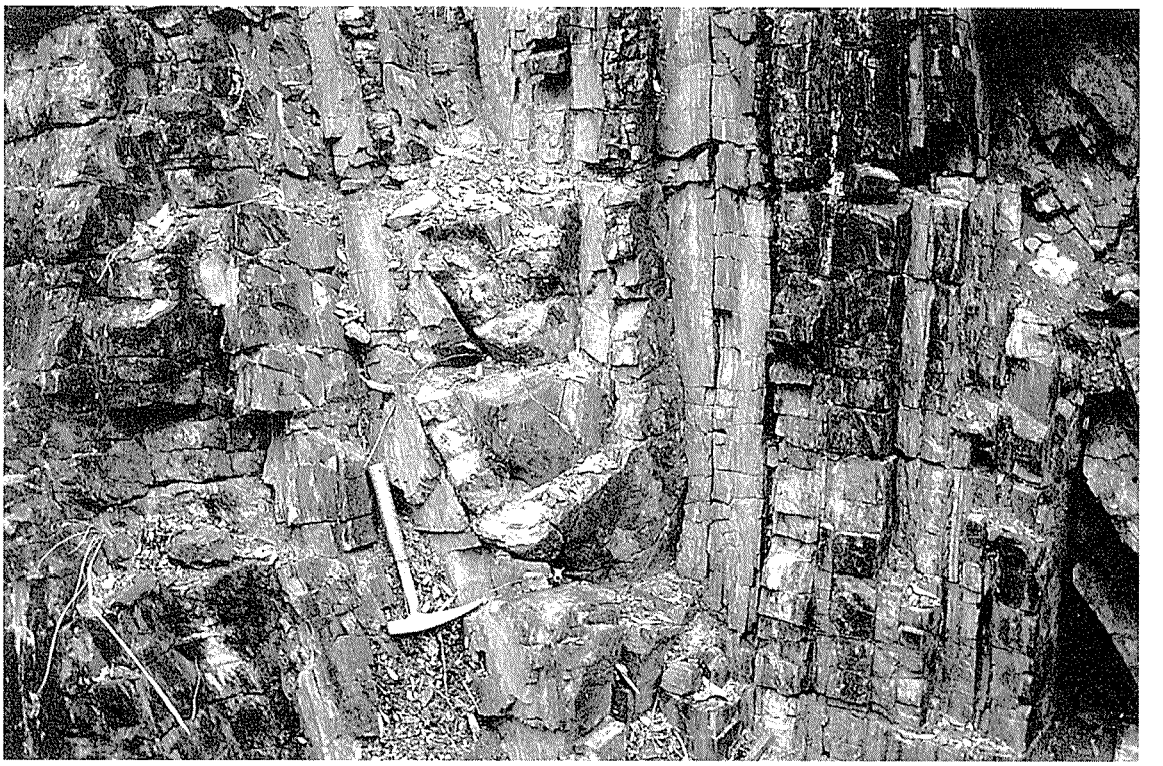

WW 324 10.03.98

Figure 26. D_2 mesoscopic fold in Chester Formation metasedimentary rocks, exposed in creek section at RAVENSTHORPE AMG 401738. Note that the fold plunges 30–40° away from the viewer (southeast)

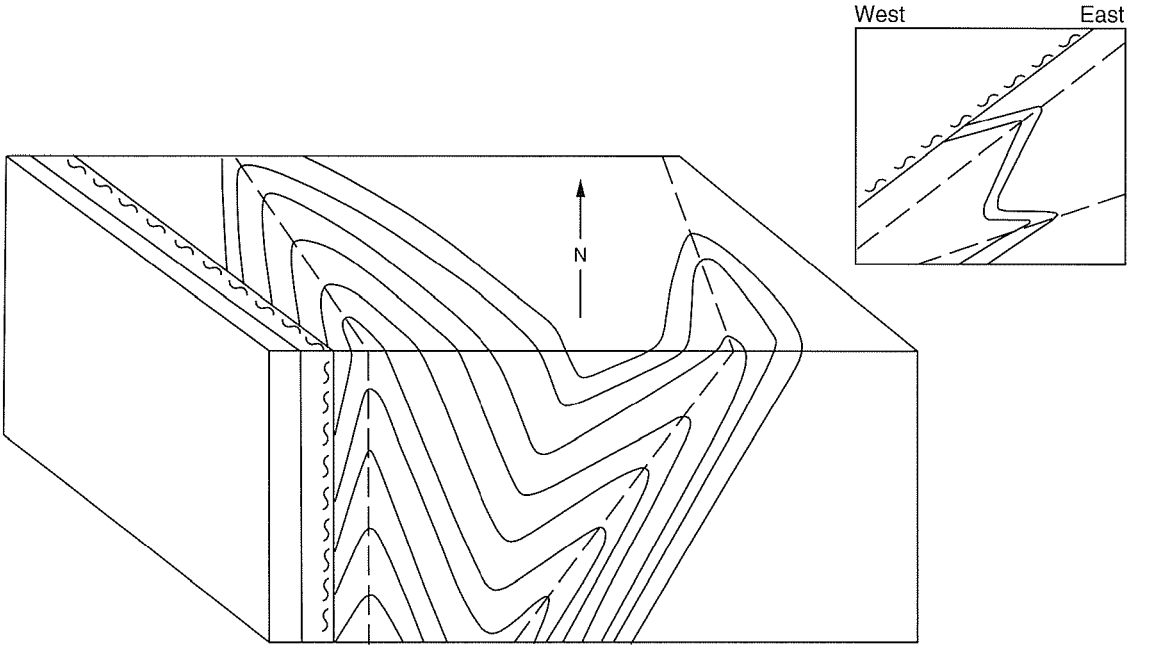

WW274 28.10.97

Figure 27. Block diagram showing shape and orientation of mesoscopic D_2 folds in Chester Formation metasedimentary rocks around RAVENSTHORPE AMG 401738. Inset shows attitude of folds after the greenstone–granitoid gneiss contact is restored to the horizontal

Structure of the Ravensthorpe Terrane

In the Ravensthorpe Terrane primary igneous textures in tonalite and primary depositional structures in volcanic rocks are widespread, except in the southwest where the volcanic rocks are pervasively foliated adjacent to the West sector of the Cocanarup greenstones. Structural interpretation is hampered by the general paucity of bedding in the Annabelle Volcanics, but several high-strain zones can be recognized, both internally and on the contacts with adjacent tectonostratigraphic units. The high-strain zones are subparallel to contact zones.

The D_2 event produced contact-parallel deformation in the Ravensthorpe Terrane. Bedding in restricted occurrences of fine-grained pyroclastic deposits is steeper than the limbs of the Beulah synform and is probably indicative of a separate (earlier) folding event (F_1). The widespread preservation of primary igneous and depositional structures in the Ravensthorpe Terrane suggests that D_1 was a relatively mild folding event.

Deformation on and adjacent to tectonic contacts with the Carlingup Terrane and the Cocanarup greenstones is described below. The following features indicate the presence of internal zones of high strain.

1. Rare exposures of mylonitized zones within the Manyutup Tonalite (e.g. COCANARUP AMG 670637).

2. East of the Ravensthorpe smelter, long thin units of recrystallized ultramafic schist within Manyutup Tonalite are interpreted as tectonically interleaved slices emplaced during contact-parallel deformation.

3. A granitic pegmatite swarm is associated with a zone of deformation and stratigraphic repetition south of Cocanarup. Elsewhere, concentrations of pegmatite dykes are interpreted as indicating zones of deformation. Local deformation of pegmatite dykes, including boudinage (e.g. COCANARUP AMG 657738), indicates that pegmatite intrusion was coincident with movement on the deformation zones.

4. Isolated calc-silicate rocks found at several locations within the Ravensthorpe Terrane are interpreted as metamorphically recrystallized zones of carbonate alteration associated with D_2 deformation.

These features have been used to interpret internal contact-parallel zones of deformation on Plate 1 (see also Fig. 7). However, it should be noted that the extrapolation of these zones beyond a limited number of observation points is poorly constrained.

Structure of the Cocanarup greenstones

Interpretation of the structural history of the Cocanarup greenstones is limited by their restricted exposure in a narrow zone between Ravensthorpe Terrane rocks and granitoid gneiss. Lithological contacts are subparallel to the greenstone–granitoid gneiss contact, and dip moderately (40–70°) east.

Both sectors of the Cocanarup greenstones — the Aerodrome and West sectors — contain a well-developed and almost pervasive foliation. The foliation is subparallel to, and becomes more intense toward, the granitoid gneiss contact. Tight to isoclinal macroscopic folds have been mapped in the Aerodrome sector. The geometry of these folds is uncertain but the pervasive foliation strikes roughly parallel to the axial planar orientation, suggesting that the folds pitch steeply to the west. Mesoscopic, isoclinal to asymmetric, inclined to overturned folds in granitoid gneiss, amphibolite and mafic gneiss have varied orientations. Mesoscopic isoclinal folds also exist in banded iron-formation, south of Elstree farm, but examples have not been observed in situ. Restoration of the macroscopic folds to their pre-Beulah synform geometry shows that they probably formed as recumbent folds lying just above a flat-lying zone of intense ductile deformation on the contact of the Cocanarup greenstones with granitoid gneiss. At least two foliations, preserved in porphyroblasts and low-strain domains (see Chapter 5), predate the main, pervasive fabric. The isoclinal folds are therefore interpreted as having formed during D_3.

The contact between the Cocanarup greenstones and granitoid gneiss is a zone of intense ductile deformation, tectonic interleaving and pegmatite intrusion. Linear fabrics, defined by elongate biotite aggregates in granitoid gneiss and in adjacent metasedimentary schists, are variably oriented but most plunge slightly north of the down-dip direction (Fig. 28). Kinematic indicators that afford confident interpretation of the sense of tectonic transport were observed at only one locality (asymmetric tails on K-feldspar megacrysts in tonalitic gneiss at COCANARUP AMG 699767). After the effects of the Beulah synform are discounted, these indicators suggest movement involved transport of greenstones from east to west on a flat-lying granitoid gneiss–greenstone contact. However, no great significance should be attached to a single observation.

Other, locally preserved, structural elements suggest a complex history of movement on the granitoid gneiss–greenstone contact. Anomalous linear fabrics include subhorizontal lineations associated with S–C fabrics that preserve evidence of dextral movement (at COCANARUP AMG 645633). This is equivalent to a displacement sense that implies southward movement of greenstones over granitoid gneiss, after the effects of the Beulah synform are discounted. Quartz boudins (at COCANARUP AMG 717836), which plunge at moderate angles to the south, record a third direction of movement.

Down-dip lineations on contacts between granitoid gneiss and greenstone are interpreted as L_3, whereas less common, shallow to moderately plunging lineations probably correlate with the earlier foliations preserved in porphyroblasts of the Cocanarup greenstones (see above).

A large enclave of high-grade greenstones lies within granitoid gneiss in the West River area, west of Cocanarup and 7 km from the main granitoid gneiss–greenstone contact. Rock types in the enclave are

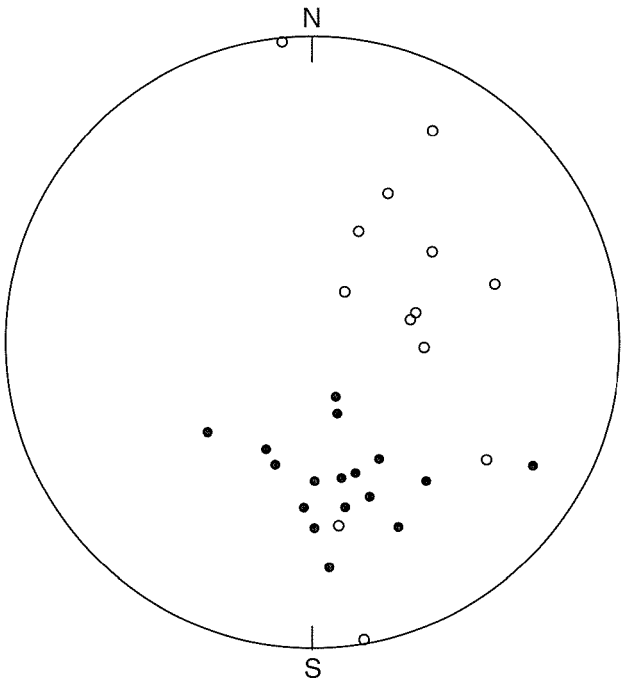

Figure 28. Stereographic projection of linear fabrics on or close to greenstone–granitoid gneiss contacts in the Ravensthorpe greenstone belt

comparable to those in the Cocanarup greenstones and the enclave is probably a result of tectonic imbrication. At West River, there are intrusive contacts as well as tectonic imbrication.

Tectonic contacts between the Ravensthorpe Terrane and adjacent tectonostratigraphic units

Contacts between the Ravensthorpe Terrane and adjacent tectonostratigraphic units are rarely exposed but tectonic contacts are inferred from the gross geometric relationships described above. Despite the poorly exposed contacts, subsurface information provides supporting evidence for a tectonic contact with the Chester Formation. At Mount McMahon, exploration drilling has revealed a zone, up to 15 m wide, of ironstone, quartz and clay on the contact between Annabelle Volcanics and the Chester Formation. The Annabelle Volcanics contain a well-developed, subvertical, contact-parallel foliation in the Mount McMahon mining area that becomes more pervasive adjacent to the Chester Formation contact. In the same area, a strongly deformed contact between Manyutup Tonalite and Chester Formation metasedimentary rocks is exposed in a creek around RAVENSTHORPE AMG 318825. This contact is associated with several contact-parallel zones of epidotization. Exploration drilling in the Mount Chester area, south of Mount McMahon, intersected broad (tens of metres) zones of pervasively foliated schist after Annabelle Volcanics adjacent to the contact with the Chester Formation. The contact is marked by 1–2 m of intensely deformed chlorite–sericite schist, and the underlying chert is brecciated over a width of 1–2 m.

Contacts between Annabelle Volcanics and Manyutup Tonalite are mostly undeformed intrusive contacts but, between Kundip and the Ravensthorpe–Esperance highway, contact-parallel shearing and alteration (chloritization, sericitization) characterize the contact of the tonalite. The presence of thin, discontinuous slices of ultramafic rock within Annabelle Volcanics near the Chester Formation contact, between Kundip and Elverdton, also suggests a tectonic contact between the two.

Contacts between Ravensthorpe Terrane greenstones and Cocanarup greenstones are not exposed. The contact between Annabelle Volcanics and metasedimentary rocks in the West sector of the Cocanarup greenstones appears to be structurally conformable with lithological contacts within the greenstone belt. Contact-parallel zones of interleaving between Manyutup Tonalite and Annabelle Volcanics are accompanied by moderate to intense strain in the volcanic rocks and broad zones of recrystallization in the tonalite. Recrystallized (medium-grained) tonalite displays a locally well-developed tectonic foliation but is more commonly characterized by subgrain development without a distinct preferred orientation. The zones of interleaving and recrystallization are interpreted as contact-parallel shears that probably formed contemporaneously with deformation on the contact with the Cocanarup greenstones.

Polymictic conglomerate in the Carlingup Terrane

Polymictic conglomerate (Fig. 29) occurs as thin fault-bound units, mainly on the northeast side of the Maydon Syncline, suggesting deposition in restricted alluvial basins, and unconformity with respect to other units of the Carlingup Terrane. Clasts of ultramafic rock and banded iron-formation, common in the Carlingup Terrane, are not present. Instead, the conglomerates have a clast population indicative of a provenance mainly in the Ravensthorpe Terrane. The conglomerate has been deformed with the enclosing mafic to ultramafic rocks. Bedding has been folded, and oriented pebbles and cobbles define a linear fabric that is colinear with D_3 lineations in the Bonnymidgup Shear Zone (Fig. 29B).

Figure 29. Two photographs of polymictic conglomerate in Bandalup Creek, at RAVENSTHORPE AMG 516759. Clasts of basalt, andesite, dacite and tonalite are set in a greywacke sand and grit matrix. Note the flattening and elongation of clasts in Figure 29B. The lineation defined by oriented clasts is approximately down-dip (parallel to handle of hammer)

Post-amalgamation deformation

Formation of the Beulah synform (east–west compression)

The Beulah synform is defined by the overall, three-dimensional shape of the Ravensthorpe greenstone belt. Although interpreted as a fold structure, it has been termed a synform because other interpretations, involving complex faulting, are possible. The Beulah synform incorporates the Carlingup Terrane, the Ravensthorpe Terrane and the Cocanarup greenstones and must therefore have formed after amalgamation of the three tectonostratigraphic units. It folds isoclinal folds in the Cocanarup greenstones as well as high-strain zones within the Ravensthorpe Terrane. Interpretation as a south-plunging fold structure is supported by an irregularly developed north–south foliation, and some mesoscopic folds with a similar orientation that occur in the Carlingup Terrane. The east–west compression that formed the Beulah synform is interpreted as D_3 in the Carlingup and Ravensthorpe Terranes but as D_4 in the Cocanarup greenstones, as each unit had a separate deformation history prior to amalgamation.

Later deformation events (north–south compression)

Late deformation in the Carlingup Terrane

The contact between Carlingup Terrane greenstones and granitoid gneiss was deformed by non-coaxial strain during the later stages of regional deformation. Gneiss and greenstones within this strongly deformed contact zone contain a strong planar fabric and a distinct lineation. Lineations plunge moderately (20–40°) to the south (Fig. 28), except where the contact has been rotated by later faults (e.g. northeast of Mount Benson). The deformation zone (referred to as the Bonnymidgup Shear Zone) diverges from the gneiss–greenstone contact to cut the northeast limb of the Maydon Syncline near Bandalup. Other anticlinal zones in smaller scale D_2 folds north of Bandalup are also sheared out by northwest-trending zones of deformation. F_2 anticlines may have initially been sheared out during D_2, but the consistent south-plunging lineation on the Bonnymidgup Shear diverges significantly from the F_2 transport direction and is attributed to a later period of deformation (D_4) during which the principal stress orientation was north–south. Metre-scale, sigmoidal pegmatite bodies and asymmetric tails on feldspar porphyroclasts (e.g. RAVENSTHORPE AMG 284880) suggest reverse movement on the Bonnymidgup Shear Zone and related subparallel structures. However, conflicting indicators related to porphyroblast asymmetry have been observed and reverse movement on the Bonnymidgup Shear Zone was probably only the latest of several periods of movement along the greenstone–granitoid gneiss contact.

Near Mount Chester (RAVENSTHORPE AMG 333802), the main foliation in the Chester Formation (S_2) has been broadly crenulated and, locally, more tightly folded around steep east–west axes. Late, open crenulation and open folding of S_0 (bedding) about east–west axes has also been observed in banded iron-formation units within Bandalup Ultramafics, on the southwestern limb of the Maydon Syncline. These open structures are also assigned to D_4. Plunge reversals in isoclinal F_1 folds (e.g. RAVENSTHORPE AMG 374780) are probably also related to D_4.

Late deformation in the Ravensthorpe Terrane and Cocanarup greenstones

The northeast-trending antiform defined by the Cocanarup greenstones west of Cocanarup is correlated with the fold to the north of Cocanarup. It is interpreted as an F_4 fold that has been refolded about an east–west F_5 fold axis (Plate 1). The orientation of lineations on the granitoid gneiss–greenstone contact in this area is consistent with the interpretation that the lineations are a rotated L_3 fabric. Formation of the F_4 fold is correlated with the same event that produced the Beulah synform.

Late faulting related to the Jerdacuttup Fault

Late (Proterozoic) faulting of all tectonostratigraphic units occurs mainly across east-northeasterly trending structures that are subparallel to the Jerdacuttup Fault. Offset lithological contacts indicate apparent dextral movement across most faults and a major component of dextral movement is also indicated by reorientation of greenstone units immediately north of the Jerdacuttup Fault. However, the Jerdacuttup Fault juxtaposes Archaean Munglinup Gneiss (metamorphosed under deep crustal conditions (Myers, 1995b)) in the south against lower grade greenstones to the north, implying a significant component of vertical movement. This also suggests that other late, subparallel faults may have accommodated subvertical movements.

Structural history of the granitoid gneiss

Archaean granitoid gneiss

Granitoid gneiss north of the Jerdacuttup Fault is structurally complex, displaying multiple fold generations, including tight isoclinal folds, and shear zones at a low angle to gneissic banding. Generally, the tectonic history of the granitoid gneiss is compatible with that observed in the adjacent greenstones. Despite the minor compositional differences between granitoid gneiss northeast of the Carlingup Terrane and that west of the Cocanarup greenstones, no compelling evidence for different deformation histories was identified.

Munglinup Gneiss

Munglinup Gneiss is well-exposed at some localities along the coast and along the Jerdacuttup River. Near Hopetoun, the gneiss is characterized by a shallowly west-dipping foliation and a subhorizontal, north–south rodding or stretching lineation. The gneissic foliation is axial planar to rare reclined folds. These relations suggest a north–south movement direction during formation of the gneiss. The gneissic fabric was subsequently gently warped about 280°. Further inland (RAVENSTHORPE AMG 335486), the gneissic banding is also oriented approximately north–south, but boudinage of monzogranitic layers, ptygmatic folding and rootless folds provide evidence of subsequent, intense ductile deformation parallel to the main fabric. Gneissic banding of rocks in the Jerdacuttup River near Arrandale is oriented approximately east–west, suggesting large-scale rotation of banding about a north–south fold axis broadly coincident with the Jerdacuttup River. At Masons Bay, gneissic banding dips shallowly to the west and south. Isoclinal folding was followed by at least two periods of folding. Folds that are overturned to the south-southeast are refolded about north–south axes. Zones of ductile deformation, oriented 320°, cut across all other structures.

Synthesis of Archaean deformation history

Figure 30 shows several interpreted cross sections through the Ravensthorpe greenstone belt. Interpreted correlations between deformation events in the various tectonostratigraphic units are shown in Table 2.

In the Carlingup Terrane, D_1 involved low-angle thrusting and recumbent folding. The transport direction during this deformation is uncertain. The nature of early deformation events in the Ravensthorpe Terrane and Cocanarup greenstones is even less clear than in the Carlingup Terrane and it is uncertain to what extent D_1 in the Carlingup Terrane can be correlated with D_1 in the other tectonostratigraphic units. Lithological differences between all three units suggest that D_1 probably evolved independently in each case.

Restoration of the Carlingup Terrane greenstones to their pre-Beulah synform geometry (Fig. 31, final panel) leaves F_2 folds (the Maydon Syncline and related folds) as overturned or recumbent folds that display eastward vergence. Similarly, the pre-Beulah synform orientation of contact-parallel structures in the Ravensthorpe Terrane become flat-lying structures, subparallel to a subhorizontal granitoid gneiss–greenstone contact and a gently inclined thrust contact with the Carlingup Terrane. The dominant down-dip lineation (L_3) in the Cocanarup greenstones and adjacent granitoid gneiss indicates east–west movement on this subhorizontal contact, once the effects of the Beulah synform are discounted. Ravensthorpe Terrane rocks overlie the Cocanarup greenstones, and both overlie a shallowly west-dipping thrust fault that separates them from the Carlingup Terrane. Internal zones of high strain within the Ravensthorpe Terrane are sub-parallel to this sole fault and are interpreted as further thrust faults.

The common subhorizontal east–west movement vector suggests that D_2 in the Carlingup Terrane and D_3 in the Cocanarup greenstones can be correlated with one another. This deformation event is interpreted as being responsible for the tectonic emplacement of the Ravensthorpe Terrane over the Carlingup Terrane, and their subsequent amalgamation. Emplacement took place across several flat-lying thrust faults, particularly the sole thrust at the contact between the Ravensthorpe Terrane and the Carlingup Terrane (represented at the present erosion level by the Chidnup Fault). Thrust faults within the Ravensthorpe Terrane suggest stacking of the tonalitic and calc-alkaline volcanic rocks, and their subsequent 'piggy-back' transport above the basal thrust slice. Reclined folds in the Chester Formation are spatially associated with the tectonic front between the Carlingup Terrane and the Ravensthorpe Terrane, and the axial planes of the reclined folds are roughly normal to the transport direction during emplacement of the Ravensthorpe Terrane (Fig. 25B).

Thin slices of ultramafic schist within the Ravensthorpe Terrane and adjacent to the basal thrust plane are interpreted as tectonic slices from the Carlingup Terrane that lubricated movement of the thrust slices. Some of these thrust faults appear to have acted as zones of weakness through which boron-rich silicic magmas travelled and subsequently crystallized as pegmatites. The tourmaline-rich pegmatite dykes display evidence of ductile deformation, including boudinage, suggesting that they were syntectonically emplaced. Tourmaline-rich units, including tourmalinites, lie at the margins of fault-bound slices of ultramafic rock within the Cocanarup greenstones and adjacent Annabelle Volcanics. These are probably related to metasomatic fluids introduced into active thrusts during terrane accretion (cf. Zhang et al., 1994). Pegmatite swarms south of Cocanarup extend into the Cocanarup greenstones, indicating that they and the Ravensthorpe Terrane were juxtaposed at the time of intrusion. Metapelitic schists in the Cocanarup greenstones, like ultramafic rocks, may have lubricated movement on thrust faults within the Ravensthorpe Terrane (Fig. 31).

The eastward vergence of D_2 folds in the Carlingup Terrane indicates that D_2 movement in this terrane was from west to east. The simplest tectonic history involves eastward transport of the Ravensthorpe Terrane over the Carlingup Terrane (Fig. 31). Eastward-directed thrusting began with the formation of overturned to recumbent folds (D_2) in the Carlingup Terrane. Anticlinal zones in these folds became sheared out as deformation progressed. Emplacement of the Ravensthorpe Terrane over the Maydon Syncline was the culminating phase of this deformation. As the Maydon Anticline was sheared out by emplacement of the Ravensthorpe Terrane, final

Figure 30. Interpreted east–west cross sections through the Ravensthorpe greenstone belt. Locations of sections A–B, C–D and E–F–G are shown on Plate 1

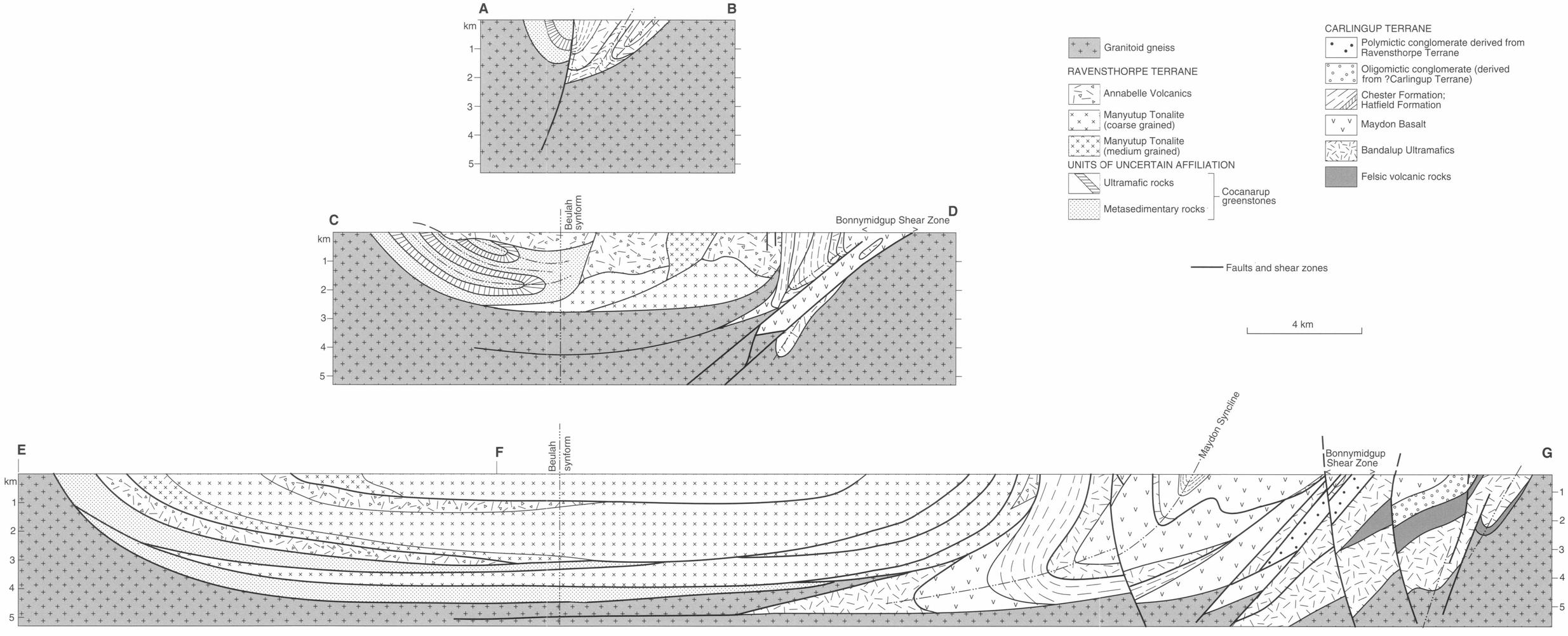
A
B
km
1
2
3
4
5
C
D
Beulah synform
Bonnymidgup Shear Zone
E
F
G
Maydon Syncline
Granitoid gneiss
RAVENSTHORPE TERRANE
Annabelle Volcanics
Manyutup Tonalite (coarse grained)
Manyutup Tonalite (medium grained)
UNITS OF UNCERTAIN AFFILIATION
Ultramafic rocks
Metasedimentary rocks
Cocanarup greenstones
CARLINGUP TERRANE
Polymictic conglomerate derived from Ravensthorpe Terrane
Oligomictic conglomerate (derived from ?Carlingup Terrane)
Chester Formation; Hatfield Formation
Maydon Basalt
Bandalup Ultramafics
Felsic volcanic rocks
Faults and shear zones
4 km
WW339
08.06.98

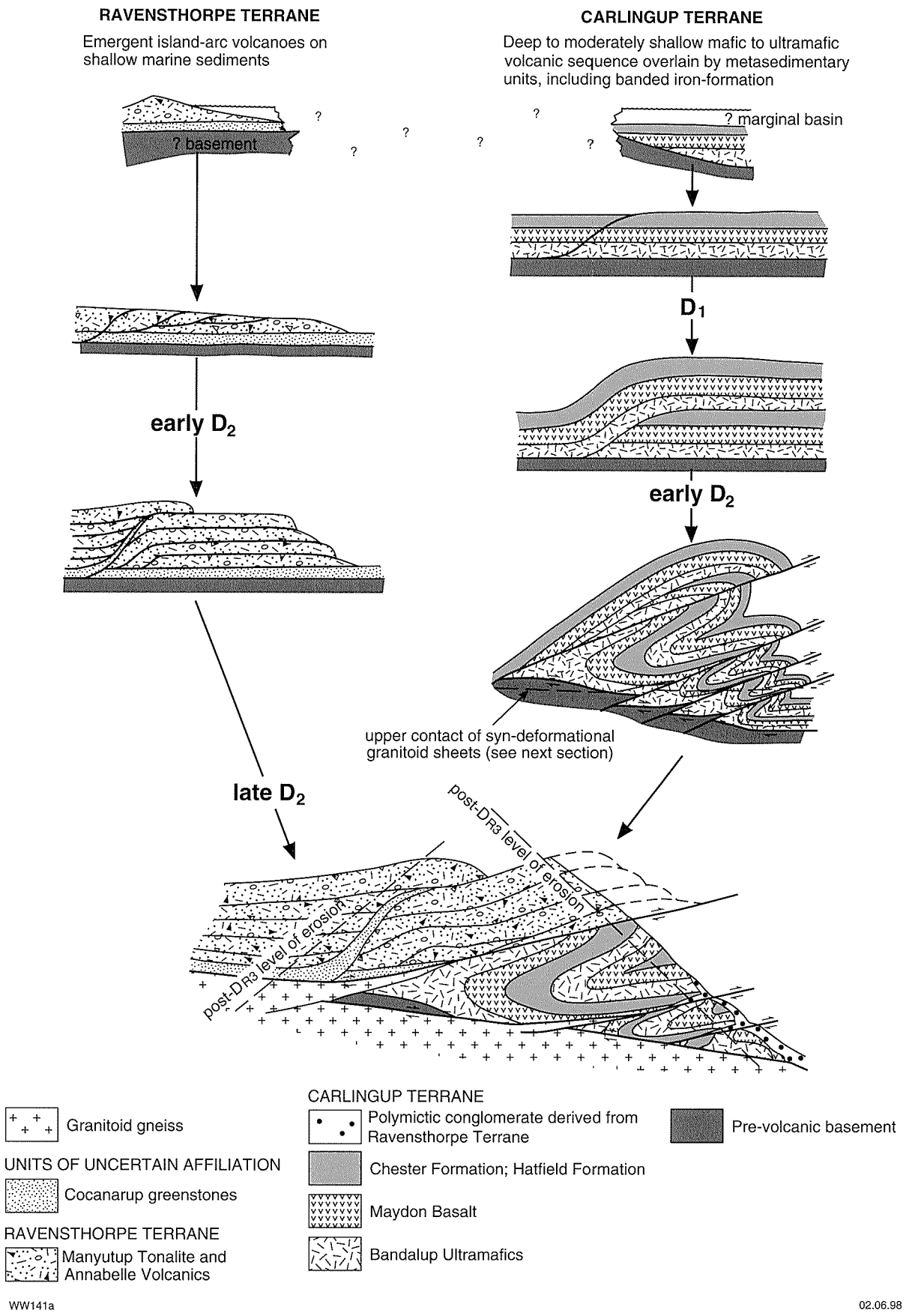

Figure 31. Schematic cross sections illustrating interpreted structural evolution of the Carlingup Terrane, Ravensthorpe Terrane and Cocanarup greenstones, up to the time of amalgamation (prior to formation of the Beulah synform)

tectonic emplacement must then have post-dated D_2 in the Carlingup Terrane. Detritus eroded from the advancing upper thrust-plate (Ravensthorpe Terrane) was deposited in alluvial basins to form the polymictic conglomerate units now interleaved with mafic and ultramafic rocks in the Carlingup Terrane (Fig. 31).

Granitoid gneiss records most of the structural events affecting the greenstones, and gneissic banding is broadly conformable with greenstone contacts. There is no evidence (e.g. abundant pegmatitic segregations, tourmaline) for a genetic link to the pegmatite dyke swarms that accompanied accretion of the two terranes. Minor compositional differences between granitoid gneiss adjacent to the Cocanarup greenstones and that adjacent to Carlingup Terrane greenstones suggest emplacement of the granitoid precursors into active, flat-lying thrust faults during the earlier periods of low-angle faulting and recumbent folding (D_1). However, continued or renewed ductile deformation along the greenstone–granitoid gneiss contact during D_2 (terrane accretion) was likely. Much of the northeast limb of the Maydon Syncline was cut out as a result of simple shear on this contact during progressive D_2 deformation.

Following amalgamation of the two terranes, the Beulah synform developed as a result of continued east–west compression, followed by a period of north–south compression. Northward transport of the Carlingup Terrane greenstones across the Bonnymidgup Shear Zone, and open east–west folds (D_4 in the Carlingup Terrane) may be correlated with more pronounced east–west folding (D_5) in the Cocanarup greenstones. Different responses to the north–south stress orientation may have been controlled by the different orientations of the granitoid gneiss–greenstone contact in each area.

A simplistic interpretation of the Beulah synform as a south-plunging fold structure places the Manyutup Tonalite structurally above the Annabelle Volcanics. It is possible that the Manyutup Tonalite was emplaced as a sill-like body within the Annabelle Volcanics and that the lower contact is exposed in the Ravensthorpe area. However, this is not the preferred interpretation as the presence of numerous plugs and dykes of medium- to fine-grained tonalite and granodiorite in the Ravensthorpe to Kundip area is consistent with features expected at the roof rather than at the floor of a granitoid intrusion. Exposure of the underlying unit (Manyutup Tonalite) south of the main outcrops of Annabelle Volcanics and in the core of the synform may be explained in the following terms:

1. A steep or irregular, not flat-lying, tonalite–volcanic rock contact prior to deformation;
2. D_2 thrust faults that formed at an angle to the original tonalite–volcanic rock contact;
3. Uplift of deeper stratigraphic levels to the south during east–west folding (D_4 in the Ravensthorpe Terrane).

Chapter 5

Archaean metamorphism

All the Archaean greenstones have been metamorphosed. The widespread occurrence of andalusite in metapelitic rocks indicates low-pressure facies metamorphism (Miyashiro, 1973). In contrast to most greenstone belts in the Yilgarn Craton, pelitic and semipelitic rocks are reasonably well-exposed in the Ravensthorpe area, providing the opportunity for a more informed discussion of the metamorphic history. This section begins with a description of metamorphic assemblages in metasedimentary rocks and identification of the relevant metamorphic isograds. These isograds are projected into adjoining areas, with varying degrees of confidence, based on metamorphic assemblages in banded iron-formation and intermediate, mafic and ultramafic rocks. Pressure and temperature estimates are based on metamorphic assemblages and garnet–biotite geothermometry. In the latter part of this section, the timing of peak metamorphic temperatures with respect to regional deformation and interpreted P–T–t paths is discussed.

Metapelitic assemblages (including epiclastic units of the Annabelle Volcanics)

Progressive metamorphism of the metasedimentary rocks is described in terms of the P–T grids presented and discussed by Yardley (1989) and Spear (1993). A summary P–T grid for metasedimentary rocks in the Ravensthorpe area is shown in Fig. 32, which shows

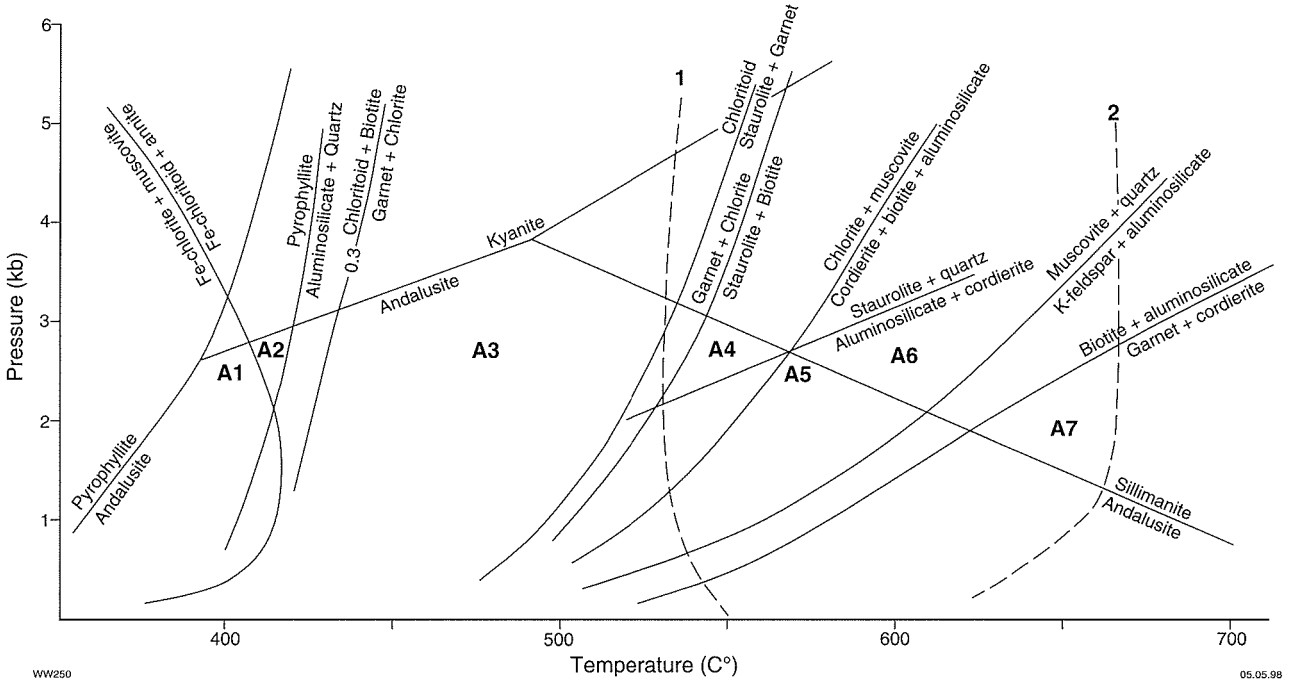

Figure 32. Detailed P–T grid for pelites and ultramafic rocks, based on Spear (1993). Note that curves 1 and 2 have been added from Gole et al. (1987). Curve 1: antigorite → talc + forsterite; Curve 2: talc + forsterite → anthophyllite. Locations A1 to A7 represent approximate metamorphic conditions for greenstones, discussed in text. The 'garnet-in' stability curve is labelled 0.3, the molar spessartine content of the garnet involved in the reaction. The curve moves to higher temperatures for $X_{sps}^{grt} < 0.3$

phase relations in the K_2O–FeO–MgO–Al_2O_3–SiO_2–H_2O (KFMASH) system. The distribution of metamorphic porphyroblast minerals in the Chester and Hatfield Formations is partly controlled by the bulk composition of the original sedimentary rocks. Thus, at many localities, porphyroblast-bearing pelites are interbedded with pelites lacking porphyroblasts. The early appearance of chloritoid and andalusite imply that porphyroblast-bearing pelites are Fe- and Al-rich.

Lowest grade metapelites, east of Kundip, are fine grained and commonly weathered, but contain biotite and lack porphyroblasts of any kind. They probably contain the assemblage quartz–chlorite–pyrophyllite–biotite–opaques(–muscovite–plagioclase). This assemblage (assemblage A1 in Fig. 32) is considered to be unstable at temperatures much above 400°C .

Northward from Kundip, the first small porphyroblasts to appear are chloritoid (field identification only, not confirmed by thin section). These porphyroblasts probably formed by reaction (1).

Fe-chlorite + pyrophyllite → Fe-chloritoid + quartz + H_2O (1)

The temperature at which this reaction takes place is uncertain but it only occurs in Fe-rich, high-Al pelites (Spear, 1993). The resultant assemblage is shown as A2 in Figure 32.

Between Kundip and Elverdton, garnet and andalusite porphyroblasts coexist, in some cases with chloritoid, and are locally abundant. It could not be determined which of andalusite and garnet developed first but it is clear that they both became stable at about the same temperature. This assemblage has also been recognized in the Hatfield Formation, around RAVENSTHORPE AMG 453743.

Further chloritoid may have been produced by reaction (2).

Fe-chlorite + muscovite → Fe-chloritoid + annite + quartz + H_2O (2)

The early paragenesis of andalusite is confined to high-Al pelites (Spear, 1993) and this mineral probably formed as result of reaction (3).

Pyrophyllite → andalusite + quartz + H_2O (3)

In the KFMASH system (Fig. 32), garnet does not become stable until temperatures that are well above the andalusite-producing reaction (1) and even above the staurolite isograd. However, the stability of garnet is significantly expanded by the addition of MnO to the bulk chemical system and this could explain the early appearance of garnet in the Chester and Hatfield Formations. Reactions (4) and/or (5) probably formed garnet.

Muscovite + chlorite → garnet + biotite + quartz + H_2O (4)

Chloritoid + biotite + H_2O → garnet + chlorite (5)

Stability of this assemblage (A3 in Fig. 32) requires temperatures of at least 400°C.

Staurolite has been identified in metapelitic rocks north of Elverdton, around Mount Chester, during this study, and by Savage (1992) in epiclastic or altered schist of the Annabelle Volcanics. Staurolite coexists with garnet and andalusite and, in the latter locality, with chloritoid. The likely staurolite-forming reactions are reactions (6) and (7).

Chloritoid → staurolite + garnet + chlorite + H_2O (6)

or

Garnet + chlorite → staurolite + biotite + H_2O (7)

The assemblage is shown as A4 in Figure 32, and requires temperatures of 500°C or more. The chloritoid-bearing assemblage noted by Savage (1992) must lie on the staurolite isograd.

Staurolite has not been observed, except as rare metastable relicts, outside the Mount Chester area. The limited occurrence of staurolite in pelitic rocks is consistent with its restricted stability range at low pressures (Fig. 32). Temperatures above the staurolite isograd are indicated by the presence of cordierite in metapelitic schist of the Chester Formation and in schist derived from epiclastic or altered facies of the Annabelle Volcanics, north and west of Mount Chester. Cordierite coexists with andalusite in some of these rocks and garnet is present in the same area. Cordierite probably formed from staurolite by reaction (8) although reactions (9) and (10) may also have been important.

Staurolite + quartz → aluminosilicate + cordierite + H_2O (8)

Chlorite + muscovite → cordierite + biotite + andalusite + H_2O (9)

Chlorite + muscovite → cordierite + biotite + quartz + H_2O (10)

At 2.5 kb, this reaction takes place at slightly less than 550°C and the assemblage is shown as A5 in Figure 32. In altered Annabelle Volcanics, however, cordierite may be stable at temperatures as low as 450°C (Fig. 34).

Northwest of the Mount McMahon area, porphyroblast-bearing assemblages in the Chester Formation contain chloritoid, andalusite and garnet, indicating a trend toward lower temperatures.

Garnet and andalusite are also stable in metasedimentary rocks of the Aerodrome sector of the Cocanarup greenstones but the sillimanite isograd is crossed near the boundary with the West sector. Sillimanite occurs firstly with, and then in place of, andalusite, south of the Ravensthorpe aerodrome. The transition from andalusite to sillimanite is expected at 590°C, at 2.5 kb; the sillimanite-bearing assemblage is shown as A6 in Figure 32.

Low-Al metapelites along the western margin of the West sector of the Cocanarup greenstones contain the assemblage quartz–biotite–plagioclase–garnet–cordierite. Aluminosilicate minerals are absent, which implies reaction (11).

$$\text{Biotite + sillimanite} \rightarrow \text{garnet + cordierite + } H_2O \qquad (11)$$

This is the highest grade assemblage in the Archaean greenstones at Ravensthorpe and is indicated as A7 in Figure 32. The assemblage indicates temperatures well above 600°C. At such temperatures, muscovite-bearing assemblages should break down according to reaction (12).

$$\text{Muscovite + quartz} \rightarrow \text{K-feldspar + sillimanite + } H_2O \qquad (12)$$

Bulk-rock compositions that are likely to record reaction (12) are not widespread in the West sector but do occur (around COCANARUP AMG 640650) as the assemblage quartz–K-feldspar–sillimanite. The pink and white mottled appearance of quartz–K-feldspar–sillimanite rocks, described in Witt (1997), may reflect incipient migmatitization of the rocks.

The presence of andalusite in metapelitic rocks in the southern part of the West sector of the Cocanarup greenstones indicates that metamorphic temperatures decrease southward from the garnet–cordierite zone. Assemblages containing garnet, andalusite and cordierite suggest conditions close to those represented by A5 in Figure 32. Relict staurolite in retrogressed cordierite porphyroblasts from these metapelites (Fig. 37G 119903, COCANARUP AMG 649582) suggests the prograde reaction (8) has taken place.

Assemblages in ultramafic rocks, mafic to intermediate rocks, and banded iron-formation

The isograds identified above, on the basis of pelitic and semipelitic units, can be extrapolated through areas underlain by other rock types with varying degrees of confidence (Fig. 33, Plate 1). This extrapolation is based mainly on assemblages in ultramafic rocks, banded iron-formation and altered rocks of the Annabelle Volcanics.

Ultramafic rocks are less sensitive to metamorphic grade than metapelites. Tremolite–chlorite assemblages after komatiite are stable over a wide range of temperatures. However, more magnesian units such as the B-zones of komatiitic flows provide some constraints. Serpentine-rich rocks react to form talc + metamorphic olivine (forsterite) between 500°C and 550°C (Gole et al., 1987) and ultramafic rocks containing metamorphic olivine are approximately equivalent to A4–A7 assemblages in pelitic and semipelitic rocks. Metamorphic olivine and pseudomorphs after metamorphic olivine have been identified in ultramafic rocks along the margins of the Ravensthorpe Terrane and the Cocanarup greenstones (Plate 1). The absence of anthophyllite in these rocks imposes a maximum temperature of approximately 650°C, above which talc and forsterite react to form anthophyllite (Curve 2, Fig. 32). The relative scarcity of late tremolite in talc–carbonate schists in the Bandalup Ultramafics, east of Kundip, is consistent with evidence from metapelites for relatively low-grade metamorphism in this area.

Although they are relatively poor indicators of metamorphic grade, assemblages in mafic rocks also indicate an increase of metamorphic grade toward the margins of the greenstone belt. Mafic gneiss along the margins of the Aerodrome sector of the Cocanarup greenstones and exposed in the West River contains clinopyroxene and hornblende. The latter displays a pleochroic scheme that exhibits distinct brown hues. The presence of clinopyroxene in mafic gneiss suggests temperatures of 650–750°C (Binns, 1964) and equivalence to assemblages A7 (Fig. 32) in pelitic and semipelitic rocks.

Banded iron-formation in most parts of the Carlingup Terrane is a banded quartz–grunerite(–magnetite) rock. The lower stability limit of grunerite is not well known (Gilbert et al., 1982). However, Ahmat (1986) considered the presence of grunerite in banded iron-formation to be indicative of amphibolite-grade metamorphism, consistent with observations from metapelitic assemblages.

Massive to irregularly banded, coarse-grained, calc-silicate rocks, found locally as float within the Ravensthorpe Terrane, are interpreted to have formed by metamorphic recrystallization of carbonated andesite. Calc-silicate assemblages are varied, but assemblages that contain quartz–diopside–calcic amphibole–K-feldspar are common and all contain prominent diopside. These rocks are typical of altered mafic to intermediate rocks metamorphosed at medium to high grades (Ahmat, 1986) and require temperatures >450°C (Yardley, 1989). They are thus equivalent to assemblages A3 and above in pelitic and semipelitic rocks. Although the full extent and form of these diopside-bearing units is poorly known, they are interpreted here as metamorphically recrystallized D_2 shear zones (see above).

Cordierite–gedrite–andalusite–quartz–plagioclase (–garnet) rocks, exposed in the West sector of the Cocanarup greenstones, are interpreted as metamorphosed, altered Annabelle Volcanics. At 2.5 kb, this assemblage is stable above about 470°C (Fig. 34). The upper temperature limit for these rocks is set, by the absence of sillimanite, at a little less than 600°C. The presence of minor relict staurolite in cordierite porphyroblasts (Fig. 37H) further constrains the metamorphic P–T conditions. There is no garnet in this rock so the most likely cordierite-forming reaction is reaction (8) (above), implying conditions equivalent to those recorded by A4 or A5 assemblages in pelitic and semipelitic rocks (Fig. 32). Similar assemblages occur at the Mount McMahon mining centre.

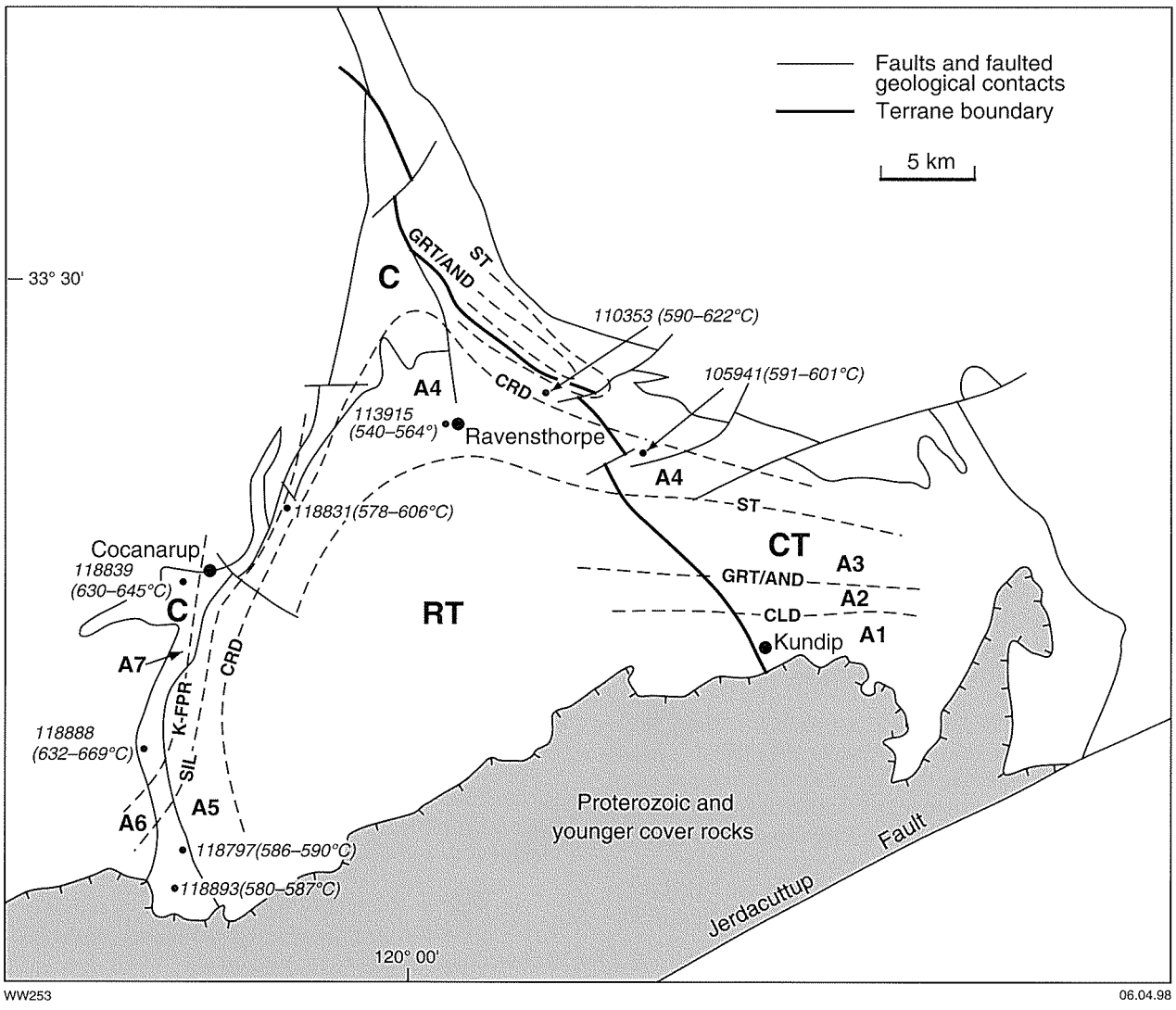

Figure 33. Interpreted isotherms for the Ravensthorpe greenstone belt, based on mineral assemblages and garnet–biotite geothermometry. Metamorphic zones and their bounding isograds (see text) are as follows: Zone A1 — chloritoid (CLD); Zone A2 — garnet–andalusite (GRT/AND); Zone A3 — staurolite (ST); Zone A4 — cordierite (CRD); Zone A5 — sillimanite (SIL); Zone A6 — K-feldspar (K-FPR) to Zone A7. Other abbreviations: Carlingup Terrane (CT), Ravensthorpe Terrane (RT), Cocanarup greenstones (C)

Pressure estimates

Metamorphic assemblages discussed above indicate a range of metamorphic conditions that vary from middle greenschist facies to upper amphibolite facies, with the highest grade assemblages occurring south of Cocanarup.

The widespread metapelitic assemblage quartz–plagioclase–biotite–garnet–andalusite (Fig. 35) suggests metamorphism under pressure conditions defined by bathozone 2 of Carmichael (1978). This bathozone corresponds to pressures of 2.2 to 3.3 kb (approximately). The pressure is further constrained to a maximum of about 2.7 kb by the appearance of cordierite before sillimanite, in metapelitic assemblages. The presence of spodumene in the Cattlin Creek pegmatite imposes minimum pressures of 2.5–3 kb during crystallization (London, 1990). The cordierite–gedrite–andalusite–quartz–plagioclase(–garnet) assemblages in altered Annabelle Volcanics imply maximum pressures of approximately 3.5 kb (Fig. 34). Slightly higher pressures are possible in the highest grade sillimanite-bearing rocks for which there are no significant pressure constraints.

Peak metamorphic assemblages in rocks throughout much of the Ravensthorpe greenstone belt appear to have equilibrated at similar pressures of 2.5–3.5 kb, thus generating a flat P–T array (Fig. 32). This P–T array should not be confused with the geothermal gradient since peak metamorphic assemblages in different rock samples may have equilibrated at different times on the P–T–t paths of each sample (Thompson and England, 1984; Yardley, 1989). In geological provinces that have undergone crustal thickening, it is not unusual for rocks with very different P–T–t paths to equilibrate at similar

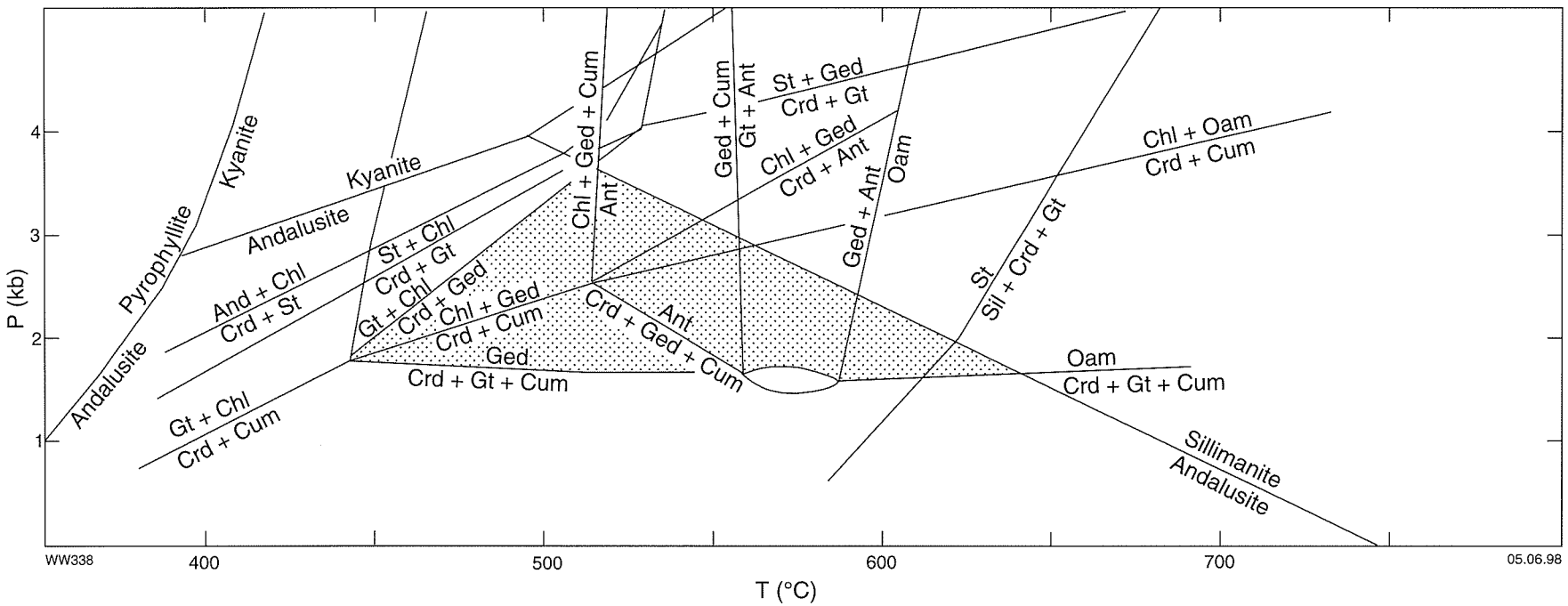

Figure 34. P–T grid for cordierite–orthoamphibole assemblages (after Spear, 1993). Shaded area shows metamorphic conditions indicated by assemblages in the southwest Ravensthorpe Terrane. Mineral names are abbreviated as follows: And andalusite; Ant anthophyllite; Chl chlorite; Crd cordierite; Cum cummingtonite; Ged gedrite; Gt garnet; Oam orthoamphibole; Sil sillimanite; St staurolite

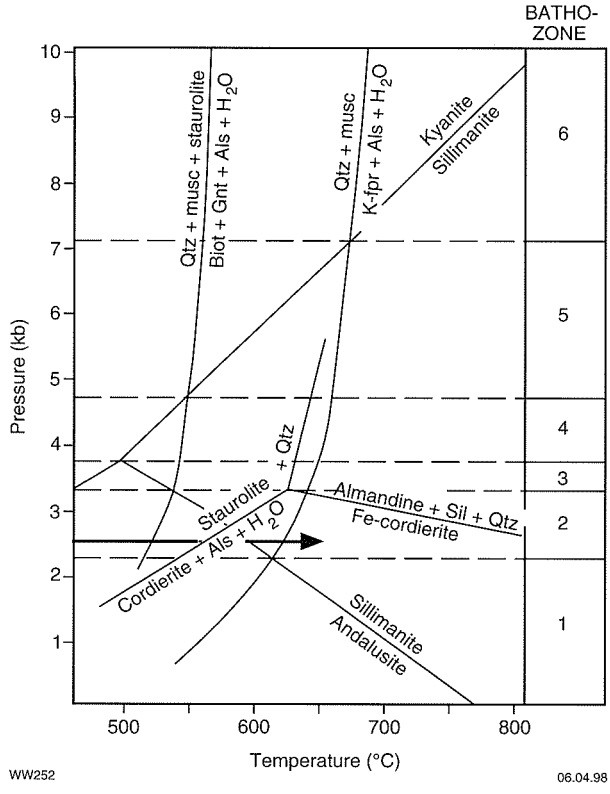

Figure 35. P–T grid (from Yardley, 1989). The arrow represents the approximate locus of metamorphic assemblages in the Ravensthorpe greenstone belt

pressures as the province is uplifted in response to erosion (England and Thompson, 1984).

Geothermometry and geobarometry

Several geothermometers and geobarometers have been applied to samples for which mineral analyses are available. Representative analyses and a discussion of the analytical method are presented in Appendix 3. Their application has had mixed results. The mostly unsuccessful application of geothermometers and geobarometers involving plagioclase may be related to slow diffusion rates of cations in plagioclase and consequent disequilibrium with other minerals in the same rock (Spear, 1993).

Temperatures determined using the Perchuk and Lavren'teva (1981) garnet–biotite geothermometer have been plotted on Plate 1. The isotherms mimic the metamorphic gradients determined from regional metamorphic assemblages, and are within, or slightly higher than, ranges determined from metamorphic assemblages. Anomalously high garnet–biotite temperatures cannot be explained by diffusion of Fe and Mg during retrograde cooling but may reflect a slight underestimation of pressure, or consumption of garnet margins during net transfer reactions and consequent disequilibrium between garnet margins and matrix biotite (Spear, 1993).

Timing relations between metamorphism and deformation

Carlingup Terrane

Evidence for timing relationships between deformation and metamorphism is preserved in porphyroblast-bearing metapelitic assemblages and associated volcanogenic rocks of the Chester Formation. The S_1 fabric is defined by quartz–biotite–opaque oxides(–plagioclase) in low-strain domains between spaced S_2 (Fig. 36) and in pressure shadows of porphyroblasts (Fig. 24). S_1 is also preserved in porphyroblasts of cordierite, as trails of opaque grains oriented at a high angle to S_2 (Fig. 36). The main foliation (S_2) is defined by a similar assemblage to that which defines S_1. It is deflected by porphyroblasts of andalusite, garnet, cordierite and staurolite (Figs 36, 37A) but is also preserved as inclusion trails within some porphyroblasts. S_2 inclusion trails are not markedly rotated with respect to the external foliation (Figs 37B, 38) indicating that porphyroblasts continued to grow after D_2 was essentially completed. Andalusite in sample 113929 (RAVENSTHORPE AMG 315846) displays evidence for two stages of growth (Fig. 37C). Early, white chiastolitic andalusite displays the characteristic cruciform arrangement of dusty inclusions (?opaques, ?carbonaceous material) but is free of silicate inclusions. Chiastolitic andalusite deflects S_2 in the enclosing schist but a later, post-D_2 overgrowth of grey, idioblastic andalusite is riddled with silicate inclusions that are continuous with, and unrotated with respect to, the external S_2. Garnet in sample 113934 also displays two stages of growth (Figs 37B, 38). In this case an inclusion-free margin overgrows an inclusion-rich porphyroblast. Garnet porphyroblasts are arranged in bands at a large angle to S_2 suggesting growth was controlled by an earlier compositional banding (?S_0). Extensional fractures between closely spaced garnet porphyroblasts are oriented normal to porphyroblast margins and are filled with fibrous quartz and grunerite that have grown parallel to S_2 (Fig. 37B). These observations suggest that peak metamorphism occurred syn- to post-D_2 but that growth of some porphyroblasts, most notably cordierite, began before S_2 formed.

The presence of chloritoid in pelites of the Chester Formation, northwest of Mount McMahon, indicates relatively low-temperature metamorphic assemblages in a zone that is confined between higher grade rocks to the east (metamorphic olivine in ultramafic rocks) and west (cordierite–gedrite assemblages in altered Annabelle Volcanics). It is possible that the isograds have been tightly folded by D_2 (Fig. 33). If this interpretation is correct, it implies that metamorphic gradients in the Carlingup Terrane were already defined before or during early D_2. This is consistent with the extended growth

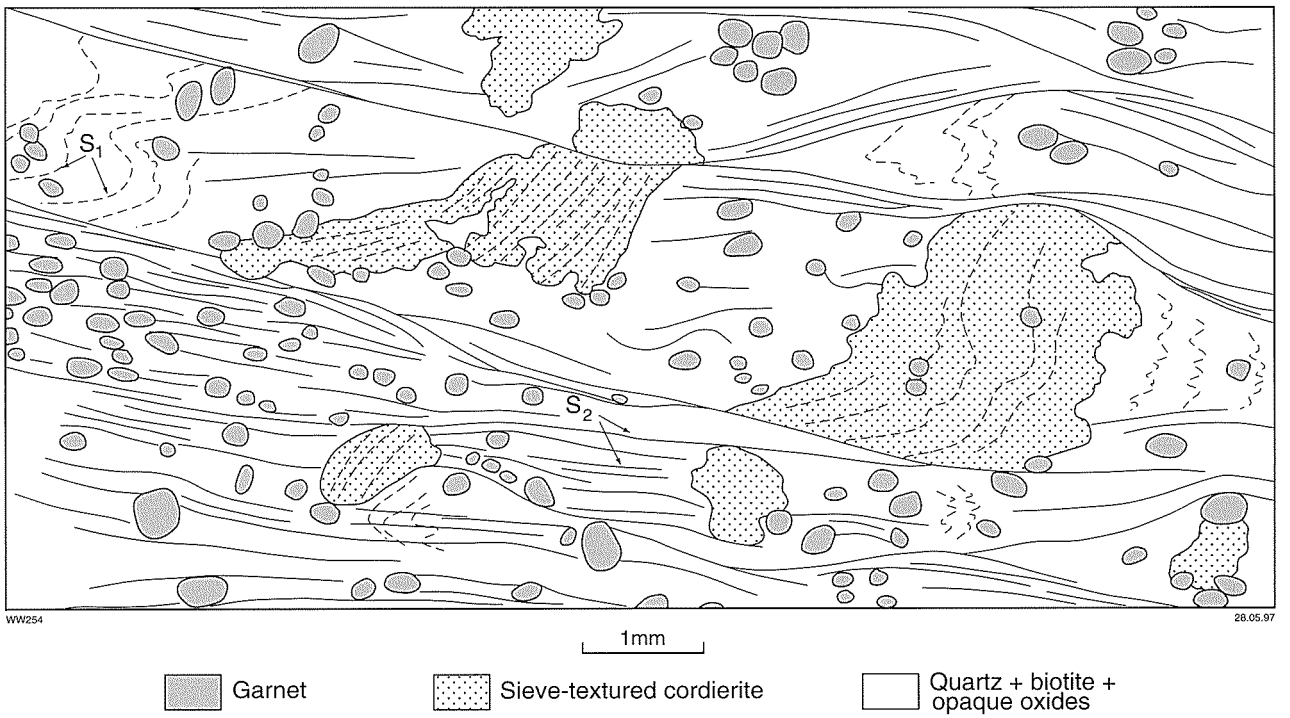

Figure 36. Sketch of mineral–fabric relations in Chester Formation metasedimentary rock. GSWA 113931, based on print of a microfiche image of a thin section

history of porphyroblasts but may be difficult to reconcile with the post-D_2 growth of porphyroblasts. If peak thermal equilibration was late, it is expected that the pre-folding isograds would decay and new isograds that are consistent with the post-folding geometry would form. A better understanding of the metamorphic patterns northwest of Mount McMahon requires more detailed studies but for the present it is concluded, on the basis of porphyroblasts–matrix fabric relations, that peak thermal metamorphism in the Carlingup Terrane was syn- to post-D_2.

Ravensthorpe Terrane

Garnet porphyroblasts in metamorphosed epiclastic or altered rocks near Ravensthorpe deflect but also overgrow the main metamorphic fabric (S_2). Inclusion trails are mostly unrotated with respect to the external foliation, suggesting late syn- to post-D_2 growth, similar to that deduced for garnet growth in the Chester Formation. Cordierite porphyroblasts also deflect S_2 but contain randomly oriented inclusions of biotite and rutile. Biotite inclusions contrast with oriented biotite (defining S_2) in the matrix suggesting the cordierite largely pre-dated D_2. This relationship is again similar to that observed for cordierite in the Chester Formation. Photomicrographs in Savage (1992) indicate that, near Mount Chester, fabric relations for porphyroblasts of staurolite, garnet, chloritoid and andalusite in schist derived from the Annabelle Volcanics are mostly consistent with late syn- to post-D_2 growth. However, some photomicrographs show staurolite with strongly rotated inclusion trails. The rotated porphyroblasts near Mount Chester indicate a period of overlap between D_2 and staurolite growth. Either staurolite began to crystallize early, with cordierite or, more probably, S_2 deformation near the tectonic front between the Carlingup and Ravensthorpe Terranes continued for a longer period than in rocks more distal from the front.

South of Cocanarup, unoriented orthoamphibole sprays in cordierite–gedrite rock suggest syn- to post-D_2 growth of andalusite, cordierite and gedrite (Fig. 39) in altered and metamorphosed Annabelle Volcanics.

Cocanarup greenstones

The main metamorphic fabric (S_3) in metapelitic schist and micaceous quartzite is defined by oriented micas. Muscovite, though commonly oriented parallel to biotite, is partly unoriented suggesting continued growth after S_3. Early foliations (S_1, S_2) are preserved as inclusion trails of quartz, biotite, sillimanite, rutile and opaque minerals in porphyroblasts of garnet (Figs 37D–E, 40, 41) and andalusite (Figs 37F, 42) and in low-strain domains between spaced S_3 foliation planes. Preservation of these early fabrics indicates initial growth of garnet and andalusite prior to the development of an S_3 fabric. Although early, rotated fabrics have also been observed in cordierite, this mineral commonly lacks inclusion trails. Andalusite and garnet porphyroblasts partly deflect but also partly overgrow S_3 indicating continued stability and growth during D_3. Furthermore, elongate andalusite porphyroblasts (up to 60×4×2 mm) at COCANARUP AMG 770755 are oriented steeply within the main metamorphic fabric, defining L_3. Prismatic sillimanite in sample

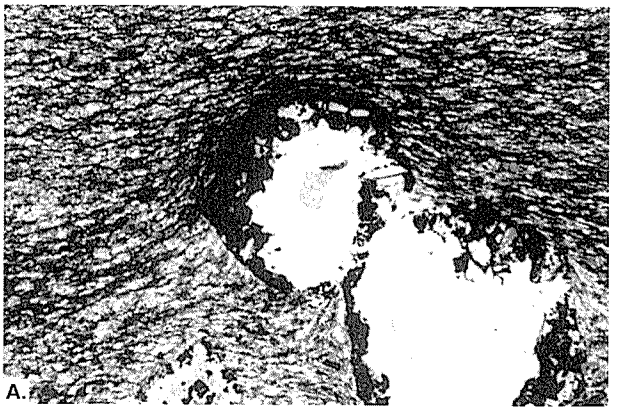
A.

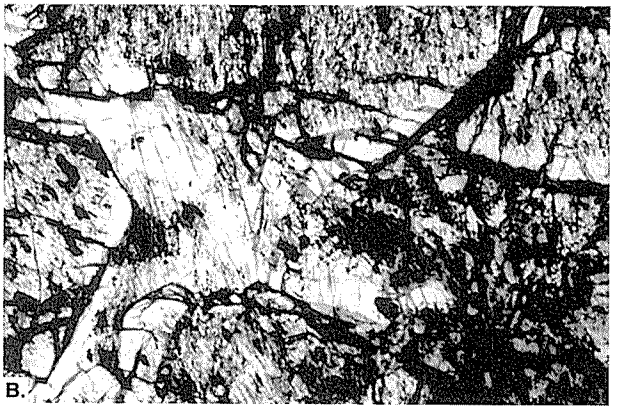
B.

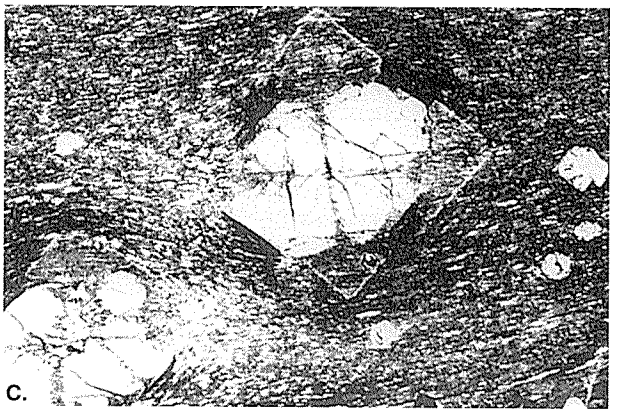
C.

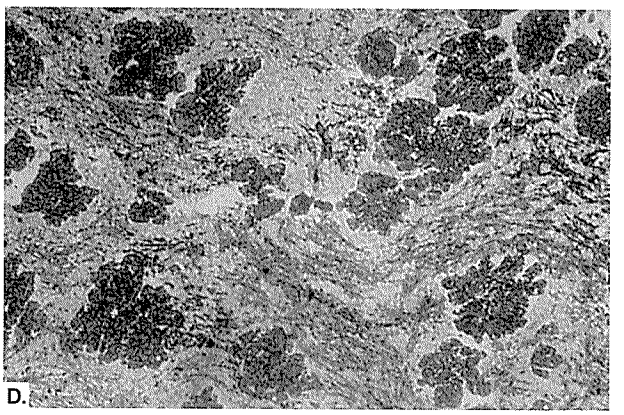
D.

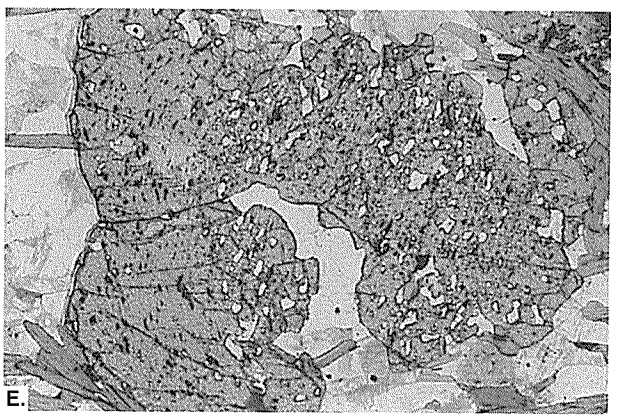
E.

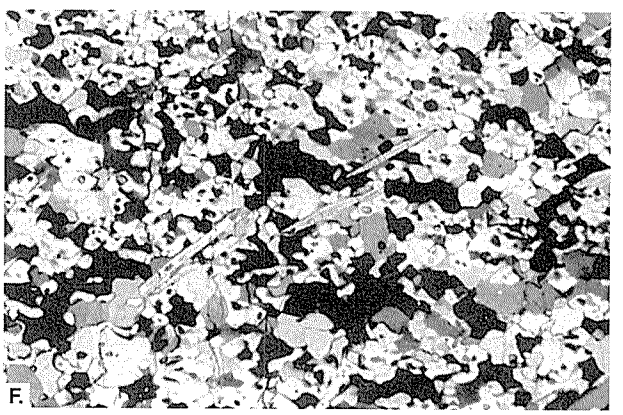
F.

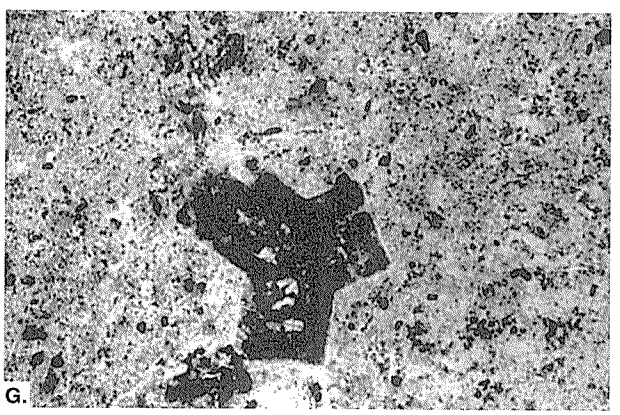
G.

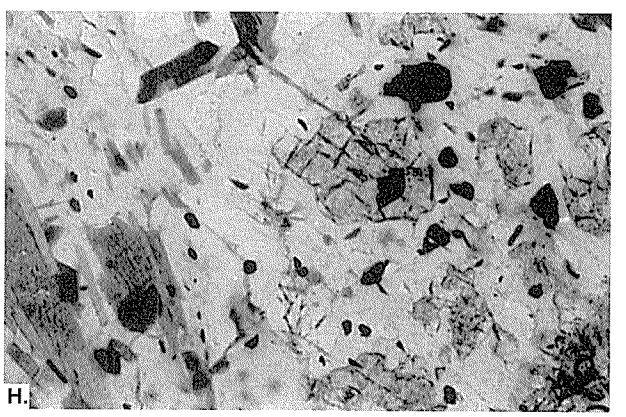
H.

WW 326

11.03.98

118832 is preserved only within andalusite porphyroblasts where it preserves an earlier fabric (S_1 or S_2) (Figs 37F, 42). These relationships suggest that, in metapelitic rocks at this locality, sillimanite grew during D_1 and D_2 but was unstable with respect to andalusite, quartz and muscovite during D_3.

Conclusions

The above observations indicate that regional metamorphic assemblages preserved in rocks at the present erosion surface were temporally related to the deformation that resulted in amalgamation of the Carlingup and Ravensthorpe Terranes (D_2 in the Carlingup Terrane and Ravensthorpe Terrane, D_3 in the Cocanarup greenstones). However, each tectonostratigraphic unit had an earlier metamorphic history locally preserved as relict tectonic fabrics in porphyroblasts and low-strain domains. These earlier histories were contemporaneous with pre-amalgamation deformation fabrics and probably developed independently in each tectonostratigraphic unit. Thus, garnet and andalusite porphyroblasts in the Cocanarup greenstones appear to have grown during pre-amalgamation deformation, whereas in the Carlingup Terrane these minerals did not begin to grow until amalgamation of the terranes. Early sillimanite in the Cocanarup greenstones contrasts with its absence in the Carlingup Terrane. Deformation associated with the Bonnymidgup Shear Zone is not associated with retrograde metamorphic assemblages, indicating that high temperature metamorphic conditions were maintained during D_4 north–south compression (D_5 in the Cocanarup greenstones).

Pressure–temperature–time (P–T–t) paths

At the present erosion level, there is widespread evidence for metamorphic crystallization at 2.5–3.5 kb (Fig. 32). However, individual rock samples preserve evidence for a complex metamorphic history and may have arrived at their present P–T points via quite different P–T–t paths (England and Thompson, 1984). Thrust tectonics of the type that juxtaposed the Ravensthorpe and Carlingup Terranes produces distinctive metamorphic P–T–t paths in rocks forming the upper and lower plates, respectively (Spear et al., 1984; Chamberlain and Karabinos, 1987). Three examples of these are shown in Figure 43. Metamorphic fabrics, combined with compositional zoning in garnet, were used to interpret qualitative P–T–t paths for tectonostratigraphic terranes in the Ravensthorpe area and compare these with predicted paths.

Reconnaissance analyses of garnets in samples 110353 and 113915 are presented in Appendix 3. Both samples are altered Annabelle Volcanics from the eastern part of the Ravensthorpe Terrane (Fig. 33). All analysed garnet porphyroblasts were greater than one mm in diameter thus minimizing erroneous results arising from diffusion during retrograde cooling (Spear, 1993). Two to four analyses were collected at the rims (<50 μ from grain boundary), margins (50–300 μ from grain boundary), interiors, and cores of individual garnet grains. More detailed analytical traverses from margin to margin across garnet grains in sample 118831 (from the Cocanarup greenstones) were performed using a

Figure 37. Metamorphic textures and fabrics in Archaean rocks

A–C: Chester Formation metasedimentary rocks
A: Deflection of S_2 around (plucked) garnet porphyroblasts. GSWA 110358, plane-polarized light, field of view approximately 4 mm
B: Fibrous quartz–grunerite oriented parallel to S_2 in extensional domains between garnet porphyroblasts. Note S_2 inclusion trails in garnet porphyroblasts. The photomicrograph is a close-up view of a portion of the thin section (GSWA 113934) shown in Figure 38, plane-polarized light, field of view approximately 4 mm
C: Two-stage growth of andalusite porphyroblasts in Chester Formation metasedimentary rocks. Early chiastolitic andalusite (white) deflects S_2 whereas later euhedral andalusite overgrows the deflected S_2 and is riddled with inclusions that preserve S_2 in the later andalusite. GSWA 113929, plane-polarized light, field of view approximately 2 mm
D–H: Ravensthorpe Terrane rocks (including Cocanarup greenstones)
D: S_1 (lower left to upper right in photomicrograph) preserved as inclusion trails in garnet porphyroblasts. Note quartz-rich haloes around garnet porphyroblasts and that S_2 is deflected by the garnet porphyroblasts. GSWA 118795, plane-polarized light, field of view approximately 12 mm
E: Two foliations (S_1 and S_2) preserved as inclusion trails in garnet porphyroblasts. The dominant foliation in the sample is oriented parallel to the long edge of the photomicrograph (see Fig. 40). GSWA 118839, plane-polarized light, field of view approximately 10 mm
F: Oriented sillimanite preserves S_1 in andalusite porphyroblast (see Fig. 42 for broader context). GSWA 118832, crossed polars, field of view approximately 2 mm
G: Relict ?andalusite in pinnitized cordierite porphyroblast. GSWA 119903A, plane-polarized light, field of view approximately 2 mm
H: Relict staurolite in pinnitized cordierite, cordierite–orthoamphibole rock. GSWA 118894, plane-polarized light, field of view approximately 2 mm

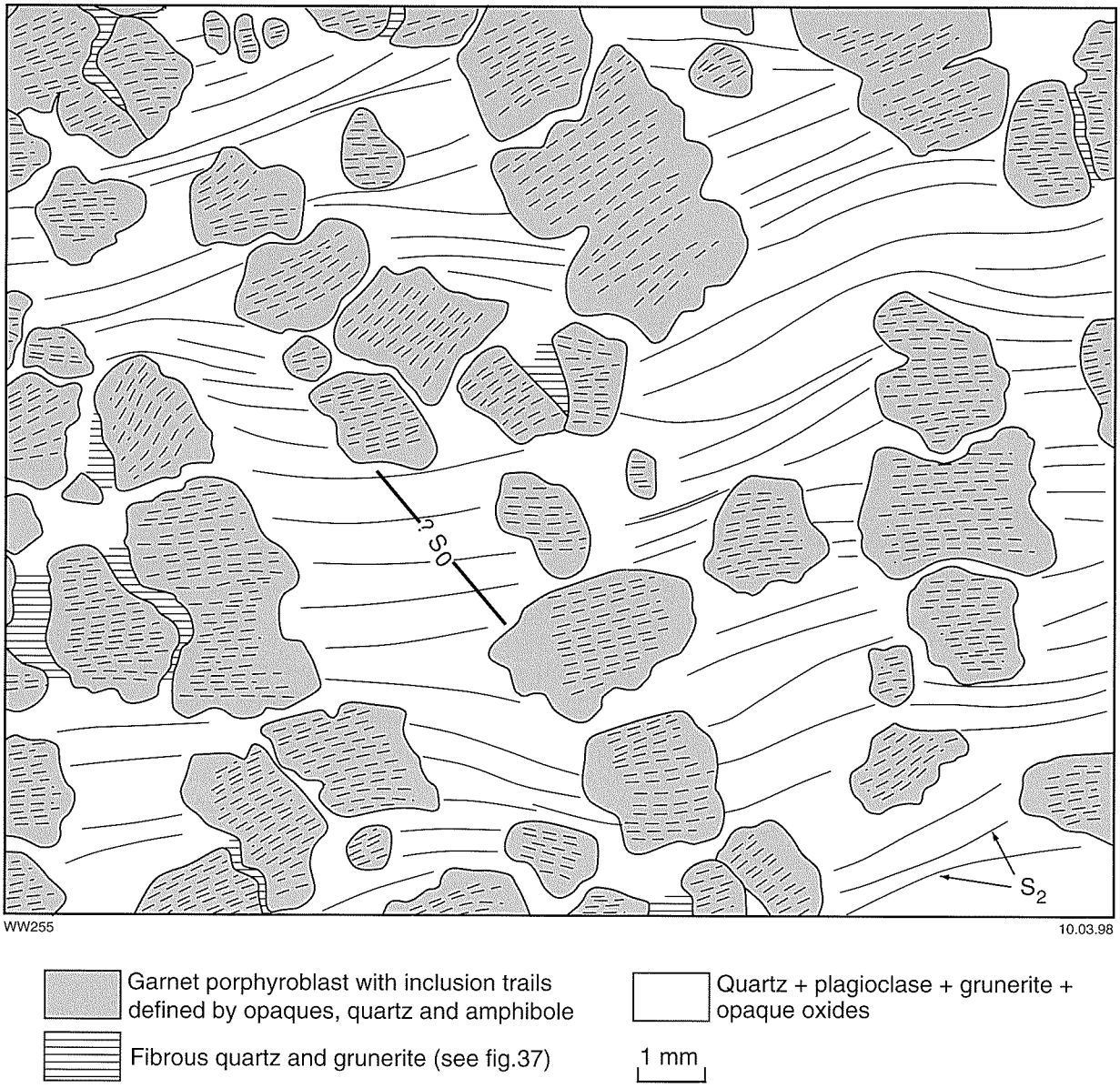

Figure 38. Sketch of mineral–fabric relations in metasedimentary rock from the Cocanarup greenstones. GSWA 113934, based on print of a microfiche image of a thin section. S_0 is bedding

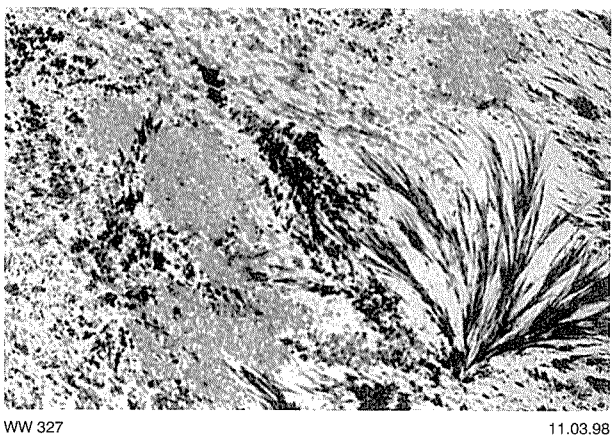

CAMECA electron microprobe. Traverses consisted of twenty-one analytical sites spaced 0.05 mm apart. Twenty-one analytical sites, from margin to core, comprised a detailed traverse across each of two garnets in sample 113915 (altered Annabelle Volcanics). The results of these data describing compositional zoning in garnet are discussed below.

Figure 39. Andalusite porphyroblasts (dark grey) and radiating sprays of gedrite in a quartz–plagioclase–biotite matrix, cordierite–orthoamphibole rock from the southwest part of the Ravensthorpe Terrane. GSWA 118796, plane-polarized light, field of view approximately 10 mm

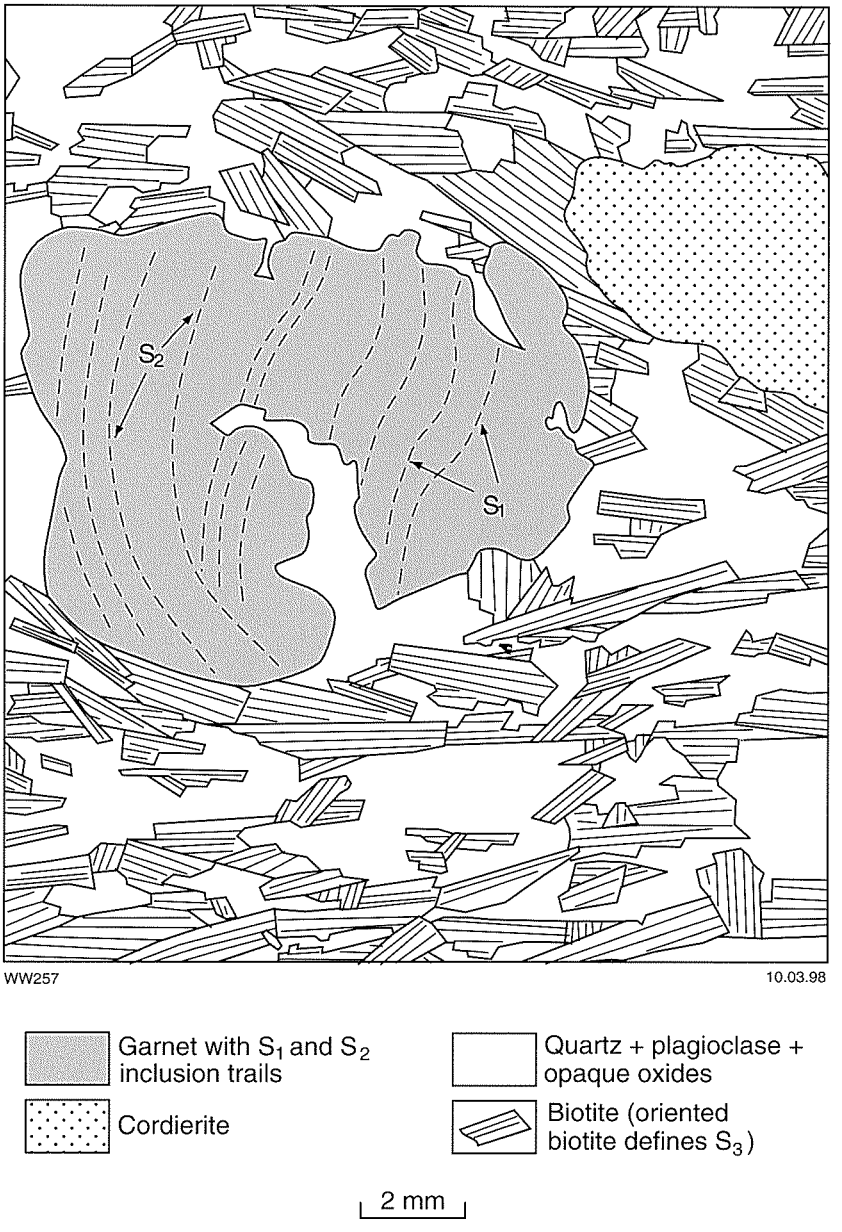

Figure 40. Sketch of mineral–fabric relations in metasedimentary rock from Cocanarup greenstones. GSWA 118839, based on print of a microfiche image of a thin section

Cocanarup greenstones and the western margin of the Ravensthorpe Terrane

Sample 118832 from the Cocanarup greenstones preserves relict, prismatic sillimanite only as inclusions in andalusite (Fig. 37F). Sillimanite is one of the minerals that define pre-S_3 fabrics but it was unstable with respect to andalusite during D_3. The period D_1 to D_3 was therefore characterized by isobaric cooling or a decrease in pressure. Two independent lines of evidence suggest the decompression path is more likely.

1. Garnet compositional zoning in the assemblage garnet–biotite–aluminosilicate–muscovite–quartz is strongly dependent upon pressure and largely independent of temperature (Fig. 44A). Sample 118831, which was collected within 2 km of 118832, contains this assemblage. The increase in the almandine component of garnet (X_{Fe}^{grt}), from core to margin, in sample 118831 (Fig. 45, see also Appendix 3) can only have been produced by decompression, assuming Fe has not been introduced by fluids (Fig. 44A). Other analysed garnets from the Cocanarup greenstones are from the metapelitic quartz–plagioclase–biotite–garnet–cordierite unit that defines the highest grade Cocanarup greenstones. These assemblages do not contain muscovite and the garnets are not systematically zoned. Interpretation of compositional zoning in these garnets is difficult

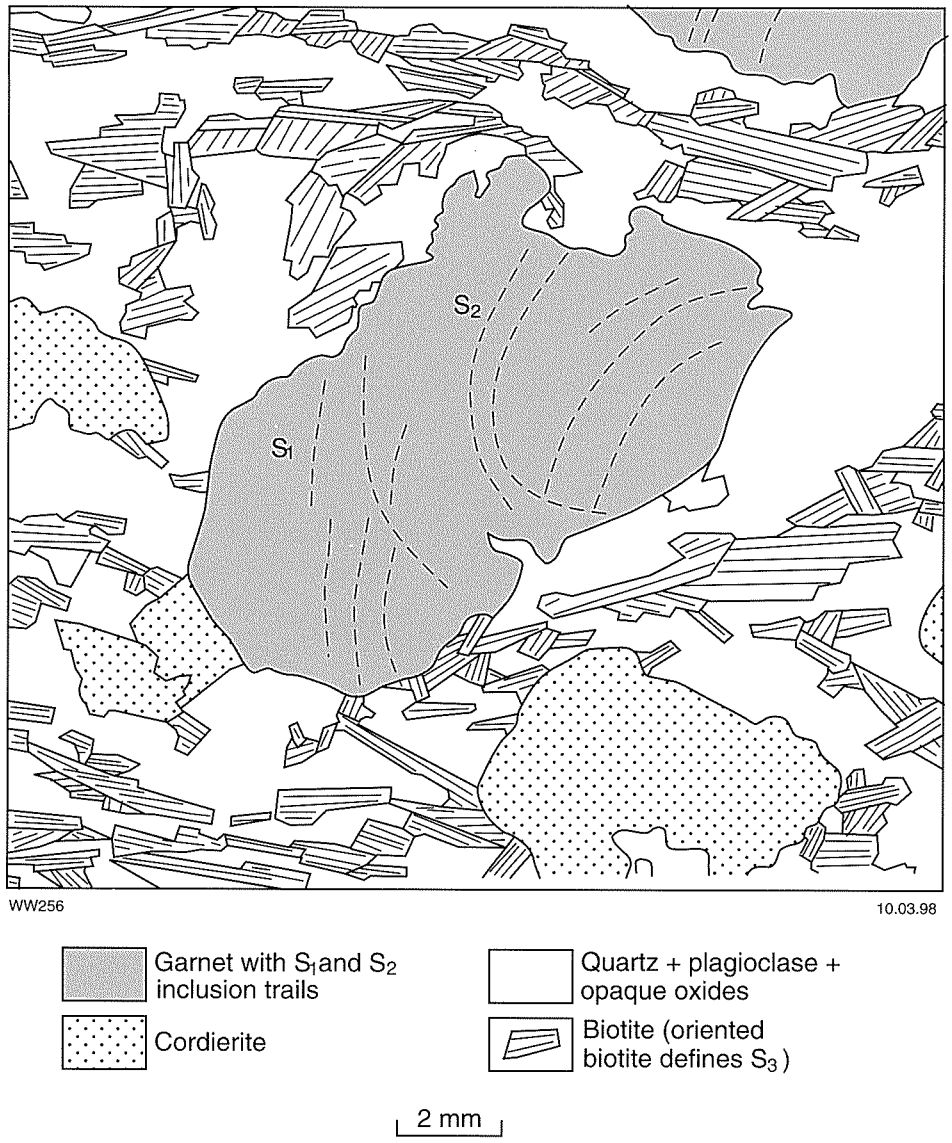

Figure 41. Sketch of mineral–fabric relations in metasedimentary rock from Cocanarup greenstones. GSWA 118839, based on print of a microfiche image of a thin section

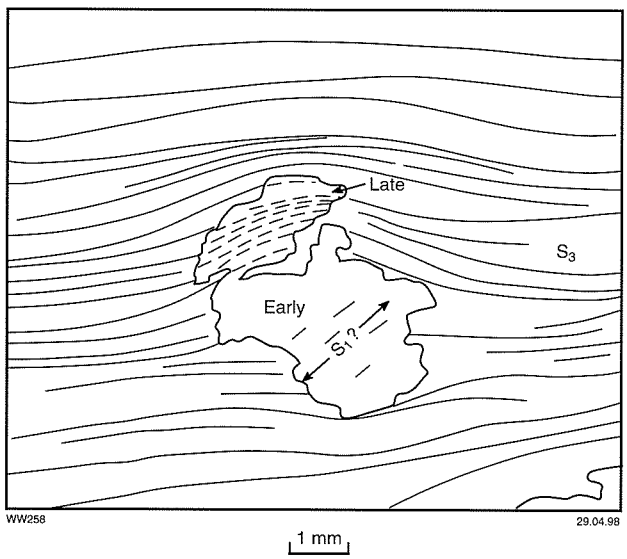

but the non-systematic variations may have been caused by net transfer or exchange effects related to the loss or formation of other Fe- and Mg-rich mineral species (Spear, 1993).

2. A decrease in temperature in sample 118832 and other rocks in the Cocanarup greenstones is not consistent with the absence of retrograde alteration of garnet, biotite and andalusite. Two further reactions of significance are indicated by textural relationships

Figure 42. Sketch of mineral–fabric relations in metasedimentary rock from Cocanarup greenstones. Note preservation of S_1 as oriented sillimanite in early andalusite (deflects S_3). Late andalusite overgrows S_3, which is preserved within the porphyroblast as inclusion trails. GSWA 118832, based on print of a microfiche image of a thin section

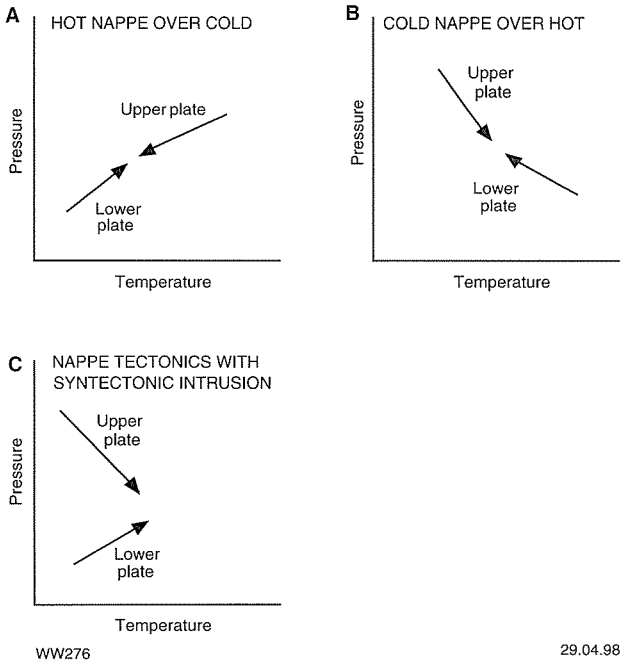

Figure 43. A and B: P–T–t paths predicted for metamorphic rocks in nappe tectonic regimes (after Spear et al., 1984). C: P–T–t path predicted for nappe tectonic regime in which syntectonic granitoid sheets are emplaced within the thrust sequence (this report)

in some samples of the Cocanarup greenstones. Relicts of staurolite in cordierite in metapelitic sample 119903 from the Last Venture mine area, south of Cocanarup, suggest reaction (8) (see above, Metapelitic assemblages). The same relationship has been observed in samples of altered Annabelle Volcanics in the vicinity. This reaction proceeds to the right in response to increasing temperature or decreasing pressure but is not compatible with a cooling path (Fig. 32).

Eastern margin of the Ravensthorpe Terrane, and the Chester Formation in the Carlingup Terrane

The absence of high-temperature minerals in relict S_1 fabrics preserved in porphyroblasts of cordierite indicates a prograde heating path for Chester Formation metasedimentary rocks but does not constrain changes in pressure. The early formation of cordierite in high-temperature pelites, compared to the syn- to post-D_2 growth of garnet, andalusite and chloritoid in lower temperature pelites is consistent with a deep heat source and progressively later peak thermal equilibration at shallower crustal levels (England and Thompson, 1984). Andraditic garnets in staurolite-bearing sample 105941 (from the Chester Formation) have been analysed but the complex compositional zoning in these garnets could not be meaningfully interpreted. Elsewhere, garnet in Chester Formation pelites is too weathered to yield meaningful analytical data.

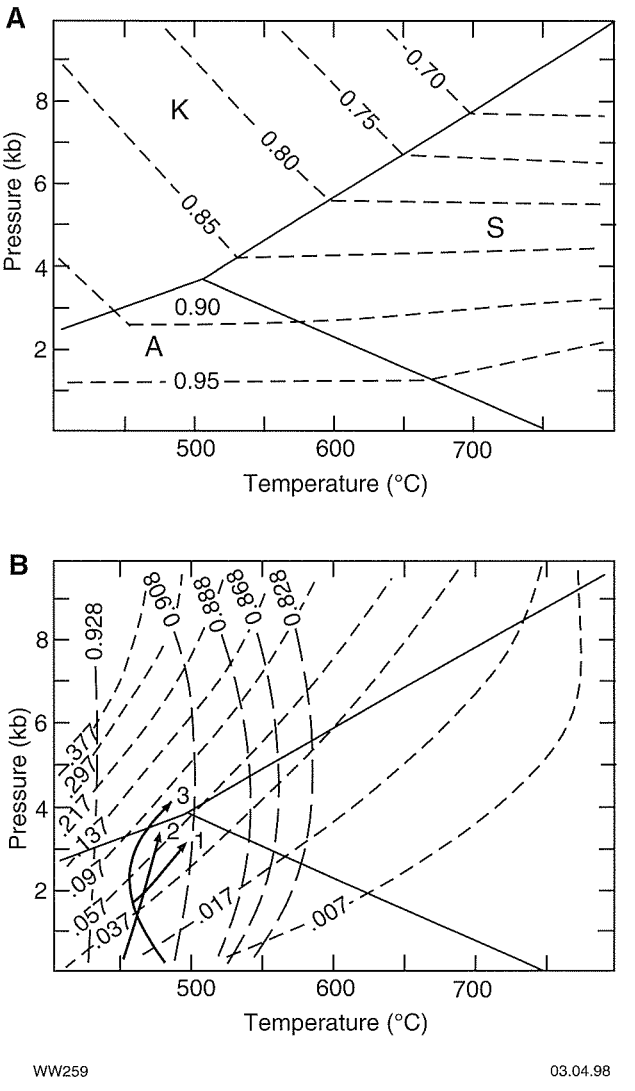

Figure 44. P–T grids showing the aluminosilicate phase boundaries and equilibrium garnet compositions (after Spear, 1993). A: X_{Fe}^{grt} in the assemblage garnet + biotite + andalusite + muscovite + quartz. B: Fe/Fe + Mg in garnet contours and X_{Ca}^{grt} contours in the assemblage garnet + biotite + chlorite + plagioclase + muscovite + quartz. Arrows indicate P–T–t paths for garnets in altered Annabelle Volcanics near Ravensthorpe, based on garnet compositions

Spear (1993) has published contours for $X_{Fe/Fe+Mg}^{grt}$ and X_{Ca}^{grt} for the assemblage garnet–biotite–chlorite–plagioclase–muscovite–quartz (Fig. 44B). Calcium zoning in garnet is particularly useful as the calcium diffuses slowly during retrograde cooling (Spear, 1993) and is therefore likely to preserve the prograde history of the garnet better than X_{Fe}^{grt}. Samples of altered Annabelle Volcanics (in Cu–Au lodes) from the Ravensthorpe area (110353 and 113915) approximate this assemblage, although the rocks lack muscovite. This may not be a serious problem since the amount of Ca, Fe, Mn and Mg in muscovite is very small compared to that in garnet, biotite, plagioclase and chlorite.

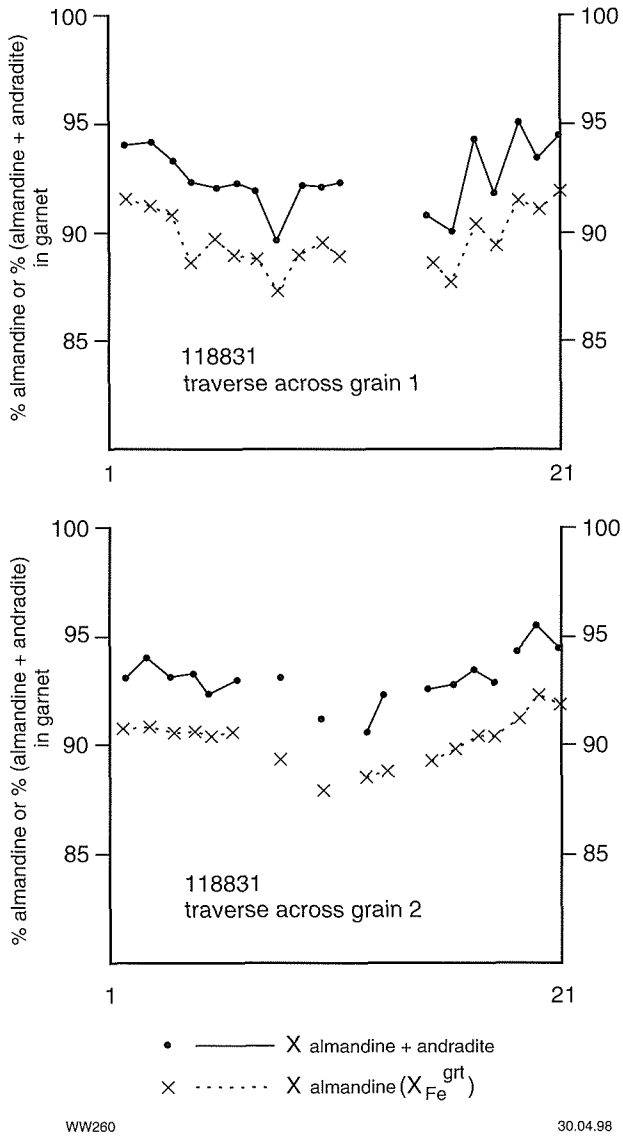

Figure 45. Results of microprobe analyses from traverses across two garnet grains (2 mm diameter) in the assemblage quartz–plagioclase–biotite–muscovite–andalusite–sillimanite–garnet–opaque minerals from Cocanarup greenstones. Points 1–21 (along base of diagram) are analytical sites spaced at 0.05 mm intervals from margin to margin. Missing points analysed inclusions of other minerals (mainly quartz). X is molecular proportion in garnet

X_{Ca}^{grt} increases regularly from core to margin in sample 110353. There is also an increase in the grossular content of garnets from sample 113915 although in this sample X_{Ca}^{grt} zoning is more complex. Increasing X_{Ca}^{grt} can be interpreted to indicate increasing pressure or decreasing temperature (Fig. 44B) but the latter is inconsistent with the prograde textural fabrics of the garnet-bearing samples. X_{Fe}^{grt} zoning in samples 110353 and 113915 is complex, and may be complicated by an andradite component. However, P–T paths defined by the intersection of $X_{Fe/Fe+Mg}^{grt}$ and X_{Ca}^{grt} contours are consistent with pressure and temperature increasing during much or all of garnet growth (Fig. 44B). More detailed analytical traverses across two garnet porphyroblasts in sample 113915 illustrates the complexity of the compositional zoning. Nevertheless, the data are consistent with a two-stage decompressional path for the garnet-bearing rock (Fig. 46).

Metamorphic isograds and causes of metamorphism

Isograds shown in Figure 33 and Plate 1 are based mainly on assemblages in metapelitic and ultramafic rocks. As the dominant metamorphic assemblages have been timed, on structural–fabric criteria, as post-dating amalgamation of the Carlingup and Ravensthorpe Terranes, the isograds have been drawn across terrane boundaries.

Metamorphism in the Ravensthorpe greenstone belt as a whole has, in the past, been interpreted as contact metamorphism related to intrusion of the Manyutup Tonalite (Sofoulis, 1958). Assemblages in Chester Formation pelites indicate variations in metamorphic grade that are parallel to the igneous contact and thus do not support this hypothesis. Furthermore, the post-crystallization emplacement of the igneous body into its

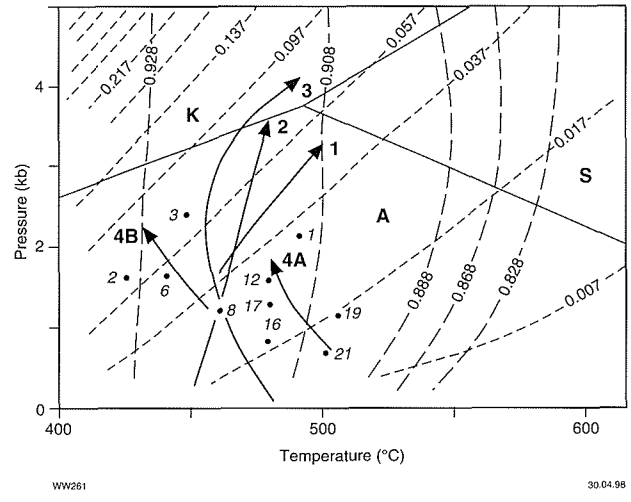

Figure 46. P–T grid showing aluminosilicate triple phase boundaries and equilibrium garnet compositions in the assemblage quartz–plagioclase–biotite–muscovite–garnet–chlorite (after Spear, 1993). Long dashed contours show $X_{grossular}$; short dashed contours show $X_{Fe/(Fe+Mg)}$. Arrows 1–3 show compositional trends for garnets (1–2 cm diameter) in the Ravensthorpe Terrane, adjacent to the terrane boundary, based on three sets of analyses (margin, intermediate and core). A more detailed (microprobe) analytical traverse across one of these garnets, from core (21) to margin (1), reveals a more complex compositional zoning that is, however, consistent with growth during two-stage (arrows 4A and 4B) tectonic loading (increasing P). Missing analytical points represent inclusions of other minerals (mainly quartz)

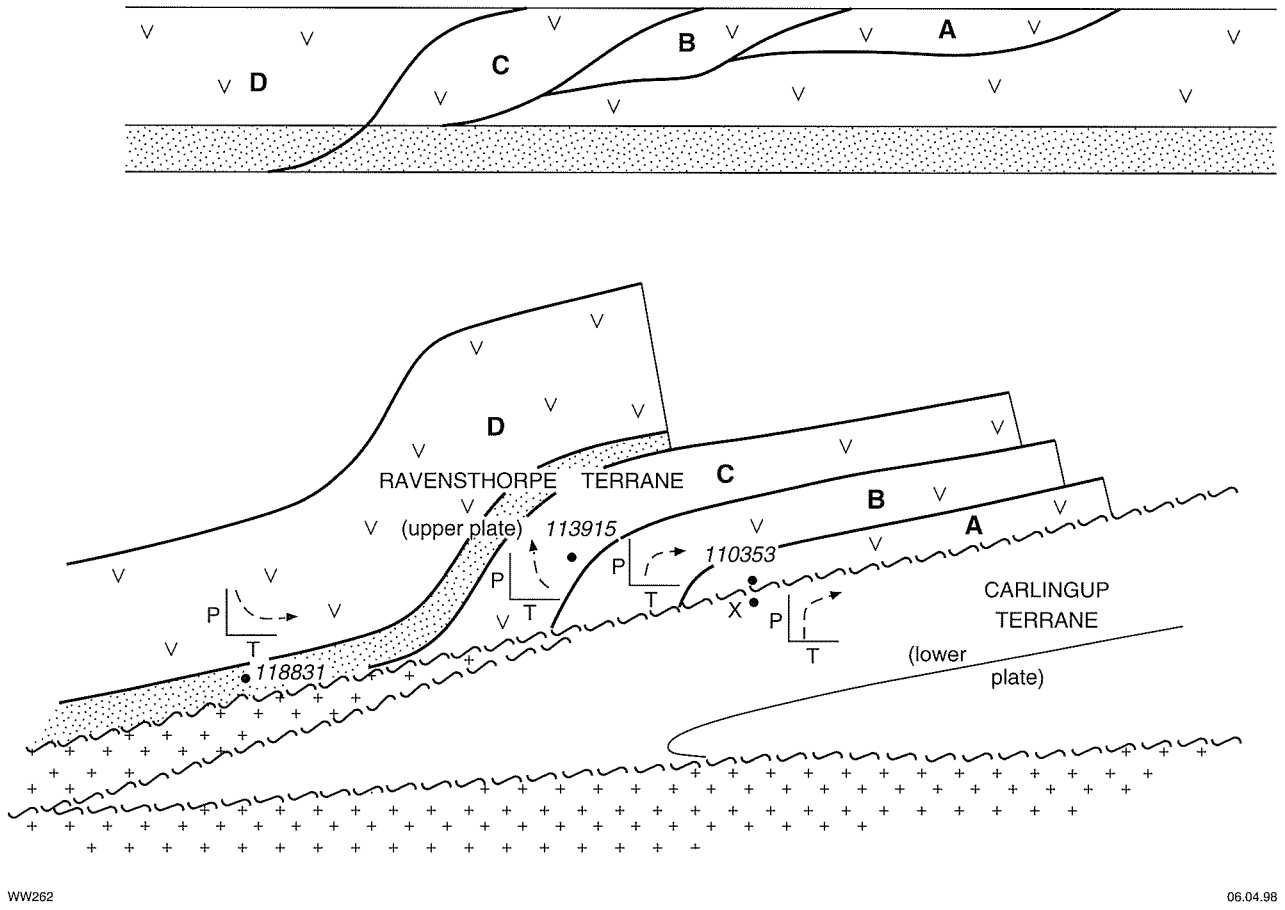

Figure 47. Schematic diagram showing relationships between thrust slices and expected P–T–t paths of metamorphic rocks in the Ravensthorpe greenstone belt. P–T paths in samples 118831, 113915 and 110353 are consistent with those expected in the upper thrust slices. No data are available from lower plate, but expected P–T path is shown by point X for completeness

present position proposed in this report cannot be reconciled with contact metamorphism of the Carlingup Terrane. Savage (1992) interpreted metamorphic assemblages in drillhole MCD–1A, near Mount Chester, as recording a contact metamorphic gradient in which temperatures decrease away from the Manyutup Tonalite contact. As these assemblages occur only in the Annabelle Volcanics, which were tectonically emplaced with the Manyutup Tonalite, it is conceivable that a contact metamorphic gradient has been preserved by assemblages at this locality. However, in a broader context, the assemblages at Mount Chester are consistent with the regional metamorphic gradients documented above. High-grade metamorphic rocks in the Ravensthorpe greenstone belt are spatially related to contacts with granitoid gneiss at the margins of the greenstone belts, not to contacts with the Manyutup Tonalite.

Although the final (present) configuration of regional metamorphic isograds appears to cut across tectonostratigraphic (terrane) contacts, there is evidence that earlier metamorphic histories of the eastern and western rocks were different. The different metamorphic histories of the Chester Formation and the eastern Ravensthorpe Terrane on the one hand, and of the western Ravensthorpe Terrane and the Cocanarup greenstones on the other, are particularly significant.

The Ravensthorpe Terrane comprises mainly andesitic and tonalitic rocks, an association that is characteristic of oceanic or continental-margin island arcs (Wilson, 1989; Whalen, 1985). These are regions of high heat-flow (Park, 1988) and it would therefore not be surprising if the Ravensthorpe Terrane were emplaced as a 'hot plate', particularly if thrusting occurred shortly after volcanism and intrusion. Following the thrust model for emplacement of the Ravensthorpe Terrane, the lower plate represented by the Chester Formation and the rest of the Carlingup Terrane would be expected to display initial compression due to loading, as the Ravensthorpe Terrane is thrust over the Carlingup Terrane (Fig. 43A). This would be followed by heating due to thermal re-equilibration (England and Richardson, 1977) as well as heat transfer from the hot upper plate (represented by the Ravensthorpe Terrane). A similar P–T history could be expected for the base of the upper plate because the Ravensthorpe Terrane is an imbricate stack of thrust slices and the lowest of these thrust slices would also record compression and heating (Fig. 47). Chester Formation metapelites display prograde metamorphic

assemblages, and garnet zoning in altered volcanic rocks from the base of the Ravensthorpe Terrane suggests increasing pressure during prograde metamorphism. Interpreted P–T paths for the Chester Formation metasedimentary rocks and the adjacent part of the Ravensthorpe Terrane are therefore consistent with those predicted for the lower plate in a thrust-tectonic regime. The pressure estimate for assemblages in Chester Formation metasedimentary rocks (<3 kb), constrained by the coexistence of chloritoid and andalusite, limits the thickness of the overlying plate, at the time of thermal equilibrium, to about 8–10 km.

Metamorphic P–T–t paths in the upper plate should record decompression and cooling (Fig. 43A). Decompressional P–T–t paths for the Cocanarup greenstones suggest this somewhat enigmatic tectono-stratigraphic unit was thrust, with the Ravensthorpe Terrane, over the Carlingup Terrane. Although a decompression path for the Cocanarup greenstones has been established, there is little evidence for extensive retrograde cooling. In fact, reactions described above suggest a heating path for the Cocanarup greenstones and adjacent Ravensthorpe Terrane rocks. Furthermore, metamorphic isograds are not parallel to the tectonic contact between the two plates (terranes), implying another source of heat that complicated patterns of thermal re-equilibration related to tectonic thickening. These patterns and the prograde decompressional P–T–t paths in the upper plate are attributed to syn-tectonic emplacement of granitoid magmas, as sheets at the base of the Ravensthorpe Terrane and the Cocanarup greenstones. These granitoids are now exposed as gneiss north and west of the Cocanarup greenstones. Similar emplacement of granitoid sheets probably also occurred at the base of the Ravensthorpe Terrane (Fig. 47). The resulting P–T–t paths in upper and lower plates are shown in Figure 43C.

Chapter 6

Geology of the Proterozoic rocks

Proterozoic dolerite dykes

Numerous Proterozoic doleritic dykes, up to several hundred metres thick, intrude the Archaean basement. The dykes are not shown on Plate 1, but are marked on RAVENSTHORPE and COCANARUP. Orientations are variable, but most fall broadly into easterly, east-northeasterly or northwest-trending groups. East-trending dykes may be members of the Widgiemooltha dyke swarm (Myers, 1990b), which is present throughout the Yilgarn Craton (Hallberg, 1987). Dykes trending northwest belong to the Boyagin dyke swarm, and those trending east-northeasterly belong to the Gnowangerup dyke swarm (Myers, 1993). The dykes become deformed close to the contact with the Mount Barren Group but do not intrude the Proterozoic rocks.

Northwest-trending amphibolite dykes intrude the Manyutup Tonalite, between Manyutup Creek and the Phillips River, in association with dacite porphyry dykes. It is not known whether they are feeders to Archaean greenstones or post-cratonization Proterozoic dykes. Although the dykes are metamorphosed, the assemblages are not readily distinguished from Proterozoic dykes, some of which have undergone extensive deuteric alteration.

Mount Barren Group

Proterozoic metasedimentary units on RAVENSTHORPE and COCANARUP were assigned to the Mount Barren Group by Thom and Chin (1984). The age of these rocks is uncertain, but is probably somewhere in the range 1550 to 1300 Ma (Myers, 1995b). Maximum ages of 1850 ± 30 Ma and 1917 ± 13 Ma are provided by the U–Pb in zircon (SHRIMP) ages of detrital zircons from orthoquartzite at Barrens Beach and No Tree Hill, respectively (Nelson, 1996). The base of the Mount Barren Group was interpreted as an unconformity by Sofoulis (1958).

Dolerite and quartz dolerite, referred to as the Cowerdup Sill by Thom and Chin (1984), has intruded the Mount Barren Group. Thom and Chin (1984) recognized and defined three stratigraphic units within the Mount Barren Group. The three units are, from oldest to youngest:

1. the Steere Formation — conglomerate, grit and dolomite (type locality at RAVENSTHORPE AMG 366680);

2. Kundip Quartzite — quartzite (type locality at RAVENSTHORPE AMG 393692);

3. Kybulup Schist — metapelitic schist and phyllite (type locality at RAVENSTHORPE AMG 296502).

A stratigraphic section through these units, all of which occur in the lowest part of the Mount Barren Group, is shown in Figure 48. Extrapolation of these units beyond the lower part of the Mount Barren Group is hampered by structural and stratigraphic complexity. Quartzite and pelitic schist units that lie above the basal section of the Mount Barren Group may represent cyclic deposition within a large, sedimentary basin or alternatively (as interpreted here, and by Thom and Chin, 1984) as thrust repetitions of Kundip Quartzite and Kybulup Schist. The largest unit of dolomite lies above the Kundip Quartzite and is therefore described here as a unit of the Kybulup Schist. Conglomerate units that lie well above the basal part of the Mount Barren Group are not associated with dolomite and these are interpreted as a local facies variant of the Kundip Quartzite. Detailed petrographic descriptions for metasedimentary rocks of the Mount Barren Group and the Cowerdup Sill can be found in Witt (1997).

Steere Formation

The Steere Formation consists of a basal conglomerate and overlying dolomite (Fig. 48). At the type locality, the conglomerate is about 5 m thick. It is overlain by several metres of bedded grit and 4 m of dolomite (Thom et al., 1984). The conglomerate and dolomite are exposed beneath Kundip Quartzite, in the side of a steep escarpment that marks the contact between the Mount Barren Group and the Archaean basement. The units are therefore more widespread than shown on RAVENSTHORPE. The Steere Formation is not laterally continuous but lenses out to the east and west of the type locality, suggesting restricted nearshore deposition or tectonic excision. The dolomite unit also lenses out to the east and west of the type locality. Further west, the conglomerate pinches out, leaving Kundip Quartzite directly overlying Archaean rocks. These lateral

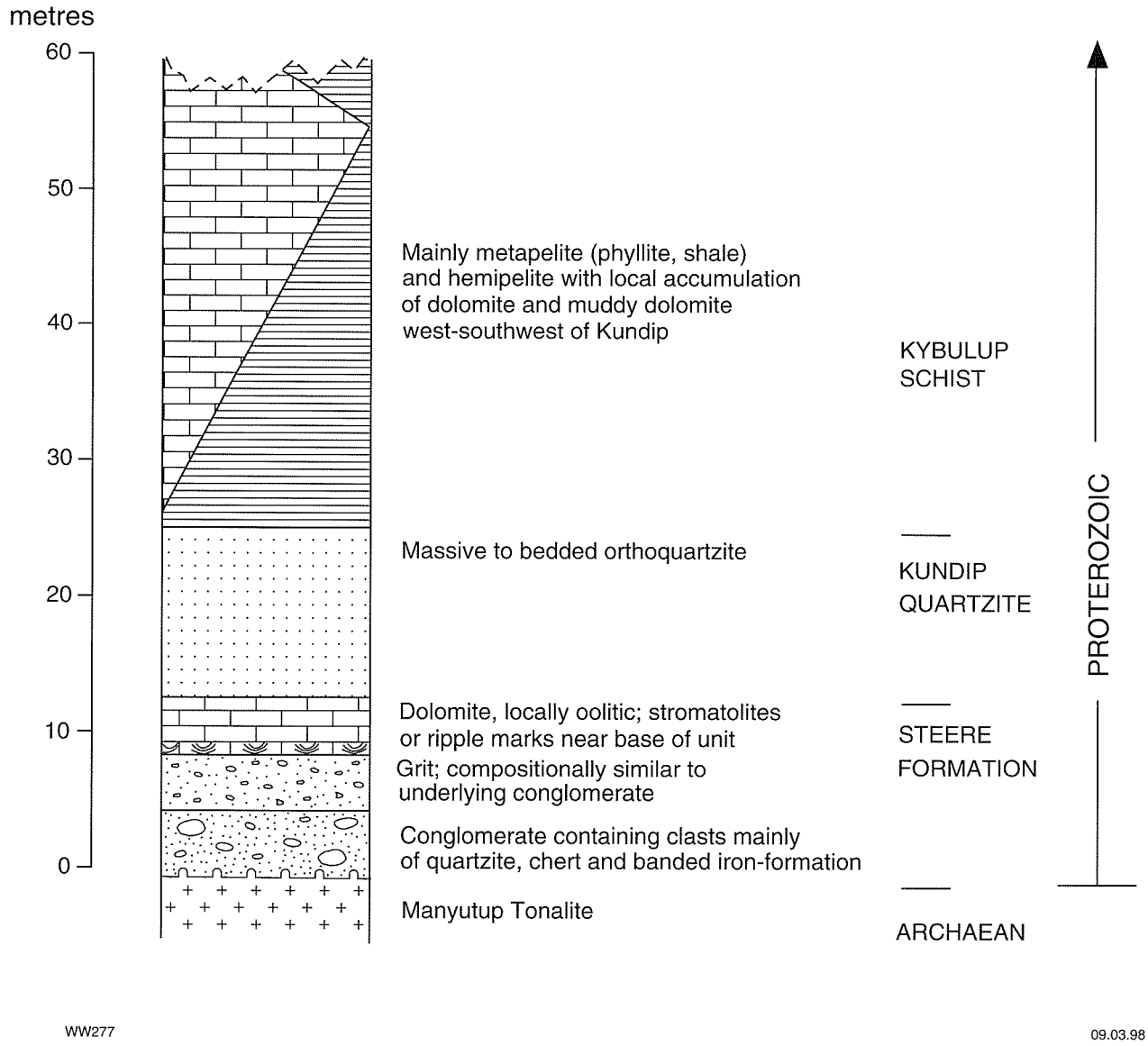

Figure 48. Stratigraphic section through the lower part of the Mount Barren Group, west of Kundip

variations in the rock sequence may reflect facies variations within the Steere Formation but may alternatively have been caused by low-angle thrust faulting on the Archaean–Proterozoic contact (see below).

Massive to weakly deformed, well-sorted to moderately well-sorted conglomerate occurs near the contact with Archaean rocks near Kundip. Well-rounded to subrounded clasts of quartzite, chert, jaspilite (?banded iron-formation), quartz and felsic volcanic rock, up to about 10 cm across, support a metamorphically recrystallized, quartz-rich matrix. The conglomerate passes upward into grit and is overlain by massive to thinly bedded, brown dolomite and dolomitic pelite. Outcrops in the Phillips River (COCANARUP AMG 735576) and west of Kundip (RAVENSTHORPE AMG 366680) have been described as stromatolitic. However, the presence of stromatolites has not been confirmed by palaeontologists, and it is possible that the structures are ripple marks.

Kundip Quartzite

Massive to coarsely bedded orthoquartzite forms a more or less continuous unit at or just above the base of the Mount Barren Group. Beds are a few centimetres to about one metre thick, and dip at 10–30°S. Low-angle, planar cross-bedding and ripple marks are common. These features suggest a shallow (above storm-wave base), marine depositional environment. East of Kundip, near Bandalup Pool, the Kundip Quartzite lenses out and Kybulup Schist directly overlies Archaean rocks. Much thicker units of strongly contorted orthoquartzite and micaceous quartzite are exposed as prominent topographic features such as the Eyre Range, Whoogarup Range and East Mount Barren. The degree of metamorphic recrystallization increases southward from the contact with Archaean rocks, and the quartzite is typically a white to grey to blue-green, fine- to medium-grained, equigranular rock with granoblastic fabric.

Thin lenses and interbeds of conglomerate are found associated with orthoquartzite at several localities between the Archaean contact and the coast. Good exposures can be seen at Barrens Beach (on RAVENSTHORPE) and at East Mylies Beach (on COCANARUP). Quartzite clasts are dominant in these units. Spectacular exposures of poorly sorted oligomictic conglomerate on the north face of the Whoogarup Range, originally mapped as breccia by Thom et al. (1984), contains subrounded to subangular quartzite clasts up to 2 m across.

Kybulup Schist

Structural complexity renders the thickness of the Kybulup Schist indeterminable. The unit varies from weathered quartz–sericite–chlorite schist and phyllite near the contact with Archaean rocks to kyanite-bearing quartz–mica schist that is well exposed on the coast, near East Mount Barren. Kyanite, garnet, staurolite and biotite form prominent porphyroblasts ≤3 mm long in the East Mount Barren area. These schists contain abundant quartz veins, many of which have quartz-poor selvages that contain coarse-grained biotite, garnet, staurolite, kyanite and chlorite.

West of Kundip, Kundip Quartzite is overlain by a substantial thickness of dolomite (locally oolitic) and calc-silicate schist. This carbonate unit appears to be a facies variation of the more typical metapelitic component of the Kybulup Schist and is interpreted to record the presence of carbonate banks surrounded by deeper water depositional environments.

Cowerdup Sill

A metamorphosed dolerite unit, known as the Cowerdup Sill, intrudes the Mount Barren Group within or adjacent to Kundip Quartzite. The Cowerdup Sill, typically about 300 m thick, is broadly conformable with the metasedimentary rocks within fault-bound blocks, but cuts across stratigraphy on a regional scale. Contacts, although rarely observed, are strongly deformed.

The Cowerdup Sill is largely mafic granophyre with abundant quartz and local K-feldspar, suggesting the precursor magma was derived by fractional crystallization of a mafic parent magma, probably in a crustal magma chamber. Pyroxenitic rocks have been observed near the base of the sill at some localities. Thom (1977) also documented petrographic and chemical zoning within the Cowerdup Sill. However, zoning due to magmatic differentiation provided way-up evidence at only a few localities.

Discussion

The Mount Barren Group metasedimentary rocks were deposited in a shallow (above storm-wave base) marine basin that was fed by quartz-rich detritus derived from a continental hinterland. Coarse clastic deposits formed in the shallower part of the basin (represented by the lowermost Mount Barren Group) together with dolomitic carbonate banks. Quartz-rich sand and silt, interbedded with mudstone, were deposited in the deeper parts of the basin. Coarse conglomerate was deposited in restricted channels within the sandstone and mudstone. Although the basal contact with Archaean rocks has been interpreted as an unconformity (Sofoulis, 1958), the contact appears to have been subject to later deformation (discussed below) and there is also evidence that the detritus that forms the Mount Barren Group was not locally derived. Part of the argument for an unconformity was the presence of chert and jaspilite pebbles in the basal conglomerate, which Sofoulis concluded were derived from the underlying Archaean rocks. This argument has been reiterated by Killick and Blackburn (1994). However, exposure of the contact between Archaean rocks and the Mount Barren Group is poor and, at most locations, the contact can only be constrained to within a few metres. The best exposure is 3 km west of Kundip, at RAVENSTHORPE AMG 366680 where, however, the basal conglomerate does not contain clasts of the tonalite that it overlies. Other rocks that are common in the adjacent craton (andesite, basalt and komatiite) are also absent or poorly represented in the Steere Formation clast population. This observation could be interpreted as indicating distal deposition from the underlying Archaean source rocks (Killick and Blackburn, 1994); local deposition over a relatively flat, mature, Archaean erosion surface; or derivation of sediments from a different terrane that advanced upon the Ravensthorpe–Carlingup cratonic assemblage from the southeast (Wetherley et al., 1994). Recent geochronological data support the third interpretation. Nelson (1996) characterized detrital zircons in Kundip Quartzite as 2770–1820 Ma in age. These ages are older than those of orthogneiss and granitoid in the Albany–Fraser Orogen and younger than those of the Ravensthorpe greenstone belt and indicate that the Mount Barren Group metasedimentary rocks were not locally derived (Nelson, 1996).

Chapter 7

Structure of the Mesoproterozoic Mount Barren Group

The structure of the Mount Barren Group is essentially that of a fold-and-thrust belt with north to northwest vergence (Fig. 49). Mesoproterozoic metasedimentary rocks of the Mount Barren Group underwent several phases of folding (Table 3) during the Albany–Fraser Orogeny and have been divided up by numerous faults. Most of the major faults are probably splays off the Jerdacuttup Fault. The Jerdacuttup Fault is a regional-scale reverse fault across which Archaean Munglinup Gneiss to the south has been uplifted and juxtaposed against the younger Proterozoic metasedimentary rocks. The faults that occur within the Mount Barren Group may, however, have had an earlier history related to folding (especially F_{B2} and F_{B3}).

Deformation on the Archaean–Proterozoic contact

The Archaean–Proterozoic contact is marked by a scarp, up to about 20 m high, formed by the gently south-dipping Kundip Quartzite (Fig. 50). Observations described in the previous section raise doubts about the local derivation of the metasedimentary rocks of the Steere Formation and the unconformable nature of the contact between Archaean and Proterozoic rocks. Although Sofoulis (1958) argued for an unconformable contact, his recognition that the Archaean–Proterozoic unconformity has been tectonized, at least locally, has been overlooked in subsequent

WW 329 11.03.98

Figure 49. East Mount Barren (near Hopetoun), formed by southeast-dipping, coarsely bedded quartzite. Metapelitic schist with porphyroblasts of kyanite, garnet and staurolite is exposed on the northern slopes of East Mount Barren (right of photo)

Table 3. Descriptions of folding events in the Mount Barren Group

Fold event	*Average orientation of axial plane*	*Plunge of fold axes*	*Fold shape, vergence*	*Timing criteria*
F_{B1}	Diverse, ?recumbent, poorly constrained	Diverse, poorly constrained	Isoclinal, vergence unknown	Fold closures in limbs of F_{B2} and F_{B3} folds
F_{B2}	East–west	Shallow to moderate (<40°)	Moderately tight to tight, overturned, vergence to north	Minor F_{B2} buckling of F_{B2} fold limbs in Whoogarup Range and west of Fortification Hill
F_{B3}	230–240°	Moderate (35–60°) southwest and northeast (shallow in areas of plunge reversal	Moderately tight to tight, overturned, vergence to northwest	Mesoscopic F_{B2} folds refolded by F_{B3} near Laurina Road
F_{B4}	Southwest to southeast	35–75° south, locally steeply to north	Open to moderately tight, small-scale, upright to steeply inclined	Small-scale buckling and warping of F_{B2} and F_{B3} folds

descriptions. Sofoulis (1958) stated that 'the plane of unconformity is also a plane of low-angle thrusting and dips 7–12° in a southerly direction'. He further judged thrusting on the contact to be 'mild' and of 'no great magnitude', and concluded that the present distribution of sedimentary units is more or less that of original deposition.

The following is cited as evidence for significant tectonic movement focused on the basal contact of the Mount Barren Group.

1. One or more tectonic fabrics are developed in pervasively foliated metapelitic schist adjacent to the contact.
2. Lithostratigraphic units display low-angle discordance with the contact. The idealized basal stratigraphy shown in Figure 48 exists only around Kundip. Elsewhere, quartzite, dolomite or even phyllitic schist directly overlies the contact.
3. Macroscopic fold structures occur within a few kilometres of the contact. Mesoscopic fold closures are also present in phyllite, within 250 m of the contact with Archaean rocks, although these reflect late, east–west compression, not northward-directed thrusting.
4. Southwest of Bandalup Pool, bedding in the basal Kundip Quartzite unit strikes northwest to north, and dips at moderate angles to the northeast, indicating a major fold axis ($?F_3$) intersection with the Archaean–Proterozoic contact in this area.

The low-angle discordance of units against the Archaean–Proterozoic contact may reflect substantial movement involving sheets of Mount Barren Group units that were thrust over the Archaean southern Yilgarn Craton foreland (Fig. 51; Plate 1). Quartz-rich units near, and to the south of, Bandalup were previously interpreted as Archaean chert (Thom et al., 1977). However, these units are associated with quartz-pebble conglomerate and are difficult to correlate with any Archaean units in the Carlingup Terrane. An alternative interpretation is that the quartz-rich units are thrust slices of the Mount Barren Group structurally overlying the Archaean. It is also notable that Abeysinghe (1996) found a nickel-rich sample of magnesite near the Archaean–Proterozoic contact, west of Kundip, and concluded that it was derived from an ultramafic rock rather than dolomite of the Steere Formation or the Kybulup Schist. It is possible that slices of Archaean ultramafic rock were brought up along low-angle thrust faults within the Mount Barren Group. Finally, it is noted that if the interpretation of Steere Formation dolomite as stromatolitic is correct, the stromatolites are upside down (Fig. 52). These structures are characterized by rounded, convex-downward surfaces separated by upward-pointing cusps, opposite to the normal arrangement for stromatolites. Therefore, if these structures are stromatolites, even the lowest dolomite units near Kundip are overturned — with radical implications for the nature of the Archaean–Proterozoic contact.

Deformation within the Mount Barren Group

The Mount Barren Group is divided into five structural domains by major northeast to east-northeast faults (Fig. 51). The northern structural domain 1 is characterized by relatively low strain and a gently refolded east–west fold of uncertain geometry. The remaining domains are more intensely deformed. Domain 2 is dominated by moderately tight, overturned folds with east–west axial planes. Domains 4 and 5 are dominated by overturned folds with northeast–southwest axial planes. Domain 3 has elements of both fold sets. The dominant fold set in each domain is characterized by vergence to the north or northwest (Figs 49, 53).

Tectonic fabrics are generally not well-preserved in orthoquartzite, conglomerate and dolomite, but up to three foliations are preserved in metapelitic schist and phyllite.

Figure 50. Scarp (about 20 m high) formed by Kundip Quartzite, west of Kundip. Bedding in quartzite dips shallowly (10–20°) to the south (away from the viewer)

The main metamorphic fabric in the schists is defined by oriented micas and fine-scale segregation of quartz and micas. Bedding is completely transposed in many samples but is locally preserved, particularly in fold hinges. Probable S–C fabrics, recognized in thin section, may be related to local zones of faulting. Thin units of mafic schist after doleritic rocks also preserve a strong tectonic fabric defined by seams of chlorite(–muscovite–biotite), which anastomose around relatively unstrained quartz and feldspar (Fig. 54A).

Domain 1 (the northern sector)

The northernmost structural domain is limited by the Archaean–Proterozoic contact to the north, and by the Phillips River Fault to the south. It is characterized by relatively low strain, although Kybulup Schist contains one or more of at least two foliations (S_{B2} and S_{B4}) at all localities. The main fold structure has an east–west fold axis (F_{B2}) that has been refolded, on a smaller scale, about northwest to north-northwest axes (F_{B4}). Photo-scale fold closures within quartzite in the limbs of F_{B2} structures (e.g. at No Tree Hill) suggest an earlier period of deformation (F_{B1}). F_{B3} folds and fabrics are poorly developed or absent throughout most of domain 1. However, chevron folds in Kybulup Schist near Pichi Rich (RAVENSTHORPE AMG 292533) have axes that trend 210–220° and refold an earlier generation of folds. The chevron-style folds may have been generated by F_{B3} structures but alternatively could be F_{B4} structures.

Bedding (S_0) and the main foliation (?S_{B2}) in schist adjacent to the Phillips River Fault, near Pichi Rich, have anomalously shallow dips to the north. These unusual attitudes may be related to drag associated with north-side-down movement across the Phillips River Fault.

Domain 2 (the north-central sector)

The north-central sector is bound by the Phillips River Fault to the north and the Annie Peak Fault to the south. It is dominated physiographically by quartzite ridges forming the Eyre Range. Prominent east–west fold structures (F_{B2}), defined by the quartzite units are steeply overturned to the north. Minor fold axes are poorly exposed, but Thom (1977) recorded a prominent linear fabric that plunges 10–40° east. S. Wetherley (1994, pers. comm.) has interpreted this fabric as an intersection lineation formed by bedding (S_0) and the F_{B2} axial planar fabric (S_{B2}), and has noted some shallow west-plunging lineations. This linear fabric indicates that F_{B2} folds in the Eyre Range plunge shallowly to moderately eastward. The F_{B2} folds are gently warped about roughly north–south axes (F_{B4}) resulting in plunge reversals east of the Eyre Range, and refolded structures west of Fortification Hill. D_{B3} is weakly developed in the north-central sector. West of Fortification Hill, a pervasive S_{B2} foliation is overprinted in zones by S_{B3} (210–230°, subvertical to 70° southeast). This deformation locally intensifies to form discrete shear zones. Rotation of S_0 in the northeast extreme of domain 2 may have been caused by F_{B3}.

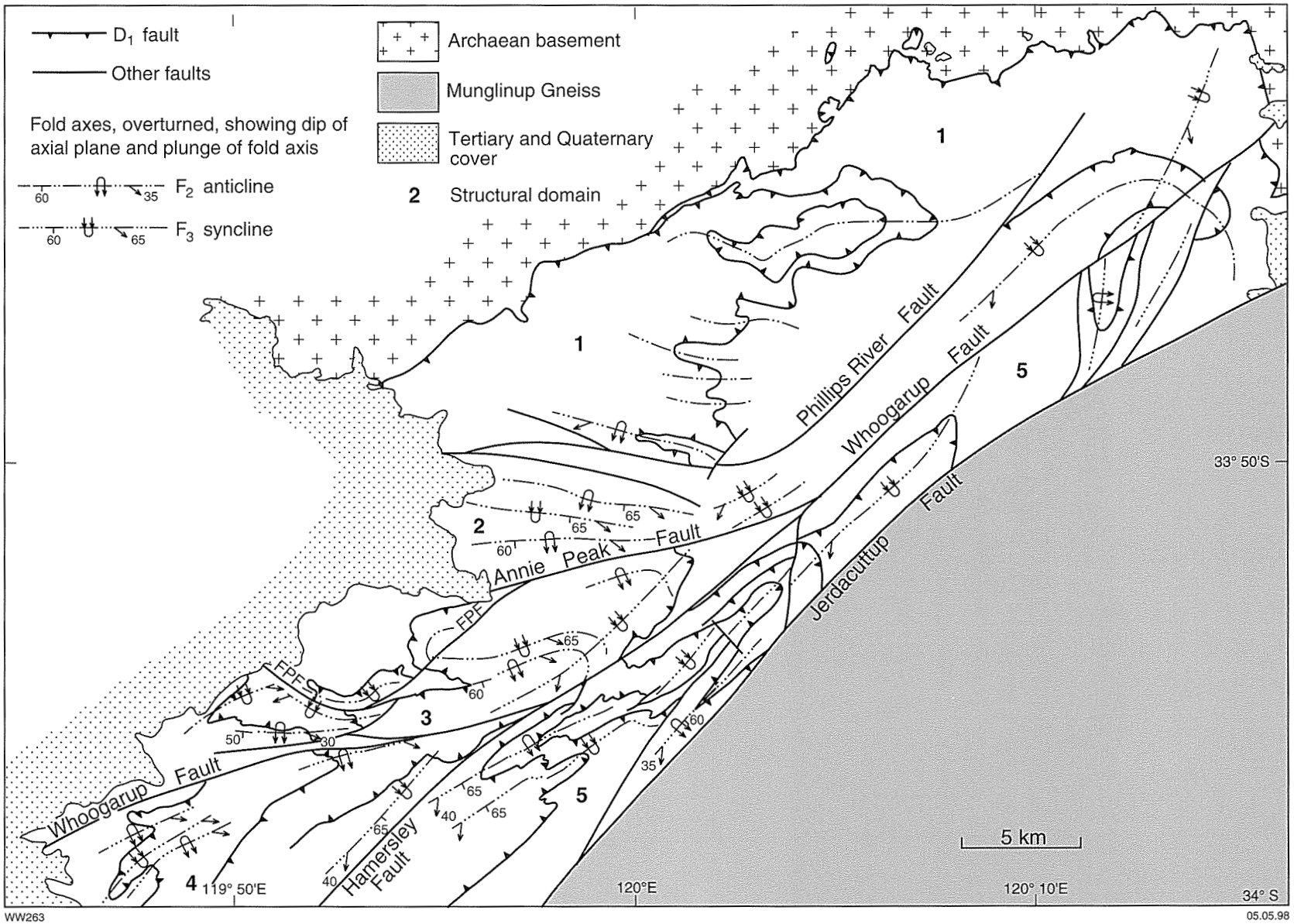

Figure 51. Main structural features and domains in the Mount Barren Group. Numbers 1–5 are structural domains (see text)

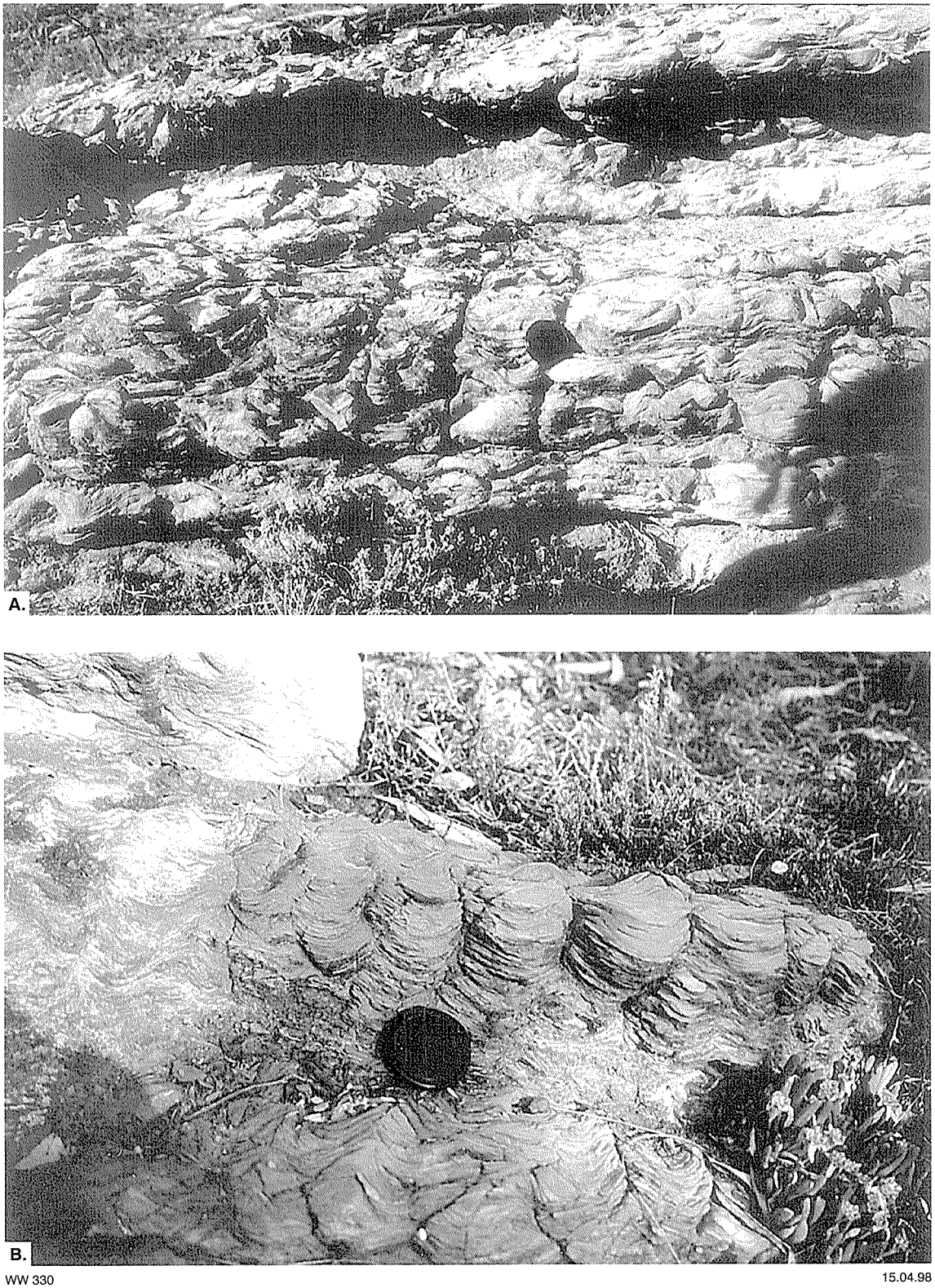

Figure 52. Structures in dolomitic sedimentary rocks of the Steere Formation, exposed in the Phillips River, south of Cocanarup (COCANARUP AMG 735576). These structures have been variously evaluated as stromatolites or ripple marks

Figure 53. Metapelitic schist (in foreground) and quartzite (bluff in background) of the Mount Barren Group, exposed at West Beach. Note moderate to steeply southeast-dipping foliation (S_{B3}) and mesoscopic F_{B3} fold closures in schists

Figure 54. Metamorphic fabrics and textures in the Mount Barren Group and Cowerdup Sill

A: Feldspar porphyroclast with asymmetric tails indicating simple shear, in quartz–chlorite–feldspar schist after mafic rock (?Cowerdup Sill). GSWA 113949, plane-polarized light, field of view approximately 2 mm
B: Early, crenulated quartz–mica foliation ($?S_{B1}$) in low-strain domain between dominant S_{B2} (lower left to upper right) in metapelitic schist from Mount Barren Group. GSWA 113956, plane-polarized light, field of view approximately 2 mm
C: Early foliation ($?S_{B1}$) preserved as inclusion trails (quartz, biotite, opaques) in garnet porphyroblast. The dominant foliation (S_{B3}, lower left to upper right) is defined by elongate staurolite porphyroblasts with numerous quartz inclusions. GSWA 113956, plane-polarized light, field of view approximately 4 mm
D: Early foliation ($?S_{B1}$) preserved as inclusion trails of quartz and opaque oxide minerals in biotite 'fish', metapelitic schist of Mount Barren Group. The dominant foliation (S_{B3}, left to right) is formed by oriented muscovite and biotite. GSWA 113953, plane-polarized light, field of view approximately 5 mm
E: Early foliation ($?S_{B1}$) preserved as inclusion trails of opaques, quartz and tourmaline in garnet porphyroblast, metapelitic schist of the Mount Barren Group. The dominant foliation (S_{B3}, lower left to upper right) is defined by quartz–mica banding and oriented muscovite (beneath garnet porphyroblast in photomicrograph). GSWA 113955, plane-polarized light, field of view approximately 1 mm
F: Biotite porphyroblast oriented at a high angle to the main foliation (S_{B3}), metapelitic schist, Mount Barren Group. The dominant foliation (S_{B3}, lower left to upper right) is defined by oriented muscovite and biotite. GSWA 113956, plane-polarized light, field of view approximately 3 mm
G: Sigmoidal inclusion trails in garnet porphyroblast define an early foliation ($?S_{B1}$) in contrast to staurolite porphyroblast (below garnet in photomicrograph) that overgrows S_{B3} (the dominant foliation, left to right but locally deflected about the top of the garnet porphyroblast). GSWA 113955, plane-polarized light, field of view approximately 2 mm
H: Sprays of sillimanite oriented at a large angle to the dominant foliation (S_{B3}), metapelitic schist, Mount Barren Group. The dominant foliation (lower left to upper right in photomicrograph) is defined by oriented biotite and muscovite. GSWA113956, plane-polarized light, field of view approximately 2 mm

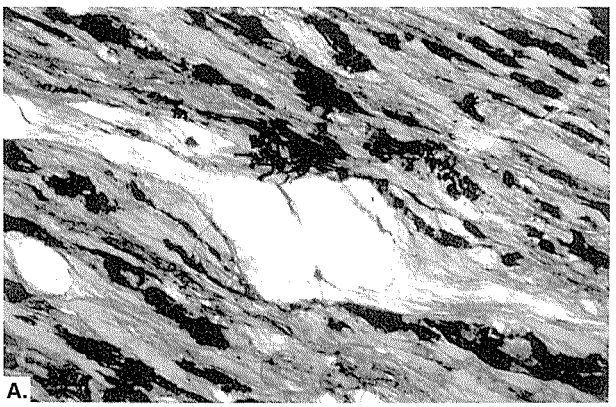
A.


B.

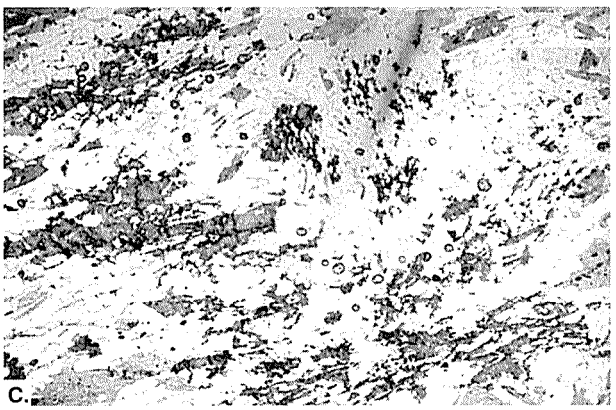
C.


D.

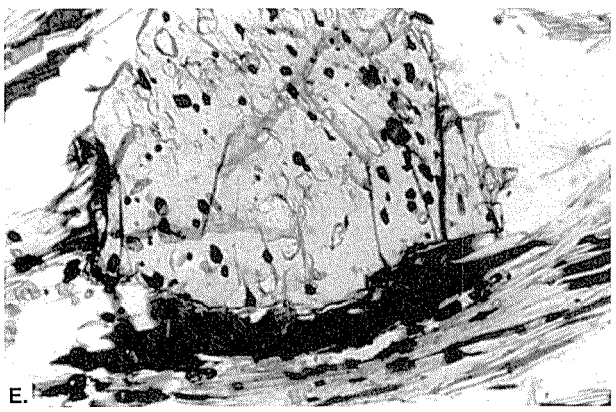
E.

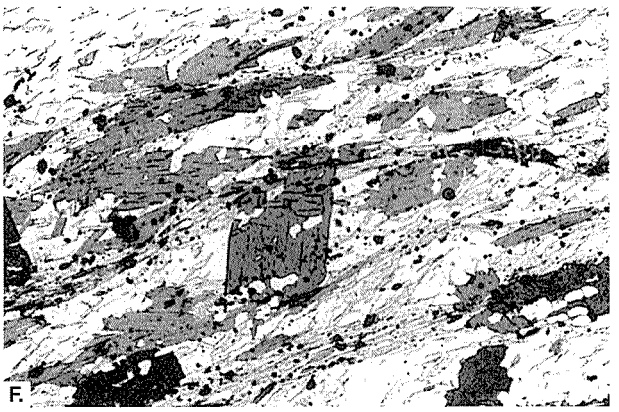
F.


G.

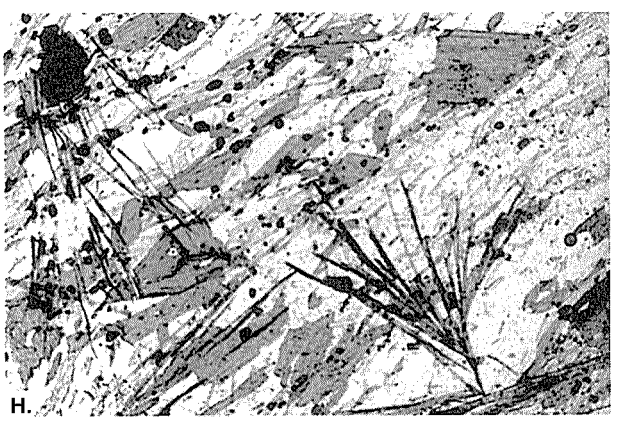
H.

WW 332 11.03.98

Domain 3 (the south-central sector)

The south-central sector, the most structurally complex domain, is bounded by the Annie Peak Fault to the north and the Whoogarup Fault to the south. East–west (F_{B2}) folds are overturned to the north. They have been refolded by a F_{B3} syncline, and are broadly warped about roughly northerly to north-northwest (F_{B4}) axes. Interference between early (F_{B1}) folds and later (F_{B4}) folds produced dome-and-basin structures in the limbs of F_{B2} and F_{B3} folds (e.g. Hamersley River, COCANARUP AMG 680438; Sepulcralis Hill, COCANARUP AMG 727447; and south of Annie Peak, COCANARUP AMG 752457 and 764464).

F_{B2} fold limbs in the Whoogarup Range are overprinted by a 230° foliation and minor folds with 230° axial planes. These latter folds could conceivably be well-developed D_{B4} folds but are interpreted as D_{B3} structures because exposures along the coast indicate that southwest-trending F_{B4} folds become less prevalent westward from West Beach.

South of Sepulcralis Hill, four separate phases of folding are exposed in Kybulup Schist. F_{B2} folds are overprinted by F_{B3} and S_{B3} (240°, axial planes dip subvertical to 70° southeast) and F_{B4}. F_{B4a} (north–south axial planes) has caused plunge reversals in F_{B2} folds. F_{B4a} folds themselves display variable plunge and pitch directions, suggesting they pre-date minor folds (F_{B4b}) that are overturned to the northeast and plunge steeply northwest.

An east–west fold axis adjacent to the Whoogarup Fault, where it is cut by the Hamersley River, may be a truncated F_{B2} fold, or may be en echelon folding resulting from a sinistral component of slip on the Whoogarup Fault.

Domain 4 (southern sector)

The southern sector is confined between the Whoogarup Fault in the north and the Hamersley Fault in the southeast. Good exposures occur along the coast. Dominant fold structures (F_{B3}) in this sector are overturned to the northwest and those around Quoin Head plunge northeast. Some minor fold axes (F_{B4}) at east Whalebone Beach have southeast-trending axial planes and fold axes that plunge 50–65° southeast. F_{B3} fold axes are closely spaced between Quoin Head and Whalebone Beach, but less well-developed between Whalebone Beach and Hamersley Inlet. Between Whalebone Beach and the Hamersley Fault, bedding and S_{B3} have been rotated into an east-southeast orientation. Minor fold asymmetry and bedding–cleavage relationships suggest the presence of a major F_{B3} synclinal axis in this location. Bedding and S_{B3} are gently warped about 190°, 70° west (F_{B4}).

Mesoscopic isoclinal folds within F_{B3} fold limbs occur in Kybulup Schist at west Whalebone Beach (COCANARUP AMG 626371) and are defined by quartz veins at Quoin Head (COCANARUP AMG 600360). These may be F_{B1} or F_{B2} folds. Although F_{B2} folds in the Eyre Range are not isoclinal, F_{B2} folds in domain 4 may have been tightened during refolding by a relatively intense D_{B3} event.

An east–west fold axis adjacent to the Whoogarup Fault could be interpreted as en echelon folding related to sinistral movement across the fault, or as an F_{B3} fold that was rotated during dextral movement on the fault.

Domain 5 (the southeastern sector)

The southeastern sector is bounded by the Hamersley Fault to the northwest and the Jerdacuttup Fault to the southeast. The dominant folds are tight to moderately open, overturned folds (F_{B3}) with axial planes that strike 230° and dip 50–70° southeast, and fold axes that plunge 35–60° southwest (Fig. 55). A weak linear fabric defined by the preferred orientation of elongate metamorphic minerals and aggregates exists locally, in zones, and plunges steeply east-southeast, approximately normal to the F_{B3} plunge direction. F_{B3} folds are also the dominant mesoscopic structures in northeastern domain 5 where Kybulup Schist is exposed near the Jerdacuttup River (RAVENSTHORPE AMG 476626).

Along the coast, S_{B3} forms a pervasive fabric but an earlier foliation is locally preserved in low-strain areas of quartz-rich bands (Fig. 54B). Isoclinal fold closures, locally preserved in the limbs of F_{B3} folds, may be F_{B1} or F_{B2} folds that have been tightened during refolding. Near Laurina Road (RAVENSTHORPE AMG 384565), pre-F_{B3} folds are exposed in weathered schist. These earlier folds are not isoclinal and are interpreted as F_{B2} rather than F_{B1} folds.

Later folding events (F_{B4}) that cause minor refolding of F_{B3} fold axes include:

1. folds with axial planes that trend 210–220°. This event produced macroscopic folds near East Mount Barren, but its effects are reduced to gentle, open warping and crenulation of F_{B3} and S_{B3} near Hamersley Inlet;

2. Southeast-trending folds that plunge 50–65° southeast.

Quartz veins

Quartz veins are common in Kybulup Schist in all areas, but well-preserved exposures are only seen along the coast, in domains 4 and 5. Abundant quartz veins at Barrens and West Beaches are mostly subparallel to S_0 and have been boudinaged and folded during F_{B3} (Fig. 56). Some veins cut across D_{B3} structures. A few veins form isoclinal folds in F_{B3} fold limbs. These observations suggest that veins formed over a protracted deformation interval involving at least D_{B2} to D_{B4}. Coarse-grained assemblages rich in kyanite–biotite (–garnet–staurolite) adjacent to these veins are interpreted as metamorphically recrystallized alteration selvages (Fig. 56).

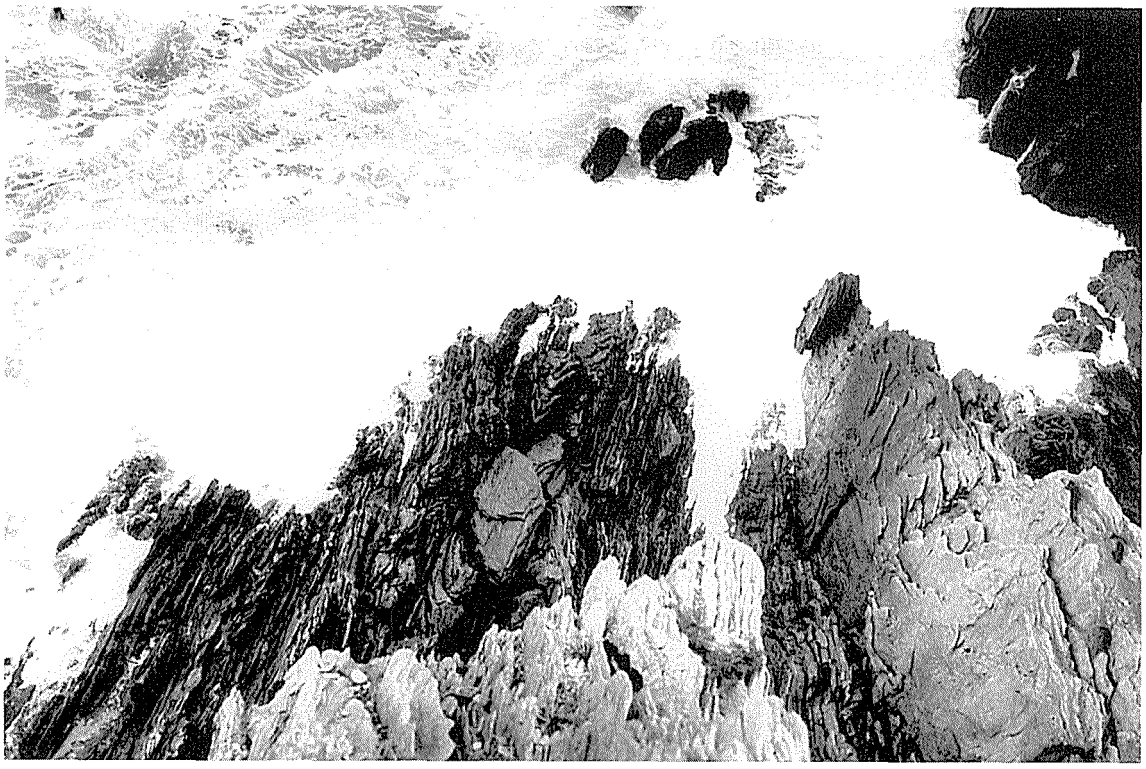

Figure 55. Mesoscopic F_{B3} folds and S_{B3} in finely interbedded metapelitic schist and micaceous quartzite in the Mount Barren Group, east end of West Beach. Axial planar foliation (S_{B3}) dips southeast (left of photo) and fold axes plunge 30–40° southwest (away from viewer). In foreground, the width of photo is about 5 m

Faults

It is likely that fault formation and movement accompanied each of the first three phases of folding. Interpreted D_{B1} low-angle thrust faults caused repetition of the original stratigraphic succession and are based on the assumption of a single transgressive sedimentary sequence (i.e. only one quartzite unit and one schist unit). The locations of these D_{B1} faults, shown on Plate 1 and in Figure 51, are not the same as those proposed by Thom (1977) and Thom et al. (1984).

Many F_{B2} and F_{B3} fold closures have been truncated by faults that are subparallel to axial planes of the folds and are interpreted to be more or less coeval with folding. For example, a truncated F_{B2} fold occurs at Fingerprint Hill (COCANARUP AMG 648429). Truncated F_{B3} folds are common along the coast between Barrens Beach and Quoin Head. Some of these faults (e.g. the Fingerprint Fault) are broadly warped in a similar fashion to F_{B2} and F_{B3} fold axes, consistent with formation prior to F_{B4}.

Faults with F_{B2} and F_{B3} axial planar orientations, including those that bound structural domains (Fig. 51; Plate 1), are largely interpreted on the basis of map and photo patterns. They are difficult to access and are only rarely exposed, along the coast. Many of these interpreted faults are coincident with prominent photo-lineaments defined by drainage. However, most of these drainage systems are choked with vegetation, preventing meaningful observations. S–C fabrics and other kinematic indicators of simple shear (Fig. 54A) observed in some schists are probably related to movements on these faults. The isolated occurrence of dolomite, interleaved with metapelitic schist, near Hamersley Inlet, suggests the presence of a major fault along which dolomite has been brought up from deeper levels. The dolomite contains numerous quartz veins and is locally brecciated. Sheeted quartz veins trend about 230° and dip steeply southeast, and are presumed to mimic the orientation of the Hamersley Fault. Similarly, a slice of ultramafic schist interleaved with metapelites at west Whalebone Beach suggests the presence of a fault, though this structure may be of less regional significance than the Hamersley Fault.

Most of the major faults shown on Fig. 51 and Plate 1 are probably splays off the Jerdacuttup Fault. These splays reactivated earlier formed faults that were related to folding and had an appropriate orientation. The increase in metamorphic grade toward the Jerdacuttup Fault (see below) suggests mainly reverse movement on the splay faults, consistent with uplifted deep crust (Munglinup Gneiss) south of the Jerdacuttup Fault. However, there is some evidence, in the form of possible en echelon folding, for a lateral component of movement across some faults. For example, structural domain 3 may have been extruded westward within a mainly north–south compressional regime.

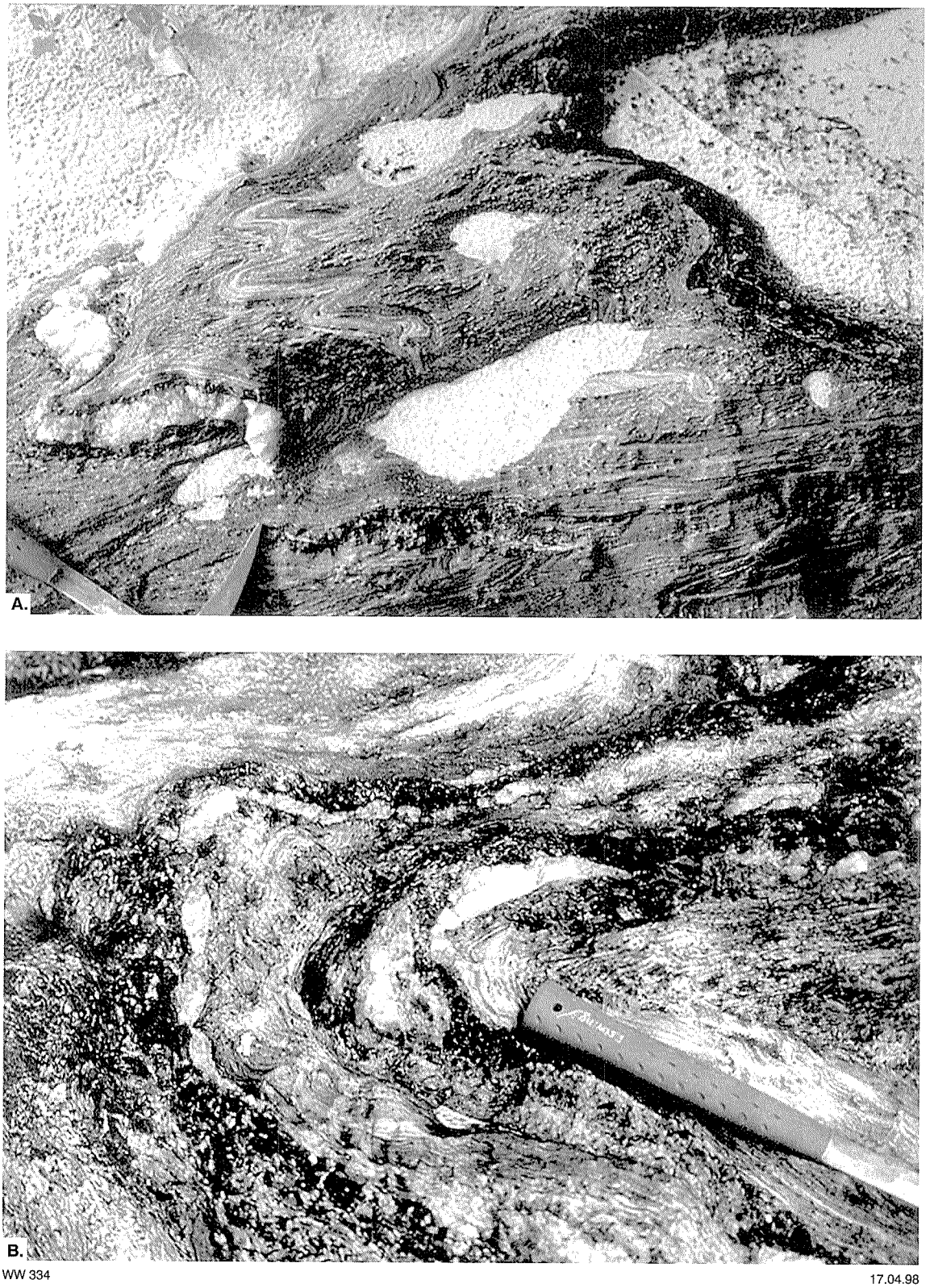

Figure 56. Mesoscopic F_{B3} folds and quartz veining in metapelitic schist, Mount Barren Group. A: Barrens Beach; B: West Beach. In both photos, note the dark selvages adjacent to veins, which consist mainly of coarse-grained biotite, garnet, staurolite and kyanite

Summary and discussion

The structure of the Mount Barren Group is essentially that of a fold-and-thrust belt with north to northwest vergence (Fig. 57). The four phases of deformation, summarized in Table 3, are equivalent to the six phases of folding reported by Wetherley et al. (1994). The extra phases of folding described by Wetherley et al. (1994) are only locally developed and are not recognized as regional events in this report. Recumbent folding (F_{B1}), which is poorly developed or more difficult to recognize than in the western part of the Mount Barren Group basin (Wetherley et al., 1994), was followed by two phases of upright to overturned folds (F_{B2} and F_{B3}). The relative timing of F_{B2} (east–west folds in domain 2) and F_{B3} (southwest-plunging folds in domain 5) is poorly constrained, although the interpretation presented here is consistent with interpretations by Wetherly et al. (1994) and Myers (1990a). Whereas F_{B2} is dominant in those parts of the basin that are closest to the Archaean craton, F_{B3} folds are increasingly dominant in more distal areas, especially between the Whoogarup and Jerdacuttup Faults.

The last phase of folding (F_{B4}), involving a range of fold orientations from southwest to southeast, had a relatively minor impact on outcrop patterns. However, this final phase of folding was responsible for the reversal of F_{B3} plunge directions east of Whalebone Beach and of F_{B2} plunge reversals elsewhere. Plunge directions are rotated about broadly north–south axes, suggesting formation in an east–west compressional regime. The orientations of fold axes during D_{B2} through to D_{B4} suggest a progressive rotation of σ_1 from north–south to east–west. Northwest and northeast F_{B4} fold axes may be related to rotation of bedding adjacent to complementary D_{B4} faults.

Each of the first three phases of folding was accompanied by movement on reverse faults, some of which caused shearing and truncation of fold closures. These faults were reactivated as splays off the Jerdacuttup Fault during the final stages of the orogenic event when deeper basement rocks to the south were uplifted and juxtaposed against younger, shallower rocks of the Mount Barren Group and the Archaean granite–greenstone terranes.

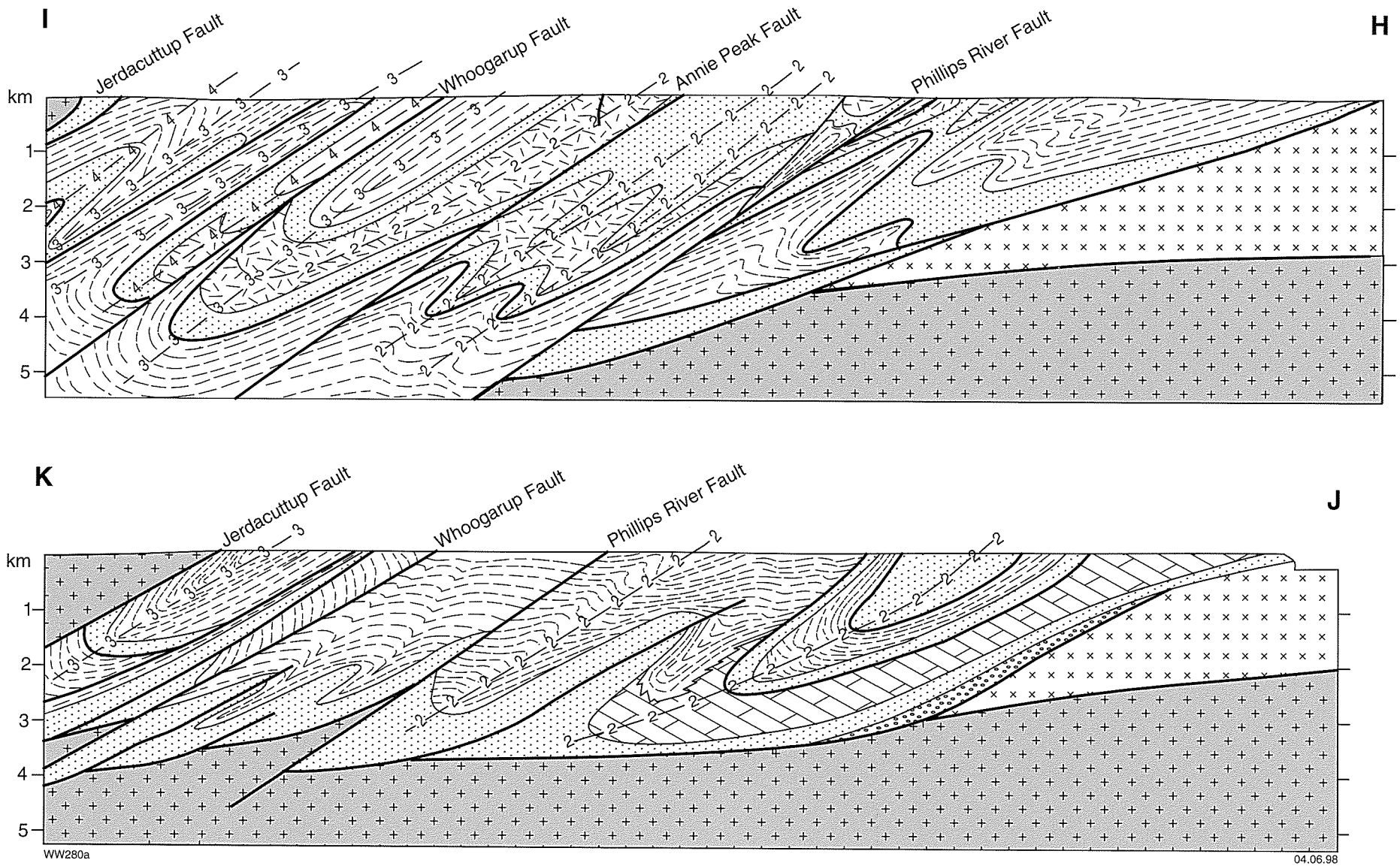
I
H
K
J
Jerdacuttup Fault
Whoogarup Fault
Annie Peak Fault
Phillips River Fault
km
1
2
3
4
5
WW280a
04.06.98

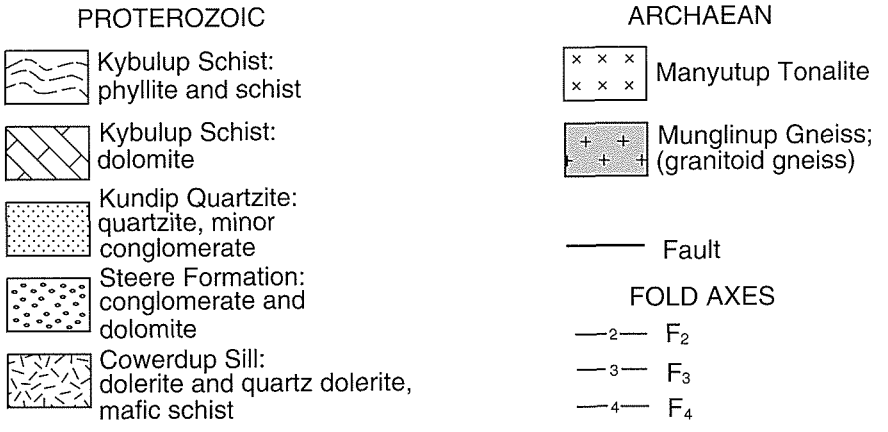

Figure 57. Interpreted cross sections through the Mount Barren Group. See Plate 1 for locations of sections H–I and J–K

Chapter 8

Proterozoic metamorphism

Regional metamorphic grades in the Mount Barren Group metasedimentary rocks are constrained by assemblages in the Kybulup Schist. The absence of biotite and chloritoid in widespread quartz–muscovite(–chlorite) schist between the contact with Archaean rocks in the north and the Phillips River Fault indicates metamorphic conditions below the biotite isograd at about 400°C (PL in Fig. 58). The presence of biotite and andalusite in pelitic rocks immediately north of the Phillips River Fault suggests that these rocks lie within the biotite zone (of Barrow, 1893; see also Myashiro, 1973; Yardley, 1989; Spear, 1993). Andalusite may have been produced by reaction (B1).

$$\text{Pyrophyllite} \rightarrow \text{andalusite} + \text{quartz} + H_2O \qquad \text{(B1)}$$

The presence of andalusite indicates pressures of <3.8 kb (Fig. 58). The local presence of high-Al rocks may result from hydrothermal alteration related to fluids that moved up the Phillips River Fault. The absence of chloritoid at these temperatures implies a relatively magnesian (Fe-poor) composition for the pelites, consistent with the paucity of biotite and chlorite at lower metamorphic grades.

The absence of any porphyroblasts in structural domains 2, 3 and 4 of the Mount Barren Group requires temperatures below about 400°C, or quite specific bulk-rock compositions that lie on the muscovite–phlogopite tie line of an AKM diagram (cf. Spear, 1993, fig. 10-6).

In structural domain 5, pelitic rocks exposed along the coast between Barrens Beach and West Beach, and immediately north and west of East Mount Barren contain the equilibrium assemblage quartz–muscovite–biotite–garnet–staurolite–kyanite. This is equivalent to the kyanite zone of Barrow (1893) and implies the elimination of chlorite by reaction (B2).

$$\text{Staurolite} + \text{chlorite} \rightarrow \text{biotite} + \text{kyanite} + H_2O \qquad \text{(B2)}$$

This reaction imposes minimum temperatures of about 600°C and 6 kb (PH in Fig. 58). An upper pressure limit is less precisely constrained to <11 kb (approximately) by the stability of ilmenite rather than rutile in kyanite-bearing schists. Therefore, assemblages in the kyanite-bearing schists between Barrens and West Beaches fall within bathozone 5 or 6 of Carmichael (1978).

Relations between metamorphic minerals and tectonic fabrics

In the West Beach – Barrens Beach area, two main fabrics have been identified. The dominant fabric, S_{B3}, is defined by fine-scale quartz–mica banding, and oriented micas. It forms a pervasive foliation that is axial planar to the main generation of folds (F_{B3}) at these localities. An earlier, bedding-parallel foliation (?S_{B1} or S_{B2}), defined by quartz–mica–tourmaline–opaque oxides, is preserved in F_{B3} fold hinges and elsewhere in low-strain domains, garnet porphyroblasts and biotite 'fish' (Figs 54B–E, G). S_{B3} is deflected around porphyroblasts of garnet. Most biotite is aligned along a spaced S_{B3} fabric and locally biotite aggregates form a linear fabric (L_{B3}) that plunges approximately normal to F_{B3} fold axes (e.g. COCANARUP AMG 751388). However, there is also some late-stage biotite that is oriented at a high angle to S_{B3} and overgrows the S_{B3} fabric (Fig. 54F). These relationships indicate an extended period of growth for garnet and biotite, beginning before D_{B3} and continuing after D_{B3}.

Unlike biotite and garnet, staurolite and kyanite porphyroblasts do not preserve the S_{B1}–S_{B2} fabric but commonly overgrow S_{B3}, and inclusion trails display little or no rotation (Figs 54G, 59). Kyanite is mostly unoriented, except in some (S_{B3}) foliation-parallel zones where it is weakly oriented approximately normal to F_{B3} fold hinges. These relationships suggest that initial staurolite and kyanite growth (late syn- to post-D_{B3}) post-dated early biotite and garnet (syn-D_{B1} to D_{B2}, to post-D_{B3}). These fabric relationships involving biotite, garnet, staurolite and kyanite are consistent with a progressive metamorphic history related to crustal overthickening in which there is a lag between deformation and thermal equilibration (England and Thompson, 1984).

Sillimanite has only been identified in one specimen (from West Beach) where it forms small sprays that grow across the main metamorphic fabric (Fig. 54H). Late growth of sillimanite may be related to prograde metamorphism, if peak thermal equilibration occurred at pressures of about 6 kb, or alternatively it may be related to decreasing pressure during uplift and erosion.

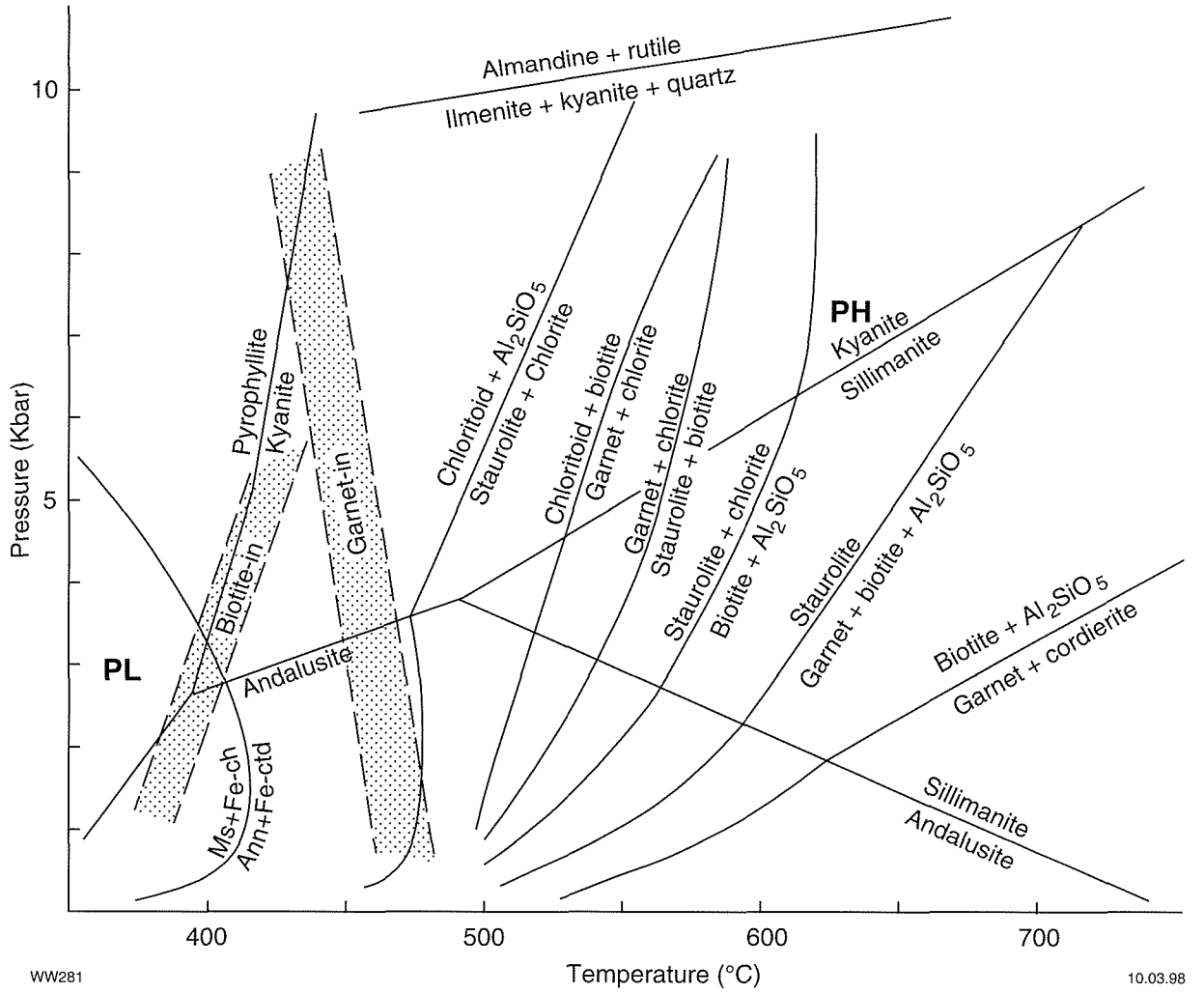

Ann	Annite
Fe-ch	Fe-chlorite
Fe-ctd	Fe-chloritoid
Ms	Muscovite

Figure 58. P–T grid for metapelitic rocks in the Mount Barren Group (after Spear, 1993), showing approximate conditions near the contact with Archaean rocks (PL) and along the coast near East Mount Barren (PH). Reaction: Almandine + rutile ——> ilmenite + kyanite + quartz is taken from Yardley (1989). Biotite-in and garnet-in reaction zones also taken from Yardley (1989)

The metapelites in the West and Barrens Beaches area contain abundant syn-D_{B1} to D_{B2} quartz veins that have been folded and boudinaged by D_{B3} (Fig. 56). The veins have selvages that contain quartz-poor biotite–garnet–kyanite assemblages. These minerals overgrow an earlier fabric defined by opaque oxide minerals (Fig. 60). The opaque oxide fabric is commonly vein-parallel but locally is complexly contorted. The high-temperature assemblage in the vein selvage is interpreted as a metamorphosed alteration selvage. Porphyroblast–fabric relationships are similar to those outside the vein selvages but biotite is unoriented or oriented at a large angle to vein margins and S_{B3}, suggesting that most of the biotite in the vein selvage formed by reaction (B2).

Discussion

The metamorphic assemblage in kyanite-bearing schists of the Mount Barren Group constrains metamorphic conditions to T >600°C and P >6kb (Fig. 58). Minimum pressure estimates are equivalent to about 20 km depth.

The late syn- to post-D_{B3} growth of kyanite suggests growth as a result of burial beneath a metasedimentary pile that was thickened, first by low-angle thrusting and recumbent folding (D_{B1}), and subsequently by relatively high-angle D_{B2} and D_{B3} folding and reverse faulting. If these events were progressive, the time lag between burial and heating (England and Richardson, 1977; England and

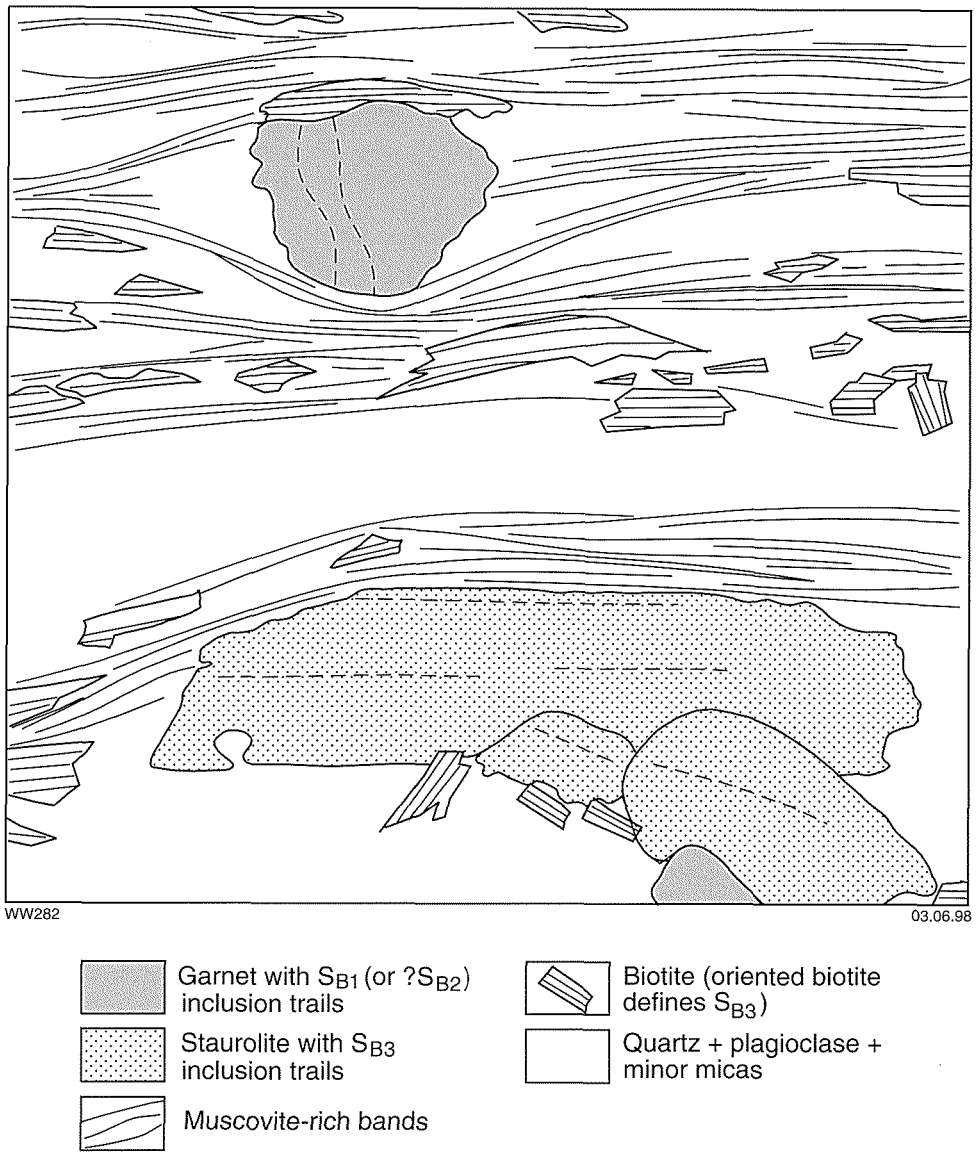

Figure 59. Sketch of mineral–fabric relations in metapelitic schist, Mount Barren Group. GSWA 113955, based on print of a microfiche image of a thin section. Note that the dominant foliation (S_{B3}) is deflected about garnet porphyroblasts near top of figure and immediately below figure but is preserved without rotation in staurolite

Thompson, 1984; Zen, 1988) may account for the restricted nature or absence of kyanite growth during D_{B1} and D_{B2}.

Uplift of deeply buried metasedimentary rocks in the West Beach and Barrens Beach area probably took place during later reactivation of syn-D_{B2} and syn-D_{B3} faults (e.g. the Whoogarup Fault). Although such faults may initially have formed during D_{B2} and D_{B3}, major uplift across the reactivated faults post-dated kyanite growth during and immediately after D_{B3}. Uplift was probably a response to isostatic re-equilibration of the over-thickened crust (England and Richardson, 1977). Passive, differential uplift across late faults produced little or no retrograde metamorphism in fault-bound blocks and no late fabric related to the uplift. The absolute timing and rate of uplift is uncertain but there is evidence that it substantially post-dated peak metamorphism, allowing time for metamorphic isograds to equilibrate with depth and become essentially flat lying. This implies relatively slow uplift rates (England and Thompson, 1984). The late faults are rarely exposed, but they have been observed along the coast between Mylies Beach and Quoin Head. The greenschist facies quartz–talc–chlorite–tremolite assemblage in a fault zone at the west end of Whalebone Beach suggests uplift was associated with retrograde metamorphism. A substantial period of time between D_{B3} and uplift is suggested by the presence of porphyroblasts on the down-thrown side of the faults, along the coast between West Beach and Quoin Head, and also on the north side of the Phillips River Fault, at Pichi Rich. Drag associated with reverse movement on southeast-dipping

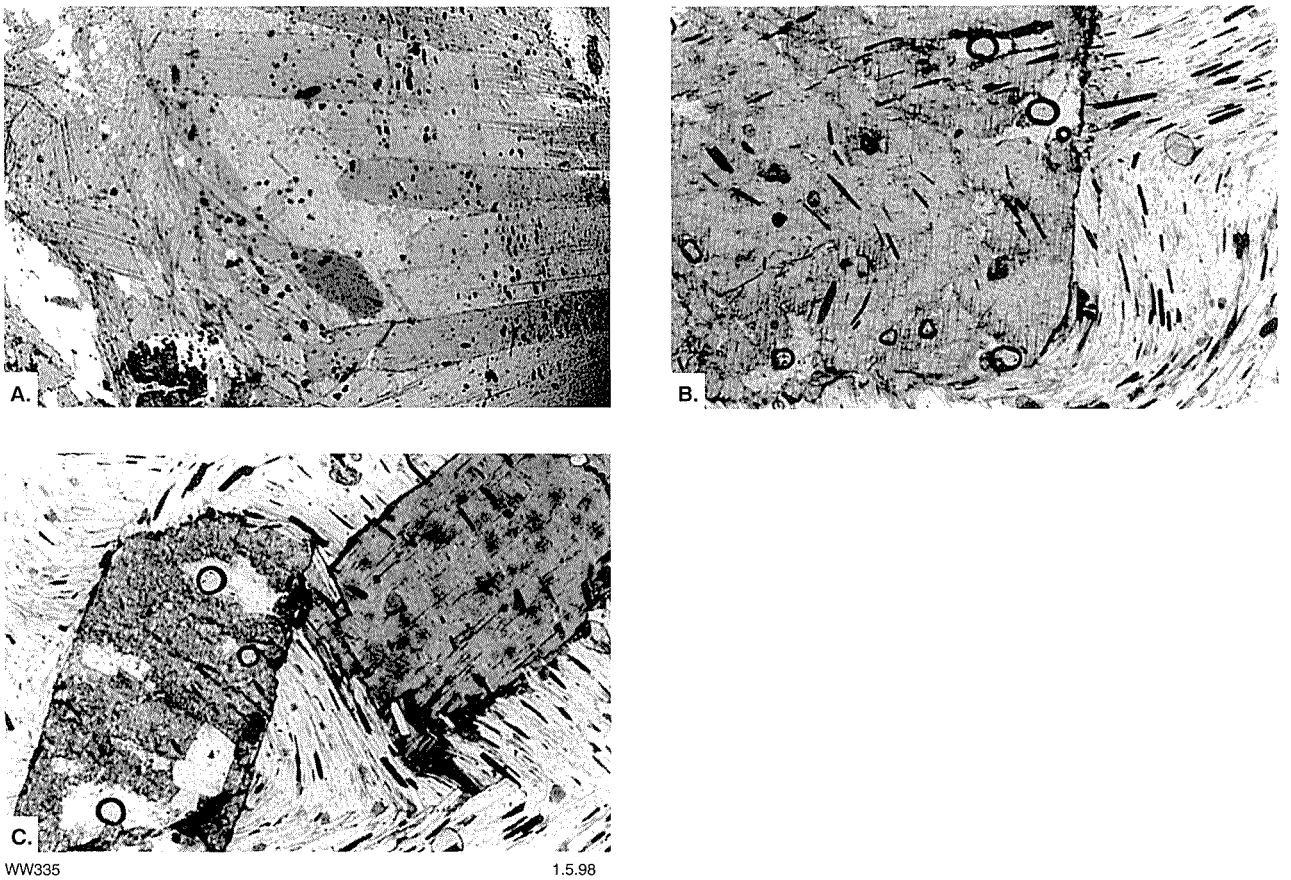

Figure 60. Metamorphic fabrics and textures in vein selvages, metapelitic schist, Mount Barren Group

A: Coarse biotite in vein selvage oriented at a high angle to vein and S_{B3} in adjacent schist. Note that S_{B3} (top to bottom of photo) in schist (left of photo) is defined by quartz–mica banding and oriented biotite, and also by opaque oxide inclusion trails in biotite-rich vein selvage. GSWA 113956, plane-polarized light, field of view approximately 1 mm
B: and C: Contorted early muscovite–opaque oxide fabric overgrown by kyanite in vein selvage. GSWA 113958, plane-polarized light, field of view approximately 0.2 mm

faults would cause local upward deflection of flat-lying metamorphic isograds adjacent to the faults. The Jerdacuttup Fault is the largest of the late faults associated with uplift. This structure has brought Archaean basement (Munglinup Gneiss) to the surface, south of the fault. Myers (1990a) has suggested that these Archaean, mainly granitoid, gneisses have been retrogressed from the granulite facies. Thus, progressively deeper crustal sections have been uplifted across these late faults, southward from the Archaean–Proterozoic contact.

The interpretation proposed here, which attributes exposure of deep crustal rocks to post-deformational differential uplift, is essentially the same as that described by Wetherley et al. (1994) but is different from that of Myers (1995a), who envisaged the deep crustal rocks as having been thrust upward during the Albany–Fraser Orogeny.

Chapter 9

Economic geology

The Ravensthorpe area has had a long history of mining and has produced a wide variety of mineral commodities. Copper was first mined in 1899 and the area produced 20 115 t of copper up until 1971 when the last operating mine (Elverdton) closed down. This total amounts to nearly half of the State's copper production. In addition, 4 000 kg of gold and 2 580 kg Ag have been produced, commonly from the same lodes that produced copper (Marston, 1979). Resource figures quoted below are from the Department's MINEDEX* database unless otherwise indicated.

Epigenetic copper, gold and silver

Descriptions of epigenetic copper–gold(–silver) mineralization in the Ravensthorpe area have been compiled by Sofoulis (1958) and Marston (1979). A recent study of mineralization around Kundip and Mount Desmond was completed by Savage (1992). During this study, a further attempt was made to evaluate the distribution and nature of this style of mineralization.

Homestake Gold of Australia Ltd and Tectonic Resources NL recently announced the discovery of base and precious metal mineralization in the Mount Barren Group metasedimentary rocks, changing a long-held perception that these rocks are unprospective. Drilling intercepts include 37 m at 0.58 g/t Au, 1.10% Cu, 5.82% Pb, 4.09% Zn and 71 g/t Ag. Little is known about this mineralization at present and it will not be discussed further in this report.

Most of the mineralization occurs in four main centres, shown in Figure 61 (Mount Cattlin, Mount McMahon, Mount Desmond and Kundip). The main copper- and gold-producing mines are shown in Table 4. Mineralization also exists at a smaller centre near Stevenson Creek, and there are several isolated deposits. Silver has been produced mainly from the Mount Cattlin, Elverdton, Flag and Mosaic mines.

* The Department of Minerals and Energy's MINEDEX database provides rapid access to information on mineral deposits and current mines in Western Australia. The mainframe database may be accessed through terminals in Perth and regional offices. See Townsend et al. (1996) for more information.

Recent exploration has been aimed at proving resources remaining in deposits that have previously been mined, particularly those at Ravensthorpe (the Mount Cattlin mining centre) and Kundip (Table 5). In the Mount Cattlin centre, remaining inferred resources at Mount Cattlin are 36 000 t at 6.28 g/t Au, 3.69 g/t Ag and 1.99% Cu, and at Marion Martin they are 48 000 t at 2 g/t Au, 1 g/t Ag and 2.28% Cu. Ongoing exploration in the Mount Cattlin centre has identified a resource of 294 kg Au at Sirdar. Attempts to identify large-tonnage, low-grade orebodies by combining the small, high-grade lodes mined in the past have so far been unsuccessful.

Distribution and host rocks

The mineralization is hosted mainly by the Annabelle Volcanics, and is mostly within about 2 km of the contact with the Manyutup Tonalite (Fig. 61). Although coarse-grained Manyutup Tonalite contains some significant mines (e.g. Elverdton–Mount Desmond), mineralization is largely confined to marginal parts of the pluton, and is commonly associated with known or suspected xenolithic blocks of volcanic rock. There is a spatial association with small, medium-grained tonalite plutons at Mount Cattlin and Mount McMahon, and microtonalitic dykes are common at all centres of mineralization. Microtonalitic dykes host at least part of the mineralization at the Flag mine, Kundip. Summary drill logs of selected diamond drillholes from the Kundip mining centre are shown in Appendix 4. Coarse-grained tonalite has been intersected in diamond drillholes at depths of between 80 and 200 m beneath the Kundip mining centre (Sofoulis, 1958). The contact between tonalite and andesitic volcanic rocks at Kundip dips southwest at about 60°.

Relatively few mines are hosted by rocks other than those belonging to the Ravensthorpe Terrane and most of these record insignificant amounts of production. The main exceptions are Hecla (in Chester Formation metasedimentary rocks) and Mosaic (in Bandalup Ultramafics).

Metal ratios and metal zoning

The metal budget in these deposits is very variable, but the presence of Au–Ag–Cu zoning is difficult to assess

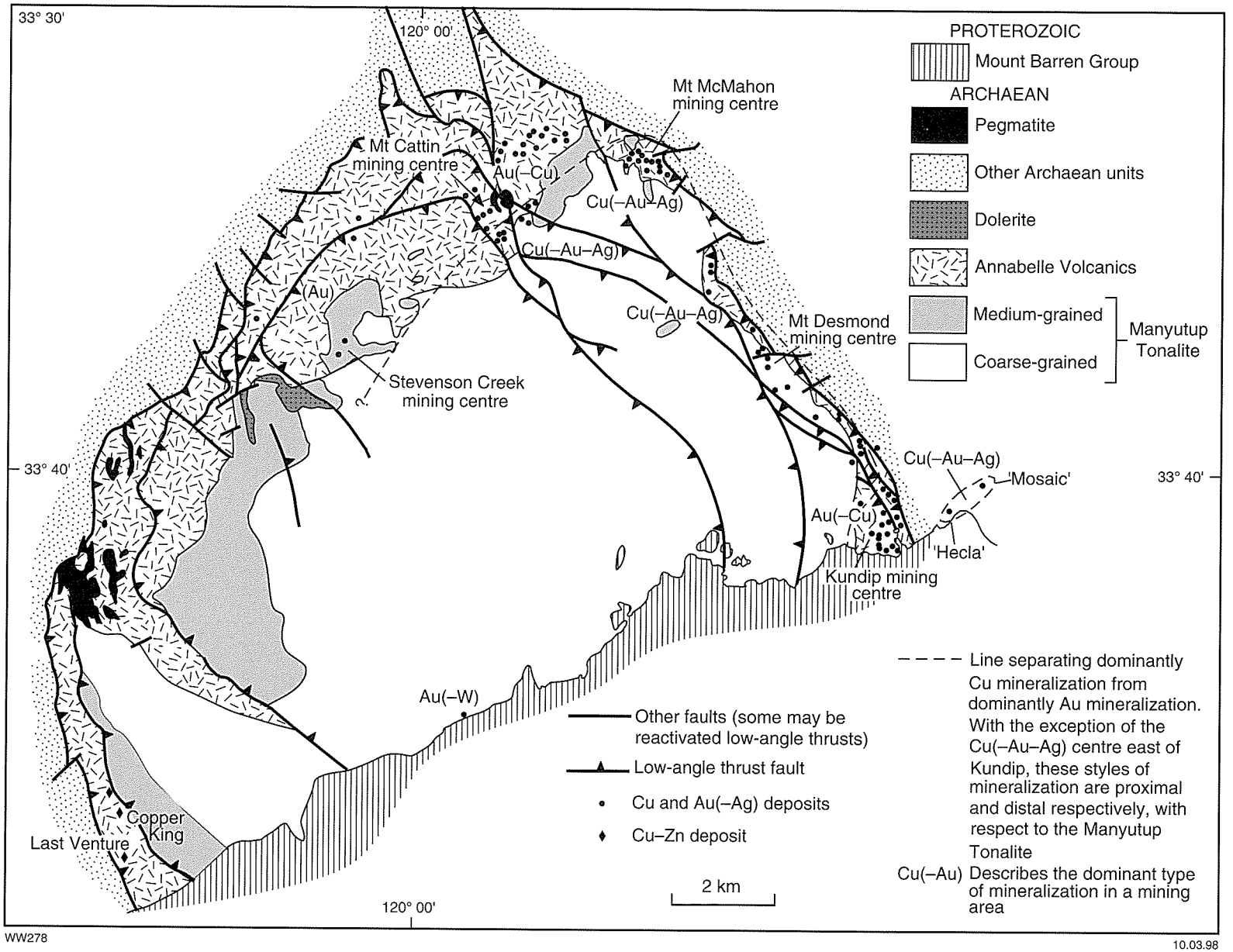

Figure 61. Distribution of precious- and base-metal deposits and metallogenic zoning, Ravensthorpe greenstone belt

Table 4. Gold and copper production, Ravensthorpe area

Mining centre	*Mine*	*Gold production (kg)*	*Copper production (tonnes)*
Kundip	Beryl	80.71	–
	Flag	306.69	253.23
	Gem	253.66	–
	Gem Consolidated	202.76	–
	Harbour View	184.27	264.42
	Hillsborough–Fairplay	–	191.98
	Two Boys	273.73	–
Mount Desmond	Desmond	–	286.08
	Elverdton	99.62	14 850.03
	Mount Desmond	–	251.58
Mount McMahon	Last Chance	–	226.83
	Mount Benson	–	185.65
	Mount Benson (East)	–	127.62
Ravensthorpe	Floater	349.90	–
	Maori Queen	133.50	–
	Marion Martin	–	773.55
	Mount Cattlin	187.64	1 323.60
	Surprise	–	219.15

SOURCES: Townsend et al. (1996)
Department of Mines (1954)

without more detailed knowledge of the subsurface distribution of the Manyutup Tonalite.

Sofoulis (1958) reported that gold-rich ores tended to pass into low-grade copper deposits at depth. There is also some evidence for lateral zonation of ore metals in that Cu–Au ratios appear to decrease with distance from the Manyutup Tonalite contact (Fig. 61). At Mount Cattlin, Cu(–Au–Ag) ores lie near the contact whereas Au-only ores occur further away from the contact. The Mount Desmond and Mount McMahon centres have produced mainly copper with some gold and silver. These centres lie mainly within or close to the Manyutup Tonalite. Savage (1992) noted that Cu:Au and Ag:Au ratios in pyrite from a diamond drillhole near Mount Chester decreased with distance from the tonalite contact. The Kundip mining centre has produced significant amounts of both gold and copper, although gold has been the more economically significant commodity. Copper-rich ores at Hecla and Mosaic are several kilometres from the nearest outcrops of Manyutup Tonalite. The Mosaic mine has yielded the ores richest in silver in the district.

Although the mines shown on Plate 1 in the Annabelle Volcanics at Kundip are annotated with yellow diamonds denoting Au(–Cu–Ag) mineralization, most mines (except for two at AMGs 239600 6272300 and 239700 6272850) could equally be annotated with red diamonds — Cu(–Au–Ag) mineralization. The mines have, in fact, produced more gold than copper but the style of mineralization is more consistent with Cu(–Au–Ag) in shears and veins.

Structural controls

Unlike the more widespread Archaean gold-only lode-style mineralization in the Yilgarn Craton, there is no

Table 5. Gold resources, Kundip mining centre

Deposit	*Resource type*	*Ore (tonnes)*	*Grade (g/t Au)*	*Contained gold (kg)*
Western Gem (open pit)	Demonstrated mineable	12 000	4.2	50
Beryl (underground)	Demonstrated mineable	10 000	22.1	22.1
Flag (open pit)	Measured mineable	16 000	4.6	74
Flag (underground)	Demonstrated mineable	8 000	22.1	177
Harbour View–Mayday (underground)	Demonstrated in situ	30 000	15.0	450
Kaolin–Glengold (open pit)	Demonstrated developable	110 000	3.2	352

SOURCE: Townsend et al. (1996)

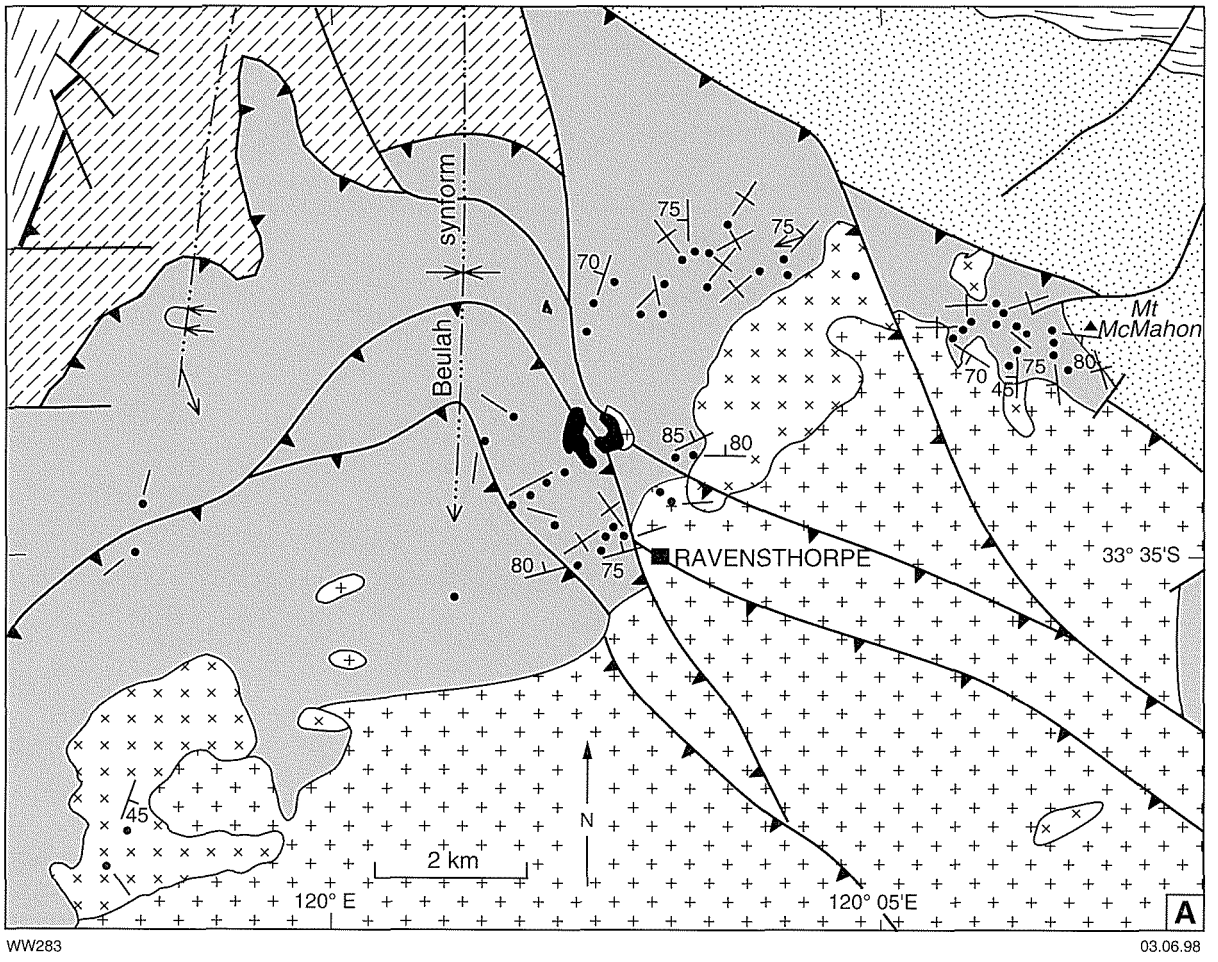

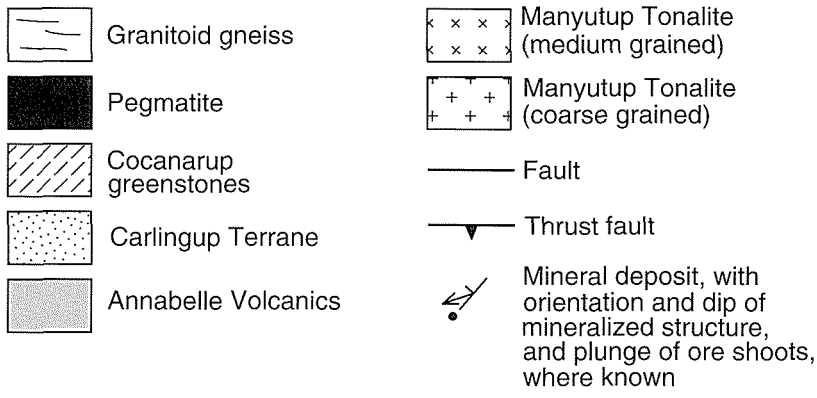

Figure 62. Location and orientation of mineralized structures at Ravensthorpe — A. the Ravensthorpe mining centre; B. Desmond and Kundip centres (on adjacent page)

association with regional strike-slip shear zones. Instead, there is an association with a broad zone of deformation and alteration, including several thrust faults, adjacent to the tectonic contact between the Ravensthorpe Terrane and the Carlingup Terrane. Many deposits lie on linear trends that are subparallel to, and approximately normal to, these regional thrust faults (Figs 61, 62). For example, east to east-northeast and northeast trends are evident in the Mount Cattlin centre; northwest and north-northeast trends are common in the Mount McMahon centre; and north-northeast, northwest and east-northeast trends in the Kundip centre. Although many of the deposits lie on these trends, their orientations do not necessarily reflect the orientation of the district-scale trends (Figs 62A, B).

At the deposit scale, mineralization is controlled by narrow (up to 2 m thick), discontinuous shear zones and quartz veins within irregular shears. The orientations and attitudes of the controlling structures are shown in

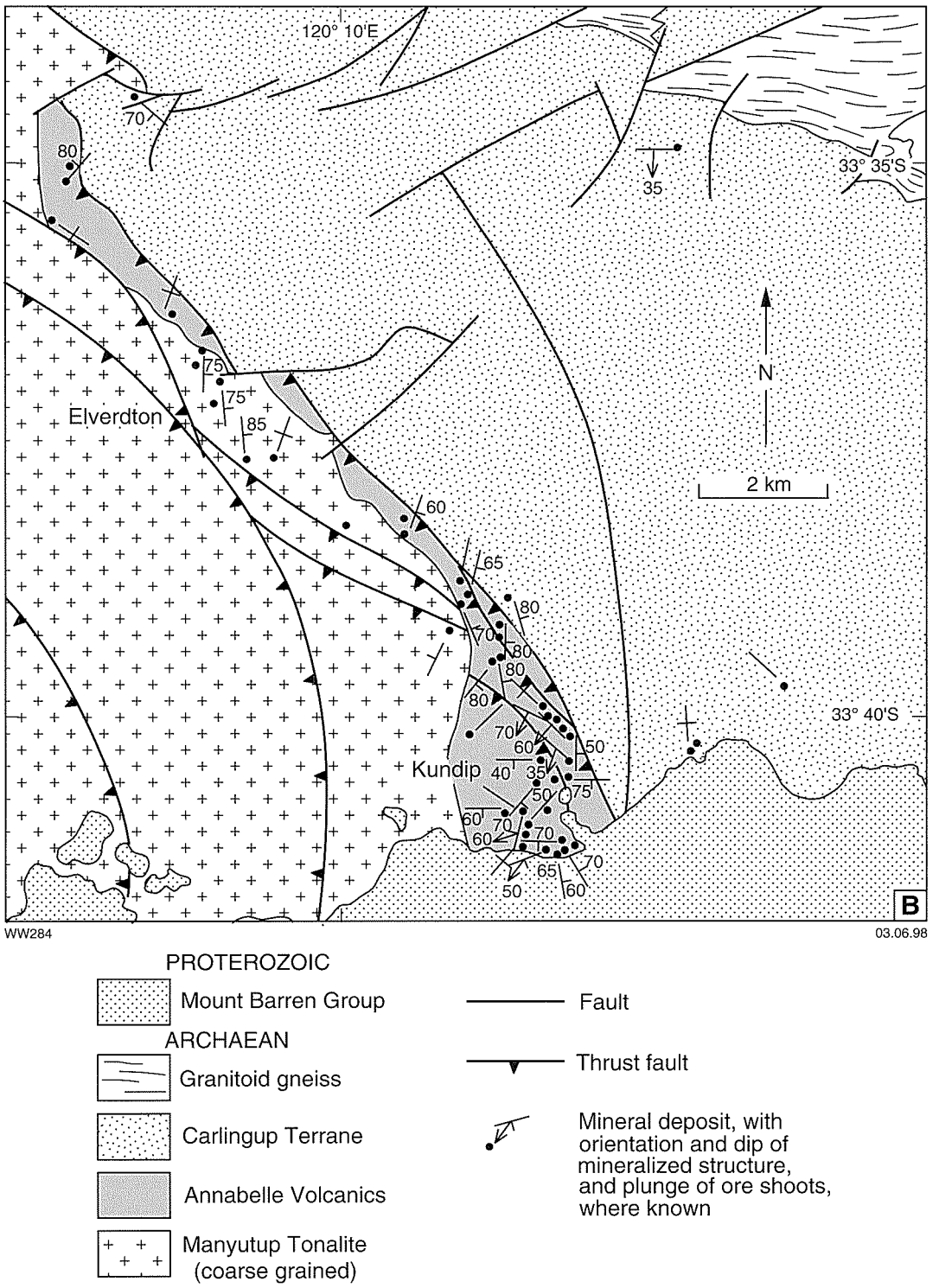

Figure 62, together with the plunge of the orebodies, where known. Sofoulis (1958) noted that gold-rich ores tend to be associated with quartz veins, whereas quartz veins are relatively uncommon or absent in copper-rich orebodies. Observations carried out during this study indicate that quartz veins are present in most copper-rich lodes but they tend to be discontinuous and form a relatively minor proportion of the mineralized lodes. The Elverdton–Mount Desmond structure is 700 m long and the Harbour View structure 600 m long, but most mineralized structures are less than 200 m long and 30 m wide (Marston, 1979).

Ore mineralogy

Gold-rich, copper-poor deposits north of Ravensthorpe tend to be low in sulfide mineral content compared to copper-rich ores that contain up to about 10% disseminated sulfides and some massive-sulfide ore. The gold–

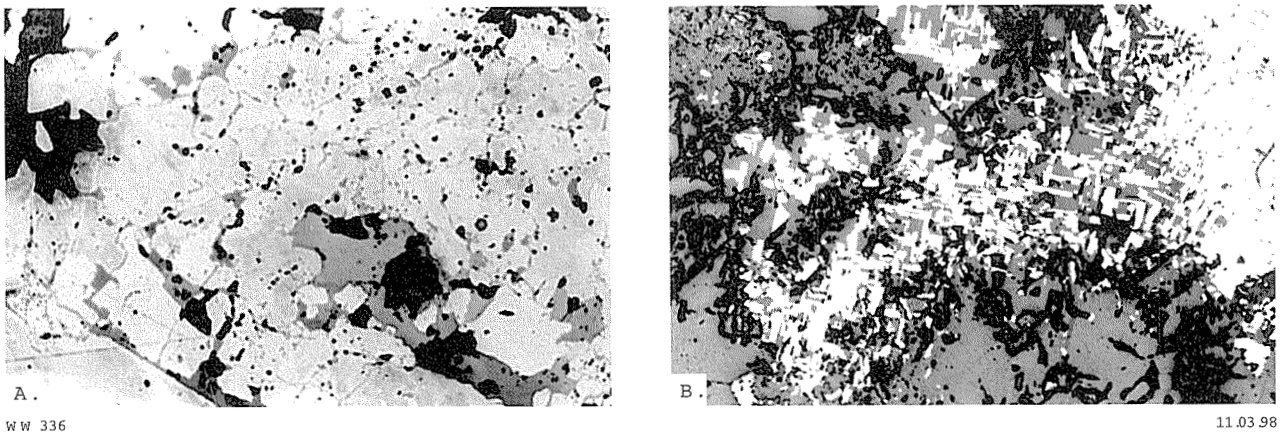

Figure 63. A: Chalcopyrite (dark grey) as inclusions, veinlets and fracture-fill in pyrite, Hillsborough–Fairplay mine, Kundip. GSWA 105994, reflected light, field of view approximately 0.1 mm. B: Skeletal pyrite, Beryl mine, Kundip. GSWA 110202, plane-polarized light, field of view approximately 0.1 mm

copper deposits at Kundip include massive and banded sulfide ore. Marston (1979) recognized three main copper-ore associations in the Ravensthorpe greenstone belt. His zinc-rich association is found only in the West sector of the Cocanarup greenstones and is discussed separately in the following section.

A quartz–gold–secondary copper minerals association is predominant in the oxidized zone, which can extend to 60 m depth. Secondary copper minerals are malachite, azurite, chalcocite, bornite and covellite. This assemblage passes downward into a chalcopyrite–gold–pyrite–magnetite(–pyrrhotite–ilmenite)–quartz association. Sulfide minerals occur as disseminations, quartz–sulfide veinlets, and veins within deformed and altered volcanic and tonalitic host rocks. Pyrite in veins is coarse and anhedral, and commonly displays evidence of cataclasis. Chalcopyrite occurs as discrete grains and as veins and inclusions in pyrite (Fig. 63A) and locally displays evidence that it formed by replacement of pyrite. In some samples, pyrite exhibits a skeletal habit suggesting rapid growth (Fig. 63B). Minor cobaltite has been recorded with this assemblage at Last Chance, and sphalerite is a minor component at Mount Benson, Elverdton, Mount Desmond and Flag. Silver occurs as tetrahedrite at Marion Martin and silver–bismuth telluride is a rare accessory at Eleverdton–Mount Desmond (Marston, 1979). Gold occurs as small inclusions, and in-filling cracks, in pyrite and chalcopyrite. Bismuth tellurides have also been reported at the gold-rich Floater deposit (Sofoulis, 1958).

Alteration

The Manyutup Tonalite and the Annabelle Volcanics display more or less pervasive styles of alteration that are far more extensive than the more intense but restricted alteration haloes associated with mineralized lodes. These pervasive styles of alteration are evidenced by secondary minerals occurring as disseminations and discontinuous veinlets.

Pervasive alteration

Pervasive alteration is widespread throughout most of the Manyutup Tonalite and comprises minor secondary minerals as disseminations, microfracture fillings and veinlets. Chlorite, epidote and rare calcite replace plagioclase and ferromagnesian minerals; biotite replaces amphibole; titanite replaces biotite and ilmenite; and hematite replaces magnetite. Traces of pyrite and chalcopyrite are commonly found in association with chlorite and epidote. Disseminated secondary minerals are locally associated with epidote–chlorite(–pyrite–chalcopyrite) veinlets. These secondary mineral assemblages constitute a pervasive propylitic alteration throughout most of the Manyutup Tonalite. Fracture- and veinlet-controlled biotite and K-feldspar (potassic alteration) in the Manyutup Tonalite are relatively rare but have been observed (e.g. around Ravensthorpe AMG 305828).

Minor biotitization and sericitization occur along macroscopic joints and fractures in Manyutup Tonalite, in a broad arc between Ravensthorpe and Kundip. This more restricted, structurally controlled alteration is probably related to deformation adjacent to the tectonic front between the Carlingup and Ravensthorpe Terranes.

Pervasive alteration in the Annabelle Volcanics is present mainly between Ravensthorpe and Kundip, in an arc that is apparently related to the tectonic front that separates the Carlingup and Ravensthorpe Terranes. In this arc, andesitic to dacitic volcaniclastic rocks contain secondary quartz, biotite, chlorite, epidote and sericite and are cut by quartz, chlorite–plagioclase and chlorite–biotite veinlets. Veinlets rich in amphibole(–plagioclase–quartz) are more common in the higher metamorphic grade rocks north and northeast of Ravensthorpe. Narrow, bleached haloes adjacent to amphibole-rich veinlets (and mafic clasts in dacite) display relatively intense sericitization. Some of these secondary minerals are associated with a D_2 foliation.

The spatial association with the tectonic front between the two terranes suggests that at least some of this alteration may be syntectonic.

Deposit-scale alteration

Alteration assemblages adjacent to mineralized veins and within mineralized shears vary from centre to centre, as follows.

Kundip centre

Several diamond drillcores from the Kundip mining centre have been logged and sampled (Appendix 4, Figs 4.1–4.4). Drillcore samples of andesitic volcanic rocks and microtonalite and tonalite porphyry dykes from the Kundip mining area are all characterized by intense propylitic alteration. Amphiboles were unstable in these rocks, which have been altered to assemblages rich in chlorite–epidote(–sulfide–carbonate).

Investigation of mineralized samples from mine dumps in the Kundip area and from diamond drillholes that intersected mineralization beneath the Flag and Gem Consolidated (Beryl) mines indicate that altered volcanic and tonalitic rocks are quartz–sericite–chlorite(–epidote–biotite–sulfide) assemblages. Alteration zones, up to a metre thick, are characterized by advanced destruction of ferromagnesian minerals and plagioclase, and the addition of chlorite, quartz and muscovite or sericite. A darkening of rock colour reflects an increase in the modal abundance of chlorite at the expense of plagioclase. The size and abundance of sulfide minerals increase with proximity to quartz–sulfide veins or central zones of shearing. The chalcopyrite:pyrite ratio also increases, from about 1:10 in distal parts of alteration zones to 1:2 in, and immediately adjacent to, veins. A narrow, bleached zone of silicification is adjacent to some veins. Minor gangue minerals in quartz–sulfide veins are magnetite, chlorite, muscovite, carbonate, albite, epidote and tourmaline.

Mount Desmond centre

Marston (1979) described quartz–plagioclase–biotite–chlorite(–hornblende) schist from the Eleverdton–Desmond mineralized system. Other mine dumps in the Mount Desmond area contain chloritized and sericitized tonalite, and quartz–plagioclase–biotite–chlorite schist after intermediate volcanic rocks.

Biotitization is the main style of alteration at the Rio Tinto and Mount Garrity mines in the Mount Chester area. Savage (1992) noted quartz–plagioclase–biotite–chlorite assemblages, associated with porphyroblasts of garnet, staurolite and chloritoid, in mineralized volcanic rocks intersected by diamond drilling in the Mount Chester area. A similar assemblage, but including andalusite, is found at an isolated mine in Chester Formation metapelites near the Ravensthorpe–Esperance highway (RAVENSTHORPE AMG 341807). Savage (1992) also noted the presence of K-feldspar and tourmaline in the drillhole samples from near Mount Chester.

Mount McMahon centre

Mineralized volcanic rocks in the Mount McMahon centre are quartz–biotite(–plagioclase–chlorite–muscovite–sulfide) schist, locally with garnet, orthoamphibole (gedrite, see Appendix 3, Table 3.5), magnetite and cordierite porphyroblasts. Oriented biotite and fine-scale mineral layering define the main shear fabric. Garnet, amphibole and cordierite are unoriented and overprint the schistosity, which is preserved as inclusion trails within the porphyroblasts. Chlorite commonly appears to be retrograde with respect to biotite.

Mount Cattlin centre

Copper lodes in volcanic rocks are quartz–plagioclase–biotite(–chlorite–sulfide) assemblages, commonly with garnet porphyroblasts and unoriented amphibole prisms. Optical properties suggest that the amphiboles are calcic (actinolite and/or hornblende and cummingtonite). Where the altered rock is foliated, garnet and amphibole porphyroblasts overprint the shear fabric, as described above (Mount McMahon centre). Quartz–sulfide veins contain smaller amounts of amphibole, biotite and magnetite. Tourmaline is common, and carbonate a minor component, in veins and alteration selvages at the gold-rich Maori Queen deposit.

Stevenson Creek centre

Biotite is the main alteration phyllosilicate in mineralized Annabelle Volcanics in the Stevenson Creek centre. Garnet porphyroblasts have not been identified.

Mineralogy and geothermometry

Mineral analyses of garnet, biotite, amphibole, plagioclase and staurolite from mineralized samples at Marion Martin (113915), Mount Benson (110353), and an unnamed deposit in Chester Formation metasedimentary rocks north of Mount Chester (105941), are presented in Appendix 3 (Tables 3.2 to 3.6). The alteration assemblages at these localities are interpreted to have equilibrated at regional metamorphic temperatures. Garnet–biotite temperatures are shown in Appendix 3 and discussed in the section on Archaean metamorphism.

Geochemistry

The results of mass balance calculations (after Gresens, 1967) for altered, mineralized samples collected from drillcore at Kundip are presented graphically in Appendix 4 (Figures 4.5 to 4.11). Epidote alteration in spaced shears in coarse-grained tonalite from KDP–2 is unmineralized. It is similar to that near the tectonic front between the Carlingup and Ravensthorpe Terranes, described in chapter 4, and is not considered further here. The remaining samples show that alteration associated with Au–Cu mineralization at Kundip involves addition of ΣFeO, MgO, S and, in most cases, SiO_2. These changes in bulk chemical composition are accompanied by loss of CaO and Na_2O. In one case (110201/110202), SiO_2 has been removed from the mineralized sample, and

in another (110201/110203), FeO has been removed rather than added. There is relatively little addition of K_2O and CO_2 compared to most mesothermal, gold-only deposits in the Yilgarn Craton.

Qualitatively similar changes in bulk chemical composition are recorded by three samples of 'unaltered microtonalite' from Kundip (Fig. 19). These samples are all characterized by intense propylitic alteration, as described above. The trace elements Cu and, to a lesser extent, Co are also enriched in these 'least altered' samples and are enriched to an even greater extent in most altered samples collected from mineralized shears or vein selvages (Fig. 19; Appendix 2, Table 2.1).

Timing

The following relationships provide constraints on the timing of propylitic alteration and copper–gold mineralization.

1. On a regional scale, mineralized alteration assemblages vary sympathetically with the present metamorphic grade of the host rocks (e.g. chlorite and sericite at Kundip, biotite and garnet at Ravensthorpe and Mount McMahon). Therefore, mineralization must have either pre-dated or else was synchronous with metamorphism (i.e. pre- to syn-terrane amalgamation).

2. Compositional zoning in garnets in alteration assemblages from the Ravensthorpe and Mount McMahon centres preserves evidence of the compression associated with tectonic loading during terrane amalgamation. This would suggest that the garnet grew during terrane accretion, either directly as part of an amphibolite facies alteration assemblage, or during metamorphic re-equilibration of an earlier alteration assemblage.

3. A lower age limit for mineralization is set by a Proterozoic dolerite dyke that cuts the mineralized lode at Mount Cattlin.

4. Copper–gold mineralization occurs mainly in tonalite and volcanic rocks of the Ravensthorpe Terrane, but is also found in Chester Formation metasedimentary rocks and Bandalup Ultramafics in the Carlingup Terrane. If mineralization in the two terranes is related, it must therefore have been synchronous with or post-dated amalgamation of the Ravensthorpe and Carlingup Terranes.

These observations provide conflicting constraints on the timing of copper–gold–silver mineralization. A post-metamorphic origin can be ruled out, but the mineralization may have formed before or during regional metamorphism and terrane accretion.

Genesis

Currently, there are two hypotheses for the origin of copper–gold(–silver) mineralization in the Ravensthorpe area. Sofoulis (1958) proposed a magmatic–hydrothermal origin in which mineralization was related to the Manyutup Tonalite. This hypothesis has been supported by Savage (1992), who viewed the mineralization as part of an Archaean porphyry copper system. Sofoulis (1958) and Savage (1992) suggested that the structures that host mineralization were generated by forceful magmatic emplacement of the Manyutup Tonalite. Marston (1979), on the other hand, suggested that ore components may have been remobilized from originally stratiform sulfide mineralization in the Annabelle Volcanics during regional deformation and metamorphism. It seems unlikely that stratiform mineralization at Kundip could be completely remobilized by regional deformation and metamorphism, particularly when volcanogenic sulfide deposits can still be recognized in amphibolite-grade rocks in the West sector of the Cocanarup greenstones (see below). However, it is possible that some of the Cu–Au(–Ag) deposits described here are synvolcanic. The structurally controlled mineralization may have formed in a subaqueous environment, in a similar manner to the structurally controlled feeder zones that underlie many volcanogenic massive-sulfide deposits (Franklin et al., 1981). A third possibility is that the copper–gold deposits are synmetamorphic and formed in a similar manner to the more widely recognized gold-only Archaean lode deposits (Groves et al., 1992; Witt, 1993).

In the following paragraphs, Cu–Au(–Ag) mineralization at Ravensthorpe is assessed in terms of three models:

- porphyry copper–gold;
- sub-seafloor volcanogenic; and
- syntectonic–synmetamorphic.

An assessment of the porphyry copper–gold model

The copper–gold mineralization is associated with calc-alkaline volcanic rocks, dominated by andesite and associated with cogenetic intrusive rocks (mainly tonalite) that have many petrographic and geochemical features in common with those that host porphyry copper–gold systems in the southwest Pacific (Hine and Mason, 1978; Titley and Beane, 1981). Other features of the Ravensthorpe copper–gold mineralization that are comparable to some or most porphyry copper systems are the association with relatively fine-grained, volumetrically small plutons and dykes; the vertical and lateral zoning of ore-metal ratios; and the widespread propylitic alteration (including chalcopyrite) in the tonalitic rocks. Increasing chalcopyrite:pyrite ratios toward the central sections of orebodies, similar to those documented at Kundip (see above), also typify some porphyry deposits (Rose, 1970). Fluid inclusion studies carried out by Savage (1992) documented the presence of highly saline (>60 wt% NaCl equivalent), high temperature (>550°C) ore fluids at Mount Chester and Kundip. These fluid characteristics are typical of those that are associated with porphyry systems (Watmuff, 1978; Beane and Titley, 1981).

Although many features of copper–gold mineralization in the Ravensthorpe area are consistent with a

porphyry copper style origin, several other features are problematic. These are as follows:

1. Although there is an apparent association of mineralization with fine-grained stocks and dykes, there is no well-developed zone of potassic alteration (biotitization) centred on these intrusions (cf. Beane and Titley, 1981). Also, despite the widespread propylitic alteration of the Manyutup Tonalite, there is no district-scale zoning of alteration types (propylitic, phyllic, potassic, calcic) comparable to that described by Chivas (1978) and Dilles and Einaudi (1992).

2. Broad zones of stockwork veining and magmatic–hydrothermal brecciation typify porphyry-style mineralization (Burnham, 1979; Beane and Titley, 1981) but are absent in the Ravensthorpe area. The relatively isolated, discontinuous quartz veins and brittle–ductile shears that carry mineralization are more typical of Archaean, mesothermal, gold-only deposits (Colvine et al., 1988; Witt, 1993).

3. Metasomatism of wallrocks adjacent to mineralized veins in porphyry deposits results in the addition of K and S, and in some cases Na and Ca (Beane and Titley, 1981; Dilles and Einaudi, 1992). This contrasts with the notable addition of Fe and Mg and depletion of Na and Ca in most deposits studied at Kundip.

4. Despite the petrographic and geochemical similarity of calc-alkaline rocks of the Ravensthorpe Terrane to those associated with porphyry copper–gold mineralization in the southwest Pacific (Hine and Mason, 1978), the whole-rock copper contents of the Ravensthorpe Terrane rocks (<30 ppm, excluding samples from the Kundip mining centre) are comparatively low.

5. The early crystallization of sulfide minerals from the Manyutup Tonalite magma implies early sulfur saturation with sequestration of Cu and negative consequences for the development of porphyry copper mineralization (Candela and Holland, 1986; Wyborn and Sun, 1994).

An assessment of the sub-seafloor synvolcanic model

The association of Cu–Au(–Ag) mineralization at Ravensthorpe with andesitic volcanic rocks, the sulfide-rich nature of the orebodies, and the nature of the alteration are all consistent with a sub-seafloor synvolcanic model (see reviews by Lydon, 1984 and Franklin et al., 1981 for this type of mineralization). Alteration associated with the lodes is similar to intense chloritic alteration and Fe–Mg metasomatism that characterizes stockwork feeder zones beneath volcanogenic massive-sulfide deposits. Zoning of ore metals and sulfide mineralogy is also a common feature of volcanogenic base-metal sulfide ore systems. The Manyutup Tonalite is a subvolcanic intrusion that was emplaced within the Annabelle Volcanics during or soon after volcanism. In this sense, the Manyutup Tonalite is comparable to subvolcanic intrusions in the Noranda–Val d'Or area of Quebec, such as the Bourlamaque batholith (Campiglio and Darling, 1976) and the Flavrian pluton (Goldie, 1978). It is also comparable to these Canadian igneous bodies in broad compositional terms (all intrusions are relatively mafic complexes comprising some or all of diorite, tonalite and trondhjemite), although there are some differences in the detailed geochemistry of the intrusions. Subvolcanic intrusions are an important component of sub-seafloor sulfide systems because they provide a heat source that drives seawater through the volcanic pile causing redistribution of chemical components, including ore elements (Barrie et al., 1993; Cathles, 1993). Cathles (1993) has demonstrated the importance of the Flavrian pluton at Noranda. He used oxygen isotope data to show how the pluton focused the flow of hydrothermal fluids into the feeder zones that underlie the Noranda massive-sulfide deposits. Similar deep penetration of seawater into the Manyutup Tonalite, at low fluid: rock ratios, would account for the widespread but volumetrically minor propylitic alteration. The association of disseminated pyrite and chalcopyrite with propylitic alteration, and the high Cu contents of metamorphic–propylitic amphibole and chlorite compared to igneous amphibole and biotite, suggest the fluids that caused propylitic alteration were enriched in copper compared to the unaltered tonalite.

There are two main problems with the sub-seafloor model for Cu–Au(–Ag) mineralization at Ravensthorpe. The first is the identification of high-temperature, high salinity ore fluids, based on fluid inclusion studies by Savage (1992). Although boiling of hydrothermal fluids is possible in a shallow sub-seafloor environment (Cathles, 1993), this phase change will not necessarily lead to a large salinity increase in the residual fluid (Franklin et al., 1981). The second problem is shared by the sub-seafloor model and the porphyry model. Both models relate mineralization to early stages in the tectonothermal evolution of the host rocks. Mineralization should therefore be confined to the Ravensthorpe Terrane. The presence of minor gold and gold–copper (–silver) mineralization in the Carlingup Terrane requires explanation (see below).

An assessment of the syntectonic–synmetamorphic model

The mineralized quartz veins and short, discontinuous shears that carry copper–gold(–silver) mineralization at Ravensthorpe are not unlike those that carry gold-only mineralization in mesothermal gold deposits elsewhere in the Yilgarn Craton (see Groves et al. (1992) and Witt and Vanderhor (in press) for overviews of this style of mineralization). However, there are several important features that distinguish the Ravensthorpe deposits from most Yilgarn mesothermal deposits. Most notable are the relatively high sulfide contents of mineralized veins and shears; the relatively high copper and silver contents of the ores; and the lateral and vertical zoning of metal ratios at Ravensthorpe. The style of alteration is also unlike that associated with mesothermal gold-only deposits. Mesothermal deposits in rocks of comparable

metamorphic grade to those at Kundip are characterized by intense carbonation and the addition of K and S. Although significant in terms of mineralization, the amount of sulfur is small. At Kundip, sulfide-rich lodes associated with carbonate-poor chloritic alteration, and the addition of Fe and Mg stand in stark contrast to typical mesothermal styles of mineralization.

Although it is an inadequate model for the bulk of the Cu–Au(–Ag) mineralization in the Ravensthorpe Terrane, minor redistribution of low-level copper and gold mineralization (associated with propylitic alteration in the Manyutup Tonalite) during terrane accretion may account for the presence of some deposits (e.g. Hecla, Mosaic) in the Carlingup Terrane. Enormous amounts of fluid can be generated during thrust tectonics and the consequent metamorphism of the lower plate to higher pressures and temperatures (Fyfe, 1990). These fluids probably migrated upward along shallowly dipping thrust faults and were focused along the basal thrust plane (the Chidnup Fault). The experimental studies of Hemley et al. (1992) and discussion of results by Hemley and Hunt (1992) indicate that copper may have been leached from the Manyutup Tonalite by rock-buffered fluids ascending along a quasi-adiabatic pressure–temperature path. Redeposition of gold and copper in higher level structures, including splays into the Carlingup Terrane, would occur in response to falling temperature, pressure, phase separation, or fluid mixing (Fig. 64).

The gold-rich, copper-poor veins in the northern part of the Mount Cattlin mining centre are less well exposed than the copper-rich lodes, and detailed studies of alteration have not been carried out. Though small, these deposits may also have formed during terrane accretion and thus be comparable to the more widespread mesothermal deposits of the Yilgarn Craton.

Conclusions

It is concluded from the above comparisons that the Cu–Au(–Ag) mineralization at Ravensthorpe best fits a model in which the mineralized veins and shears are part of a discharge zone within a sub-seafloor hydrothermal system. The relatively small orebodies in each of the four main mining centres may lie beneath massive-sulfide deposits that formed at higher stratigraphic levels. Alternatively, they may represent relatively small-scale zones of discharge involving hydrothermal fluids with limited ore metal concentrations that were dispersed at the sea floor. If overlying massive-sulfide bodies did form, they have since been removed by erosion, or tectonically displaced across thrust faults within the Ravensthorpe Terrane. The tectonic model proposed in this report predicts that any massive-sulfide bodies that lay above the feeder zones at Mount Cattlin, Mount McMahon, Elverdton and Kundip have been removed by erosion. Other orebodies may be found elsewhere within the Annabelle Volcanics, for example in thrust slices beneath surface exposures of Manyutup Tonalite.

Witt (1995) suggested a syntectonic model for the Cu–Au(–Ag) mineralization at Ravensthorpe, whereby metamorphic dewatering of metasedimentary rocks in the Carlingup Terrane produced fluids that were focused up the gently inclined Chidnup Fault and overlying Ravensthorpe Terrane. Low-grade porphyry-style mineralization in the Manyutup Tonalite was redistributed into higher level veins and shears, mainly in the hanging wall of the Chidnup Fault. This model was strongly influenced by the presence of some Cu–Au (–Ag) mineralization in Carlingup Terrane rocks. Porphyry- and synvolcanic-styles of mineralization should be confined to one or other of the two terranes as they were only accreted with one another during regional deformation and metamorphism. The reinterpretation proposed here is prompted by the newly acquired data on alteration geochemistry and a re-examination of several aspects of the mineralization, particularly the sulfide-rich nature of the orebodies. The problem of how to reconcile the presence of Cu–Au(–Ag) mineralization in the Carlingup Terrane with the accretionary tectonic model still requires explanation. The deposits in the Carlingup Terrane (primarily Hecla and Mosaic) are poorly exposed. It is possible they represent synvolcanic mineralization that formed independently of the sea-floor systems in the Ravensthorpe Terrane. For example, there are extensive stratiform, massive-sulfide deposits in the Chester Formation (described below) to which Hecla and Mosaic may be related. Felsic volcanic rocks exposed near Hecla and Mosaic display a strong hydrothermal overprint. These rocks are strongly silicified, carbonated, chloritized and sericitized, and contain minor disseminated sulfide minerals. Such alteration may be part of a larger hydrothermal system that also includes the mineralization at Hecla and Mosaic.

Alternatively, synvolcanic mineralization in the Ravensthorpe Terrane may have been remobilized during regional deformation and redeposited in footwall splays off the Chidnup Fault (Fig. 64). Gold-rich veins in the northern part of the Mount Cattlin mining centre may also have formed at this stage.

Stratabound base-metal sulfides at West River

In the West River area, three metamorphosed, stratabound copper–zinc sulfide deposits occur in the Annabelle Volcanics within a large area of quartz–biotite–plagioclase–gedrite–cordierite(–andalusite–garnet) rock. The orebodies strike northwest to north-northwest, and are steeply dipping parallel to the foliation in the enclosing intermediate gneiss. The largest of these deposits (Last Venture) has produced 43 t Cu, and exploration drilling in the mine area has intersected several metre-widths of Cu–Zn mineralization (summarized in Marston, 1979).

Details of alteration zoning are uncertain as mineralization is not exposed in situ. Samples collected from mine dumps at Last Venture are massive to banded, coarse-grained quartz–plagioclase–biotite

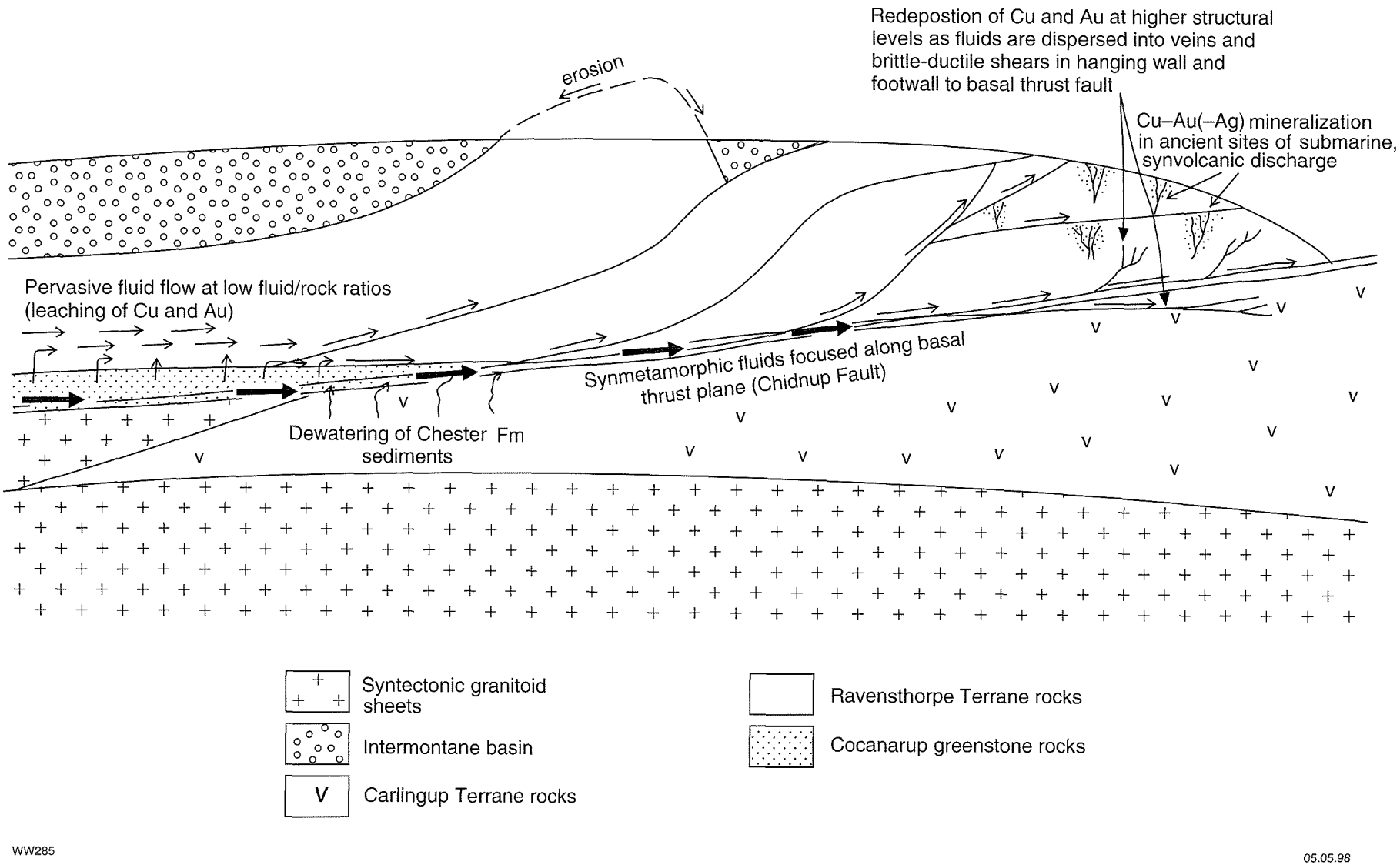

Figure 64. Syntectonic–synmetamorphic model for partial redistribution of volcanogenic Cu–Au mineralization (?and new generation of vein gold deposits) in the Ravensthorpe area

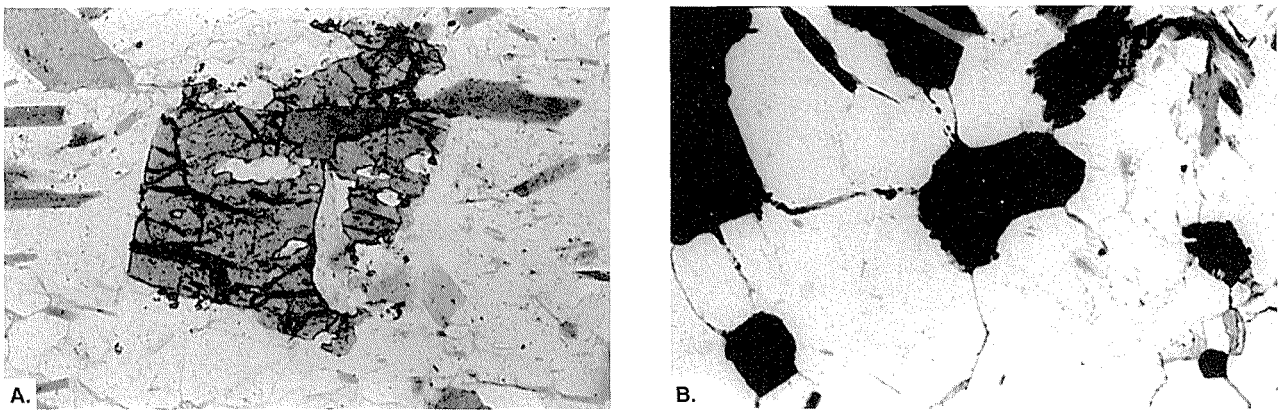

Figure 65. A: Intergrown gahnite (dark grey, subhedral) and sphalerite (mid grey, anhedral), Copper King mine. GSWA 118882, plane-polarized light, field of view approximately 0.5 mm. B: Well-annealed quartz–pyrite (opaque) textures reflecting metamorphism of the base-metal deposit, Last Venture mine. GSWA 118894, plane-polarized light, field of view approximately 0.5 mm

(–muscovite)–cordierite–orthoamphibole rocks with minor disseminated, vein- and veinlet-controlled sulfides. Minor garnet has also been identified in some samples. Samples from Copper King are similar to those from Last Venture, but contain andalusite and only minor cordierite. Accessory minerals include ilmenite, apatite and tourmaline. Pyrrhotite, pyrite and chalcopyrite are variably altered to secondary sulfides and oxides. Zinc occurs as sphalerite and gahnite (Fig. 65A). Mineral analyses are given in Appendix 3 (Table 3.6). The orthoamphibole is gedrite rather than anthophyllite as previously reported (Thom et al., 1984; Marston, 1979).

Quartz veins have been boudinaged, disrupted and ptygmatically folded. There are no late quartz veins. Oriented micas and fine-scale quartz–biotite banding preserve an early deformation fabric in most samples. Although quartz–biotite fabrics record deformation during metamorphic recrystallization, fabric relations involving other minerals in the alteration assemblage indicate a substantial component of static recrystallization. Cordierite, andalusite and garnet porphyroblasts are subequant and overprint the early quartz–biotite fabric. Gedrite occurs as radiating sprays of columnar to acicular crystals up to 2 cm long (Fig. 39). The porphyroblasts contain inclusion trails of quartz, feldspar, biotite, gahnite and opaque minerals. Sulfide–silicate intergrowths and well-annealed quartz–sulfide triple points (Fig. 65B) indicate high-temperature static recrystallization of the mineralized assemblage. Retrograde chlorite and sericitic alteration of plagioclase, andalusite and cordierite is widespread.

These deposits were interpreted as metamorphosed volcanogenic base-metal sulfide deposits by Marston (1979). Cordierite–orthoamphibole assemblages are typical of metamorphosed mafic to intermediate rocks that have been chloritized during sea-floor hydrothermal alteration and are commonly associated with volcanogenic massive-sulfide deposits (Lydon, 1984). The cordierite–gedrite assemblage at West River is interpreted to be altered and metamorphosed Annabelle Volcanics. The deposits at West River therefore constitute a similar style of mineralization to that which occurs in lower grade metamorphic rocks between Ravensthorpe and Kundip. The West River deposits lie in an area where dacitic rocks are prevalent, which may account for the Zn-rich character of these deposits.

Stratiform sulfides in the Chester Formation, Carlingup Terrane

Stratiform, massive to bedded gossanous limonite forms ridges along the Ravensthorpe Range that total many kilometres of strike length. These limonitic horizons grade along strike into chert and banded iron-formation of the Chester Formation. Similar limonitic gossan units are found within the Hatfield Formation. Drilling beneath these gossanous horizons has intersected massive pyrite and bedded, pyritic shale and chert at Mount McMahon (Gray and Gleeson, 1951a), and finely bedded pyritic shale at Mount Chester (Savage, 1992; Vesanto, 1992). No economic concentrations of base metals or gold are associated with these pyritic intersections. However, Cu–Au(–Ag) mineralization at Hecla may be related to this style of mineralization. Pipe-like zones of alteration and veining below limonitic horizons, equivalent to feeder zones in well-documented volcanogenic massive-sulfide deposits, have not been identified and there is no physical link with the sea-floor alteration systems in the Ravensthorpe Terrane.

The pyritic horizons in the Chester and Hatfield Formations are extensive, tabular bodies, interbedded with metamorphosed shale, siltstone and sandstone.

Although both formations contain a minor component of intermediate to felsic rocks of probable volcanic origin, the pyritic horizons are not intimately associated with volcanic rocks. The pyritic units are therefore akin to the sedimentary–exhalative, sediment-hosted, stratiform massive-sulfide deposits of Lydon (1984). They are distinct from the structurally controlled, synvolcanic mineralization in the Ravensthorpe Terrane that is comparable to the volcanogenic, volcanic-hosted, massive-sulfide deposits of Lydon (1984). The scale of the pyrite mineralization, and its association with a mainly sedimentary or mixed sedimentary–volcanic sequence of rocks suggests similarities to deposits formed in large, continental rift zones, such as at Bergslagen, Sweden and in the Iberian Pyrite Belt (Galley, 1993). Some of the massive pyrite units are associated with porphyroblast-bearing, high-Al pelites. These high-Al pelites may reflect the presence of large-scale, semi-conformable, sea-floor alteration zones within the sedimentary rock sequence. The local presence of manganiferous sedimentary rocks, and iron-rich metapelites and silicate-facies banded iron-formation in the Chester Formation, are other features in common with the host-rock sequences at Bergslagen and in the Iberian Pyrite Belt (Galley, 1993).

Although exploration in the Chester Formation and the Hatfield Formation has so far located only barren, pyritic metasedimentary rocks, there has been no systematic prospecting of the gossanous horizons. Iron-rich, silicate-facies banded iron-formation and metapelitic rocks in the Chester Formation are associated with felsic volcanic or volcaniclastic rocks. This association (shown as *Acf* on RAVENSTHORPE) constitutes an attractive exploration target because it is present in the ore environment of many Archaean and younger volcanogenic, base-metal, massive-sulfide deposits (Franklin et al., 1981; Lydon, 1984).

Nickel

Exploration during the 1960s and 1970s revealed the presence of nickel-sulfide mineralization in the Carlingup Terrane, at several localities east of Ravensthorpe. The Number 8 deposit contains an indicated resource of 249 900 t averaging 1.95% Ni (Marston, 1984). This deposit, and several other prospects described by Marston (1984), occurs along the strongly deformed northeastern limb of the Maydon Syncline. Disruption of the original sulfide orebodies into several smaller, separated deposits during regional deformation (especially D_2 and D_4, Carlingup Terrane) has made exploration difficult, and mining uneconomic.

The deposits are contained in serpentinized dunite and peridotite that have been metamorphosed to tremolite-rich assemblages and talc–forsterite(–anthophyllite) rock. Talc–carbonate schist occurs in widespread deformation zones. The Number 8 deposit consists of minor massive to brecciated sulfide ore within a larger shoot of disseminated sulfides. Disseminated sulfides in talc–forsterite assemblages (matrix ore) occur in triangular interstices between prismatic metamorphic olivine crystals. The ore shoot plunges 30° southeast, approximately co-linear with the main tectonic lineation (L_4) in this area. Disseminated ore contains up to 2% Ni, and massive-sulfide ore up to 18% Ni. The main sulfides are pentlandite and pyrrhotite with minor pyrite and chalcopyrite.

At Bandalup Hill, nickel is also found in lateritic deposits, up to 80 m thick, which have developed over ultramafic rocks (Marston, 1984). Metallurgical problems have prevented mining of a resource of 15.4 Mt of lateritic ore averaging 1.4% Ni.

Nickel mineralization has so far been identified only in the Carlingup Terrane. RAVENSTHORPE (Witt, 1996a) shows several lenses and units of ultramafic rock that do not appear on the 1:250 000-scale map. There is potential for undiscovered concentrations of nickel sulfides in these units, especially in the upper Bandalup Creek area where ultramafic caprock was previously mapped as laterite. Sulfide orebodies in this location are remote from the Bonnymidgup Shear Zone and are likely to be less deformed. However, high-MgO komatiitic rocks, which host nickel-sulfide mineralization on RAVENSTHORPE and elsewhere (Lesher, 1989), appear to be uncommon in other newly identified ultramafic units. The occurrence of magnesite, south of the Jerdacuttup Fault (see Magnesite, below) warrants further investigation.

Lithium, tantalum

Pegmatite dyke swarms are widespread in the Cocanarup and Ravensthorpe areas and are thought to have been emplaced within thrust planes, mainly in Ravensthorpe Terrane rocks. These structures probably provided access for pegmatitic magmas derived from deeper, unexposed sources. There is no evidence to suggest that the pegmatites were derived from the Manyutup Tonalite, as suggested by Sofoulis (1958).

Descriptions of the pegmatite at Cattlin Creek can be found in Sofoulis (1958), Blockley (1980), and Witt (1992). The pegmatite is a thin sheet (up to a few metres thick), which dips shallowly to the east-northeast. It contains lithium in the form of lepidolite and spodumene. The latter mineral forms spectacular crystals up to a metre long. Minor mineral components include tourmaline, amblygonite, montebrasite, cassiterite and Ta–Nb oxide minerals. The fractionated nature of the pegmatite is indicated by the presence of pink to green tourmaline (elbaite). Production of spodumene from Cattlin Creek has accounted for 6 670 kg Li_2O, and Hill (1976) reported reserves of 1.3 Mt of spodumene. This pegmatite has also yielded a small amount of tantalite and contains a further 120 000 t at 0.09% tantalum (Resource Information Unit, 1993).

Flat-lying pegmatite sheets on COCANARUP become progressively smaller and more fractionated northward, toward Cocanarup. Tourmaline is a minor to abundant constituent of these dykes, and commonly occurs in vuggy pockets, several centimetres across, within the pegmatites. The more fractionated pegmatites contain

lepidolite and zinnwaldite, but spodumene has not been recorded. They also contain minor amounts of amblygonite, lithiophilite and Ta–Nb oxide minerals (Witt, 1992).

Manganese, cobalt

Massive to bedded manganese-oxide ore occurs as stratiform deposits in both Archaean and Proterozoic metasedimentary rocks in the Ravensthorpe area. The more significant deposits are contained in Kybulup Schist near the Hamersley River Gorge (COCANARUP AMG 679441) where there are some shallow workings. These have been described by Gray and Gleeson (1951b) and Sofoulis (1958) and are generally regarded as being too small and too low-grade (approximately 33% Mn) to be economic. Other manganiferous metapelites were noted in this general area during fieldwork on COCANARUP. Three samples collected for analysis contain anomalous concentrations of Co, Ni and some base metals, as well as Mn (Table 6).

Other occurrences of manganese in Chester Formation metasedimentary rocks near Elverdton and Kundip have been recorded by de la Hunty (1963). A sample of manganese ore from Mount Chester was examined by X-ray powder diffractometry, X-ray powder photography and energy dispersive X-ray analysis. The sample consists mainly of pyrolusite with subordinate cryptomelane, quartz and goethite. Sofoulis (1958) mentioned up to 2% Co (cobalt) in manganiferous ores in the Ravensthorpe district but does not specify which deposits were sampled.

Table 6. Whole-rock trace element analyses of Mn-rich metasedimentary rocks from the Mount Barren Group

Sample number	*119933A*	*119933B*	*119934*
		Parts per million	
Ag	<2	<2	2
As	324	208	114
Au (ppb)	?12	?27	?14
Ba	274	395	125
Bi	4	<4	<4
Cd	<5	7	<5
Ce	6	9	9
Co	161	239	141
Cr	26	83	17
Cu	667	690	292
Ga	<3	5	<3
Ge	<3	<3	<3
La	22	30	24
Mn	43 000	94 100	158 700
Mo	<2	<2	<2
Nb	<7	<7	<7
Ni	448	429	1 010
Pb	67	35	7
Rb	2	17	<2
Sb	21	4	<4
Sn	<4	4	4
Sr	105	124	101
Ta	<5	<5	<5
Te	<6	<6	<6
Th	<2	3	<2
U	6	6	2
V	152	351	92
W	34	40	68
Y	38	20	19
Zn	1 050	911	383
Zr	21	60	27

NOTE: Au in ppb

Magnesite

Several occurrences of magnesite in the Ravensthorpe area have been described by Abeysinghe (1996), who recognized two types of deposit.

The main areas are on RAVENSTHORPE, around Bandalup and Bandalup Creek, and east of Kundip. Most deposits developed over Archaean ultramafic and mafic rocks during Cainozoic weathering. Large areas mapped as magnesite, and probably underlain by ultramafic rocks, are also shown south of the Jerdacuttup Fault, east of the Jerdacuttup River. One sample from this area analysed by Abeysinghe (1996), proved to be limestone (1.63% MgO). Magnesite and dolomite are found in close association at several localities along the track west from Kundip. Although this magnesite probably formed by Cainozoic weathering of Proterozoic dolomite, one sample analysed by Abeysinghe (1996) contained elevated Ni contents, suggesting derivation from Archaean or Proterozoic ultramafic rocks.

Magnesite of higher quality is found at the base of the Pallinup Siltstone where this unit overlies Archaean ultramafic rocks. Deposits formed by hydrothermal replacement of the siltstone with magnesia derived from underlying ultramafic rocks and transported in alkaline groundwater. The most significant deposit is at Bandalup where production of coarse, nodular magnesite has been intermittent. The deposit yielded 67 945 t of magnesite, between 1959 and 1984. Reserves are estimated at 1.252 Mt containing 18.2% $MgCO_3$.

Talc

Recent exploration southwest of Kundip has targeted altered Proterozoic dolomite and has identified limited quantities of talc in the Mesoproterozoic Mount Barren Group. The talc is a high-grade bedded product suitable for use in the cosmetics industry (Abeysinghe, 1996).

Spongolite

Spongolite is widespread within the Pallinup Siltstone, in the southern parts of RAVENSTHORPE and COCANARUP. Spongolite has been used as a building stone in Hopetoun and Ravensthorpe, but could also find application as an insulating or abrasive material. An old spongolite quarry at Twertup is currently listed as a tourist site by the Department of Conservation and Land Management (CALM).

Chapter 10

Summary and conclusions

There are three major Precambrian tectonic units represented on RAVENSTHORPE and COCANARUP — from northwest to southeast these are:

- the southern Archaean Yilgarn Craton;
- the Mount Barren Group; and
- Munglinup Gneiss.

The latter two units are assigned to the Mesoproterozoic Albany–Fraser Orogen (Myers, 1990a).

The Archaean craton contains an enclave of greenstones that is surrounded by granitic rocks, mainly granitoid gneiss, to the west, north and east. The greenstones comprise two tectonostratigraphic terranes (the Carlingup and Ravensthorpe Terranes) and a third component of uncertain affiliation (the Cocanarup greenstones). These tectonostratigraphic units form part of the Southern Cross Superterrane of Myers (1995a).

The Carlingup Terrane contains metamorphosed komatiite, basalt, sedimentary rocks and minor dacitic to rhyolitic volcanic rocks. Metasedimentary rocks include chert, banded iron-formation and manganese-rich and sulfide-rich metasedimentary rocks. The presence of chert and banded iron-formation, and the paucity of cross bedding and graded bedding in clastic deposits, suggests a low-energy, shallow-water depositional environment, comparable to the widespread 'platform greenstones' elsewhere in the Yilgarn Craton (Groves and Batt, 1984). The association of this sedimentary sequence with ultramafic to mafic volcanic and felsic volcanic rocks suggests a submarine, continental rift depositional setting for the Carlingup Terrane. Single zircons from rhyolite yield U–Pb isotope data that Nelson (1995) has interpreted to yield a depositional age of 2958 ± 4 Ma. Komatiitic ultramafic rocks contain subeconomic concentrations of nickel–iron sulfide minerals. There are massive to bedded pyritic horizons in the sedimentary Chester Formation and Hatfield Formation that display some similarities with sulfide-rich orebodies in the Iberian Pyrite Belt. Early, layer-parallel deformation may have caused structural repetition of the original stratigraphic sequence and much or all of the exposed Carlingup Terrane greenstones may be allocthonous with respect to their original depositional environment.

The Ravensthorpe Terrane comprises a calc-alkaline intrusive–extrusive association that has been dated at c. 2990–2970 Ma (Savage et al. 1995). The Annabelle Volcanics unit is mainly andesite, with lesser basalt and dacite, and minor to rare rhyolite. The volcanic sequence is dominated by pyroclastic to epiclastic agglomerate, lapilli tuff and tuff and resedimented equivalents. Clasts are entirely volcanic or subvolcanic; hyaloclastite and mafic to intermediate lavas are rare or absent. The abundance of agglomerate, poorly developed bedding, rapid lateral and vertical facies variations, and the absence of non-volcanogenic sedimentary interbeds, suggest a submarine depositional environment continually fed by abundant volcanogenic debris. The absence of hyaloclastite and pillowed lavas suggest the volcanic source was subaerial. Although submarine mass-flows can transport debris long distances from a volcanic source, the Annabelle Volcanics unit is intruded by co-genetic tonalite and this suggests it has not been transported large distances from the magmatic centre. The deposits are typical of those associated with mass wastage of emergent, calc-alkaline volcanic cones (Cas and Wright, 1987).

Calc-alkaline volcanic–tonalite associations are uncommon elsewhere in the Yilgarn Craton, although a few calc-alkaline centres have been documented in other parts of the Southern Cross Superterrane (Hallberg et al., 1976) and also in other parts of the Yilgarn Craton (Giles, 1981). K-poor granitoids are very uncommon in the Yilgarn Craton, although some small plutons of tonalite and diorite have been recorded (Watkins and Hickman, 1990; Roth et al., 1990; Witt and Davy, 1997).

Andesitic stratovolcanoes, such as those that were the source of volcanogenic debris in the Annabelle Volcanics, typically occur in continental margin settings as components of continental or oceanic island arcs (Fisher and Schminke, 1984; Wilson, 1989). Volcanic centres in these types of tectonic settings are commonly associated with porphyry copper mineralization (Beane and Titley, 1981). Sofoulis (1958) and Savage (1992) interpreted the copper–gold mineralization in the Ravensthorpe district in these terms. Calc-alkaline volcanic rocks in volcanic arcs also contain volcanogenic base-metal sulfide deposits and, in this report, the Cu–Au(–Ag) mineralization at Ravensthorpe is reinterpreted as sub-seafloor, synvolcanic, mineralized feeder or discharge zones. Stratabound Cu–Zn deposits in the Annabelle Volcanics at West River are also of synvolcanic origin, but are more closely associated with dacitic volcanic rocks.

Early stages of deformation occurred independently of one another in the two terranes. Granitoid (mainly granodiorite and monzogranite) sheets were emplaced below the greenstones during this early deformation and were later deformed together with the greenstones. Following earlier stages of deformation in each terrane, the Ravensthorpe Terrane was thrust, most probably from west to east, over the Carlingup Terrane. The eastward-verging, overturned Maydon Syncline formed during this event, as did thrust stacking within the Ravensthorpe Terrane. The Ravensthorpe Terrane consists of several thrust slices, which were transported 'piggy-back' fashion above the main basal thrust. Ultramafic rocks, probably derived from the Carlingup Terrane, were caught up as tectonic slices in the basal and overlying thrust planes and aided transport by lubricating thrust surfaces. Thrust planes also acted as zones of weakness that accommodated intrusion of boron-rich pegmatite dykes and hydrothermal fluids during deformation. Some of these pegmatites carry spodumene, tantalum–niobium oxides, apatite–lithiophilite, and elbaite-rich tourmaline. Granitoid sheets continued to be emplaced at the base of the greenstones during accretion.

The Cocanarup greenstones comprise mainly metasedimentary rocks with some ultramafic rocks (especially in the Aerodrome sector). The metasedimentary rocks are not readily correlated with those of the Chester Formation in the Carlingup Terrane. The Cocanarup greenstones may represent either lateral facies variants of the Chester Formation, or, more probably, unrelated sedimentary rocks that lay beneath the Ravensthorpe Terrane rocks, or were deposited in a marine basin between the original depositional sites of the Ravensthorpe and Carlingup Terranes. Associated ultramafic rocks may have been deposited with the sediments, or alternatively may have become interleaved with the metasedimentary rocks during transport.

Metamorphism commenced in each terrane prior to amalgamation but the dominant metamorphic assemblages preserved at the current erosion level developed during accretion as the rocks adjusted to the new P–T conditions imposed by deformation and granitoid intrusion. Syn-amalgamation intrusion of granitoid sheets was facilitated by movement on low-angle structures during accretion of the two terranes. Pre-amalgamation lineations preserved locally at the margin of the Cocanarup greenstones suggest that granitoid emplacement may have commenced during the earliest stages of accretion. Compositional differences between granitoid gneiss west of the Cocanarup greenstones and that northeast of the Carlingup Terrane also suggest initial emplacement prior to complete amalgamation. However, the metamorphic history of the greenstones requires a continued thermal input from granitoid intrusions during terrane accretion.

The final metamorphic patterns appear to be largely independent of terrane boundaries, but show some correlation with granitoid gneiss–greenstone contacts. Metamorphic grade varies from middle greenschist facies (≤400°C) to upper amphibolite facies (>600°C). There is evidence for decompressional P–t paths in some samples from the Cocanarup greenstones. For this reason, the Cocanarup greenstones are interpreted as forming part of the upper plate (together with the Ravensthorpe Terrane) during thrusting and accretion. Andesitic rocks at the leading edge of the upper plate preserve evidence for compressional P–t paths. Both upper plate (Ravensthorpe Terrane) and lower plate (Carlingup Terrane) display evidence for prograde heating paths as a consequence of heat introduced from crystallizing granitoid sheets.

The absence of kyanite in Carlingup Terrane pelites, and pressure estimated at 2.5 kb during prograde metamorphism of the Chester Formation, limits the thickness of the overthrust plate to 7–9 km. However, a thicker upper plate is permissible if erosion and uplift kept pace with thermal equilibration. The presence of polymictic conglomerate units dominated by tonalitic and calc-alkaline volcanic clasts in the Carlingup Terrane attests to contemporaneous thrusting and erosion of the Ravensthorpe Terrane rocks.

Large quantities of fluid derived from metasedimentary rocks in the lower plate (and from the Cocanarup greenstones within the upper plate) would probably have moved upward along the basal and overlying thrust planes. These fluids may have leached copper and gold from low-level mineralization in the Manyutup Tonalite (Hemley and Hunt, 1992). Thus, copper, gold and silver from synvolcanic deposits in the Annabelle Volcanics may have been partly remobilized and redeposited in footwall splays in the Carlingup Terrane. Some of the copper-poor, gold-rich veins in both terranes may also have formed at this time.

Post-amalgamation deformation events did not impart pervasive fabrics. Following amalgamation of the Ravensthorpe and Carlingup Terranes, the greenstones and underlying granitoid gneiss were deformed together to form the Beulah synform. A change in the regional stress field from east–west to north–south was accompanied by northward transport of the greenstones over granitoid gneiss across the Bonnymidgup Shear Zone and weak folding about east–west axes (most obviously in the Cocanarup area). Amphibolitic rocks in the Bonnymidgup Shear Zone, and linear fabrics defined by hornblende in amphibolite, indicate that amphibolite facies regional metamorphism was maintained during these later stages of deformation. Emplacement of small biotite monzogranite and granodiorite plutons post-dated the main stages of orogenesis.

At around 2500 ± 100 Ma, and again between 1600 and 1300 Ma (Myers, 1993), dolerite dykes were emplaced during rifting of the Archaean supercontinent, a fragment of which became the present-day Yilgarn Craton.

Deposition of quartz-rich Mount Barren Group sediments some time in the period between 1550 and 1300 Ma (Myers, 1993) may have been related to this rifting event but the provenance of these sediments is not yet resolved. An alternative proposal is that the Mount Barren Group was deposited in a foreland basin to East Antarctica as the East Antarctica continental plate

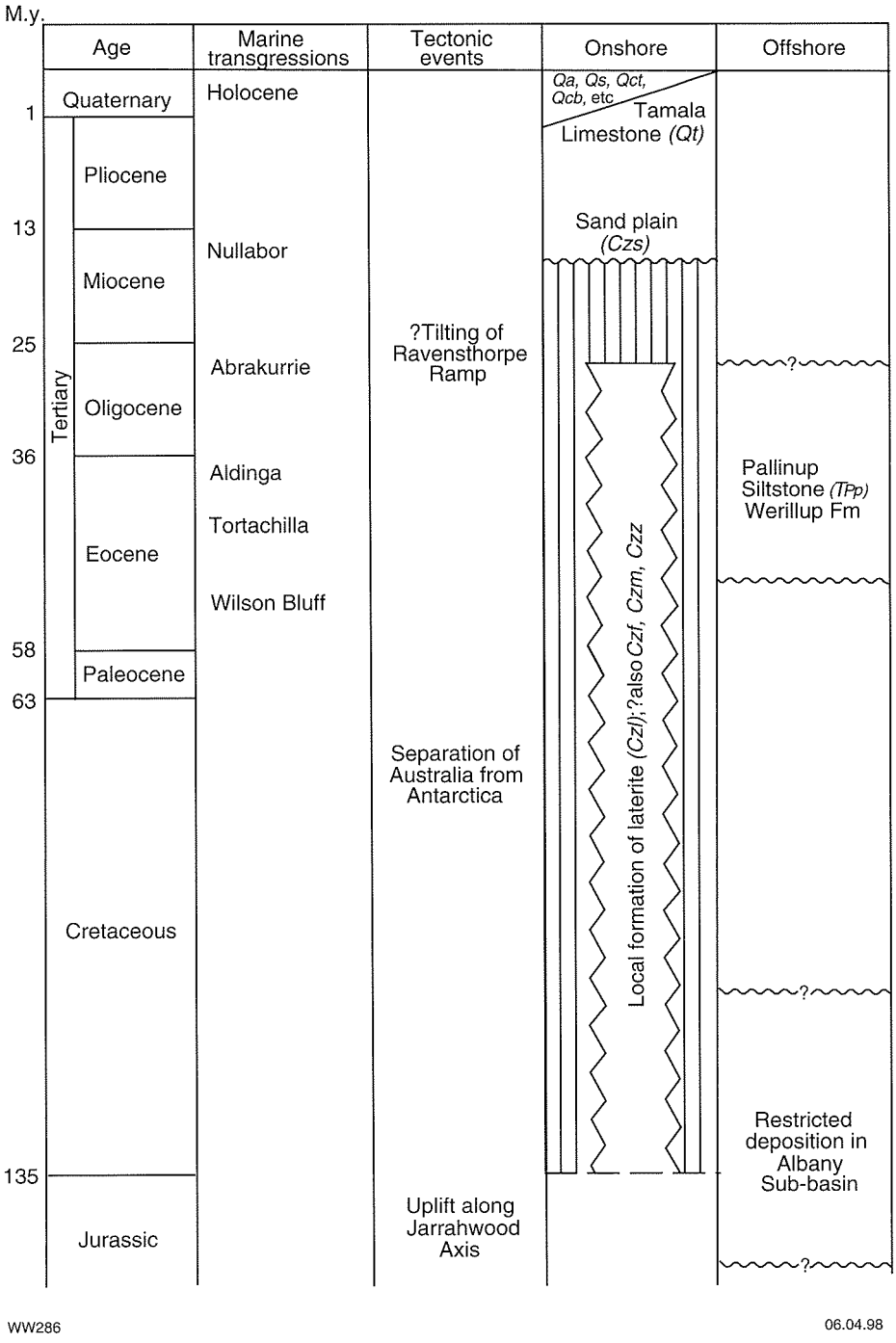

Figure 66. Stratigraphic column (Upper Jurassic to present) showing main tectonic and depositional events in the Ravensthorpe–Hopetoun area

approached the Yilgarn Craton immediately prior to the Albany–Fraser Orogeny (Nelson et al., 1995).

A northward-verging fold-and-thrust belt was formed by deformation of Mount Barren Group sedimentary rocks, during the Albany–Fraser Orogeny, at around 1300 Ma (Myers, 1993). The Albany–Fraser Orogeny brought together the southern Yilgarn Craton and a second plate, preserved now mainly as Mesoproterozoic orthogneiss of the Biranup and Nornalup Complexes in Australia (Myers, 1993, 1995b) and in the Bunger Hills, Antarctica (Nelson et al., 1995). Five stages of deformation are recognized in the Mount Barren Group. The first three stages are probably related to progressive transport of the sedimentary rocks northward across the southern Yilgarn foreland, although little is known about D_{B1}, which produced low-angle thrusts and recumbent folds. The principal stress direction during D_{B2} was oriented north–south but swung to the northwest during D_{B3}. Peak metamorphic conditions at P = >6kb, and

T = 600°C were reached in the deeper parts of the structural complex during and immediately after D_{B3}. During this deformation of the Mount Barren Group, new faults developed and old ones were reactivated within the Archaean foreland, causing limited movement or 'jostling' of adjacent blocks of Archaean crust.

The final phase of folding (D_{B4}) in the Mount Barren Group produced a variety of small-scale structures, including warping about north–south fold axes. This phase of deformation may have occurred during westward transport of the Albany–Fraser Orogen over the Yilgarn Craton between 1270 and 1180 Ma (Nelson et al., 1995).

Deep crustal sections were uplifted south of the Jerdacuttup Fault and related faults, possibly as a result of gravitational collapse or isostatic readjustment following crustal thickening during the Albany–Fraser Orogeny. These movements brought kyanite-bearing metapelites and Munglinup Gneiss to their present level of exposure, adjacent to much lower grade rocks. The granulite facies Munglinup Gneiss, with a protolith age of approximately 2630 Ma (Nelson et al., 1995; Myers, 1995b), was deformed and recrystallized at amphibolite facies during the Albany–Fraser Orogeny, but displays no evidence of earlier (Archaean) deformation (Myers, 1995b).

Little is known about the geological evolution of the Ravensthorpe area between the termination of the Albany–Fraser Orogeny and initial uplift along the Jarrahwood Axis. Much of the Yilgarn Craton was exposed to sub-aerial conditions during this time (Butt, 1988). Uplift along the Jarrahwood Axis probably occurred during the Jurassic (Clarke, 1994) and preceded the separation of Australia from Antarctica during the late Cretaceous (Hocking, 1990). Rejuvenation of the southward-flowing river systems may have accompanied this separation.

Laterite developed onshore, from the Cretaceous up to early Tertiary (Fig. 66). The Plantagenet Group, including the Pallinup Siltstone, was deposited offshore during the mid- to late-Eocene Aldinga transgression (Clarke, 1994). Further tilting of the Ravensthorpe Ramp, possibly during the Oligocene, is indicated by a slight southward dip for the base of the Plantagenet Group (Hocking, 1990). Erosion during this period dissected the Pallinup Siltstone and stripped much of the Tertiary laterite from underlying Precambrian rocks (Fig. 66).

Onshore deposition of an extensive sandplain postdated the last major transgression, which occurred during the mid-Miocene (Hocking and Cockbain, 1990). Tamala Limestone was deposited in a marine, nearshore environment during the Quaternary and was later partly exposed during a subsequent marine regression. Reworking of the Tamala Limestone, the late Tertiary sandplain, and other, earlier, units, continues to the present time, contemporaneous with nearshore deposition of beach sand, and local deposition of aeolian sand, silt in freshwater swamps, and river channel deposits.

Acknowledgements

Outokumpu Australia Pty Ltd provided regional geological maps and aeromagnetic images of the Archaean portions of RAVENSTHORPE and COCANARUP. The Centre for Electron Microscopy (University of Western Australia) and CSIRO, Floreat Park, are acknowledged for ensuring access to their analytical facilities. The author has benefited from discussions with Simon Wetherley and Mark Savage. A visit to the field area with Tim Griffin, John Myers, Cees Swager and Stephen Wyche, in late 1993, stimulated many of the ideas presented in this report. However, final responsibility for the contents rest with the author. Stephen Wyche is further acknowledged for a review of an earlier version of this report.

References

ABEYSINGHE, P. B., 1996, Talc, pyrophyllite and magnesite in Western Australia: Western Australia Geological Survey, Mineral Resources Bulletin 16, 118p.

AHMAT, A. L., 1986, Metamorphic patterns in the greenstone belts of the Southern Cross Province, Western Australia: Western Australia Geological Survey, Report 19, Professional Papers for 1984, p. 1–21.

ARNDT, N. T., NALDRETT, A. J., and PYKE, D. R., 1977, Komatiitic and iron-rich tholeiitic lavas of Munro Township, northeast Ontario: Journal of Petrology, v. 18, p. 319–369.

ARTH, J. G., and BARKER, F., 1976, Rare-earth partitioning between hornblende and dacitic liquid and implications for the genesis of trondhjemitic–tonalitic magmas: Geology, v. 4, p. 534–536.

BARLEY, M. E., 1986, Incompatible-element enrichment in Archean basalts: A consequence of contamination by older sialic crust rather than mantle heterogeneity: Geology, v. 14, p. 947–950.

BARRIE, C. T., LUDDEN, J. N., and GREEN, A. H., 1993, Geochemistry of volcanic rocks associated with Cu–Zn and Ni–Cu deposits in the Abitibi Subprovince: Economic Geology, v. 88, p. 1341–1358.

BARROW, G., 1893, On an intrusion of muscovite–biotite gneiss in the southeastern Highlands of Scotland, and its accompanying metamorphism: Quarterly Journal of the Geological Society of London, v. 49, p. 330–358.

BATEMAN, P. C., and CHAPPELL, B. W., 1978, Crystallization, fractionation, and solidification of the Tuolomne Intrusive Series, Yosemite National Park, California: Geological Society of America Bulletin, v. 90, p. 465–482.

BEANE, R. E., and TITLEY, S. R., 1981, Porphyry copper deposits Part II. Hydrothermal alteration and mineralization: Economic Geology, 75th Anniversary Volume, p. 214–215, 235–269.

BEESON, J., DELOR, C. P., and HARRIS, L. B., 1988, A structural and metamorphic traverse across the Albany Mobile Belt, Western Australia: Precambrian Research, v. 40/41, p. 117–136.

BINNS, R. A., 1964, Zones of progressive regional metamorphism in the Willyama Complex, Broken Hill district, New South Wales: Journal of the Geological Society of Australia, v. 11, p. 283–330.

BLOCKLEY, J. G., 1980, The tin deposits of Western Australia with special reference to the associated granites: Western Australia Geological Survey, Mineral Resources Bulletin 12, 184p.

BLUNDY, J. D., and HOLLAND, T. J. B., 1990, Calcic amphibole equilibria and a new amphibole–plagioclase geothermometer: Contributions to Mineralogy and Petrology, v. 104, p. 208–224.

BURNHAM, C. W., 1979, Magmas and hydrothermal fluids, *in* Geochemistry of Hydrothermal Ore Deposits *edited by* H. L. BARNES: New York, John Wiley and Sons.

BUTT, C. R. M., 1988,Genesis of lateritic and supergene deposits in the Yilgarn Block, Western Australia, *in* Bicentennial Gold 88, Extended Abstracts Oral Programme *edited by* A. D. T. GOODE and I. L. BOSMA: Geological Society of Australia Abstract Series no. 22, p. 359–364.

CALM (Department of Conservation and Land Management), 1991, Fitzgerald River National Park Management Plan 1991–2001: Department of Conservation and Land Management, Management Plan no. 15, 133p.

CAMPIGLIO, C., and DARLING, R., 1976, The geochemistry of the Archaean Bourlamaque batholith, Abitibi, Quebec: Canadian Journal of Earth Sciences, v. 13, p. 972–986.

CANDELA, P. A., and HOLLAND, H. D., 1986, A mass transfer model for copper and molybdenum in magmatic hydrothermal systems: the origin of porphyry-type ore deposits: Economic Geology, v. 81, p. 1–19.

CARMICHAEL, D. M., 1978, Metamorphic bathozones and bathograds: a measure of the depth of post-metamorphic uplift and erosion on a regional scale: American Journal of Science, v. 278, p. 769–797.

CAS, R. A. F., and WRIGHT, J. V., 1987, Volcanic successions modern and ancient: London, Allen and Unwin.

CATHLES, L. M., 1993, Oxygen isotope alteration in the Noranda mining district, Abitibi greenstone belt, Quebec: Economic Geology, v. 88, p. 1483–1511.

CHAMBERLAIN, C. P., and KARABINOS, P., 1987, Influence of deformation on pressure–temperature paths of metamorphism: Geology, v. 15, p. 42–44.

CHIVAS, A. R., 1978, Porphyry copper mineralization at the Koloula Igneous Complex, Guadalcanal, Solomon Islands: Economic Geology, v. 73, p. 645–677.

CLARKE, J. D. A., 1994, Evolution of the Lefroy and Cowan palaeodrainage channels, Western Australia: Australian Journal of Earth Sciences, v. 41, p. 55–68.

COLVINE, A. C., FYON, J. A., HEATHER, K. B., MARMONT, S., SMITH, P. M., and TROOP, D. G., 1988. Archean lode gold deposits in Ontario: Ontario Geological Survey, Miscellaneous Paper 139, 136p.

COPE, R. N., 1975, Tertiary epeirogeny in the southern part of Western Australia: Western Australia Geological Survey, Annual Report for 1974, p. 40–46.

DAVY, R., AND LEONARD, E. L., 1989, Orientation geochemical study, Fitzgerald River National Park area. Western Australia Geological Survey, Record 1989/13, 16p.

de la HUNTY, L. E., 1963, The geology of the manganese deposits of Western Australia: Western Australia Geological Survey, Bulletin 116, 122p.

DEPARTMENT of MINES, 1954, List of cancelled Gold Mining Leases which have produced gold: Western Australia Department of Mines, Perth, Government Printer, 271p.

DILLES, J. H., and EINAUDI, M. T., 1992, Wall-rock alteration and hydrothermal flow paths about the Ann-Mason porphyry copper deposit, Nevada — a 6 km vertical reconstruction: Economic Geology, v. 87, p. 1963–2001.

DONALDSON, C. H., 1976, An experimental investigation of olivine morphology: Contributions to Mineralogy and Petrology, v. 57, p. 187–213.

ENGLAND, P. C., and RICHARDSON, S. W., 1977, Influence of erosion upon the mineral facies of rocks from different metamorphic

environments: Journal of the Geological Society, v. 134, p. 201–213.

ENGLAND, P. C., and THOMPSON, A. B., 1984, Pressure–temperature–time paths of regional metamorphism. I. Heat transfer during the evolution of regions of thickened continental crust: Journal of Petrology, v. 25, p. 894–928.

FISHER, R. V., and SCHMINKE, H.-U., 1984, Pyroclastic rocks: Springer-Verlag, Berlin.

FRANKLIN, J. M., SANGSTER, D. F., and LYDON, J. W., 1981, Volcanic-associated massive sulphide deposits: Economic Geology, 75th Anniversary Volume, p. 485–627.

FRIDRICH, C. J. and MAHOOD, G. A., 1984, Reverse zoning in the resurgent intrusions of the Grizzly Peak cauldron, Sawatch Range, Colorado: Geological Society of America Bulletin, v. 95, p. 779–787.

FYFE, W. S., 1990, Prospecting for the 1990s: the integration of tectonics and geochemical transport processes, *in* Stable isotopes and fluid processes in mineralization *edited by* H. K. HERBERT and S. E. HO: University of Western Australia, Geology Department and University Extension Service, Publication no. 23, p. 1–16.

GALLEY, A.G., 1993, Characteristics of semi-conformable alteration zones associated with volcanogenic massive sulfide districts: Journal of Geochemical Exploration, v. 48, p. 175–200.

GEE, R. D., BAXTER, J. L., WILDE, S. A., and WILLIAMS, I. R., 1981, Crustal development in the Yilgarn Block, Western Australia, *in* Archaean Geology *edited by* J. E. GLOVER and D. I. GROVES: International Archaean Symposium, 2nd, Perth, W.A., 1980, Proceedings: Geological Society of Australia Special Publication no. 7, p. 43–56.

GILBERT, M. C., HELZ, R. T., POPP, R. K., and SPEAR, F. S., 1982, Experimental studies of amphibole stability, *in* Amphiboles: Petrology and experimental phase relations *edited by* D. R. VEBLEN and P. H. RIBBE: Reviews in Mineralogy, Volume 9B, Mineralogical Society of America, 390p.

GILES, C. W., 1981, Archaean calc-alkaline volcanism in the Eastern Goldfields Province, Western Australia, *in* Archaean Geology *edited by* J. E. GLOVER and D. I. GROVES: International Archaean Symposium, 2nd, Perth, W. A., 1980, Proceedings: Geological Society of Australia Special Publication no. 7, p.275–286.

GOLDIE, R., 1978, Magma mixing in the Flavrian pluton, Noranda area, Quebec: Canadian Journal of Earth Sciences, v. 15, p. 132–144.

GOLE, M. J., BARNES, S. J., and HILL, R. E. T., 1987, The role of fluids in the metamorphism of komatiites, Agnew nickel deposit, Western Australia: Contributions to Mineralogy and Petrology, v. 96, p. 151–162.

GRAY, N. M., and GLEESON, J. S., 1951a, Report on pyrite — Mount McMahon, Phillips River Goldfield: Western Australia Geological Survey, Annual Report for 1949, p. 110.

GRAY, N. M., and GLEESON, J. S., 1951b, Report on manganese deposits in and adjacent to the Phillips River Goldfield: Western Australia Geological Survey, Annual Report for 1949, p. 61–68.

GRESENS, R. L., 1967, Composition–volume relationships of metasomatism: Chemical Geology, v. 2, p. 47–65.

GRIFFIN, T. J., 1990, Southern Cross Province, *in* Geology and mineral resources of Western Australia *edited by* A. F. TRENDALL: Western Australia Geological Survey, Memoir 3, p. 60–77.

GROMET, L. P., and SILVER, L. T., 1987, REE variations across the Peninsula Ranges Batholith: implications for batholithic petrogenesis and crustal growth in magmatic arcs: Journal of Petrology, v. 28, p. 5–125.

GROVES, D. I. and BATT, W. D., 1984, Spatial and temporal variations of Archaean metallogenic associations in terms of evolution of granitoid–greenstone terrains with particular emphasis on Western Australia, *in* Archaean Geochemistry *edited by* A. KRONER, G. N. HANSON, and A. M. GOODWIN: Berlin, Springer-Verlag, p. 73–98.

GROVES, D. I., BARLEY, M. E., BARNICOAT, A. C., CASSIDY, K. F., FARE, R. J., HAGEMANN, S. G., HO, S. E., HRONSKY, J. M. A., MIKUCKI, E. J., MUELLER, A.G., McNAUGHTON, N. J., PERRING, C. S., RIDLEY, J. R., and VEARNCOMBE, J. R., 1992, Sub-greenschist to granulite-hosted Archaean lode-gold deposits of the Yilgarn Craton: a depositional continuum from deep-sourced hydrothermal fluids in crustal-scale plumbing systems, *in* The Archaean: Terrains, processes and metallogeny *edited by* J. E. GLOVER and S. E. HO: University of Western Australia, Geology Department (Key Centre) and University Extension Service, Publication no. 22, p. 325–337.

HALLBERG, J. A., 1987, Post-cratonization mafic and ultramafic dykes of the Yilgarn Block: Australian Journal of Earth Sciences, v. 34, p. 135–150.

HALLBERG, J. A., JOHNTOM, C., and BYE, S. M., 1976, The Archaean Marda Dam igneous complex, Western Australia: Precambrian Research, v. 3, p. 111–136.

HANSON, G. N. 1978, The application of trace elements to the petrogenesis of igneous rocks of granitic composition: Earth and Planetary Science Letters, v. 38, p. 26–43.

HEMLEY, J. J., and HUNT, J. P., 1992, Hydrothermal ore-forming processes in the light of studies in rock-buffered systems II. Some general geologic applications: Economic Geology, v. 87, p. 23–43.

HEMLEY, J. J., CYGAN, G. L., FEIN, J. B., ROBINSON, G. R., and D'ANGELO, W. M., 1992, Hydrothermal ore-forming processes in the light of studies in rock-buffered systems: I. Iron–copper–zinc–lead sulfide solubility relations: Economic Geology, v. 87, p. 1–22.

HILL, W. B., 1976, Pegmatite minerals (mica, beryl, lithium, feldspars) — Western Australia, *in* Economic geology of Australia and Papua New Guinea, Volume 4. Industrial Minerals and Rocks *edited by* C. L. KNIGHT: Australasian Institute of Mining and Metallurgy, Monograph 8, p. 235–240.

HILL, R. E. T., GOLE, M. J., and BARNES, S. J., 1987, Physical volcanology of komatiites: A field guide to komatiites between Kalgoorlie and Wiluna, Eastern Goldfields Province, Yilgarn Block, Western Australia: Geological Society of Australia (W. A. Division), Excursion Guide no. 1, 74p.

HINE, R., and MASON, D. R., 1978, Intrusive rocks associated with porphyry copper mineralization, New Britain, Papua New Guinea: Economic Geology, v. 73, p. 749–760.

HOCKING, R. M., 1990, Bremer Basin, *in* Geology and mineral resources of Western Australia *edited by* A. F. TRENDALL: Western Australia Geological Survey, Memoir 3, p. 561–563.

HOCKING, R. M., and COCKBAIN, A. E., 1990, Regolith, *in* Geology and mineral resources of Western Australia *edited by* A. F. TRENDALL: Western Australia Geological Survey, Memoir 3, p. 591–602.

IRVINE, T. N., and BARAGAR, W. R. A., 1979, A guide to the chemical classification of the common volcanic rocks: Canadian Journal of Earth Sciences, v. 8. p. 523–548.

ISHIHARA, S., 1977, The magnetite-series and ilmenite-series granitic rocks: Mining Geology, v. 27, p. 293–305.

KILLICK M. F., and BLACKBURN, G. V., 1994, Sedimentology of the mid-Proterozoic Mount Barren Group, *in* Australian Geological Convention, 12th Perth, W. A., 1994, Abstracts *edited by* M. FREEMAN: Geological Society of Australia, Abstracts Series, no. 37, p. 504.

LE MAITRE, R.W., 1989, A classification of igneous rocks and glossary of terms: Blackwell, Oxford, 193p.

LESHER, C. A., 1989, Komatiite-associated nickel sulphide deposits, *in* Ore deposits associated with magmas *edited by* J. A. WHITNEY and A. J. NALDRETT: Reviews in Economic Geology, no. 4, p. 45–101.

LONDON, D., 1990, Internal differentiation of rare-element pegmatites; a synthesis of recent research: Geological Society of America, Special Paper 246, p. 35–50.

LYDON, J. W., 1984, Ore deposit models — 8. Volcanogenic massive sulphide deposits Part I. A descriptive model: Geoscience Canada, v. 11, p. 195–202.

MARSTON, R. J., 1979, Copper mineralization in Western Australia: Western Australia Geological Survey, Mineral Resources Bulletin 13, 208p.

MARSTON, R. J., 1984, Nickel mineralization in Western Australia: Western Australia Geological Survey, Mineral Resources Bulletin 14, 271p.

MONGER, J. W. H., SOUTHER, J.G., and GABRIELSE, H., 1972, Evolution of the Canadian Cordillera: A plate tectonic model: American Journal of Science, v. 272, p. 577–602.

MORRIS, P. A., 1993, Archaean mafic and ultramafic volcanic rocks, Menzies to Norseman, Western Australia: Western Australia Geological Survey, Report 36, 107p.

MYASHIRO, A., 1973, Metamorphism and metamorphic belts: London, George Allen and Unwin.

MYERS, J. S., 1990a, Albany–Fraser Orogen, *in* Geology and mineral resources of Western Australia *edited by* A. F. TRENDALL: Western Australia Geological Survey, Memoir 3, p. 255–264.

MYERS, J. S., 1990b, Mafic dyke swarms, Yilgarn Craton, *in* Geology and mineral resources of Western Australia *edited by* A. F. TRENDALL: Western Australia Geological Survey, Memoir 3, p. 126–127.

MYERS, J. S., 1992, Tectonic evolution of the Yilgarn Craton, Western Australia, *in* The Archaean: Terrains, processes and metallogeny *edited by* J. E. GLOVER and S. E. HO: University of Western Australia, Geology Department (Key Centre) and University Extension Service, Publication no. 22, p. 265–274.

MYERS, J. S., 1993, Precambrian history of the West Australian Craton and adjacent orogens: Annual Review of Earth and Planetary Sciences, v. 21, p. 453–485.

MYERS, J. S., 1995a, The generation and assembly of an Archaean supercontinent: evidence from the Yilgarn Craton, Western Australia, *in* Early Precambrian processes *edited by* M. P. COWARD and A. C. RIES: Geological Society Special Publication no. 95, p. 143–154.

MYERS, J. S., 1995b, Esperance, Western Australia: Western Australia Geological Survey, 1:1 000 000 Geological Series, Explanatory Notes, 10p.

MYERS, J. S., and HOCKING, R. M., (compilers) 1988, Geological map of Western Australia: Western Australia Geological Survey.

NELSON, D. R., 1995, Compilation of SHRIMP U–Pb zircon geochronology data, 1994: Western Australia Geological Survey, Record 1995/3, 244p.

NELSON, D. R., 1996, Compilation of SHRIMP U–Pb zircon geochronology data, 1995: Western Australia Geological Survey, Record 1996/5, 168p.

NELSON, D. R., MYERS, J. S., and NUTMAN, A. P., 1995, Timing of events in the mid-Proterozoic Albany–Fraser Orogen, Western Australia, and implications for Gondwana correlations: Australian Journal of Earth Sciences, v. 42, p. 481–496.

PARK, R.G., 1988, Geological structures and moving plates: Glasgow and London, Blackie.

PERCHUK, L. L. and LAVREN'TEVA, I. V., 1981, Experimental investigation of exchange equilibria in the system cordierite–garnet–biotite, *in* Kinetics and equilibrium in mineral reactions *edited by* S. K. SAXENA: Springer-Verlag, New York, p. 199–240.

PERRING, R. J., 1991, First annual report, West River E74/131, E74/138, March 18, 1990 to March 17, 1991: Pancontinental Mining Ltd (unpublished report).

REDMAN, B. A., and KEAYS, R. R., 1985, Archaean basic volcanism in the Eastern Goldfields Province, Yilgarn Block, Western Australia: Precambrian Research, v. 30, p. 113–152.

RESOURCE INFORMATION UNIT, 1993, Register of Australian Mining 1993/94, *edited by* D. WILKINSON: Resource Information Unit, Subiaco, Western Australia.

ROSE, A. W., 1970, Zonal relations of wallrock alteration and sulfide distribution at porphyry copper deposits: Economic Geology, v. 65, p. 920–936.

ROTH, E., BENNETT, J. M., and SYMONS, P. M., 1990, Boddington and Black Flag: Anomalous Archaean gold deposits, *in* Gold deposits of the Archaean Yilgarn Block, Western Australia: Nature, genesis and exploration guides *edited by* S. E. HO, D. I. GROVES and J. M. BENNETT: University of Western Australia, Geology Department and University Extension Service, Publication no. 20, p. 189–194.

SAVAGE, M., 1992, A study on the source and nature of Cu–Au–Ag mineralization in the Phillips River Goldfield, Ravensthorpe, Western Australia: University of Western Australia, M.Sc. thesis (unpublished).

SAVAGE, M., BARLEY, M. E., and McNAUGHTON, N. J., 1995, SHRIMP U–Pb geochronology of 2.95 to 3.0 Ga felsic igneous rocks at Ravensthorpe, Yellowdine Terrane, Yilgarn Craton, *in* Australian Conference on geochronology and isotope geoscience, Workshop Programme and Abstracts: Western Australia Curtin University of Technology, Perth, p. 30.

SOFOULIS, J., 1958, The geology of the Phillips River Goldfield: Western Australia Geological Survey, Bulletin 110, 145p.

SPEAR, F. S., 1993, Metamorphic phase equilibria and Pressure–Temperature–Time paths: Mineralogical Society of America, Monograph, 799p.

SPEAR, F. S., SELVERSTONE, J., HICKMOTT, D., CROWLEY, P., and HODGES, K. V., 1984, P–T paths from garnet zoning: A new technique for deciphering tectonic processes in crystalline terranes: Geology, v. 12, p. 87–90.

STIX, J., 1991, Subaqueous, intermediate to silicic-composition explosive volcanism: a review: Earth Science Reviews, v. 31, p. 21–53.

STRECKEISEN, A., 1976, To each plutonic rock its proper name: Earth Science Reviews, no. 12, p. 1–33.

SUN, S. S., and NESBITT, R. W., 1978, Petrogenesis of Archaean ultrabasic and basic volcanics: Evidence from rare earth elements: Contributions to Mineralogy and Petrology, v. 65, p. 301–325.

SWAGER, C. P., WITT, W. K., GRIFFIN, T. J., AHMAT, A. L., HUNTER, W. M., McGOLDRICK, P. J., and WYCHE, S., 1992, Late Archaean granite–greenstones of the Kalgoorlie Terrane, Yilgarn Craton, Western Australia: *in* The Archaean: Terrains, processes and metallogeny *edited by* J. E. GLOVER and S. E. HO: University of Western Australia, Geology Department (Key Centre) and University Extension Service, Publication no. 22, p. 107–122.

TAYLOR, S. R., and McLENNAN, S. M., 1985, The continental crust: Its composition and evolution: Blackwell, Oxford, 312p.

THOM, R., 1977, The evolution of Proterozoic rocks near the Fraser Front at Ravensthorpe, Western Australia: University of London, PhD thesis (unpublished).

THOM, R., and CHIN, R. J., 1984, Bremer Bay, Western Australia: Western Australia Geological Survey, 1:250 000 Geological Series, Explanatory Notes, 20p.

THOM, R., LIPPLE, S. L., and SANDERS, C. C., 1977, Ravensthorpe, Western Australia: Western Australia Geological Survey, 1:250 000 Geological Series Explanatory Notes, 40p.

THOM, R., CHIN, R. J., and HICKMAN, A. H., 1984, Newdegate, Western Australia: Western Australia Geological Survey, 1:250 000 Geological Series Explanatory Notes, 24p.

THOMPSON, A. B., and ENGLAND, P. C., 1984, Pressure–temperature–time paths of regional metamorphism. II. Their inference and interpretation using mineral assemblages in metamorphic rocks: Journal of Petrology, v. 25, p. 929–955.

TITLEY, S. R., and BEANE, R. E., 1981, Porphyry copper deposits Part I. Geologic settings, petrology and tectonogenesis: Economic Geology, 75th Anniversary Volume, p. 214–235, 263–265.

TOWNSEND, D. B., 1994, Mineral deposits of the Albany 1:1 000 000 sheet: Western Australia Geological Survey, Record 1993/4, 80p.

TOWNSEND, D. B., PRESTON, W. A., and COOPER, R. W., 1996, Mineral resources and locations, Western Australia: digital dataset from MINEDEX: Geological Survey of Western Australia, Record 1996/13, 19p.

VALLANCE, T.G., 1967, Mafic rock alteration and the isochemical development of some cordierite–anthophyllite rocks: Journal of Petrology, v. 8, p. 84–96.

VESANTO, J., 1992, Annual technical report for year ending 15 September 1992 on VMS-type base metals exploration: Exploration Licence 74/56, Mount Chester: Outokumpu Exploration Australia Pty Ltd (unpublished).

WATKINS, K. P., and HICKMAN, A. H., 1990, Geological evolution and mineralization of the Murchison Province, Western Australia: Geological Survey of Western Australia, Bulletin 137, 267p.

WATMUFF, G., 1978, Geology and alteration–mineralization zoning in the central portion of the Yandera porphyry copper prospect, Papua New Guinea: Economic Geology, v. 73, p. 829–856.

WETHERLEY, S., 1995, Clockwise pressure–temperature–time paths for the Proterozoic Mount Barren Group, Albany–Fraser Province, Southwestern Australia, *in* Precambrian '95 Program and Abstracts (unedited): École Polytechnique de Montreal, Canada, p. 263.

WETHERLEY, S., HARRIS, L. B., and RIDLEY, J. R., 1994, The tectonic setting of the Mount Barren Group, Albany–Fraser Orogen, W.A.: Implications for basin-formation and subsequent deformation during a compressional orogeny in eastern Gondwana, *in* Australian Geological Convention, 12th, Perth, W. A. 1994, Abstracts *edited by* M. FREEMAN: Geological Society of Australia, Abstracts Series, no. 37, p. 458–459.

WHALEN, J. B., 1985, Geochemistry of an island-arc plutonic suite: the Uasilau–Yau Yau Intrusive Complex, New Britain, P.N.G.: Journal of Petrology, v. 26, p. 603–632.

WILSON, M., 1989, Igneous petrogenesis: A global tectonic approach: London, Unwin Hyman.

WITT, W. K., 1992, Heavy-mineral characteristics, structural settings, and parental granites of pegmatites in Archaean rocks of the eastern Yilgarn Craton: Western Australia Geological Survey, Record 1992/10, 54p.

WITT, W. K., 1993, Gold mineralization in the Menzies–Kambalda region, Eastern Goldfields, Western Australia: Western Australia Geological Survey, Report 39, 165p.

WITT, W. K., 1995, Terrane accretion and Cu–Au mineralization at a province boundary: the Ravensthorpe greenstone belt, Western Australia: Western Australia Geological Survey, Annual Review 1994–95, p. 47–50.

WITT, W. K., 1996a, Ravensthorpe, sheet 2930, W. A.: Western Australia Geological Survey, 1:100 000 Geological Series.

WITT, W. K., 1996b, Cocanarup, sheet 2830, W. A.: Western Australia Geological Survey, 1:100 000 Geological Series.

WITT, W. K., 1997, Geology of the Ravensthorpe and Cocanarup 1:100 000 sheets: Western Australia Geological Survey, 1:100 000 Geological Series Explanatory Notes, 26p.

WITT, W. K., and DAVY, R., 1997, Geology and geochemistry of granitoid rocks in the southwest Eastern Goldfields Province, Western Australia: Western Australia Geological Survey, Report 49, 137p.

WITT, W. K., and VANDERHOR, F., in press, Diversity within a unified model for Archaean gold mineralization in the Yilgarn Craton of Western Australia: An overview of the mesothermal gold deposits: Ore Geology Reviews.

WYBORN, D., and SUN, S. S., 1994, Sulphur-undersaturated magmatism — a key factor for generating magma-related copper–gold deposits: Australian Geological Survey Organisation, Research Newsletter, v. 21, p. 7–8.

YARDLEY, B. W. D., 1989, An introduction to metamorphic petrology: London, Longman.

ZEN A. E., 1988, Thermal modelling of stepwise anatexis in a thrust-thickened sialic crust: Transactions of the Royal Society of Edinburgh, Earth Sciences, v. 79, p. 223–235.

ZHANG, J. S., PASSCHIER, C. W., SLACK, J. F., FLIERVOET, T. F., and de BOORDER, H., 1994, Cryptocrystalline Permian tourmalinites of possible metasomatic origin in the Orobic Alps, Northern Italy: Economic Geology, v. 89, p. 391–396.

Appendix 1

Mineralogy of the Manyutup Tonalite

The minerals amphibole, plagioclase, biotite and secondary chlorite from several samples of the Manyutup Tonalite were analysed on a JEOL 6400 scanning electron microscope (SEM) at the Centre for Electron Microscopy, University of Western Australia (UWA). Analytical conditions were 15 kV and 3×10^{-9}Å. Analytical spectra were collected for 60 seconds. A copy of the analytical file, SIL15H.ZAF, is reproduced in Table 1.1. The chemistry of metamorphic minerals in the Archaean greenstones is documented in Tables 1.3–1.6.

Additionally, reconnaissance analyses for copper in several minerals in two samples of Manyutup Tonalite were carried out using the CAMECA SX-50 Microprobe at Commonwealth Scientific and Industrial Research Organisation (CSIRO), Floreat Park. Mineral analyses were carried out at 30.2 kV and 450 nÅ, for 200 seconds. One analysis was run for 400 seconds. Metallic copper was used as the standard. The lower limit of detection is estimated to have been 6 ppm Cu. The analytical file TRC00407.DAT is reproduced as Table 1.2. Results are presented in Table 1.7 and discussed in Chapter 3.

Table 1.1. Analytical file SIL15H.ZAF used for mineral microanalysis at the Centre for Electron Microscopy, UWA

		FWHM		*Range-1*		*Range-2*		*C/s/nÅ*	*Brem*	*ZAF*	*Standard*
Si	Ka	84	90	55	115	0	0	1313.54	1.8594	2.9285	Wollastonite
Ti	Ka	222	229	205	263	0	0	727.22	0.6649	5.0171	Pure Ti
Al	Ka	71	77	45	95	0	0	1107.11	1.8302	2.6555	CAAL
Cr	Ka	267	274	250	316	0	0	520.09	0.5200	5.3813	Pure Cr
Fe	Ka	316	324	299	371	13	49	375.37	0.3976	5.7541	Pure Fe
Ni	Ka	369	378	352	433	23	57	255.07	0.3119	6.0608	Pure Ni
Mn	Ka	291	299	274	343	0	0	441.40	0.4652	5.6652	Pure Mn
Mg	Ka	60	66	35	84	0	0	872.84	1.7587	2.5141	Periclase
Ca	Ka	181	188	165	218	0	0	877.36	0.9374	3.9616	Wollastonite
Na	Ka	49	55	28	72	0	0	397.98	1.4950	1.7659	Albite
K	Ka	162	169	146	198	0	0	904.50	1.0137	3.6597	Orthoclase
C	Ka	128	134	110	161	0	0	1045.03	1.2041	3.4072	Apatite

Table 1.2. Analytical file TRC00407.DAT used for copper analyses of silicate minerals, CSIRO

Method	*Spectrometer*	*Element*	*Peak*	*Bg offsets*		*C/s/nÅ/100%*
Mnticu30	1	Mn	24010	200	200	2350
Mnticu30	2	Ti	31435	200	200	3150
Mnticu30	3	Cu	38251	200	200	1510

Method	*Spectrometer*	*Crystal*	*Bias*	*Gain*	*Dead time*	*Base line*	*Window*	*Mode*
Mnticu30	1	PET	1345	120	2	750	4000	DIFF
Mnticu30	2	PET	1345	120	2	500	4000	DIFF
Mnticu30	3	LIF	1811	120	2	750	2750	DIFF

Table 1.3. Selected analyses of amphiboles from the Manyutup Tonalite

	Sample 113991								
	hb-1	*hb-2*	*hb-3*	*hb-5*	*hb-7*	*hb-8*	*hb-9*	*hb-10*	*hb-14*
					Percentage				
SiO_2	46.63	44.61	46.62	46.36	46.31	46.13	46.14	46.40	46.81
TiO_2	0.19	0.34	0.43	0.44	0.75	0.48	0.77	0.82	0.59
Al_2O_3	8.60	9.67	8.59	9.22	8.90	8.42	8.70	8.99	9.08
FeO	16.96	17.92	17.77	17.07	17.72	17.98	18.07	17.90	18.14
MnO	0.21	0.22	0.33	0.31	0.31	0.00	0.39	0.18	0.22
MgO	11.09	9.90	10.75	10.75	10.80	10.28	10.18	10.97	10.60
CaO	11.82	11.46	11.81	11.60	11.54	11.32	11.05	11.84	11.78
Na_2O	0.68	0.94	0.79	0.82	0.91	0.67	0.96	0.71	0.76
K_2O	0.26	0.39	0.29	0.23	0.36	0.27	0.32	0.28	0.39
Total	**96.44**	**95.44**	**97.37**	**96.81**	**97.59**	**95.55**	**96.64**	**98.09**	**98.37**
Mg#	54.0	50.0	52.0	53.0	52.0	51.0	50.0	52.0	51.0
Si/Al	6.30	5.29	6.07	5.89	5.66	6.35	5.94	5.51	5.83
Al^{vi}	0.405	0.447	0.360	0.442	0.339	0.397	0.370	0.317	0.390
Origin	Ign	Ign	Ign	Ign	Ign	Ign	Ign	Ign	Ign

	Sample 113991 (cont.)									
	hb-15	*hb-16*	*hb-17*	*hb-18*	*hb-19*	*hb-12*	*hb-13*	*hb-4*	*hb-6*	*hb-11*
						Percentage				
SiO_2	46.03	46.71	46.56	46.32	46.26	45.25	45.13	42.75	42.70	42.68
TiO_2	0.26	0.48	0.66	0.58	0.89	0.27	0.57	0.26	0.47	0.29
Al_2O_3	9.55	9.03	9.11	9.06	9.21	11.32	10.31	12.74	12.41	13.29
FeO	18.18	18.18	18.33	18.07	17.91	17.93	18.52	19.55	19.14	19.52
MnO	0.24	0.33	0.27	0.33	0.25	0.36	0.20	0.21	0.00	0.33
MgO	10.48	10.70	10.53	10.26	10.15	9.68	9.60	8.46	8.49	8.72
CaO	12.02	11.71	11.43	11.77	11.14	11.86	11.75	11.51	11.59	11.72
Na_2O	0.91	0.80	0.76	0.83	0.73	1.11	0.80	1.06	1.10	1.26
K_2O	0.24	0.32	0.31	0.31	0.32	0.42	0.41	0.36	0.47	0.51
Total	**97.91**	**98.27**	**97.96**	**97.59**	**96.87**	**98.19**	**97.30**	**96.92**	**96.38**	**97.87**
Mg#	51.0	51.0	51.0	50.0	50.0	49.0	48.0	44.0	44.0	43.0
Si/Al	5.46	5.73	5.65	5.85	5.81	4.90	5.11	3.94	4.09	3.82
Al^{vi}	0.414	0.363	0.364	0.409	0.427	0.604	0.493	0.621	0.631	0.669
Origin	Ign	Ign	Ign	Ign	Ign	Trans	Trans	Met	Met	Met

	Sample 113978							
	hb-20	*hb-25*	*hb-26*	*hb-27*	*hb-28*	*hb-29*	*hb-32*	*hb-33*
					Percentage			
SiO_2	48.45	48.90	50.39	48.98	51.14	51.27	50.12	51.99
TiO_2	0.26	0.37	0.00	0.00	0.18	0.35	0.19	0.00
Al_2O_3	9.01	8.57	6.31	7.74	6.53	5.75	7.42	5.09
FeO	13.86	13.97	14.53	14.49	15.40	15.66	14.54	13.67
MnO	0.30	0.27	0.50	0.28	0.66	0.46	0.35	0.14
MgO	12.98	13.57	14.92	13.85	15.02	15.18	14.28	15.65
CaO	11.30	11.23	9.80	10.32	9.08	8.96	10.41	10.24
Na_2O	0.70	0.76	0.30	0.32	0.53	0.49	0.60	0.00
K_2O	0.00	0.09	0.00	0.00	0.07	0.00	0.00	0.00
Total	**96.85**	**97.73**	**96.74**	**95.97**	**98.60**	**98.11**	**97.91**	**96.78**
Mg#	63.0	63.0	65.0	63.0	64.0	63.0	64.0	67.0
Si/Al	6.71	6.65	7.72	6.91	7.49	7.49	7.20	10.06
Al^{vi}	0.489	0.390	0.129	0.291	0.120	0.044	0.250	0.117
Origin	Ign	Ign	Ign	Ign	Ign	Ign	Ign	Ign

Table 1.3. (continued)

	Sample 113978 (cont.)							
	hb-34	*hb-21*	*hb-22*	*hb-31*	*hb-35*	*hb-23*	*hb-24*	*hb-30*
					Percentage			
SiO_2	49.69	46.25	47.870	47.71	47.78	46.40	45.83	45.79
TiO_2	0.31	1.74	0.77	1.45	0.37	0.23	0.30	2.36
Al_2O_3	7.90	9.75	9.49	9.53	9.80	10.44	11.37	9.57
FeO	15.31	13.78	15.59	13.74	14.45	14.61	14.99	15.74
MnO	0.43	0.24	0.30	0.32	0.26	0.23	0.29	0.40
MgO	14.05	12.32	12.89	13.00	12.63	12.57	11.69	11.80
CaO	10.11	11.15	10.38	11.42	11.38	10.88	11.20	11.14
Na_2O	0.75	0.88	0.76	0.67	0.73	0.60	0.84	0.68
K_2O	0.00	0.18	0.26	0.15	0.14	0.10	0.00	0.11
Total	**98.54**	**96.31**	**97.73**	**97.97**	**97.55**	**96.05**	**96.51**	**97.59**
Mg#	62.0	62.0	60.0	63.0	0.61	0.61	58.0	57.0
Si/Al	6.41	5.37	5.42	5.68	5.93	5.15	4.90	4.79
Al^{vi}	0.217	0.420	0.332	0.404	0.500	0.477	0.587	0.249
Origin	Ign	Trans	Trans	Trans	Trans	Met	Met	Met

	Sample 113985							
	hb-39	*hb-40*	*hb-44*	*hb-45*	*hb-46*	*hb-49*	*hb-51*	*hb-36*
					Percentage			
SiO_2	47.31	47.32	46.41	48.09	49.57	47.96	47.92	44.36
TiO_2	0.78	0.60	0.52	0.36	0.00	0.64	0.16	0.18
Al_2O_3	8.01	7.56	9.79	8.33	6.47	7.44	8.68	11.72
FeO	16.03	17.32	16.54	18.43	18.68	17.05	17.62	17.01
MnO	0.00	0.00	0.14	0.42	0.66	0.00	0.40	0.00
MgO	11.42	11.70	10.96	11.48	12.31	12.19	11.65	9.39
CaO	11.54	10.52	11.31	9.41	9.25	10.26	9.77	11.40
Na_2O	0.62	0.67	0.92	0.85	0.54	0.39	0.77	1.21
K_2O	0.53	0.46	0.32	0.29	0.12	0.54	0.14	0.23
Total	**96.39**	**96.36**	**96.93**	**97.74**	**97.61**	**96.54**	**97.10**	**95.50**
Mg#	56.0	55.0	54.0	53.0	54.0	56.0	54.1	50.0
Si/Al	7.06	6.56	5.71	6.05	7.20	6.65	6.06	4.99
Al^{vi}	0.406	0.249	0.500	0.267	0.106	0.227	0.333	0.739
Origin	Ign	Ign	Ign	Ign	Ign	Ign	Ign	Met

	Sample 113985 (cont.)							
	hb-37	*hb-38*	*hb-41*	*hb-42*	*hb-43*	*hb-47*	*hb-48*	*hb-50*
					Percentage			
SiO_2	44.42	43.38	46.28	46.16	46.32	45.46	44.25	45.47
TiO_2	0.30	0.44	0.40	0.36	0.50	0.14	0.30	0.39
Al_2O_3	12.33	13.30	10.42	9.83	9.60	11.98	12.91	11.81
FeO	17.19	17.56	17.00	17.43	17.97	17.06	17.49	16.92
MnO	0.00	0.00	0.19	0.00	0.25	0.00	0.17	0.18
MgO	9.36	8.76	10.42	10.68	10.81	10.11	9.36	9.94
CaO	11.43	11.56	11.07	11.80	10.14	11.36	11.24	11.50
Na_2O	1.20	1.34	0.90	0.82	0.78	1.14	1.19	1.00
K_2O	0.23	0.27	0.26	0.38	0.54	0.22	0.25	0.17
Total	**96.45**	**96.61**	**96.93**	**96.45**	**97.01**	**97.48**	**97.16**	**97.43**
Mg#	49.0	47.0	52.0	52.0	52.0	51.4	48.8	51.1
Si/Al	4.71	4.24	5.54	5.55	5.34	4.87	4.35	4.95
Al^{vi}	0.758	0.811	0.576	0.481	0.384	0.700	0.743	0.694
Origin	Met	Met	Met	Met	Met	Met	Met	Met

Table 1.3. (continued)

	Sample 113992							
	hb-52	*hb-53*	*hb-54*	*hb-55*	*hb-56*	*hb-57*	*hb-58*	*hb-59*
					Percentage			
SiO_2	40.18	39.71	40.12	40.76	39.85	40.52	40.14	40.20
TiO_2	0.51	0.34	0.27	0.43	0.24	0.43	0.39	0.44
Al_2O_3	11.88	12.37	12.42	11.66	12.11	11.87	12.01	12.26
FeO	26.17	25.93	25.91	25.65	26.07	25.92	25.91	25.33
MnO	0.00	0.15	0.17	0.00	0.00	0.00	0.00	0.00
MgO	4.37	4.10	4.11	4.53	4.08	4.24	4.13	4.19
CaO	11.29	11.26	11.35	11.35	11.26	11.07	11.13	11.17
Na_2O	1.14	1.09	1.38	1.23	1.22	1.37	1.22	1.05
K_2O	0.88	0.88	0.88	0.80	0.84	0.79	0.87	0.92
Total	**96.91**	**96.33**	**97.10**	**96.77**	**96.18**	**96.63**	**96.31**	**96.00**
Mg#	22.9	22.0	22.0	23.9	21.8	22.6	22.1	22.7
Si/Al	3.69	3.59	3.68	3.944	3.714	3.87	3.80	3.82
Al^{vi}	0.490	0.558	0.587	0.533	0.561	0.555	0.564	0.621
Origin	?	?	?	?	?	?	?	?

	Sample 119928											
	hb-7	*hb-8*	*hb-10*	*hb-11*	*cum-1*	*cum-2*	*cum-3*	*cum-4*	*cum-5*	*cum-6*	*cum-9*	*cum-12*
							Percentage					
SiO_2	46.01	46.30	46.40	45.39	55.74	54.68	54.83	55.15	52.22	55.07	54.78	54.06
TiO_2	0.55	0.46	0.30	0.52	0.00	0.00	0.00	0.00	0.00	0.00	0.00	0.00
Al_2O_3	10.61	10.43	10.34	10.86	0.38	0.52	0.55	0.44	3.98	0.30	0.33	1.85
FeO	17.22	17.23	16.92	17.35	25.43	24.84	25.02	24.66	22.42	25.23	24.41	23.47
MnO	0.00	0.00	0.00	0.00	0.48	0.53	0.58	0.61	0.28	0.58	0.50	0.63
MgO	10.72	10.95	10.77	10.63	17.36	16.95	17.15	17.26	15.03	17.40	17.15	16.51
CaO	11.20	11.46	11.30	11.32	0.62	0.60	0.52	0.56	4.37	0.40	0.49	2.46
Na_2O	1.17	1.02	0.90	1.18	0.00	0.00	0.00	0.00	0.00	0.00	0.00	0.00
K_2O	0.26	0.25	0.24	0.36	0.00	0.07	0.00	0.00	0.10	0.00	0.00	0.00
Total	**97.73**	**98.10**	**97.16**	**97.61**	**100.00**	**98.12**	**98.65**	**98.69**	**98.40**	**98.97**	**97.65**	**98.98**
Mg#	52.6	53.1	53.1	52.2	54.9	54.9	55.0	55.5	54.4	55.1	55.6	55.6
Si/Al	5.14	5.21	5.54	4.86	1332	726	295	$>10^5$	20.05	532	$>10^5$	46.1
Al^{vi}	0.517	0.494	0.556	0.505	0.058	0.079	0.067	0.075	0.305	0.036	0.057	0.146
Origin	?Met	?Met	?Met	?Met	Met	Met	Met	Met	Met	Met	Met	Met

	Sample 119929								
	hb-13	*hb-15*	*hb-16*	*hb-17*	*hb-19*	*hb-20*	*hb-22*	*hb-23*	*hb-24*
					Percentage				
SiO_2	45.91	45.95	46.11	45.96	45.73	49.57	46.36	45.15	45.26
TiO_2	0.30	0.30	0.32	0.48	0.81	0.67	0.27	0.66	0.52
Al_2O_3	11.32	11.50	11.58	11.12	10.94	7.19	9.58	11.02	10.57
FeO	16.36	16.19	16.05	16.63	16.43	18.74	15.46	16.65	16.25
MnO	0.16	0.00	0.19	0.00	0.16	0.58	0.00	0.14	0.00
MgO	10.69	10.69	11.06	10.89	10.84	13.95	11.38	10.61	10.77
CaO	11.47	11.62	11.46	11.73	11.34	7.37	11.82	11.57	11.50
Na_2O	0.99	1.05	0.91	1.03	1.00	0.64	0.78	1.04	0.89
K_2O	0.19	0.17	0.25	0.15	0.17	0.16	0.12	0.13	0.18
Total	**97.40**	**97.46**	**97.93**	**98.00**	**97.42**	**98.88**	**95.77**	**96.98**	**95.94**
Mg#	53.8	54.1	55.1	53.9	54.0	57.0	56.7	53.2	54.1
Si/Al	5.10	5.13	4.95	5.01	4.97	8.95	6.07	4.85	5.18
Al^{vi}	0.632	0.672	0.625	0.573	0.537	0.426	0.541	0.541	0.550
Origin	Ign	Ign	Ign	Ign	Ign	Ign	Ign	Ign	Ign

Table 1.3. (continued)

	Sample 119929 (cont.)								
	hb-25	*hb-26*	*hb-27*	*hb-30*	*hb-31*	*hb-14*	*hb-18*	*hb-28*	*hb-29*
					Percentage				
SiO_2	45.05	47.02	46.20	46.37	46.28	45.79	45.48	43.82	43.83
TiO_2	0.26	0.57	0.37	0.25	0.32	0.16	0.20	0.13	0.28
Al_2O_3	11.44	9.67	10.16	10.31	10.24	12.07	12.26	12.65	13.14
FeO	16.20	15.52	15.74	15.75	16.03	16.92	16.48	16.42	17.09
MnO	0.00	0.25	0.00	0.00	0.00	0.00	0.00	0.00	0.00
MgO	10.40	11.62	11.08	11.29	11.35	10.68	10.34	9.72	9.31
CaO	11.63	11.62	11.50	11.61	11.48	11.83	11.86	11.32	11.48
Na_2O	0.99	0.89	0.74	1.10	0.83	1.00	1.04	1.10	1.19
K_2O	0.16	0.16	0.09	0.15	0.17	0.19	0.15	0.15	0.18
Total	**96.14**	**97.32**	**95.89**	**96.83**	**96.70**	**98.65**	**97.81**	**95.31**	**96.50**
Mg#	53.4	57.1	55.6	56.1	55.8	52.9	52.8	51.3	49.3
Si/Al	5.02	5.90	5.75	5.64	5.48	4.71	4.80	4.49	4.32
Al^{vi}	0.668	0.498	0.581	0.576	0.531	0.649	0.726	0.770	0.793
Origin	Ign	Ign	Ign	Ign	Ign	Trans	Met	Met	Met

	Sample 113987			*Sample 119948*					
	hb-33	*hb-34*	*hb-36*	*hb-1*	*hb-4*	*hb-5*	*hb-6*	*hb-7*	*hb-8*
					Percentage				
SiO_2	44.37	45.16	44.30	47.31	47.00	47.00	46.95	47.21	46.67
TiO_2	0.00	0.00	0.00	0.00	0.75	0.50	0.72	0.69	0.56
Al_2O_3	12.05	12.07	12.82	9.19	9.32	8.50	9.22	9.74	9.93
FeO	16.64	16.48	17.76	15.52	16.53	17.15	17.81	16.79	16.45
MnO	0.23	0.26	0.27	0.20	0.30	0.31	0.44	0.21	0.24
MgO	9.48	9.63	9.02	11.32	10.82	11.15	11.24	10.92	10.65
CaO	10.84	10.96	10.94	11.64	11.26	9.87	10.14	11.35	11.05
Na_2O	1.29	1.19	1.31	0.56	0.80	0.65	0.94	1.05	0.73
K_2O	0.20	0.14	0.16	0.00	0.21	0.12	0.16	0.28	0.24
Total	**95.10**	**95.89**	**96.56**	**95.73**	**96.99**	**95.25**	**97.63**	**98.25**	**96.54**
Mg#	50	49	52	43	46	46	47	46	46
Si/Al	4.90	5.11	4.51	6.81	6.17	6.23	5.41	5.90	5.93
Al^{vi}	0.771	0.798	0.783	0.573	0.493	0.364	0.316	0.505	0.562
Origin	?	?	?	Ign	Ign	Ign	Ign	Ign	Ign

	Sample 119948 (cont.)							*Sample 119930*	
	hb-9	*hb-11*	*hb-2*	*hb-3*	*hb-10*	*hb-12*	*hb-13*	*hb-45*	*hb-46*
					Percentage				
SiO_2	46.85	47.29	44.76	44.71	45.21	44.93	45.18	43.32	43.91
TiO_2	0.43	0.57	0.00	0.00	0.36	0.27	0.25	0.16	0.18
Al_2O_3	10.49	9.86	11.99	11.87	11.85	12.00	12.76	13.05	11.67
FeO	16.21	16.75	16.54	16.43	16.91	16.72	16.72	18.44	17.81
MnO	0.00	0.36	0.00	0.00	0.36	0.21	0.15	0.00	0.00
MgO	10.67	10.87	9.54	9.60	9.50	9.72	9.67	9.59	10.29
CaO	11.53	11.19	11.59	11.46	11.61	11.51	11.72	11.23	11.09
Na_2O	0.73	1.00	0.86	0.80	1.18	0.69	0.80	1.43	1.66
K_2O	0.22	0.25	0.20	0.12	0.21	0.19	0.26	0.23	0.13
Total	**97.13**	**98.13**	**95.48**	**94.99**	**97.19**	**96.23**	**97.51**	**97.58**	**95.92**
Mg#	46	46	49	50	50	49	49	48.1	50.7
Si/Al	5.91	5.91	5.12	5.15	5.03	4.89	4.73	3.88	4.28
Al^{vi}	0.649	0.523	0.805	0.796	0.736	0.734	0.803	0.619	0.515
Origin	Ign	Ign	Met	Met	Met	Met	Met	?Met	?Met

Table 1.3. (continued)

	Sample 119930 (cont.)									
	hb-47	*hb-48*	*hb-49*	*hb-50*	*hb-51*	*hb-52*	*hb-53*	*cum-42*	*cum-43*	*cum-44*
						Percentage				
SiO_2	43.28	45.82	43.65	43.12	43.94	42.17	44.30	53.73	53.52	53.10
TiO_2	0.24	0.37	0.34	0.33	0.28	0.29	0.23	0.00	0.00	0.00
Al_2O_3	12.53	10.40	11.68	12.21	11.50	13.77	11.09	0.46	0.20	0.27
FeO	17.55	17.85	18.21	17.99	18.15	18.58	17.82	25.00	25.50	25.13
MnO	0.17	0.00	0.00	0.00	0.00	0.00	0.00	0.70	0.72	0.51
MgO	9.65	10.64	9.82	9.64	10.02	9.14	10.01	16.73	16.80	16.60
CaO	11.30	11.20	11.11	11.36	11.25	11.27	11.17	0.57	0.53	0.55
Na_2O	1.47	1.23	1.34	1.51	1.39	1.43	0.99	0.00	0.00	0.20
K_2O	0.23	0.20	0.28	0.23	0.21	0.32	0.15	0.00	0.00	0.00
Total	**96.42**	**97.70**	**96.45**	**96.39**	**96.91**	**97.19**	**95.89**	**97.35**	**97.29**	**96.51**
Mg#	49.5	51.3	49.0	48.8	49.6	46.7	50.0	54.4	54.0	54.1
Si/Al	4.11	5.07	4.27	4.09	4.35	3.56	4.68	–	–	–
Al^{vi}	0.630	0.469	0.526	0.576	0.511	0.648	0.536	0.036	0.000	0.000
Origin	?Met	?Met	?Met	?Met	?Met	?Met	?Met	Met	Met	Met

	Sample 113982						
	hb-57	*hb-58*	*hb-59*	*hb-60*	*hb-61*	*hb-62*	*hb-63*
				Percentage			
SiO_2	47.90	48.12	46.95	46.94	47.07	47.42	47.03
TiO_2	0.92	1.26	0.85	0.64	0.61	0.92	0.45
Al_2O_3	6.39	6.05	7.26	6.74	7.07	7.11	7.08
FeO	17.83	17.89	18.24	18.02	17.63	18.23	18.22
MnO	0.39	0.48	0.36	0.54	0.39	0.43	0.30
MgO	11.30	11.53	10.75	11.13	11.46	11.09	11.35
CaO	11.56	11.04	11.38	11.42	11.73	11.48	11.72
Na_2O	0.90	0.96	1.12	1.19	1.10	1.20	0.88
K_2O	0.08	0.00	0.23	0.20	0.22	0.12	0.31
Total	**97.27**	**97.35**	**97.15**	**96.84**	**97.27**	**98.19**	**97.35**
Mg#	53.0	53.5	51.2	52.4	53.7	52.0	52.6
Si/Al	7.50	7.40	6.67	6.80	6.63	6.65	6.53
Al^{vi}	0.169	0.092	0.225	0.155	0.182	0.184	0.169
Origin	Ign	Ign	Ign	Ign	Ign	Ign	Ign

	Sample 113982 (cont.)						
	hb-64	*hb-54*	*hb-55*	*hb-56*	*hb-2*	*hb-3*	*hb-5*
				Percentage			
SiO_2	47.55	42.90	42.56	43.17	41.27	42.49	42.40
TiO_2	1.15	0.25	0.50	0.39	0.34	0.44	0.42
Al_2O_3	6.55	11.16	11.43	11.76	12.46	11.47	12.04
FeO	18.58	20.35	20.57	20.45	20.96	20.34	20.92
MnO	0.47	0.00	0.24	0.38	0.42	0.19	0.33
MgO	11.18	8.53	8.39	8.41	7.85	8.32	8.36
CaO	11.00	11.71	11.57	11.79	11.56	11.57	11.60
Na_2O	1.21	1.23	1.51	1.25	1.42	1.38	1.57
K_2O	0.15	0.42	0.52	0.57	0.57	0.61	0.54
Total	**97.83**	**96.54**	**97.28**	**98.17**	**96.86**	**96.81**	**98.17**
Mg#	51.8	42.8	42.1	42.3	40.0	42.2	41.6
Si/Al	6.74	4.28	4.03	4.09	3.58	4.09	3.78
Al^{vi}	0.097	0.475	0.438	0.494	0.478	0.475	0.442
Origin	Ign	Met	Met	Met	Met	Met	Met

NOTE: Small discrepancies in totals of the columns reflect rounding off or, if >0.01, minor amounts of oxides not shown in tabulations
Mineral abbreviations are: cum cummingtonite; hb hornblende
– not determined

Table 1.4. Selected analyses of biotite from the Manyutup Tonalite

	113991			*113978*			*113984*			
	bi-3	*bi-4*	*bi-5*	*bi-6*	*bi-10*	*bi-11*	*bi-17*	*bi-18*	*bi-21*	*bi-23*
					Percentage					
SiO_2	35.62	35.17	36.32	36.62	37.85	37.84	35.05	35.08	35.66	35.40
TiO_2	1.88	2.27	2.32	1.54	1.51	1.48	1.62	1.70	1.83	1.68
Al_2O_3	16.66	16.05	16.28	16.54	16.99	16.80	15.60	15.71	15.60	15.44
FeO	19.51	19.57	19.59	15.13	15.87	15.84	22.26	21.61	22.56	22.93
MnO	0.00	0.00	0.00	0.00	0.00	0.00	0.25	0.22	0.22	0.21
MgO	10.88	10.87	10.67	14.17	14.32	14.39	8.44	8.92	8.65	8.69
K_2O	8.97	8.80	10.04	7.66	8.69	8.96	9.82	10.07	9.89	9.87
Total	**93.53**	**92.72**	**95.21**	**91.65**	**95.23**	**95.31**	**93.03**	**93.32**	**94.41**	**94.23**
Mg#	50.0	50.0	49.0	63.0	62.0	62.0	40.3	42.4	40.6	40.3

	113984 (cont.)	*119928*		*113987*		*119948*			*113982*	
	bi-24	*bi-1*	*bi-2*	*bi-12*	*bi-13*	*bi-1*	*bi-2*	*bi-6*	*bi-21*	*bi-22*
					Percentage					
SiO_2	35.44	36.78	36.22	37.39	37.55	36.93	36.32	36.34	35.24	35.59
TiO_2	1.57	1.38	1.44	1.54	1.47	1.60	1.66	1.67	2.18	2.16
Al_2O_3	15.64	16.59	16.22	16.37	16.20	16.41	16.09	16.21	16.14	16.07
FeO	22.74	18.42	18.67	18.02	17.66	17.82	17.91	18.46	20.98	20.58
MnO	0.20	0.00	0.00	0.00	0.00	0.00	0.00	0.00	0.00	0.00
MgO	8.64	13.30	12.88	12.42	12.80	12.34	11.99	12.43	10.80	9.92
K_2O	9.93	8.48	8.09	9.17	9.36	9.90	9.42	8.61	9.33	9.58
Total	**94.16**	**94.96**	**93.51**	**94.91**	**95.04**	**95.00**	**93.39**	**93.81**	**94.68**	**94.11**
Mg#	40.4	56.3	55.1	55.0	56.0	55.0	54.0	55.0	47.8	46.2

NOTE: Small discrepancies in totals of the columns reflect rounding off or, if >0.01, minor amounts of oxides not shown in tabulations

Table 1.5. Selected chlorite analyses, Manyutup Tonalite

	113985						*119929*	
	bi-12 biotite	*bi-13 biotite*	*bi-14 biotite*	*ch-1 biotite*	*ch-2 biotite*	*ch-3 biotite*	*bi-8 biotite*	*bi-9 biotite*
					Percentage			
SiO_2	28.80	28.10	30.42	25.31	25.20	25.92	29.39	29.23
TiO_2	1.46	1.21	1.40	0.00	0.00	0.00	1.13	1.22
Al_2O_3	16.87	17.60	16.77	21.46	21.78	21.00	17.46	18.37
FeO	25.22	24.30	22.94	22.60	22.91	22.49	20.82	20.86
MnO	0.00	0.00	0.00	0.00	0.19	0.15	0.00	0.00
MgO	14.61	14.87	13.27	17.28	16.80	17.24	16.83	16.04
CaO	0.57	0.28	0.21	0.00	0.00	0.00	0.53	0.95
K_2O	–	–	–	–	–	–	–	–
Total	**87.53**	**86.36**	**87.22**	**86.65**	**86.87**	**86.88**	**86.34**	**86.84**
Mg#	50.8	52.2	50.8	57.7	56.6	57.7	59.0	57.8

Table 1.5. (continued)

	113987				*119948*			
	ch-2 hornblende	*ch-5 hornblende*	*ch-6 biotite*	*ch-8 biotite*	*bi-3 biotite*	*ch-1 biotite*	*ch-3 biotite*	*ch-5 hornblende*
				Percentage				
SiO_2	26.59	25.85	26.19	26.15	29.32	26.64	25.86	25.80
TiO_2	0.12	0.00	0.00	0.00	1.05	0.00	0.00	0.00
Al_2O_3	20.57	20.54	21.27	21.01	17.23	19.68	21.31	20.99
FeO	21.04	20.67	20.71	20.64	21.57	21.15	21.36	21.91
MnO	0.31	0.00	0.00	0.24	0.00	0.00	0.15	0.00
MgO	19.09	18.84	18.58	18.94	14.94	18.98	17.86	17.58
CaO	0.00	0.00	0.21	0.00	0.94	0.00	0.00	0.00
K_2O	0.00	0.00	0.00	0.00	1.04	0.00	0.00	0.00
Total	**87.60**	**85.91**	**86.75**	**86.98**	**86.10**	**86.45**	**86.54**	**86.29**
Mg#	62.0	62.0	62.0	62.0	55.0	62.0	60.0	59.0

	119948 (cont.)			*119930*			
	ch-7 hornblende	*ch-8 hornblende*	*ch-9 hornblende*	*ch-12 hornblende*	*ch-13 hornblende*	*bi-16 biotite*	*bi-17 biotite*
				Percentage			
SiO_2	26.77	26.24	26.68	25.29	25.38	32.04	28.58
TiO_2	0.00	0.00	0.00	0.00	0.00	2.46	1.31
Al_2O_3	20.43	21.24	20.98	20.45	20.73	16.07	15.87
FeO	21.40	21.63	20.82	23.14	23.71	21.07	24.02
MnO	0.00	0.00	0.27	0.00	0.00	0.00	0.00
MgO	19.12	18.34	19.30	17.24	16.77	14.47	14.45
CaO	0.00	0.00	0.00	0.00	0.00	0.99	0.39
K_2O	0.00	0.00	0.00	0.00	0.00	3.33	1.23
Total	**87.72**	**87.45**	**88.05**	**86.25**	**86.59**	**90.81**	**85.85**
Mg#	61.0	60.0	62.0	57.1	55.8	55.0	51.7

NOTE: Small discrepancies in totals of the columns reflect rounding off or, if >0.01, minor amounts of oxides not shown in tabulations
Chlorite is after biotite or hornblende; original mineral is listed below chlorite sample number
– not determined

Table 1.6. Selected analyses of plagioclase from the Manyutup Tonalite

	Sample 113991								
	plag-1 core	*plag-2* ——	*plag-3* ——	*plag-4* ——	*plag-5* ——>	*plag-6 margin*	*plag-7*	*plag-8*	*plag-9*
					Percentage				
SiO_2	58.27	58.93	59.85	59.55	59.47	58.90	58.71	58.81	59.85
Al_2O_3	27.66	26.63	26.94	26.38	26.10	26.17	26.80	26.23	25.81
FeO	0.00	0.00	0.00	0.00	0.00	0.00	0.00	0.00	0.00
CaO	8.99	8.28	7.86	7.76	7.30	7.70	8.12	7.69	7.12
Na_2O	6.64	7.10	7.12	7.41	7.63	7.08	6.78	7.07	7.32
K_2O	0.12	0.07	0.07	0.00	0.00	0.00	0.00	0.00	0.00
Total	**101.68**	**101.01**	**101.85**	**101.09**	**100.49**	**99.85**	**100.41**	**99.80**	**99.82**
X_{An}	42.5	39.0	37.7	36.6	34.6	37.5	39.8	37.5	35.0
X_{Ab}	56.8	60.6	61.9	63.4	65.4	62.5	60.2	62.5	65.0
X_{Or}	0.6	0.4	0.4	–	–	–	–	–	–

Table 1.6. (continued)

	Sample 113978								
	plag-10 calcic core	*plag-11 calcic core*	*plag-12 overgrowth*	*plag-13 margin*	*plag-15 calcic core*	*plag-16 calcic core*	*plag-14 overgrowth*	*plag-17* ——	*plag-18* ——>
					Percentage				
SiO_2	49.63	47.14	59.92	60.09	50.31	49.21	59.68	54.80	55.16
Al_2O_3	32.86	33.70	25.51	25.61	32.99	33.27	26.37	29.46	29.34
FeO	0.00	0.00	0.00	0.00	0.00	0.00	0.00	0.00	0.00
CaO	15.38	16.54	6.70	7.04	15.57	15.74	7.51	11.34	10.94
Na_2O	2.82	1.69	7.84	7.74	2.72	2.48	7.56	5.02	5.23
K_2O	0.00	0.00	0.00	0 .00	0.00	0.00	0.00	0.11	0.00
Total	**100.69**	**99.06**	**99.98**	**100.48**	**101.60**	**100.70**	**101.12**	**100.72**	**100.67**
X_{An}	75.1	84.4	32.1	33.4	76.0	77.8	35.4	55.2	53.6
X_{Ab}	24.9	15.6	67.9	66.6	24.0	22.2	64.6	44.2	46.4
X_{Or}	–	–	–	–	–	–	–	0.6	–

	Sample 113978 (cont.)		*Sample 113985*						
	plag-19 ——>	*plag-20 margin*	*plag-26 core*	*plag-25* ——	*plag-24* ——	*plag-23* ——	*plag-22* ——>	*plag-21 margin*	*plag-33 core*
					Percentage				
SiO_2	55.29	59.82	58.75	58.44	54.39	56.88	57.88	58.97	55.32
Al_2O_3	29.42	26.52	26.90	26.54	29.02	27.65	26.96	26.26	29.35
FeO	0.00	0.00	0.00	0.00	0.00	0.00	0.00	0.00	0.00
CaO	10.86	7.83	7.92	8.21	11.20	9.51	8.43	7.78	11.03
Na_2O	5.51	7.44	6.94	6.78	4.98	6.08	6.45	7.18	5.06
K_2O	0.00	0.00	0.00	0 .00	0.12	0.00	0.00	0.07	0.00
Total	**101.08**	**101.61**	**100.51**	**99.98**	**99.71**	**100.21**	**99.72**	**100.41**	**100.76**
X_{An}	52.1	36.8	38.6	40.1	55.0	46.3	41.9	37.3	54.6
X_{Ab}	47.8	63.2	61.3	59.9	44.3	53.6	58.1	62.3	45.3
X_{Or}	–	–	–	–	0.7	–	–	0.4	–

	Sample 113985 (cont.)					*Sample 113984*			
	plag-32 ——	*plag-31* ——	*plag-30* ——	*plag-29* ——>	*plag-28 margin*	*plag-36 core*	*plag-37* ——	*plag-38* ——	*plag-40* ——>
					Percentage				
SiO_2	55.64	59.07	54.82	56.38	59.04	59.58	61.32	65.52	63.35
Al_2O_3	29.49	26.80	29.71	28.67	26.06	24.75	23.07	23.82	22.94
FeO	0.00	0.00	0.00	0.00	0.00	0.00	0.00	0.00	0.00
CaO	11.35	8.23	11.37	9.97	7.60	6.10	4.47	4.85	4.00
Na_2O	5.12	6.82	4.80	5.99	7.01	7.60	8.65	8.73	8.96
K_2O	0.00	0.25	0. 00	0.09	0.00	0.00	0.12	0.00	0.00
Total	**101.60**	**101.17**	**100.70**	**101.10**	**99.70**	**98.04**	**97.64**	**99.91**	**99.25**
X_{An}	55.1	39.4	56.7	47.6	37.5	30.7	22.0	23.5	19.8
X_{Ab}	44.9	59.1	43.3	51.8	62.5	69.3	77.2	76.5	80.2
X_{Or}	–	1.4	–	0.5	–	–	0.7	–	–

Table 1.6. (continued)

	Sample 113984 (cont.)					*Sample 113992*			
	plag-43 ——>	*plag-34 margin*	*plag-49*	*plag-51*	*plag-53*	*plag-54*	*plag-55*	*plag-57*	*plag-56*
					Percentage				
SiO_2	63.11	62.20	62.94	65.86	59.45	64.43	67.53	63.78	62.90
Al_2O_3	22.63	23.35	22.96	21.29	24.40	22.39	20.22	22.95	22.85
FeO	0.00	0.00	0.00	0.00	0.00	0.00	0.00	0.00	0.00
CaO	3.76	4.40	4.08	1.78	7.78	3.35	0.64	3.96	4.74
Na_2O	9.48	8.88	9.24	10.60	7.62	9.83	11.02	9.26	9.19
K_2O	0.14	0.00	0.10	0.00	0.11	0.12	0.00	0.00	0.00
Total	**99.12**	**98.84**	**99.33**	**99.53**	**100.86**	**100.11**	**99.41**	**99.96**	**99.68**
X_{An}	17.8	21.5	19.5	8.5	35.8	15.7	3.1	19.1	22.2
X_{Ab}	81.3	78.5	79.9	91.5	63.5	83.6	96.9	80.9	77.8
X_{Or}	0.8	–	0.6	–	0.6	0.7	–	–	–

	Sample 113992 (cont.)		*Sample 119928*						
	plag-61	*plag-62*	*plag-1*	*plag-2*	*plag-7*	*plag-10*	*plag-11*	*plag-12*	*plag-13*
					Percentage				
SiO_2	63.92	63.37	60.70	62.21	60.59	59.13	59.46	58.79	57.72
Al_2O_3	22.67	23.58	25.89	24.72	26.01	26.21	26.59	26.91	27.69
FeO	0.00	0.00	0.00	0.00	0.00	0.00	0.00	0.00	0.00
CaO	3.64	4.72	6.99	5.72	7.10	7.75	7.90	8.29	9.24
Na_2O	9.44	8.81	7.55	8.60	7.72	7.32	7.16	6.66	6.32
K_2O	0.00	0.00	0.00	0.00	0.00	0.00	0.00	0.00	0.00
Total	**99.81**	**100.48**	**101.13**	**101.24**	**101.42**	**100.41**	**101.10**	**100.66**	**101.18**
X_{An}	17.6	22.8	33.8	26.9	33.7	36.9	37.9	40.7	44.7
X_{Ab}	82.4	77.1	66.2	73.1	66.0	63.1	62.1	59.3	55.3
X_{Or}	–	–	–	–	–	–	–	–	–

	Sample 119929							*Sample 113987*	
	plag-15	*plag-16*	*plag-21 core*	*plag-20 ——*	*plag-19 ——*	*plag-18 ——>*	*plag-17 margin*	*plag-23 calcic core*	*plag-22 ——>*
						Percentage			
SiO_2	57.58	58.49	59.01	58.19	56.95	57.26	57.83	57.87	62.75
Al_2O_3	27.58	27.02	26.90	27.51	27.69	27.85	28.07	27.18	25.04
FeO	0.00	0.00	0.00	0.00	0.00	0.00	0.00	0.00	0.00
CaO	9.26	8.49	7.93	8.68	9.55	9.41	9.48	8.98	6.02
Na_2O	6.25	6.68	6.87	6.66	5.77	5.87	6.08	6.87	8.43
K_2O	0.00	0.08	0.08	0.00	0.00	0.00	0.00	0.00	0.00
Total	**100.67**	**100.76**	**100.79**	**101.03**	**99.97**	**100.39**	**101.47**	**100.89**	**102.25**
X_{An}	45.0	41.1	38.7	41.9	47.8	47.0	46.3	41.9	28.3
X_{Ab}	55.0	58.5	60.8	58.1	52.2	53.0	53.7	58.1	71.7
X_{Or}	–	0.4	0.5	–	–	–	–	–	–

Table 1.6. (continued)

	Sample 113987 (cont.)								
	plag-24 ——	*plag-25* ——>	*plag-26 margin*	*plag-32 core*	*plag-31* ——	*plag-30* ——	*plag-29* ——	*plag-28* ——>	*plag-27 margin*
					Percentage				
SiO_2	61.27	61.83	61.50	61.40	58.76	59.14	59.35	60.51	62.13
Al_2O_3	24.38	24.84	24.63	24.94	26.39	26.18	26.50	25.60	23.83
FeO	0.00	0.00	0.00	0.00	0.00	0.00	0.00	0.00	0.00
CaO	6.01	6.18	6.14	6.42	8.32	7.91	8.12	7.34	5.47
Na_2O	8.21	8.14	8.20	8.00	7.01	6.95	6.87	7.51	8.42
K_2O	0.00	0. 00	0.00	0.00	0.07	0.00	0.00	0.00	0.00
Total	**99.88**	**100.99**	**100.47**	**100.76**	**100.55**	**100.17**	**100.84**	**100.96**	**99.85**
X_{An}	28.8	29.6	29.3	30.7	39.5	38.6	39.5	35.1	26.4
X_{Ab}	71.2	70.4	70.7	69.3	60.1	61.4	60.5	64.9	73.6
X_{Or}	–	–	–	–	0.4	–	–	–	–

	Sample 119948								*Sample 119930*	
	plag-1	*plag-2*	*plag-10 core*	*plag-9* ——	*plag-8* ——	*plag-7* ——	*plag-6* ——>	*plag-5 margin*	*plag-33*	*plag-35*
						Percentage				
SiO_2	63.22	61.46	65.79	66.73	66.64	67.12	67.72	68.78	60.10	58.65
Al_2O_3	23.00	23.97	21.77	20.68	20.76	20.84	20.57	21.13	25.34	26.09
FeO	0.00	0.00	0.00	0.00	0.00	0.00	0.00	0.00	0.00	0.00
CaO	5.38	5.18	2.62	1.09	1.83	1.17	1.10	1.59	7.02	7.52
Na_2O	7.94	8.52	10.11	10.74	10.40	11.01	10.94	11.17	7.72	7.16
K_2O	0.00	0.21	0.00	0.33	0.00	0.15	0.00	0.00	0.00	0.00
Total	**99.53**	**99.34**	**100.30**	**99.57**	**99.62**	**100.29**	**100.33**	**102.68**	**100.33**	**99.42**
X_{An}	27.2	24.8	12.5	5.2	8.9	5.5	5.3	7.3	33.5	36.7
X_{Ab}	72.8	74.0	87.5	92.9	91.1	93.6	94.7	92.7	66.5	63.3
X_{Or}	–	1.2	–	1.9	–	0.8	–	–	–	–

	Sample 119930 (cont.)									
	plag-40 core	*plag-39* ——	*plag-38* ——	*plag-37* ——>	*plag-36 margin*	*plag-45 core*	*plag-44* ——	*plag-43* ——	*plag-42* ——>	*plag-41 margin*
						Percentage				
SiO_2	58.69	59.21	58.37	55.94	59.58	58.73	58.73	58.65	59.41	59.65
Al_2O_3	26.02	25.80	26.01	28.02	25.34	25.96	25.48	25.87	25.56	25.28
FeO	0.00	0.00	0.00	0.00	0.00	0.00	0.00	0.00	0.00	0.00
CaO	7.99	7.30	7.87	9.93	6.96	7.61	7.36	7.36	6.91	6.68
Na_2O	6.95	7.36	7.11	5.95	7.59	7.52	7.53	7.30	7.54	7.59
K_2O	0.00	0.00	0.00	0.00	0.07	0.08	0.00	0.00	0.00	0.00
Total	**99.66**	**99.66**	**99.35**	**99.84**	**99.54**	**99.90**	**99.10**	**99.19**	**99.41**	**99.19**
X_{An}	38.8	35.4	38.0	48.0	33.5	35.7	35.1	35.8	33.6	32.7
X_{Ab}	61.2	64.6	62.0	52.0	66.1	63.9	64.9	64.2	66.4	67.3
X_{Or}	–	–	–	–	0.4	0.4	–	–	–	–

Table 1.6. (continued)

	Sample 113982									
	plag-46 core	*plag-47* ——	*plag-48* ——	*plag-49* ——>	*plag-50 margin*	*plag-6 core*	*plag-4* ——	*plag-3* ——	*plag-2* ——>	*plag-1 margin*
						Percentage				
SiO_2	57.26	56.91	58.26	57.23	57.04	57.02	58.17	59.84	59.52	61.96
Al_2O_3	27.23	27.79	26.63	26.92	27.57	27.29	27.01	25.75	25.65	24.21
FeO	0.00	0.00	0.00	0.00	0.00	0.00	0.00	0.00	0.00	0.00
CaO	8.98	9.73	8.33	8.94	9.64	9.07	6.42	7.43	7.19	5.39
Na_2O	6.35	6.00	6.89	6.41	6.07	6.37	6.77	7.16	7.59	8.64
K_2O	0.00	0.00	0.00	0.00	0.07	0.00	1.17	0.00	0.12	0.07
Total	**99.82**	**100.43**	**100.10**	**99.50**	**100.40**	**99.76**	**99.54**	**100.52**	**100.07**	**100.27**
X_{An}	43.9	47.2	40.0	43.5	46.8	44.0	32.0	36.0	34.1	25.6
X_{Ab}	56.1	52.8	60.0	56.5	53.2	56.0	61.0	62.8	65.2	74.4
X_{Or}	–	–	–	–	–	–	7.0	1.2	0.7	–

NOTE: Small discrepancies in totals of the columns reflect rounding off or, if >0.01, minor amounts of oxides not shown in tabulations
– not determined

Table 1.7. Microprobe copper analyses of silicate minerals — Manyutup Tonalite

Mineral analysis	*Comments*	*Cu content (ppm)*	*Analytical time (secs)*
GSWA 119929 Coarse-grained tonalite (low-SiO_2 suite)			
Am-16	Igneous	<lld	200
Am-19	Igneous	<lld	200
Am-13	Igneous	<lld	200
Am-28 (1)	Metamorphic	42	400
Am-28 (2)	Metamorphic	14	200
Plag		<lld	200
Plag		<lld	200
Plag		<lld	200
Plag		<lld	200
Plag		<lld	200
Bi-8 (1)		<lld	200
Bi-8 (2)		<lld	200
GSWA 113985 Medium-grained tonalite (low-SiO_2 suite)			
Hb-48	Metamorphic	<lld	200
Hb-50	Metamorphic	<lld	200
Hb-43	Metamorphic	17	200
Hb-37 (1)	Metamorphic	<lld	200
Hb-37 (2)	Metamorphic	<lld	200
Hb-41	Metamorphic	<lld	200
Hb-44	Igneous	<lld	200
			200
Plag		<lld	200
Plag		<lld	200
			200
Ch-3 (1)	After biotite	40	200
Ch-3 (2)	After biotite	19	200
Ch-3 (3)	After biotite	42	200
Bi-13	After biotite	<lld	200
Bi-4	After biotite	36	200
Ch-2	After biotite	<lld	200
Bi-12	After biotite	<lld	200

NOTE: Mineral abbreviations are: am amphibole; bi biotite; ch chlorite; cum cummingtonite; hb hornblende; plag plagioclase
lld lower limit of detection

Appendix 2

Whole-rock geochemistry of the Manyutup Tonalite and Annabelle Volcanics

Sixty-four samples of Manyutup Tonalite and Annabelle Volcanics, and their altered equivalents, were analysed for major elements and a range of trace elements at the Chemistry Centre, Western Australia. Results are presented in Table 2.1. Major elements were analysed by X-ray fluorescence spectroscopy (XRF) using fused glass discs. FeO was determined by titration with potassium dichromate. Loss on ignition (LOI) was measured gravimetrically after heating to 1100°C. Most trace elements were analysed by XRF using pressed powder pellets. Rare earth elements and Li, Sc, Ta, Th and Y were quantified using inductively coupled plasma mass spectrometry. Gold contents were determined following a lead-based fire assay technique. Silver was analysed using flame atomic absorption spectrometry. Fluoride concentrations were quantified using a selective ion electrode technique following pyrohydrolysis. Details of the analytical methods can be found in Witt et al. (1996) and Crawford et al. (1996).

References

CRAWFORD, R. A., FAULKNER, J. A., SANDERS, A. J., LEWIS, J. D., and GOZZARD, J. R., 1996, Geochemical mapping of the Glengarry 1:250 000 sheet: Western Australia Geological Survey, Explanatory Notes, 59p.

WITT, W. K., DAVY, R., HUNTER, W. M., and PESCUD, L., 1996, Geochemical analyses of Archaean acid to intermediate igneous rocks, including granitoids, minor intrusions and volcanic rocks, southwest Eastern Goldfields Province, Western Australia: Western Australia Geological Survey, Record 1995/2, 55p.

Table 2.1 Whole-rock geochemical data, Ravensthorpe Terrane

	110201	110201A	110201B	110202	110203	110204A	110204B	110205	110206	110207	110208
Rock code	*Agytm*	*Agytm*[a]	*Agytm*[a]	*Agytm*[a]	*Agytm*[a]	*Agytm*[a]	*Agytm*[a]	*Aaix*	*Aaix*	*Aaix*[a]	*Aaix*[a]
AMG											
Suite	*High-SiO_2*	*High-SiO_2*	*High-SiO_2*	*Low-SiO_2*	*High-SiO_2*	*High-SiO_2*	*High-SiO_2*	*Low-SiO_2*	*Low-SiO_2*	*Low-SiO_2*	*Low-SiO_2*
Drillhole	*BD-13*	*BD-13*	*BD-13*	*BD-13*	*BD-13*	*BD-13*	*BD-13*	*FD-15*	*FD-13*	*FD-13*	*FD-13*
Depth (m)	*174–175*	*174–176*	*174–177*	*173.2*	*165.5*	*160*	*160*	*113–114*	*236–237*	*230*	*194*
						Percentage					
SiO_2	67.7	67.8	67.3	50.9	69.8	67.4	62.9	57.7	58.1	45.4	50.4
TiO_2	0.35	0.34	0.33	0.24	0.33	0.3	0.35	0.43	0.44	0.77	0.9
Al_2O_3	15.1	15	14.4	14.1	14.5	13.4	15.4	16.2	16.4	12.4	13.8
Fe_2O_3	1.17	1.43	1.96	4.64	1.12	2.14	3.37	1.54	1.87	5.37	4.01
FeO	3.86	3.58	3.92	9.34	2.56	5.05	4.51	6.58	6.17	13.6	11.3
MnO	0	0	0	0.1	0	0	0	0.09	0.14	0.15	0.12
MgO	1.69	1.72	1.9	8.28	1.72	2.67	2.82	5.62	4.77	8.07	5.83
CaO	1.38	1.15	1.09	0.48	0.41	0.34	0.2	2.25	4.08	0.89	1.63
Na_2O	4.82	5.04	4.72	2.95	4.94	0.44	0.4	3.3	3.42	0.55	1.19
K_2O	0.97	0.97	0.89	0.43	1.45	2.84	3.84	0.76	0.55	0.72	1.22
P_2O_5	0.08	0.08	0.08	0.05	0.07	0.07	0.08	0.08	0.09	0.06	0.1
S	0.11	0.21	0.5	2.09	0.27	0.84	1.66	0	0	2.64	1.96
LOI	2.22	2.08	2.15	4.48	2.02	3.35	3.1	4.29	3.26	5.08	3.67
Total	**99.45**	**99.4**	**99.24**	**98.08**	**99.19**	**98.84**	**98.63**	**98.84**	**99.29**	**95.7**	**96.13**
CO_2	0.15	0.21	0.15	0.31	0	0.32	0.22	0.95	0.73	0.47	1.45
						Parts per million					
Cr	13	17	13	10	12	11	11	140	141	294	244
Ni	17	16	16	108	15	18	19	141	127	68	91
Co	16	20	nd	150	20	34	50	28	33	134	51
V	50	47	48	44	45	38	44	103	86	244	258
Sc	nd	6	6	7	6	6	6	nd	nd	31	33
Cu	97	117	676	5 000	373	320	467	37	14	6 000	437
Pb	0	12	26	38	7	6	7	0	0	2 600	2 900
Zn	25	26	29	122	27	118	119	46	45	5 500	248
W	7	9	nd	7	7	7	6	4	0	5	16
Mo	0	0	0	3	0	0	0	0	0	2	2
As	5	4	6	69	6	8	17	0	4	12	0
B	29	18	26	91	10	39	42	26	8	8	12
Ag	2	4	6	10	4	5	5	2	4	11	5
Au	0.02	0.03	2.23	nd	0.07	0.05	nd	0.01	0	1.99	0.7
Rb	30	27	23	12	40	69	91	28	19	27	42
Ba	166	161	154	91	84	469	532	88	117	112	194
Sr	126	114	100	44	71	12	11	108	120	20	25
Ga	17	15	16		16	15	18	15	15	27	21
Li	49	0	65	155	45	87	79	43	21	72	39
Nb	0	0	0	0	0	0	0	0	0	0	0
Zr	139	143	133	106	139	110	127	147	154	51	100
Y	8	9	11	8	9	9	12	15	18	4	6
Th	3	2	3	2	3	2	3	3	3	0	0
La	7	7	10	25	5	8	20	7	9	0	8
Ce	15	11	13	39	16	7	29	12	15	0	0
Pr	nd	nd	nd	nd	nd	nd	nd	nd	nd	nd	nd
Nd	nd	nd	nd	nd	nd	nd	nd	nd	nd	nd	nd
Sm	nd	nd	nd	nd	nd	nd	nd	nd	nd	nd	nd
Eu	nd	nd	nd	nd	nd	nd	nd	nd	nd	nd	nd
Gd	nd	nd	nd	nd	nd	nd	nd	nd	nd	nd	nd
Tb	nd	nd	nd	nd	nd	nd	nd	nd	nd	nd	nd
Dy	nd	nd	nd	nd	nd	nd	nd	nd	nd	nd	nd
Ho	nd	nd	nd	nd	nd	nd	nd	nd	nd	nd	nd
Er	nd	nd	nd	nd	nd	nd	nd	nd	nd	nd	nd
Tm	nd	nd	nd	nd	nd	nd	nd	nd	nd	nd	nd
Yb	nd	nd	nd	nd	nd	nd	nd	nd	nd	nd	nd
Lu	nd	nd	nd	nd	nd	nd	nd	nd	nd	nd	nd

Table 2.1 (continued)

	110209	*110210*	*110211*	*110212*	*110213*	*110214A*	*110214B*	*110217*	*110218*	*110219*	*110220*
Rock code	*Aʌyd*	*Agytm*	*Agyd*	*Agyt*	*Agydm*	*Agyt*[a]	*Agyt*[a]	*Aʌyd*	*Aʌyd*	*Agytm*	*Agytm*
AMG											
Suite	*High-SiO_2*	*High-SiO_2*	*Low-SiO_2*	*High-SiO_2*	*Low-SiO_2*	*High-SiO_2*	*High-SiO_2*	*High-SiO_2*	*High-SiO_2*	*High-SiO_2*	*High-SiO_2*
Drillhole	*BD-25*	*BD-25*	*BD-25*	*KDP-2*	*KDP-2*	*KDP-2*	*KDP-2*	*FD-11*	*FD-11*	*BD-35*	*BD-34*
Depth (m)	*119–119.5*	*123.7–124.7*	*74.8–76.0*	*116–118.8*	*119*	*119.1–119.4*	*119.1–119.5*	*189–189.5*	*179.5–180.5*	*131–132*	*94.0–94.7*
						Percentage					
SiO_2	62.4	67.1	49.4	68.6	57.5	67	67.1	68.4	65.4	66.5	67.9
TiO_2	0.45	0.35	0.77	0.32	0.5	0.33	0.28	0.43	0.3	0.34	0.34
Al_2O_3	14.1	15.1	14.7	16.3	18.4	16.3	14.9	14.1	15.7	15	15.3
Fe_2O_3	1	0.67	4.3	0.89	1.63	0.66	2.13	1.02	0.63	0.94	1.02
FeO	3.99	2.8	7.96	1.95	4.11	1.87	1.43	3.49	2.31	4.49	3.92
MnO	0.07	0	0.18	0	0.08	0	0	0	0	0	0
MgO	2.64	1.36	6.74	1.27	3.57	1.21	0.79	1.52	1.45	2.43	1.76
CaO	4.27	2.84	9.58	4.96	6.55	4.69	7.18	1.86	3.41	0.79	0.91
Na_2O	1.36	4.65	1.29	4.9	5.29	4.68	2.85	4.34	4.59	1.72	5.16
K_2O	2.41	1.33	0.1	0.37	0.25	0.56	0.6	1.11	1.61	2.74	1.03
P_2O_5	0.15	0.08	0.06	0.08	0.11	0.08	0.08	0.08	0.07	0.08	0.08
S	0.08	0.02	0.1	0	0	0	0	0.1	0.01	0.02	0.15
LOI	2.77	1.65	3.84	0.88	1.38	1.13	1.28	1.87	1.6	3.14	2.06
Total	**95.69**	**97.95**	**99.02**	**100.52**	**99.37**	**98.51**	**98.62**	**98.32**	**97.08**	**98.19**	**99.63**
CO_2	3.15	1.94	0.84	0.44	0.29	0.29	0.49	0.84	2.42	0.66	0.37
						Parts per million					
Cr	40	13	71	11	24	12	11	18	56	13	15
Ni	45	18	72	23	57	25	20	21	32	17	19
Co	19	9	50	11	21	11	5	14	8	21	18
V	62	56	252	45	110	47	54	52	47	47	50
Sc	nd	nd	nd	nd	nd	6	7	nd	nd	nd	nd
Cu	36	92	134	18	122	8	8	97	19	127	52
Pb	0	0	0	5	6	8	4	5	11	0	0
Zn	35	27	92	31	72	32	20	28	51	21	15
W	0	4	0	0	0	4	0	6	4	6	5
Mo	0	2	0	0	0	2	2	2	0	0	2
As	0	0	0	0	0	0	0	0	0	0	9
B	25	17	66	0	0	0	16	15	22	22	23
Ag	3	5	5	2	4	5	5	7	2	2	4
Au	0.01	0.01	0.02	0	0.01	0.01	0.02	0.02	0.01	0.36	0.06
Rb	65	38	0	8	4	13	20	34	48	67	25
Ba	404	247	33	107	77	147	157	192	171	380	196
Sr	61	109	126	358	344	331	387	119	145	19	89
Ga	16	18	14	18	21	17	17	16	17	10	17
Li	26	16	21	16	16	25	16	14	11	18	28
Nb	9	0	0	0	8	0	0	7	0	0	0
Zr	204	141	64	115	115	121	126	191	143	136	140
Y	21	7	17	7	30	8	9	15	10	9	8
Th	4	3	0	4	2	4	3	4	2	3	2
La	14	10	6	16	17	15	16	13	12	10	8
Ce	31	17	0	32	37	31	28	26	24	21	18
Pr	nd	nd	nd	nd	nd	nd	nd	nd	nd	nd	nd
Nd	nd	nd	nd	nd	nd	nd	nd	nd	nd	nd	nd
Sm	nd	nd	nd	nd	nd	nd	nd	nd	nd	nd	nd
Eu	nd	nd	nd	nd	nd	nd	nd	nd	nd	nd	nd
Gd	nd	nd	nd	nd	nd	nd	nd	nd	nd	nd	nd
Tb	nd	nd	nd	nd	nd	nd	nd	nd	nd	nd	nd
Dy	nd	nd	nd	nd	nd	nd	nd	nd	nd	nd	nd
Ho	nd	nd	nd	nd	nd	nd	nd	nd	nd	nd	nd
Er	nd	nd	nd	nd	nd	nd	nd	nd	nd	nd	nd
Tm	nd	nd	nd	nd	nd	nd	nd	nd	nd	nd	nd
Yb	nd	nd	nd	nd	nd	nd	nd	nd	nd	nd	nd
Lu	nd	nd	nd	nd	nd	nd	nd	nd	nd	nd	nd

Table 2.1 (continued)

Rock code	*113978* Agrtm	*113979* Agrt(px)	*113980* Agrt	*113981* Agrt	*113982* Agrt	*113983* Agrt	*113984* Agrt	*113985* Agrtm	*113986* Agrt	*113987* Agrt	*113988* Agrt
AMG	*249823*	*251822*	*252820*	*271824*	*292799*	*288778*	*289785*	*274830*	*328767*	*330759*	*329755*
Suite	*Low-SiO_2*	*Low-SiO_2*	*Low-SiO_2*	*High-SiO_2*	*High-SiO_2*	*High-SiO_2*	*High-SiO_2*	*High-SiO_2*	*High-SiO_2*	*High-SiO_2*	*High-SiO_2*
Drillhole Depth (m)											
						Percentage					
SiO_2	55.9	51.5	54.1	67.5	67	68.5	72.8	62.5	70.2	66.9	71.5
TiO_2	0.51	1.53	0.4	0.38	0.38	0.45	0.26	0.47	0.37	0.46	0.33
Al_2O_3	16.8	15.1	17.1	15.4	15.4	15.4	13.7	15.9	14.2	15.8	14.4
Fe_2O_3	1.79	3.84	1.38	1.31	1.43	1.21	0.97	1.35	1.16	1.68	1.01
FeO	5.2	9.75	5.74	2.25	2.41	2.4	1.56	3.94	2.24	2.41	1.88
MnO	0.13	0.21	0.12	0	0.05	0	0	0.07	0	0.05	0
MgO	5.67	3.03	6.63	1.34	1.45	1.11	0.63	2.42	0.84	1.53	0.81
CaO	7.79	8.31	8.51	4.28	4.72	4.46	2.76	5.81	3.62	4.07	3.31
Na_2O	3.04	3.19	2.38	4.63	4.36	4.34	4.72	4.01	4.5	4.59	4.68
K_2O	0.86	0.44	0.46	0.93	0.91	0.96	1.47	0.79	1	0.78	1.11
P_2O_5	0.07	0.26	0.06	0.09	0.08	0.1	0.06	0.1	0.07	0.11	0.07
S	0	0.06	0	0	0	0	0	0	0	0	0
LOI	1.64	3.22	2.14	1.92	1.06	0.93	0.74	1.96	1.18	1.27	1.14
Total	**99.4**	**100.44**	**99.02**	**100.03**	**99.25**	**99.86**	**99.67**	**99.32**	**99.38**	**99.65**	**100.24**
CO_2	0.22	0.18	0.22	0.18	0.11	0.33	0.18	0.11	0.22	0.15	0.15
						Parts per million					
Cr	149	0	216	31	23	9	8	74	10	13	7
Ni	138	17	182	28	32	18	13	66	16	24	15
Co	30	39	36	10	11	11	6	21	9	12	7
V	180	189	138	55	51	57	29	100	36	63	37
Sc	nd	nd	nd	nd	nd	nd	nd	nd	nd	nd	nd
Cu	20	93	34	31	13	19	20	89	17	22	13
Pb	0	0	0	4	7	0	8	7	0	6	7
Zn	45	149	41	49	45	45	33	59	39	48	38
W	0	5	0	0	0	0	0	0	4	0	0
Mo	0	0	0	0	0	2	0	0	0	0	0
As	4	0	0	0	0	0	0	0	0	0	0
B	0	23	11	37	0	0	0	21	0	6	0
Ag	4	5	4	2	2	5	2	6	7	3	1
Au	0	0.01	0	0	0	0	0	0	nd	nd	0
Rb	47	21	57	37	28	29	41	26	31	18	39
Ba	136	90	91	293	208	220	421	180	274	200	323
Sr	139	210	154	256	193	203	125	192	160	211	160
Ga	16	22	16	18	16	16	15	17	17	15	16
Li	125	28	403	22	25	22	23	22	0	23	20
Nb	0	9	0	0	0	0	7	0	0	0	7
Zr	90	193	74	158	143	197	142	143	260	152	160
Y	14	47	14	10	13	12	18	13	13	12	14
Th	0	0	0	2	4	3	6	3	4	4	5
La	7	18	8	11	14	16	21	11	17	15	17
Ce	9	30	14	25	27	26	40	24	30	24	37
Pr	nd	nd	nd	nd	nd	nd	nd	nd	nd	nd	nd
Nd	nd	nd	nd	nd	nd	nd	nd	nd	nd	nd	nd
Sm	nd	nd	nd	nd	nd	nd	nd	nd	nd	nd	nd
Eu	nd	nd	nd	nd	nd	nd	nd	nd	nd	nd	nd
Gd	nd	nd	nd	nd	nd	nd	nd	nd	nd	nd	nd
Tb	nd	nd	nd	nd	nd	nd	nd	nd	nd	nd	nd
Dy	nd	nd	nd	nd	nd	nd	nd	nd	nd	nd	nd
Ho	nd	nd	nd	nd	nd	nd	nd	nd	nd	nd	nd
Er	nd	nd	nd	nd	nd	nd	nd	nd	nd	nd	nd
Tm	nd	nd	nd	nd	nd	nd	nd	nd	nd	nd	nd
Yb	nd	nd	nd	nd	nd	nd	nd	nd	nd	nd	nd
Lu	nd	nd	nd	nd	nd	nd	nd	nd	nd	nd	nd

Table 2.1 (continued)

Rock code	*113989* Agyt	*113990* Agyt	*113991* Agyt	*113992* Agytm	*113993* Agyt	*113994* Agyt	*119908* Agyt	*119909* Agyt	*119910* Agyt	*119911* Agyt	*119912* Agytm
AMG	*319754*	*224776*	*773745*	*753763*	*224726*	*225720*	*226743*	*226743*	*746700*	*770699*	*774700*
Suite	*High-SiO_2*	*High-SiO_2*	*High-SiO_2*	*High-SiO_2*	*High-SiO_2*	*High-SiO_2*	*High-SiO_2*	*High-SiO_2*	*High-SiO_2*	*High-SiO_2*	*High-SiO_2*
Drillhole Depth (m)											
						Percentage					
SiO_2	70.9	69.6	65.1	70.9	71.2	69.2	69.4	69.9	67.5	69.8	73.3
TiO_2	0.33	0.23	0.47	0.41	0.29	0.31	0.26	0.27	0.36	0.33	0.22
Al_2O_3	14.1	16.2	15.8	13.2	14.6	15.4	16.6	15.5	15.9	15.2	14.5
Fe_2O_3	1.4	0.93	1.54	1.54	1	1.15	1.04	1.23	1.34	0.95	1.03
FeO	1.73	1.36	2.98	3.22	1.73	1.76	1.16	1.53	2.34	1.82	1.17
MnO	0	0	0.05	0	0	0	0	0	0	0	0
MgO	0.78	0.61	1.83	0.67	0.96	1.08	0.73	1.09	1.4	1	0.5
CaO	3.54	3.54	5.4	3.13	3.98	4.4	3.92	3.82	4.4	3.93	3.4
Na_2O	4.41	5.14	4.03	5.22	4.53	4.49	5.75	5	4.75	4.92	4.83
K_2O	0.96	1.33	0.97	0.47	0.46	0.56	0.81	1.04	0.89	0.77	0.76
P_2O_5	0.07	0.05	0.11	0.09	0.05	0.07	0.07	0.07	0.08	0.08	0.07
S	0	0	0	0	0	0	0	0	0	0	0
LOI	0.95	0.85	1.29	1.01	1.18	1.35	0.68	1.05	1.09	1.58	0.56
Total	**99.17**	**99.84**	**99.57**	**99.86**	**100.59**	**99.77**	**100.42**	**100.5**	**100.05**	**100.38**	**100.34**
CO_2	0.22	0.29	0.29	0.26	0.18	0.11	0.15	0.11	0.15	0.15	0.22
						Parts per million					
Cr	9	12	40	12	13	12	12	21	24	19	10
Ni	15	14	43	17	19	22	8	27	33	27	12
Co	9	4	15	14	8	7	5	8	10	9	4
V	35	21	68	34	35	43	28	42	54	51	17
Sc	nd	nd	nd	nd	nd	nd	3.8	4.6	8.6	2.5	4.8
Cu	15	11	33	17	13	15	19	8	35	10	6
Pb	5	8	5	0	4	5	5	4	6	5	5
Zn	38	30	49	12	36	35	37	51	53	35	41
W	0	0	0	0	0	0	0	0	0	0	0
Mo	2	2	0	2	2	2	2	0	0	0	0
As	0	0	0	0	0	0	0	0	0	0	0
B	0	8	0	7	0		nd	nd	nd	nd	nd
Ag	4	3	2	3	3	4	0	0	0	0	0
Au	0	0	0	0.01	0	0.01	2	0	2	0	0
Rb	33	41	28	11	13	13	23	32	25	28	20
Ba	206	444	194	142	111	129	196	211	339	160	168
Sr	183	170	196	94	288	284	508	300	254	288	211
Ga	15	16	17	16	15	17	18	17	18	15	16
Li	20	20	24	10	23	25	23	27	26	24	26
Nb	0	7	0	11	0	0	3	5	3	3	5
Zr	169	113	148	298	116	124	128	110	124	129	153
Y	10	6	16	36	4	3	8.3	9.3	19.1	4	4.9
Th	6	19	4	9	4	2	5.4	6.2	2.1	13.4	9.9
La	13	57	19	29	8	11	14.1	nd	19.2	nd	nd
Ce	27	90	39	61	14	16	28.8	nd	101	nd	nd
Pr	nd	nd	nd	nd	nd	nd	3.3	nd	5.4	nd	nd
Nd	nd	nd	nd	nd	nd	nd	10.5	nd	21	nd	nd
Sm	nd	nd	nd	nd	nd	nd	2.5	nd	5.8	nd	nd
Eu	nd	nd	nd	nd	nd	nd	1.2	nd	1.9	nd	nd
Gd	nd	nd	nd	nd	nd	nd	3	nd	6.3	nd	nd
Tb	nd	nd	nd	nd	nd	nd	0.3	nd	0.8	nd	nd
Dy	nd	nd	nd	nd	nd	nd	1.6	nd	4	nd	nd
Ho	nd	nd	nd	nd	nd	nd	0.3	nd	0.7	nd	nd
Er	nd	nd	nd	nd	nd	nd	0.8	nd	1.9	nd	nd
Tm	nd	nd	nd	nd	nd	nd	0.1	nd	0.3	nd	nd
Yb	nd	nd	nd	nd	nd	nd	0.8	nd	1.7	nd	nd
Lu	nd	nd	nd	nd	nd	nd	0.1	nd	0.2	nd	nd

Table 2.1 (continued)

Rock code	*119913* Agryd	*119914* Agrt	*119915* Agrt	*119916* Agrt	*119917* Agryd	*119918* Agrt	*119919* Agrt	*119920* Agrqd	*119921* Agrt	*119922* Agrqd	*119923* Agrt
AMG	774700	774699	776725	775737	775737	761730	772743	751731	772730	775720	67965
Suite	High-SiO_2	High-SiO_2	High-SiO_2	High-SiO_2	High SiO_2	High-SiO_2	High SiO_2	Low-SiO_2	High-SiO_2	Low-SiO_2	High-SiO_2
Drillhole											
Depth (m)											
						Percentage					
SiO_2	72.5	71.8	66.3	66.9	76	68.1	65.5	55.5	71.7	55.2	69.8
TiO_2	0.1	0.22	0.39	0.34	0.08	0.39	0.47	0.22	0.24	1.49	0.29
Al_2O_3	15.7	14.7	16.2	15.8	14	16.4	15.8	14.4	15.3	14.4	15.3
Fe_2O_3	0.52	1.11	1.44	1.16	0.55	1.3	1.45	1.28	0.95	3.67	1.19
FeO	0.44	1.37	2.32	2.22	0.57	2.11	2.9	5.08	1.2	7.86	1.42
MnO	0	0	0.05	0	0	0	0.07	0.1	0	0.15	0
MgO	0.39	0.87	1.47	1.49	0.24	1.06	1.81	7.89	0.65	1.52	0.95
CaO	2.68	3.73	5.07	4.56	0.74	4.27	5.38	9.02	3.84	6.62	3.84
Na_2O	5.88	4.67	4.71	4.8	6.29	5.1	4.24	2.3	5.09	3.68	5.44
K_2O	1.07	0.61	0.55	0.71	1.42	0.99	0.83	0.35	0.62	0.61	0.47
P_2O_5	0.04	0.03	0.09	0.09	0.04	0.1	0.11	0.04	0.07	0.35	0.08
S	0	0	0	0	0	0	0	0	0	0	0
LOI	0.5	0.94	1.38	1.23	0.63	0.77	1.12	2.55	0.85	3.16	0.89
Total	**99.82**	**100.05**	**99.97**	**99.3**	**100.56**	**100.59**	**99.68**	**98.73**	**100.51**	**98.71**	**99.67**
CO_2	0.18	0.26	0.07	0.04	0.37	0.04	0.15	0.07	0.07	0.26	0.37
						Parts per million					
Cr	12	15	25	37	8	17	41	530	13	17	18
Ni	12	23	32	39	9	22	47	356	17	26	21
Co	0	8	12	11	0	11	16	39	5	31	8
V	6	41	64	0	3	46	69	99	31	193	38
Sc	12	2.5	0.2	8.2	1.2	6.2	9.5	18.8	4	20.8	16.8
Cu	9	6	18	21	6	10	30	28	13	24	11
Pb	11	5	7	5	7	6	5	4	5	4	5
Zn	24	31	51	53	30	47	50	68	31	132	39
W	0	0	0	0	0	0	0	0	0	0	0
Mo	0	0	0	0	0	0	0	0	0	0	0
As	0	0	0	0	0	0	0	0	0	0	0
B	nd	nd	nd	nd	nd	nd	nd	nd	nd	nd	nd
Ag	0	0	0	0	0	0	0	0	0	0	0
Au	2	0	2	2	2	3	3	3	0	10	2
Rb	36	19	14	22	44	26	25	12	17	13	12
Ba	412	142	154	284	452	255	246	62	197	165	188
Sr	573	252	258	242	150	227	197	187	259	261	304
Ga	18	16	18	20	17	20	18	14	17	28	19
Li	23	28	30	24	17	29	30	28	23	14	16
Nb	0	0	5	0	0	4	6	0	3	14	5
Zr	74	118	150	102	68	156	166	42	125	192	122
Y	1.9	2	12.6	14.4	4.6	10	13.8	5	5.6	46.7	15
Th	5.6	30.9	3.6	3.4	4.4	6.9	1.9	1.3	3.7	6.9	6.3
La	nd	66.5	nd	11.3	21.4	nd	12.1	6.5	18.2	35.5	nd
Ce	nd	100	nd	27.4	38.7	nd	27.6	12.2	33.2	70.3	nd
Pr	nd	11.8	nd	3.5	4.2	nd	3.3	1.4	3.1	11.8	nd
Nd	nd	32.4	nd	14.4	13.6	nd	13	5.1	10.3	48.6	nd
Sm	nd	2.6	nd	3.9	2.7	nd	2.9	0.9	1.7	12.5	nd
Eu	nd	1.3	nd	1.4	1	nd	1	0.6	1.2	4.5	nd
Gd	nd	5.1	nd	4.1	2.6	nd	3.4	1.5	2.3	14.3	nd
Tb	nd	0.2	nd	0.5	0.2	nd	0.5	0.2	0.2	2.1	nd
Dy	nd	0.9	nd	3.1	1.1	nd	2.5	1.1	1.2	11.5	nd
Ho	nd	0.1	nd	0.6	0.2	nd	0.5	0.2	0.2	2.3	nd
Er	nd	0.3	nd	1.7	0.5	nd	1.4	0.6	0.6	6.5	nd
Tm	nd	0	nd	0.2	0.1	nd	0.2	0.1	0.1	0.9	nd
Yb	nd	0.2	nd	1.5	0.4	nd	1.3	0.6	0.6	5.5	nd
Lu	nd	0.1	nd	0.2	0.1	nd	0.2	0.1	0.1	0.8	nd

Table 2.1 (continued)

	119924	119925	119926	119927	119928	119929	119930	119931	119948
Rock code	*Agyt*	*Agyt*	*Agyt*	*Agyt*	*Agyt*	*Agyt*	*Agytm*	*Agytm*	*Agyt*
AMG	*676650*	*671649*	*664646*	*658647*	*659658*	*760622*	*676604*	*666610*	*284700*
Suite	*High-SiO_2*	*High-SiO_2*	*High-SiO_2*	*High-SiO_2*	*High-SiO_2*	*Low-SiO_2*	*High-SiO_2*	*High-SiO_2*	*High-SiO_2*
Drillhole									
Depth (m)									
					Percentage				
SiO_2	67.5	67.7	70.9	66.3	66.6	58.2	66.2	68.3	63.3
TiO_2	0.33	0.35	0.29	0.35	0.34	0.54	0.44	0.48	0.39
Al_2O_3	16.3	15.4	14.8	15.9	15.8	18.7	15.6	14.5	17.3
Fe_2O_3	1.02	1.5	1.06	1.05	0.81	1.75	1.33	1.26	1.41
FeO	1.78	1.94	1.56	2.33	2.56	3.58	2.98	2.63	2.66
MnO	0	0	0	0	0	0.07	0.05	0.03	0.05
MgO	0.9	1.42	0.71	1.59	1.55	2.78	1.87	1.73	1.94
CaO	4.34	4.36	3.49	4.82	4.88	7.66	5.69	5.3	5.99
Na_2O	4.95	4.66	4.13	4.67	4.6	4.24	4.18	4.65	4.45
K_2O	1.02	0.91	0.83	0.59	0.44	0.32	0.3	0.24	0.67
P_2O_5	0.1	0.07	0.08	0.07	0.07	0.14	0.09	0.1	0.11
S	0	0	0	0	0	0	0	0	0
LOI	1.13	1.42	0.96	1.34	1.08	1.75	1.14	0.81	1.8
Total	**99.37**	**99.73**	**98.81**	**99.01**	**98.73**	**99.73**	**99.87**	**100.03**	**100.07**
CO_2	0.59	0.4	0.22	0.4	0.33	0.11	0.22	0.37	0.04
					Parts per million				
Cr	9	34	19	28	29	31	49	45	29
Ni	13	37	18	43	41	72	55	56	51
Co	6	9	6	12	11	23	16	14	17
V	45	54	29	60	53	121	76	90	79
Sc	6	8	4.6	8	7.4	15.6	15.4	10.8	8.6
Cu	13	12	8	9	21	21	17	10	38
Pb	4	4	7	5	5	5	4	4	4
Zn	35	40	45	45	41	56	39	10	47
W	0	0	0	0	0	0	0	0	0
Mo	0	0	0	0	0	0	0	0	0
As	0	0	0	0	0	0	0	0	0
B	nd	nd	nd	nd	nd	nd	nd	nd	nd
Ag	0	0	0	0	0	0	0	0	0
Au	5	0	0	0	2	2	5	4	5
Rb	29	26	30	17	15	7	7	6	18
Ba	231	174	264	162	136	89	98	97	164
Sr	296	238	234	217	259	299	184	142	259
Ga	18	16	16	17	18	21	17	16	18
Li	36	28	48	41	30	18	18	16	30
Nb	4	5	4	4	4	6	5	7	4
Zr	134	130	144	128	129	102	177	192	102
Y	13.6	22.3	19.7	19	19.3	30.4	32.3	51	23.5
Th	9.4	10.7	12.2	8.9	9.8	3.1	2.6	24	6
La	nd	nd	40.3	nd	nd	29.9	30.7	nd	29.8
Ce	nd	nd	67.8	nd	nd	67.3	70.4	nd	60.8
Pr	nd	nd	7.7	nd	nd	9.9	10.6	nd	7.4
Nd	nd	nd	27.6	nd	nd	39.8	43.9	nd	28.8
Sm	nd	nd	5.6	nd	nd	7.4	8.2	nd	5.5
Eu	nd	nd	1.9	nd	nd	2.1	2.3	nd	1.8
Gd	nd	nd	7.4	nd	nd	8.7	9.9	nd	7.2
Tb	nd	nd	0.9	nd	nd	1.2	1.2	nd	0.8
Dy	nd	nd	4.8	nd	nd	6.5	6.9	nd	4.8
Ho	nd	nd	0.8	nd	nd	1.2	1.2	nd	0.8
Er	nd	nd	2.1	nd	nd	3.4	3.7	nd	2.5
Tm	nd	nd	0.3	nd	nd	0.5	0.5	nd	0.4
Yb	nd	nd	2.2	nd	nd	3.3	3.4	nd	2.5
Lu	nd	nd	0.3	nd	nd	0.5	0.5	nd	0.4

NOTES: LOI: loss on ignition (includes CO_2 but CO_2 is shown separately below the total)
nd: no data
0: below detection limit
(a) altered

CODES:

Manyutup Tonalite

Agyt coarse-grained tonalite
Agytm medium-grained tonalite
Agyt(px) pyroxene-bearing tonalite
Agyyd dacite porphyry
Agydm medium-grained diorite
Agyqd coarse-grained quartz diorite
Agyd dolerite

Annabelle Volcanics

AAix andesite
AAyd dacite porphyry
AAm basalt

Appendix 3

Metamorphic mineralogy and geothermobarometry of the Ravensthorpe greenstones

Metamorphic minerals from the Archaean greenstones were analysed by a JEOL 6400 scanning electron microscope (SEM) at the Centre for Electron Microscopy, University of Western Australia. Analytical conditions were 15 kV and 3×10^{-9}Å. Analytical spectra were collected for 60 seconds. A copy of the analytical file, SIL15H.ZAF, is reproduced as Table 1.1 (Appendix 1). Garnets were analysed at their rims, margins, interiors and cores (see Chapter 5). More detailed traverses of selected garnet grains used a CAMECA SX-50 Microprobe at Commonwealth Scientific and Industrial Research Organisation (CSIRO), Floreat Park. The analytical file (GARNETBS) is reproduced as Table 3.1. Results of mineral analyses are presented in Tables 3.2 to 3.6.

Garnet

Garnet formulae were calculated using GWBASIC GARNET, a program developed by J. Lewis, GSWA. Garnets are all almandine-rich with a low but variable andradite component. Many garnets display compositional zoning, which is discussed in more detail below. The most Fe-rich garnets ($X_{Fe}\geq85$) are from andalusite-bearing schist (GSWA sample number 118831, *Ald* on COCANARUP) in the Cocanarup greenstones. Garnetiferous quartz–plagioclase–biotite schist (118839, 118888, *Alg*) contains relatively Mg-rich garnet (X_{Fe} = 75–85). The remaining garnet analyses are from mineralized environments. Garnet from copper–gold lodes in the Ravensthorpe area is found in Annabelle Volcanics (110353, 113915) and in the Chester Formation (105941). The former have X_{Fe} = 81–88 and have a significant andradite component. Garnets in cordierite–gedrite assemblages and associated with Cu–Zn mineralization have X_{Fe} in the range 75–89. Those from Last Venture (118893) contain up to 19 mole% spessartine. Those from Copper King (118797) have lower Mn but contain a significant andradite component. Garnets from non-mineralized environments in the Chester and Hatfield Formations were too weathered for meaningful analysis.

The garnets display compositional zoning of variable degree and nature. Most have relatively Fe-rich rims (within 50 μ of the grain boundary in grains with a diameter of 1–20 mm) interpreted to reflect garnet growth during post-peak metamorphic cooling (Spear, 1993).

Biotite

Mg/(Mg+Fe) (Mg#) for biotite varies between 22.0 and 51.7. Most values are between 28 and 45. The lowest Mg#s (22–24) are from sample 118831, an andalusite-bearing schist (*Ald*) with Fe-rich garnet, from the Cocanarup greenstones. The highest Mg#s (50.2–51.7) are from a garnet–cordierite–biotite schist (sample 118839, *Alg* on COCANARUP).

Chlorite

Chlorite in samples 105941 and 110353, both from Cu–Au lodes, appears to be in textural equilibrium with biotite.

Table 3.1. Analytical file GARNETBS used for detailed analytical traverses of garnet grains

Line (standard)	*Spectrometer*	*Crystal*	*Time (secs)*	*Peak*	*Bg offsets*	*Base line*	*Window*	*C/s/nÅ*	*ZAF*
Si Ka (SMFO)	1	TAP	20	27737	500 500	500	4000	1772.00	2.440
Ti Ka (TI)	2	PET	20	31447	400 -100	500	0	962.64	5.017
Al Ka (MICL)	1	TAP	20	32445	500 500	500	3500	2004.00	2.696
Cr Ka (CR)	2	PET	20	26225	500 500	500	0	776.71	5.381
Fe Ka (SMFA)	3	LIF	20	48083	500 500	500	0	254.00	5.176
V Ka (V)	3	LIF	20	62159	400 400	500	0	170.43	5.302
Mn Ka (MN)	3	LIF	20	52191	800 800	500	0	247.91	5.665
Mg Ka (SMFO)	1	TAP	20	38454	500 500	500	3500	1406.00	2.099
Ca Ka (WOLL)	2	PET	20	38385	500 500	500	0	850.00	3.962
Na Ka (ANOR)	1	TAP	60	46306	500 500	500	3000	784.71	1.740

The samples have Mg#s of about 41 (110353) and 33 (110353).

Amphibole

Calcic amphiboles from para-amphibolite near Cocanarup (sample 118838) are magnesio-hornblende (Mg# approximately 70). Those from the same unit near the southern end of the Cocanarup greenstones (sample 118891) are actinolitic hornblende (Mg# approximately 55).

Orthoamphiboles from mineralized environments are Fe-rich gedrites. Sample 110353 from the Mount McMahon Cu–Au centre have Mg# = 25–27. Those from the Last Venture Cu–Zn mine have Mg# = 28–30. Intergrowths indicative of exsolution were not observed.

Staurolite

Staurolite was observed in mineralized metapelitic rocks of the Chester Formation (sample 105941) and as relicts in cordierite in cordierite–gedrite rock from the Last Venture mine (sample 118894). Both varieties are Fe-rich (Mg# = 8–13).

Cordierite

Most cordierite was too altered for analysis. However, fresh cordierite in cordierite–gedrite rock from the Last Venture mine has a Mg# = 53.5.

Plagioclase

Plagioclase compositions are very variable, reflecting the range of rock types. Plagioclase from metapelites (*Alg* on COCANARUP) from the Cocanarup greenstones contains An_{30} (approximately) with cores up to An_{36}. The andalusite-bearing schist (*Ald* on COCANARUP) contains more calcic plagioclase with a very variable composition (An_{48-65}). Para-amphibolite near Cocanarup contains sodic oligoclase (An_{10-12}) but at the southern end of the Cocanarup belt the same unit contains a much more calcic plagioclase (An_{88-95}). Cordierite–gedrite rock at Last Venture contains An_{33-45}, whereas at Copper King the plagioclase is slightly less calcic (An_{23-26}). Plagioclase from the Marion Martin Cu–Au mine, at Ravensthorpe, contains An_{30-35}.

The garnet–biotite geothermometer

Results of application of the garnet–biotite geothermometer to samples containing these minerals are summarized in Table 3.2. Garnet and biotite analyses were collected at two or more sites in each sample. Garnet grains were analysed at several points along a traverse from the rim to the core. The following points are pertinent:

1. Temperature determinations assumed a pressure of 3 kb, but the Fe:Mg partitioning curves between garnet and biotite are steep and temperature determinations assuming a pressure of 2.5 kb are only a few degrees lower.

2. Fe-rich compositions from garnet rims (within about 50 μ of the grain boundary) gave relatively low metamorphic temperatures, interpreted to record growth during retrograde cooling. Analyses from garnet margins (50–300 μ from the grain boundary), in combination with biotite from between 50 and 1000 μ of the garnet margin, were used to determine peak metamorphic temperatures. This combination of analyses is expected to give a temperature that most closely approaches peak metamorphic temperatures, although it will probably underestimate peak metamorphic temperature due to diffusion of Fe and Mg during retrograde cooling (Spear, 1993).

3. Intrasample variations in the calculated peak metamorphic temperature is associated with the range of Fe/Mg ratios in biotite. For example, $Fe/Fe+Mg_{biotite}$ in sample 118831 (site 1) varied from 0.75 to 0.78, which translated into a temperature difference of 28°C.

4. Larger variations in calculated peak metamorphic temperatures reflect the variable composition of garnet margins within the same sample. Temperature determinations on different garnet grain margins in sample 118831 varied by >50°C, reflecting variation in $Fe/Fe+Mg_{garnet\ margin}$ of 0.94 to 0.95.

5. Compositional zoning in grains with a diameter of <1 mm are likely to be dominated by the effects of diffusion during retrograde cooling and will considerably underestimate the peak metamorphic temperature (Spear, 1993).

The garnet–biotite geothermometers of Perchuk and Lavren'teva (1981), Hodges and Spear (1982) and Indares and Martignole (1985) were applied to the data in Table 3.2. Data from the margins of garnet grains with a diameter of >1 mm, and nearby biotite, were used to compare the performance of the geothermometers. The geothermometer of Indares and Martignole (1985) is designed for granulitic assemblages. It gave temperatures that were consistently lower than the other two, and mostly plotted outside the temperature range defined by the mineral assemblage. The geothermometers of Hodges and Spear (1982) mostly, and that of Perchuk and Lavren'teva (1981) consistently, calculated peak metamorphic temperatures within, or close to, the temperature range defined by the metamorphic assemblage.

The plagioclase–amphibole geothermometer

The plagioclase–amphibole geothermometers of Blundy and Holland (1990) and Spear (1980) were applied to mafic paragneiss samples near Cocanarup (118838) and south of Cocanarup (118891). A pressure of 3 kb has been assumed. Temperatures determined for sample 118838 using the geothermometer of Blundy and Holland (1990) gave temperatures comparable to those determined for

metapelites using the garnet–biotite geothermometer of Perchuk and Lavren'teva (1981). Temperatures determined using the Spear (1980) geothermometer were comparatively low. The very calcic plagioclase in sample 118891 yielded temperatures 60–100°C lower than those predicted by metamorphic assemblages in associated pelites, using the Blundy and Holland (1990) geothermometer, whereas temperatures determined using the Spear (1980) geothermometer were unreasonably high.

The garnet–aluminosilicate–plagioclase geobarometer

Pressures were determined using three versions of the garnet–aluminosilicate–plagioclase (GASP) geobarometer (Hodges and Spear, 1982; Ghent, 1976; Aranovich and Podlesskiy, 1982) but results are considered unreliable. The three sets of pressure determinations, using the same mineral analyses, differed by as much as 5 kb. The pressures so determined were commonly outside the range indicated by metamorphic mineral assemblages. The results that most closely and consistently matched the 2.5–3 kb range indicated by metamorphic mineral assemblages were those achieved using the Aranovich and Podlesskiy (1982) geobarometer. These gave pressures of 2–2.5 kb on sample 118831, and around 3.2 to 4.2 kb for sample 118893. Temperatures of 600°C and 550°C, respectively, were assumed, consistent with those indicated by metamorphic mineral assemblages.

The plagioclase–amphibole geobarometer

The combined geothermobarometer of Plyusnina (1982), based on partitioning of calcium and aluminium between plagioclase and amphibole, was applied to the two paramphibolite samples (118838 and 118891 from the Cocanarup greenstones). Sample 118838 yielded reasonable pressures of 2–3 kb, but temperatures that were much lower than predicted by metamorphic mineral assemblages. Plagioclase in sample 118891 was too calcic for application of this geothermobarometer.

References

ARANOVICH, L. Y., and PODLESSKIY, K. K., 1982, The equilibrium garnet + sillimanite + quartz + cordierite: experimental calculation: Mineralogicheskiy Zhurnal, v. 4, p. 20–32.

BLUNDY, J. D., and HOLLAND, T. J. B., 1990, Calcic amphibole equilibria and a new amphibole–plagioclase geothermometer: Contributions to Mineralogy and Petrology, v. 104, p. 208–224.

GHENT, E. D., 1976, Plagioclase–garnet–Al_2SiO_5–quartz: a potential geobarometer–geothermometer: American Mineralogist, v. 61, p. 710–714.

HODGES, K. V., and SPEAR, F. S., 1982, Geothermometry, geobarometry and the Al_2SiO_5 triple point at Mount Moosilauke, New Hampshire: American Mineralogist, v. 67, p. 1118–1134.

INDARES, A., and MARTIGNOLE, J., 1985, Biotite–garnet geothermometry in the granulite facies: the influence of Ti and Al in biotite: American Mineralogist, v. 70, p. 272–278.

PERCHUK, L. L. and LAVREN'TEVA, I. V., 1981, Experimental investigation of exchange equilibria in the system cordierite–garnet–biotite, *in* Kinetics and equilibrium in mineral reactions *edited by* S. K. SAXENA: Springer-Verlag, New York, p. 199–240.

PLYUSNINA, L. P., 1982, Geothermometry and geobarometry of plagioclase–hornblende-bearing assemblages: Contributions to Mineralogy and Petrology, v. 80, p. 140–146.

SPEAR, F. S., 1980, NaSi–CaAl exchange equilibrium between plagioclase and amphibole: Contributions to Mineralogy and Petrology, v. 72, p. 33–41.

SPEAR, F. S., 1993, Metamorphic phase equilibria and Pressure–Temperature–Time paths: Mineralogical Society of America, Monograph, 799p.

Table 3.2. Garnet analyses

Quartz–plagioclase–sillimanite–andalusite–garnet–biotite–muscovite–opaques

	118831 site 1				*118831 site 2 (grain 1)*			*118831 (grain 2)*	
	gt-9 rim grain	*gt-10 margin*	*gt-11 interm.*	*gt-12 core*	*gt-2 margin*	*gt-4 interm.*	*gt-5 core*	*gt-7 margin*	*gt-8 margin*
			2 mm diameter			*1 mm diam.*			*1.5 mm diam.*
					Percentage				
SiO_2	36.60	36.66	36.69	37.13	36.39	36.40	36.60	36.46	36.72
TiO_2	0.00	0.00	0.00	0.00	0.00	0.00	0.00	0.00	0.00
Al_2O_3	21.05	21.33	21.18	21.34	21.14	20.94	21.11	21.23	21.07
Cr_2O_3	0.00	0.00	0.00	0.00	0.00	0.00	0.00	0.00	0.00
FeO(t)	38.93	37.91	38.27	37.24	38.66	37.27	37.93	38.18	38.00
MnO	0.57	0.69	0.98	1.03	0.71	0.98	1.15	0.75	0.88
MgO	0.81	1.10	1.32	1.14	1.27	1.42	1.48	1.38	1.39
CaO	1.44	1.30	1.42	2.26	1.34	1.81	1.88	1.34	1.39
Na_2O	0.00	0.00	0.00	0.00	0.00	0.00	0.00	0.00	0.00
Total	**99.40**	**98.99**	**99.86**	**100.14**	**99.51**	**98.82**	**100.15**	**99.34**	**99.45**
X_{alm}	90.97	89.76	88.11	86.18	89.16	86.45	86.67	88.55	88.07
X_{pyr}	3.37	4.64	5.42	4.70	5.22	5.87	6.03	5.71	5.74
X_{sps}	1.35	1.65	2.29	2.41	1.66	2.30	2.66	1.76	2.07
X_{grs}	4.31	3.94	4.19	6.70	3.96	5.38	4.64	3.98	4.13
X_{and}									
Fe/Fe+Mg	0.977	0.951	0.942	0.956	0.945	0.936	0.935	0.939	0.939
Garnet–biotite temperatures (°C)									
$T_{bi\text{-}9}$	522	578	611	588	–	–	–	–	–
$T_{bi\text{-}10}$	514	579	–	–	–	–	–	–	–
$T_{bi\text{-}11}$	537	606	–	–	–	–	–	–	–
$T_{bi\text{-}1}$	–	–	–	–	625	656	661	–	–
$T_{bi\text{-}5}$	–	–	–	–	611	642	647	–	–
$T_{bi\text{-}6}$	–	–	–	–	–	–	–	633	636

Quartz–plagioclase–biotite–garnet–cordierite–opaques–apatite

	118839 site 1					*118839 site 3*			
	gt-15 rim grain	*gt-14 margin*	*gt-13 margin*	*gt-16 core*	*gt-18 core*	*gt-19 rim*	*gt-20 margin*	*gt-21 margin*	*gt-23 core*
			5 mm diameter				*1 mm diam.*		
					Percentage				
SiO_2	38.28	37.53	38.13	37.86	37.58	38.03	37.85	38.01	37.95
TiO_2	0.00	0.00	0.00	0.00	0.00	0.00	0.00	0.00	0.00
Al_2O_3	22.17	22.03	22.06	21.58	21.56	21.72	22.11	22.03	21.73
Cr_2O_3	0.00	0.00	0.00	0.00	0.00	0.00	0.00	0.00	0.00
FeO(t)	35.67	34.14	34.04	33.61	33.73	35.16	34.79	34.02	33.35
MnO	0.68	0.64	0.66	0.60	0.85	0.71	0.73	0.61	0.48
MgO	3.79	4.35	4.49	4.20	4.33	3.89	4.33	4.91	5.10
CaO	1.15	1.39	1.70	1.88	1.72	1.09	1.46	1.41	1.56
Na_2O	0.00	0.00	0.00	0.00	0.00	0.00	0.00	0.00	0.00
Total	**101.73**	**100.09**	**101.08**	**99.73**	**99.78**	**100.60**	**101.27**	**100.99**	**100.17**
X_{alm}	80.0	77.02	75.83	76.19	75.78	79.53	77.11	75.27	74.23
X_{pyr}	15.15	17.49	17.83	16.97	17.34	15.68	17.11	19.37	20.24
X_{sps}	1.54	1.46	1.49	1.38	1.93	1.63	1.64	1.37	1.08
X_{grs}	3.30	4.02	4.85	5.46	4.95	3.16	4.15	4.00	4.45
X_{and}									
Fe/Fe+Mg	0.841	0.815	0.810	0.818	0.814	0.835	0.818	0.795	0.786
Garnet–biotite temperatures (°C)									
$T_{bi\text{-}19}$	–	–	–	–	–	601	624	655	668
$T_{bi\text{-}22}$	–	–	–	–	–	612	636	668	681
$T_{bi\text{-}13}$	594	630	637	626	631	–	–	–	–
$T_{bi\text{-}14}$	601	631	645	633	639	–	–	–	–

Table 3.2. (continued)

Quartz–plagioclase–biotite–garnet–andalusite–chlorite–gedrite–opaques

	118893 site 1				
	gt-16 rim grain	*gt-3 margin*	*gt-7 interm.*	*gt-9 interm.*	*gt-14 core*
			5 mm diameter		
			Percentage		
SiO_2	37.12	37.60	37.28	37.51	37.32
TiO_2	0.00	0.00	0.00	0.00	0.00
Al_2O_3	21.31	21.36	20.94	21.17	21.08
Cr_2O_3	0.00	0.00	0.00	0.00	0.00
FeO(t)	34.86	33.78	30.95	30.02	29.37
MnO	2.76	3.74	6.89	7.86	8.21
MgO	2.47	2.56	2.12	2.09	1.90
CaO	1.62	1.87	2.06	2.23	2.30
Na_2O	0.00	0.00	0.00	0.00	0.00
Total	**100.14**	**100.91**	**100.24**	**100.89**	**100.18**
X_{alm}	78.99	75.86	69.71	67.36	66.72
X_{pyr}	9.98	10.25	8.54	8.36	7.69
X_{sps}	6.33	8.51	15.78	17.86	18.89
X_{grs}	4.70	5.38	5.57	6.41	6.69
X_{and}	–	–	0.40	–	–
Fe/Fe+Mg	0.888	0.881	0.891	0.889	0.897
Garnet–biotite temperatures (°C)					
$T_{bi\text{-}2}$	576	–	–	–	–
$T_{bi\text{-}4}$	575	587	569	–	559
$T_{bi\text{-}6}$	554	–	–	–	–
$T_{bi\text{-}7}$	568	580	562	–	552

Quartz–plagioclase–biotite–garnet–cordierite

	118888 site 1				*118888 site 2*			
	gt-18 rim grain	*gt-20 margin*	*gt-21 interm.*	*gt-23 core*	*gt-34 rim*	*gt-31 margin*	*gt-30 interm.*	*gt-27 interm.*
		5 mm diameter				*5 mm diam.*		
				Percentage				
SiO_2	37.77	38.34	37.84	37.87	38.40	38.31	38.21	37.75
TiO_2	0.00	0.00	0.00	0.00	0.00	0.00	0.00	0.00
Al_2O_3	21.25	21.18	21.20	21.29	21.13	21.50	20.99	21.00
Cr_2O_3	0.00	0.00	0.00	0.00	0.00	0.00	0.00	0.00
FeO(t)	37.27	37.03	36.49	36.87	36.85	36.47	36.37	36.29
MnO	0.64	0.52	0.48	0.68	0.53	0.46	0.54	0.82
MgO	2.69	3.06	3.02	2.96	2.61	3.01	2.73	3.03
CaO	1.07	1.27	1.48	1.37	0.94	1.54	1.52	1.20
Na_2O	0.00	0.00	0.00	0.00	0.00	0.00	0.00	0.00
Total	**100.69**	**101.40**	**100.51**	**101.04**	**100.45**	**101.29**	**100.36**	**100.09**
X_{alm}	84.54	82.82	82.43	82.68	85.15	82.37	83.03	82.28
X_{pyr}	10.88	12.32	12.18	11.84	10.80	12.12	11.22	12.32
X_{sps}	1.47	1.19	1.10	1.55	1.25	1.05	1.26	1.89
X_{grs}	3.11	2.45	4.14	3.94	2.17	4.46	3.25	2.79
X_{and}	–	1.23	0.15	–	0.63	–	1.24	0.71
Fe/Fe+Mg	0.886	0.870	0.871	0.875	0.887	0.872	0.881	0.870
Garnet–biotite temperatures (°C)								
$T_{bi\text{-}17}$	627	656	656	649	–	–	–	–
$T_{bi\text{-}20}$	640	669	–	–	–	–	–	–
$T_{bi\text{-}23}$	–	–	–	–	625	657	636	659
$T_{bi\text{-}26}$	–	–	–	–	601	632	613	634

Table 3.2. (continued)

Quartz–biotite–chlorite–gedrite–garnet

	110353 site 2			*110353 site 3*			
	gt-9 rim grain	*gt-8 margin*	*gt-7 margin*	*gt-2 rim*	*gt-3 margin*	*gt-4 interm.*	*gt-5 core*
		20 mm diameter			*20 mm diam.*		
				Percentage			
SiO_2	37.49	38.02	37.35	37.54	36.92	37.46	37.19
TiO_2	0.00	0.00	0.00	0.00	0.00	0.00	0.00
Al_2O_3	20.86	21.04	20.70	21.08	20.67	20.71	20.49
Cr_2O_3	0.00	0.00	0.00	0.00	0.00	0.00	0.00
FeO(t)	37.12	37.42	37.14	37.21	37.29	37.16	37.40
MnO	0.27	0.00	0.00	0.20	0.23	0.22	0.00
MgO	1.71	2.25	2.16	2.13	2.08	2.14	1.92
CaO	2.27	1.75	1.76	1.67	1.81	1.76	1.74
Na_2O	0.00	0.00	0.00	0.00	0.00	0.00	0.00
Total	**99.72**	**100.48**	**99.11**	**99.83**	**99.00**	**99.45**	**98.74**
X_{alm}	85.59	85.61	85.81	85.84	85.58	85.42	86.76
X_{pyr}	7.05	9.23	8.95	8.76	8.54	8.84	8.02
X_{sps}	0.63	0.00	0.00	0.47	0.54	0.52	0.00
X_{grs}	6.32	4.44	4.47	4.94	4.89	4.20	3.94
X_{and}	0.41	0.72	0.77	0.00	0.45	1.02	1.28
Fe/Fe+Mg	0.924	0.903	0.906	0.907	0.910	0.907	0.917
Garnet–biotite temperatures (C°)							
$T_{bi\text{-}9}$	564	614	607	–	–	–	–
$T_{bi\text{-}8}$	572	622	616	–	–	–	–
$T_{bi\text{-}3}$	–	–	–	595	590	596	575
$T_{bi\text{-}6}$	–	–	–	598	593	599	578

Quartz–andalusite–biotite–chlorite–garnet–staurolite

	105941 site 1 (grain 1)				*105941 site 2 (grain 2)*				*105941 site 4*			
	gt-19 rim grain	*gt-20 margin*	*gt-22 interm.*	*gt-23 core*	*gt-15 rim*	*gt-16 margin*	*gt-17 interm.*	*gt-18 core*	*gt-10 rim*	*gt-11 margin*	*gt-12 interm.*	*gt-13 core*
		1 mm diameter				*1 mm diam.*				*2 mm diam.*		
						Percentage						
SiO_2	35.41	36.28	35.98	36.25	36.94	36.54	36.46	36.17	36.54	36.15	36.32	36.25
TiO_2	0.00	0.00	0.00	0.00	0.00	0.00	0.00	0.00	0.00	0.00	0.00	0.00
Al_2O_3	20.13	20.78	20.35	20.74	21.24	21.05	20.67	21.04	21.08	20.54	20.69	21.02
Cr_2O_3	0.00	0.00	0.00	0.00	0.00	0.00	0.00	0.00	0.00	0.00	0.00	0.00
FeO(t)	38.10	38.20	37.20	36.60	37.78	37.67	38.29	37.68	37.64	36.55	36.47	35.61
MnO	1.19	1.27	2.13	2.79	1.14	1.21	1.29	1.55	1.07	1.60	2.14	3.32
MgO	1.31	1.60	1.31	1.22	1.43	1.53	1.66	1.50	1.51	1.47	1.49	1.50
CaO	1.92	2.01	2.20	1.96	1.81	1.98	1.79	1.94	1.80	2.15	2.39	2.33
Na_2O	0.00	0.25	0.20	0.24	0.23	0.00	0.27	0.00	0.00	0.00	0.34	0.00
Total	**98.06**	**100.39**	**99.37**	**99.80**	**100.57**	**99.98**	**100.43**	**99.88**	**99.64**	**98.59**	**99.85**	**100.03**
X_{alm}	87.99	86.26	84.38	83.56	86.25	86.22	86.04	86.65	86.15	84.32	82.63	81.41
X_{pyr}	5.52	6.57	5.43	5.02	5.82	6.24	6.79	6.18	6.16	6.06	6.12	6.17
X_{sps}	2.85	2.97	5.01	6.52	2.64	2.80	3.00	3.63	2.48	3.75	4.99	7.76
X_{grs}	0.66	1.51	2.05	3.59	5.29	4.74	1.50	2.83	5.21	5.52	4.25	3.55
X_{and}	2.99	2.69	3.13	1.31	0.00	0.00	2.68	0.71	0.00	0.35	2.02	1.12
Fe/Fe+Mg	0.941	0.929	0.939	0.943	0.937	0.932	0.927	0.933	0.933	0.933	0.931	0.929
Garnet–biotite temperatures (C°)												
$T_{bi\text{-}20}$	561	597	565	556	578	591	604	587	–	–	–	–
$T_{bi\text{-}18}$	565	601	569	560	582	595	608	592	–	–	–	–

Table 3.2 (continued)

Quartz–plagioclase–biotite–garnet–opaques

	113915 site 2					*113915 site 1*					
	gt-1 rim grain	*gt-2 margin*	*gt-3 margin 15 mm diameter*	*gt-4 interm.*	*gt-5 core*	*gt-6 rim*	*gt-7 margin*	*gt-11 margin 15 mm diam.*	*gt-8 margin*	*gt-9 interm.*	*gt-10 core*
						Percentage					
SiO_2	36.81	36.75	36.17	36.67	36.31	36.78	35.77	36.09	36.29	36.14	36.42
TiO_2	0.00	0.00	0.00	0.00	0.00	0.00	0.00	0.00	0.00	0.00	0.00
Al_2O_3	20.95	20.82	20.54	21.15	20.78	20.93	20.62	20.69	20.51	20.38	20.48
Cr_2O_3	0.00	0.00	0.00	0.00	0.00	0.00	0.00	0.00	0.00	0.00	0.00
FeO(t)	36.66	36.13	38.42	36.18	38.81	36.53	35.78	35.69	36.83	38.12	37.56
MnO	0.50	0.61	0.71	0.63	0.54	0.67	0.59	0.50	0.72	0.87	0.79
MgO	2.26	1.89	2.45	1.99	2.33	2.43	1.87	1.95	1.75	2.16	2.41
CaO	2.50	3.50	1.30	3.56	1.42	2.57	3.08	2.87	2.81	1.56	1.52
Na_2O	0.22	0.00	0.00	0.00	0.00	0.20	0.00	0.00	0.00	0.00	0.27
Total	**99.90**	**99.70**	**99.59**	**100.18**	**100.19**	**100.11**	**97.71**	**97.79**	**98.91**	**99.23**	**99.45**
X_{alm}	82.75	81.52	86.64	81.87	87.46	81.99	83.18	82.70	83.80	86.16	84.43
X_{pyr}	9.15	7.67	8.41	8.09	8.39	9.85	7.79	8.05	7.19	8.72	9.86
X_{sps}	1.15	1.41	1.66	1.46	1.26	1.54	1.40	1.17	1.68	2.04	1.84
X_{grs}	6.14	8.36	0.00	7.62	0.00	5.01	6.92	8.07	5.72	0.00	1.14
X_{and}	0.80	1.05	3.29	0.96	2.89	1.61	0.71	0.00	1.61	3.08	2.72
Fe/Fe+Mg	0.900	0.914	0.911	0.910	0.913	0.893	0.914	0.911	0.921	0.908	0.895
Garnet–biotite temperatures (C°)											
$T_{bi\text{-}4}$	–	–	–	–	–	–	–	–	–	–	–
$T_{bi\text{-}6}$	–	–	–	–	–	600	556	564	540	570	593

Quartz–plagioclase–biotite–garnet–gedrite–andalusite–cordierite–opaques

	118797 site 1					*118797 site 3*			
	gt-20 rim grain	*gt-19 margin*	*gt-18 margin 1 mm diameter*	*gt-17 interm.*	*gt-16 core*	*gt-12 rim*	*gt-13 margin*	*gt-14 interm.*	*gt-15 core*
					Percentage		*3 mm diam.*		
SiO_2	35.96	36.48	36.24	36.82	36.11	36.29	35.91	35.91	35.93
TiO_2	0.00	0.00	0.00	0.00	0.00	0.00	0.00	0.00	0.00
Al_2O_3	20.26	20.84	20.50	21.00	20.59	20.65	20.61	20.69	20.48
Cr_2O_3	0.00	0.00	0.00	0.00	0.00	0.00	0.00	0.00	0.00
FeO(t)	38.93	38.82	38.04	38.25	37.38	37.88	37.86	37.02	37.10
MnO	0.76	0.76	0.78	0.82	0.85	0.59	0.74	1.66	1.41
MgO	2.02	2.40	2.26	2.53	2.47	2.47	2.40	2.48	2.37
CaO	1.06	0.98	0.95	0.91	1.02	0.85	1.13	1.19	1.16
Na_2O	0.00	0.20	0.00	0.00	0.23	0.23	0.00	0.28	0.00
Total	**98.99**	**100.48**	**98.77**	**100.33**	**98.65**	**98.96**	**98.65**	**99.23**	**98.45**
X_{alm}	88.42	87.24	86.91	86.31	85.60	86.49	86.96	84.35	85.07
X_{pyr}	6.64	8.36	9.30	10.24	10.20	10.15	9.48	8.94	9.68
X_{sps}	1.79	1.76	1.82	1.89	1.99	1.38	1.75	3.92	3.32
X_{grs}	0.00	0.00	0.66	0.71	0.75	0.78	0.00	0.00	0.00
X_{and}	3.16	2.64	1.31	0.86	1.46	1.21	1.82	2.80	1.92
Fe/Fe+Mg	0.930	0.912	0.903	0.894	0.893	0.895	0.902	0.904	0.898
Garnet–biotite temperatures (°C)									
$T_{bi\text{-}16}$	552	583	576	596	595	–	–	–	–
$T_{bi\text{-}17}$	–	588	–	–	–	–	–	–	–
$T_{bi\text{-}19}$	–	597	–	–	–	–	–	–	–
$T_{bi\text{-}12}$	–	–	–	–	–	595	590	600	591
$T_{bi\text{-}10}$	–	–	–	–	–	–	586	–	–

NOTE: The calculated metamorphic temperatures (T_{bi}) are determined from the above garnet analyses, and biotite analyses from Table 3.3

Table 3.3. Representative biotite analyses

	118831 site 1			*118831 site 2*			*118839 site 3*		*118893 site 1*			
	bi-9	*bi-10*	*bi-11*	*bi-1*	*bi-5*	*bi-6*	*bi-19*	*bi-22*	*bi-2*	*bi-4*	*bi-6*	*bi-7*
						Percentage						
SiO_2	33.59	32.78	33.05	33.00	32.98	32.95	34.62	35.28	34.02	34.60	35.28	34.30
TiO_2	1.71	2.04	1.59	1.95	2.33	1.91	2.57	2.59	1.24	1.28	1.35	1.18
Al_2O_3	20.24	19.57	19.66	19.08	20.52	20.82	17.58	18.16	17.51	17.62	18.19	17.73
FeO(t)	24.73	25.66	26.95	27.81	25.95	25.42	19.23	19.12	21.42	21.44	19.88	21.10
MnO	0.00	0.00	0.00	0.00	0.00	0.00	0.00	0.00	0.00	0.00	0.00	0.00
MgO	4.39	4.80	4.37	4.39	4.38	4.24	11.54	10.82	9.43	9.47	9.87	9.70
CaO	0.00	0.00	0.00	0.00	0.00	0.00	0.00	0.00	0.00	0.00	0.00	0.00
Na_2O	0.00	0.00	0.00	0.00	0.00	0.20	0.24	0.21	0.00	0.00	0.00	0.00
K_2O	9.51	8.72	8.96	9.00	9.08	9.05	7.83	8.49	8.49	8.10	8.77	8.72
Total	**94.17**	**93.57**	**94.58**	**95.23**	**95.24**	**94.59**	**93.61**	**94.67**	**92.11**	**92.51**	**93.34**	**92.73**
Mg#	24.0	25.0	22.4	22.0	23.1	22.9	51.7	50.2	44.0	44.0	46.9	45.0

	118894 site 3		*118894 site 4*			*118888 site 1*		*118888 site 2*		*110353 site 2*	
	bi-10	*bi-11*	*bi-13*	*bi-14*	*bi-15*	*bi-17*	*bi-20*	*bi-23*	*bi-26*	*bi-8*	*bi-9*
						Percentage					
SiO_2	34.77	35.29	35.69	34.94	34.01	35.21	35.01	35.61	35.19	33.06	34.07
TiO_2	1.23	1.23	1.41	1.41	1.30	2.73	2.65	2.66	2.40	1.30	1.37
Al_2O_3	18.72	18.91	20.01	20.72	18.80	18.02	18.32	19.08	18.93	17.72	17.49
FeO(t)	24.26	23.58	22.82	21.35	23.78	22.17	22.61	22.04	20.57	25.35	23.33
MnO	0.00	0.00	0.00	0.00	0.00	0.00	0.00	0.00	0.00	0.00	0.00
MgO	7.54	7.82	7.67	7.65	7.63	7.60	7.29	7.51	7.89	7.41	7.12
CaO	0.00	0.00	0.00	0.00	0.00	0.00	0.00	0.00	0.00	0.00	0.00
Na_2O	0.00	0.00	0.00	0.00	0.00	0.00	0.00	0.00	0.00	0.00	0.41
K_2O	8.64	8.90	9.20	9.09	7.48	9.08	9.16	9.23	9.00	7.41	8.55
Total	**95.16**	**95.73**	**96.79**	**95.16**	**92.99**	**94.81**	**95.04**	**96.13**	**93.98**	**92.25**	**92.34**
Mg#	35.7	37.1	37.4	39.0	36.4	37.9	36.5	37.8	40.6	34.3	35.2

	110353 site 3		*105941 site 1*		*105941 site 3*		*105941 site 2*		*113915 site 1*	
	bi-3	*bi-6*	*bi-18*	*bi-20*	*bi-11*	*bi-12*	*bi-13*	*bi-15*	*bi-4*	*bi-6*
						Percentage				
SiO_2	35.65	35.20	33.12	32.87	33.27	33.10	33.44	33.49	33.95	34.05
TiO_2	1.23	1.46	1.52	1.38	1.48	1.46	1.34	1.72	1.29	1.37
Al_2O_3	18.08	17.99	19.58	19.42	19.20	19.53	19.84	19.87	16.59	17.46
FeO(t)	23.18	23.26	24.60	24.75	24.68	25.34	24.71	24.46	23.21	22.99
MnO	0.00	0.00	0.00	0.00	0.00	0.00	0.00	0.00	0.00	0.00
MgO	7.43	7.33	5.58	5.74	5.74	5.63	5.83	5.62	8.46	8.33
CaO	0.00	0.00	0.00	0.00	0.00	0.00	0.00	0.00	0.00	0.00
Na_2O	0.25	0.52	0.25	0.27	0.42	0.49	0.00	0.30	0.62	0.42
K_2O	8.77	8.91	8.81	8.66	8.62	8.33	9.29	9.06	8.57	8.92
Total	**94.59**	**94.67**	**93.47**	**93.09**	**93.42**	**93.87**	**94.45**	**94.53**	**92.69**	**93.54**
Mg#	36.4	36.0	28.8	29.2	29.3	28.4	29.6	29.1	39.4	39.2

Table 3.3 (continued)

	118797		*118797*		*118797*	
	site 1		*site 2*		*site 3*	
	bi-16	*bi-17*	*bi-19*	*bi-20*	*bi-10*	*bi-12*
			Percentage			
SiO_2	33.86	33.38	33.88	33.60	33.92	33.65
TiO_2	1.49	1.58	1.43	1.54	1.39	1.44
Al_2O_3	18.16	18.34	18.12	18.36	18.24	17.83
FeO(t)	22.22	22.71	22.97	23.19	21.90	22.71
MnO	0.00	0.00	0.00	0.00	0.00	0.00
MgO	8.20	8.14	7.85	8.14	8.14	8.28
CaO	0.00	0.00	0.00	0.00	0.00	0.00
Na_2O	0.00	0.00	0.63	0.40	0.55	0.24
K_2O	8.49	7.91	8.44	8.12	8.34	8.03
Total	**92.42**	**92.06**	**93.32**	**93.35**	**92.48**	**92.18**
Mg#	39.7	39.0	37.9	38.5	39.9	39.4

Table 3.4. Representative chlorite analyses

	110353		*110353*		*105941*		*105941*		*105941*	
	site 2		*site 3*		*site 1*		*site 3*		*site 2*	
	ch-1	*ch-2*	*ch-3*	*ch-4*	*ch-12*	*ch-14*	*ch-5*	*ch-6*	*ch-9*	*ch-11*
					Percentage					
SiO_2	23.45	23.60	23.42	23.92	21.71	21.83	22.18	22.08	21.66	21.51
Al_2O_3	21.40	21.79	22.00	21.61	23.54	23.07	22.59	22.79	23.36	23.14
FeO	29.01	29.03	29.51	29.46	32.01	31.96	32.39	32.47	32.38	32.52
MgO	11.57	11.48	11.56	11.42	8.85	9.16	9.13	9.21	9.17	8.80
Total	**85.43**	**85.90**	**86.48**	**86.41**	**86.12**	**86.17**	**86.42**	**86.55**	**86.57**	**86.45**
Mg#	41.6	41.4	41.1	40.9	33.0	33.8	33.4	33.6	33.6	32.6

Table 3.5. Representative analyses of amphibole, staurolite and cordierite

	118838		*118894*	*118894*		*118894*		*118891*	
	site 3		*site 3*	*site 1*		*site 4*		*site 1*	
	hb-2	*hb-4*	*ged 3*	*sta-3*	*sta-4*	*cord-1*	*cord-4*	*hb-5*	*hb-8*
					Percentage				
SiO_2	49.16	50.40	41.28	28.57	28.25	49.50	49.21	49.76	50.57
TiO_2	0.84	0.59	0.00	0.16	0.38	0.00	0.00	0.42	0.48
Al_2O_3	6.38	5.36	17.76	55.21	55.63	33.73	33.68	6.36	6.26
FeO(t)	11.13	13.43	30.93	13.16	13.38	9.94	10.07	17.15	16.51
MnO	0.27	0.00	0.28	0.00	0.00	0.00	0.00	0.33	0.41
MgO	15.84	16.65	6.98	1.19	1.37	6.42	6.49	11.41	11.54
CaO	10.63	8.63	0.10	0.00	0.00	0.00	0.00	11.38	11.33
Na_2O	1.99	1.55	1.60	0.00	0.00	1.01	0.42	0.27	0.40
K_2O	0.20	0.10	0.00	0.00	0.00	0.00	0.30	0.11	0.19
Total	**96.44**	**96.71**	**98.90**	**98.29**	**99.01**	**100.60**	**100.19**	**97.20**	**97.69**
Mg#	71.7	68.8	28.6	8.3	9.3	53.5	53.5	54.3	55.5

Table 3.5 (continued)

	118891 site 2		*110353* site 1			*105941* site 2	*118797* site 2	
	hb-1	*hb-2*	*ged-1*	*ged-4*	*ged-5*	*sta-2*	*ged-1*	*ged-3*
					Percentage			
SiO_2	50.47	50.41	39.63	39.79	39.15	26.67	37.96	40.35
TiO_2	0.48	0.46	0.00	0.00	0.00	0.27	0.00	0.00
Al_2O_3	6.00	6.09	19.21	17.75	18.91	53.77	18.79	16.52
FeO(t)	17.00	16.93	30.65	30.44	30.19	15.39	30.15	30.17
MnO	0.29	0.27	0.00	0.00	0.00	0.00	0.17	0.00
MgO	11.53	11.64	5.78	6.37	5.97	1.30	6.59	7.70
CaO	11.33	11.44	0.10	0.00	0.13	0.00	0.16	0.16
Na_2O	0.36	0.45	2.14	1.64	1.80	0.00	1.69	1.35
K_2O	0.17	0.22	0.00	0.00	0.00	0.00	0.00	0.00
Total	**97.64**	**97.90**	**97.51**	**96.00**	**96.16**	**97.40**	**95.64**	**96.41**
Mg#	54.7	55.1	25.2	27.2	26.1	13.3	28.0	31.3

Table 3.6. Representative plagioclase analyses

	118831 site 1			*118838 site 3*			*118839 site 1*		*118839 site 3*		*118893 site 1*	
	pl-4	*pl-5*	*pl-7*	*pl-4 margin*	*pl-1 interm.*	*pl-7 core*	*pl-8*	*pl-9*	*pl-17 rim*	*pl-14 core*	*pl-4*	*pl-6*
							Percentage					
SiO_2	56.48	53.55	52.72	65.64	65.90	64.90	60.36	60.08	60.71	58.60	57.22	58.43
Al_2O_3	28.19	30.06	30.26	22.20	21.98	22.04	24.96	24.85	25.17	26.32	27.52	26.74
FeO (t)	0.00	0.00	0.00	0.00	0.00	0.00	0.00	0.00	0.00	0.00	0.00	0.00
CaO	10.04	12.29	12.80	2.44	2.16	2.25	6.33	6.30	6.27	7.64	9.31	8.17
Na_2O	5.95	4.40	3.92	9.96	9.93	10.07	8.04	8.09	8.12	7.22	6.15	6.98
K_2O	0.00	0.00	0.00	0.00	0.00	0.00	0.00	0.00	0.00	0.00	0.00	0.00
Total	**100.66**	**100.30**	**99.70**	**100.24**	**99.97**	**99.26**	**99.70**	**99.33**	**100.27**	**99.78**	**100.21**	**100.32**
X_{An}	48.3	60.7	64.4	11.9	10.7	11.0	30.3	30.1	29.9	36.9	45.5	39.2
X_{Ab}	57.7	39.3	35.6	88.1	89.3	89.0	69.7	69.9	70.1	63.1	54.4	60.7
X_{Or}	–	–	–	–	–	–	–	–	–	–	–	–

	118894 site 2		*118894* site 5	*118888* site 1		*118888* site 2		*118891* site 1		*118891* site 2	
	pl-9	*pl-12*	*pl-16*	*pl-19*	*pl-20*	*pl-23*	*pl-24*	*pl-6*	*pl-8*	*pl-3*	*pl-4*
						Percentage					
SiO_2	59.48	59.23	60.45	61.35	61.00	61.41	62.11	45.67	45.24	46.98	47.04
Al_2O_3	26.55	26.63	26.28	24.94	25.39	25.03	24.19	34.89	34.59	34.37	34.52
FeO (t)	0.00	0.00	0.00	0.00	0.00	0.00	0.00	0.00	0.00	0.00	0.00
CaO	7.75	7.83	7.03	6.29	6.75	6.55	5.66	18.38	18.47	17.62	18.01
Na_2O	7.43	7.28	7.76	7.92	7.80	7.83	7.65	0.75	0.54	1.27	1.09
K_2O	0.00	0.00	0.00	0.00	0.00	0.10	0.49	0.00	0.00	0.12	0.00
Total	**101.19**	**100.96**	**101.52**	**100.49**	**100.93**	**100.92**	**100.31**	**99.68**	**98.84**	**100.36**	**100.67**
X_{An}	36.6	37.3	33.3	30.5	32.4	31.4	28.2	93.2	95.0	87.8	90.1
X_{Ab}	63.4	62.7	66.6	69.5	67.6	68.0	68.9	6.8	5.0	11.4	9.9
X_{Or}	–	–	–	–	–	0.05	2.9	–	–	0.7	–

Table 3.6. (continued)

	113915			*118797*		*118797*		*118797*		
	site 1			*site 1*		*site 2*		*site 3*		
	pl-19	*pl-4*	*pl-5*	*pl-13*	*pl-14*	*pl-16*	*pl-17*	*pl-7*	*pl-9*	*pl-10*
					Percentage					
SiO_2	61.35	59.94	58.56	63.15	61.99	62.44	62.11	62.22	62.02	62.22
Al_2O_3	24.94	24.47	25.30	23.93	24.05	24.17	23.97	24.18	23.94	23.92
FeO (t)	0.00	0.00	0.00	0.00	0.00	0.00	0.00	0.00	0.00	0.00
CaO	6.29	6.28	7.17	4.83	5.37	5.19	5.20	5.30	4.99	4.92
Na_2O	7.92	8.24	7.41	8.84	8.65	8.52	8.62	8.75	8.57	8.66
K_2O	0.00	0.00	0.00	0.12	0.00	0.00	0.00	0.00	0.00	0.00
Total	**100.49**	**98.94**	**98.44**	**100.87**	**100.06**	**100.32**	**99.90**	**100.45**	**99.53**	**99.72**
X_{An}	30.5	29.6	34.8	23.0	25.5	25.2	25.0	25.1	24.3	23.9
X_{Ab}	69.5	70.4	65.2	76.3	74.5	74.8	75.0	74.9	75.6	76.1
X_{Or}	–	–	–	0.7	–	–	–	–	–	–

Appendix 4

Drillhole sections and mass balance diagrams for altered, mineralized rocks from the Kundip mining centre

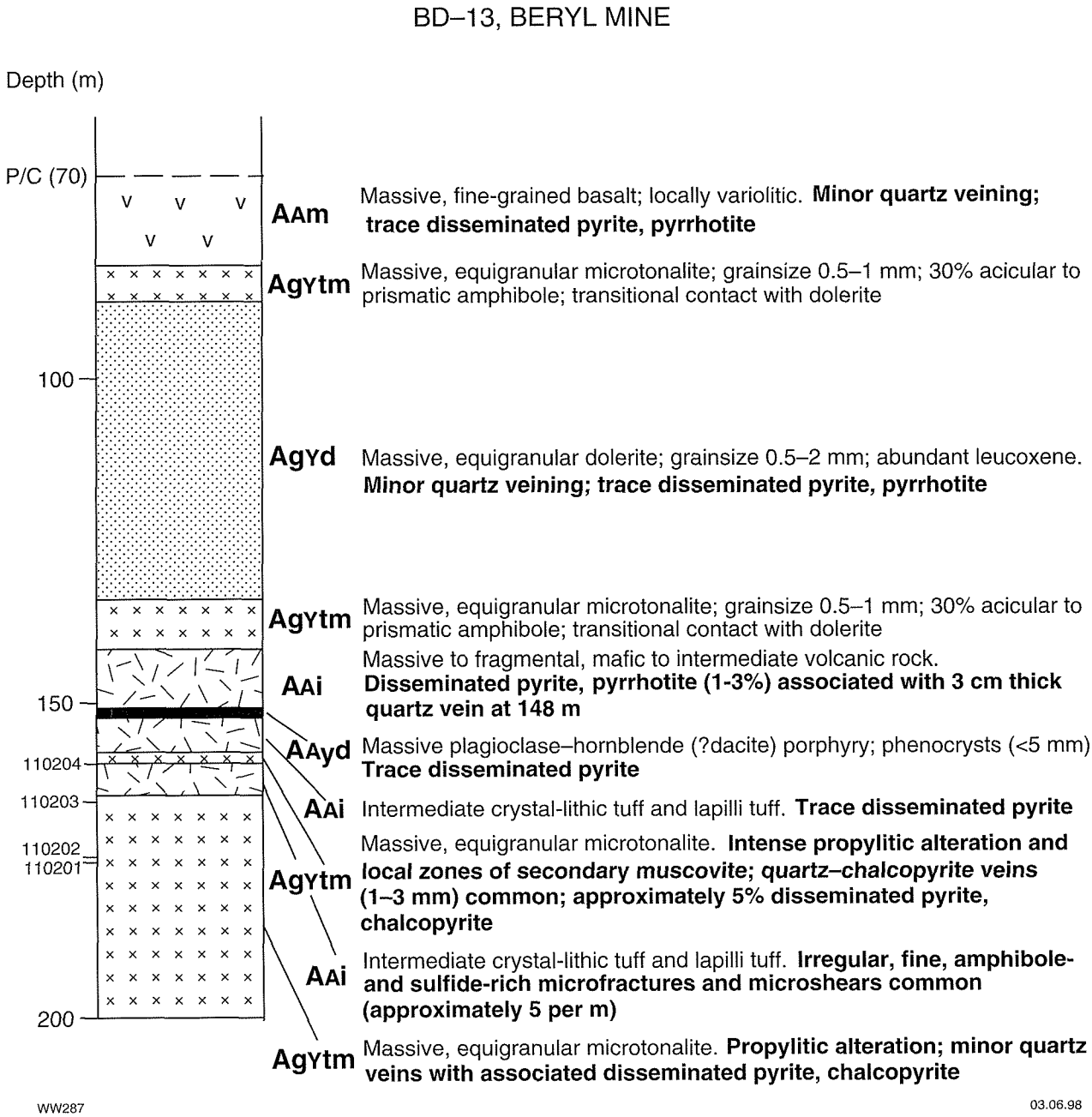

Figure 4.1. Summary log, diamond drillhole BD–13, Beryl mine, Kundip. All units metamorphosed under greenschist facies conditions. GSWA nos 110201–110204 show location of geochemical samples

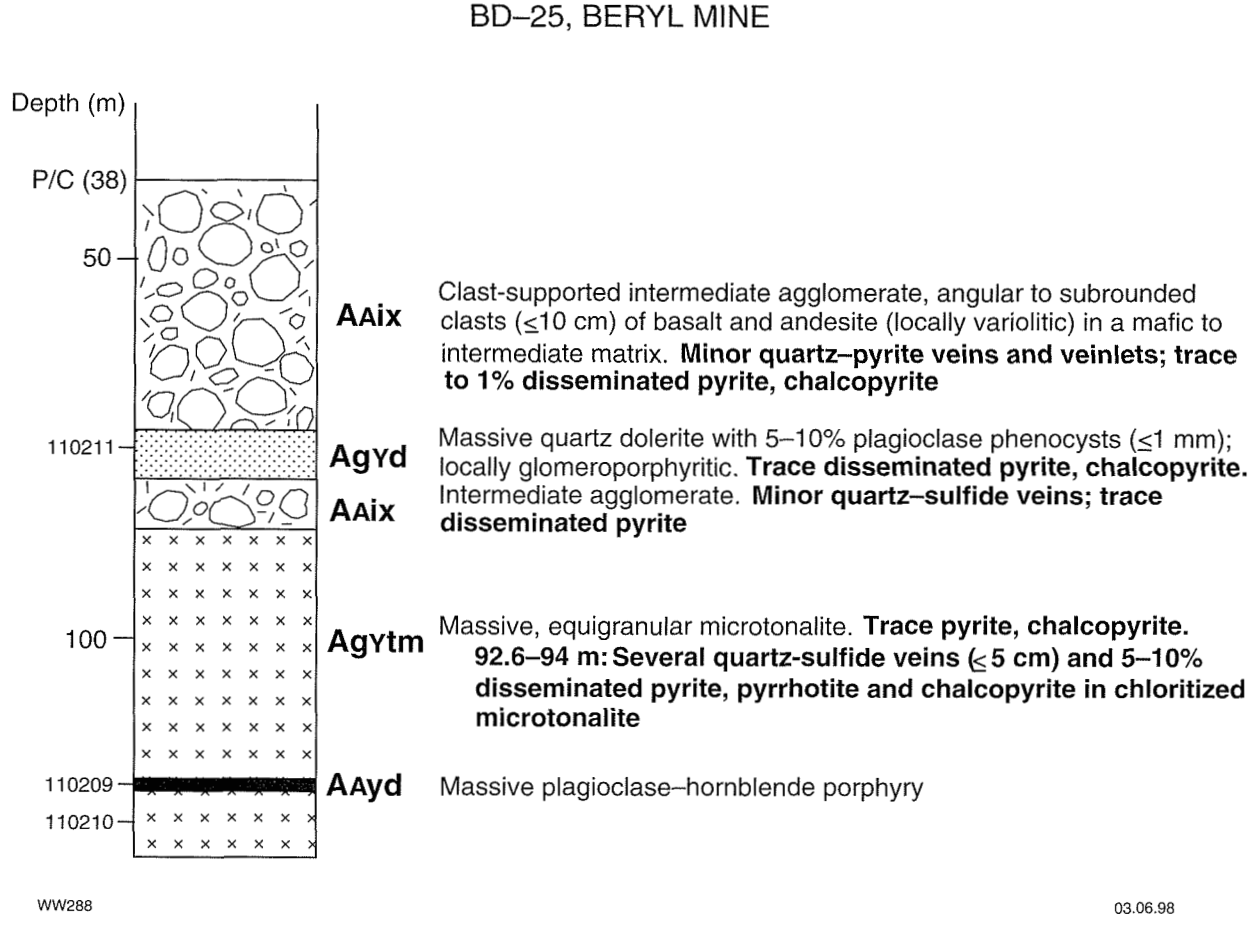

Figure 4.2. Summary log, diamond drillhole BD–25, Beryl mine, Kundip. All units metamorphosed under greenschist facies conditions. GSWA nos 110209–110211 show location of geochemical samples

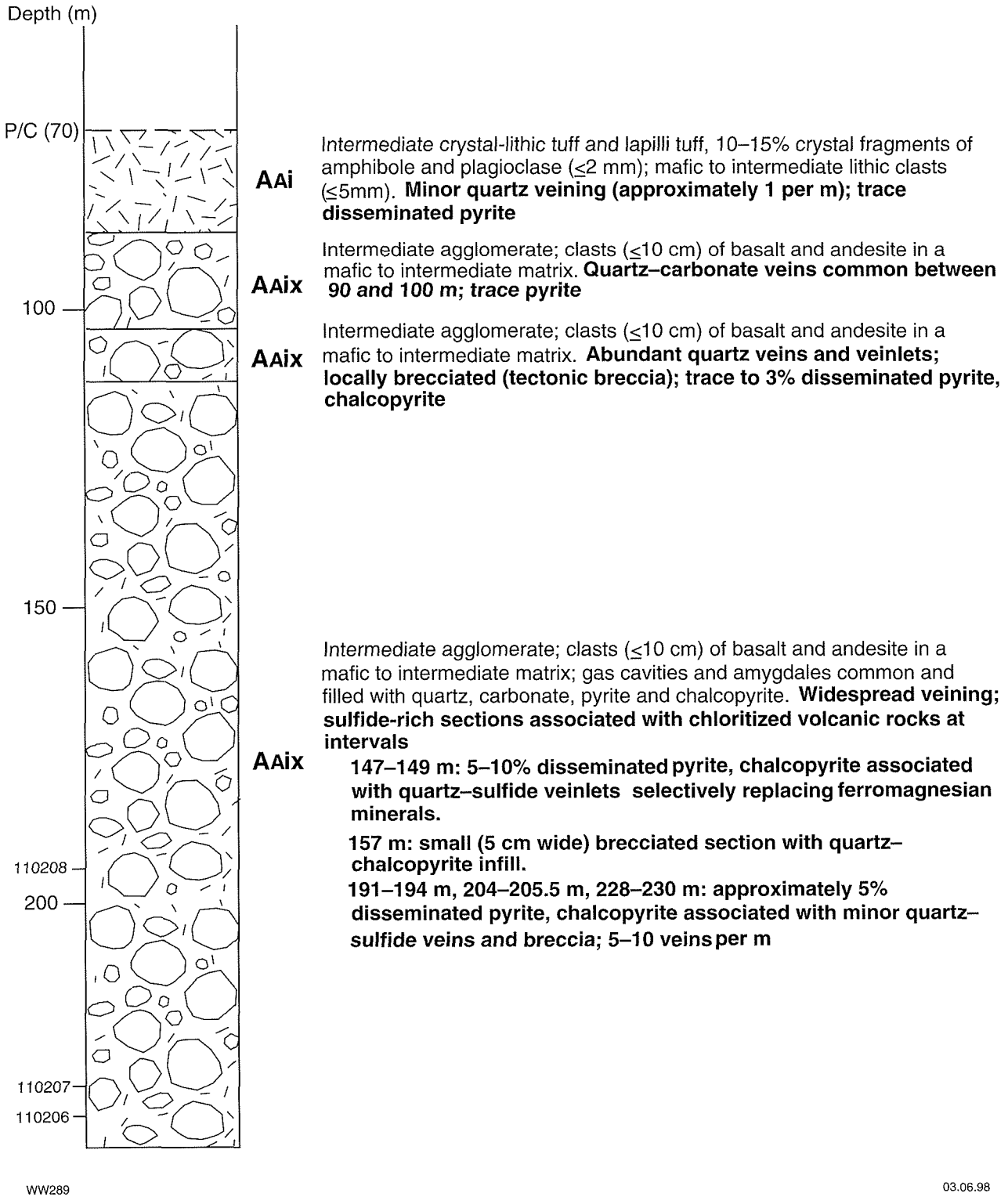

Figure 4.3. Summary log, diamond drillhole FD–13, Flag mine, Kundip. All units metamorphosed under greenschist facies conditions. GSWA nos 110206–110208 show location of geochemical samples

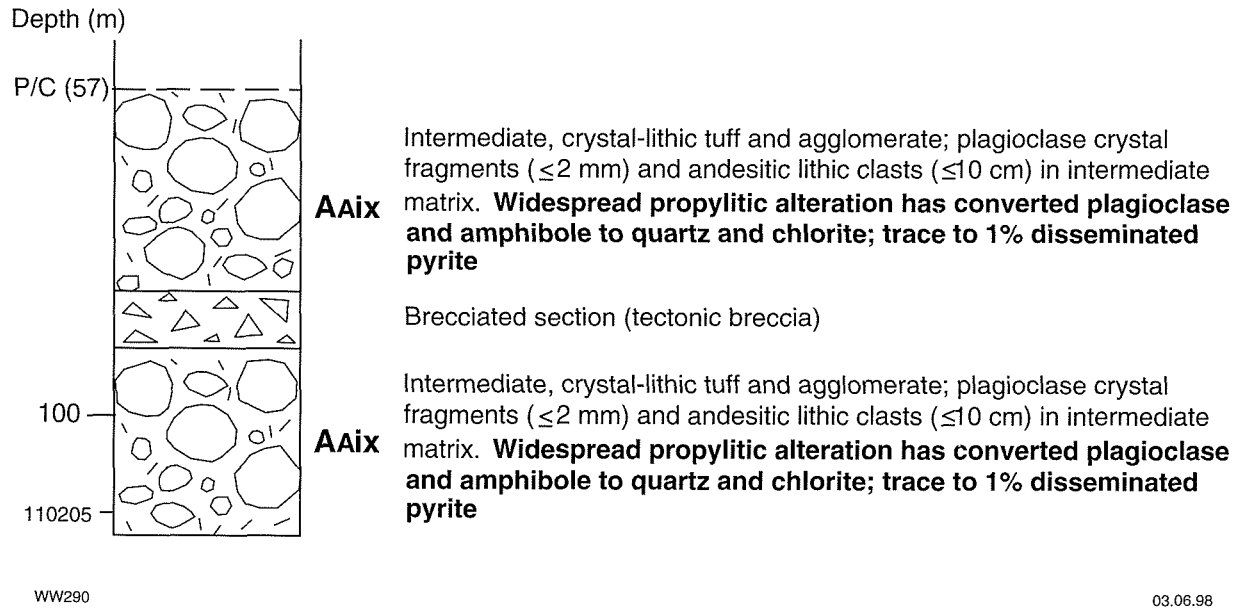

Figure 4.4. Summary log, diamond drillhole FD–15, Flag mine, Kundip. All units metamorphosed under greenschist facies conditions. GSWA no 110205 shows location of geochemical samples

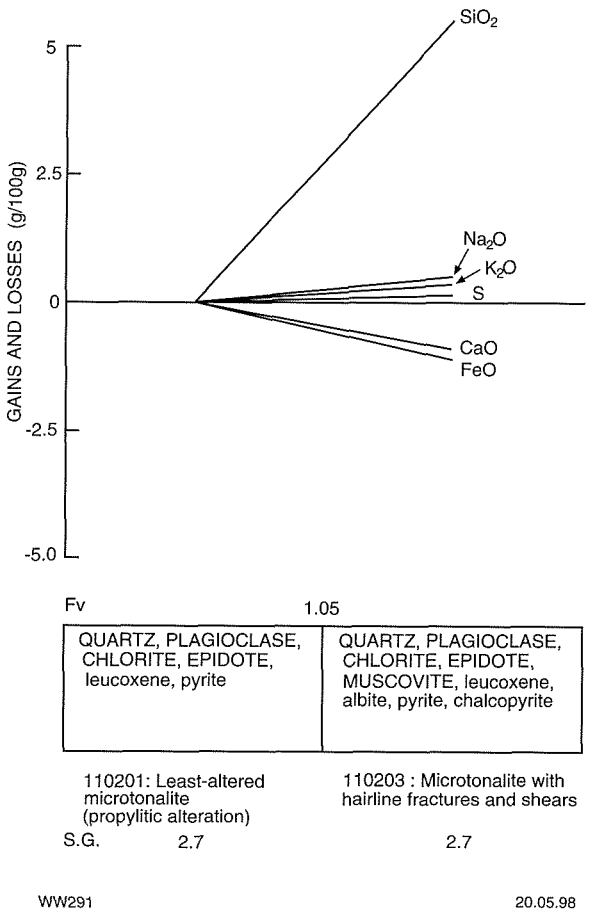

Figure 4.5. Mass balance diagram showing gains and losses associated with alteration and mineralization, Beryl mine, BD–13, 173.2 m. Microtonalite with hairline fractures and shears associated with chlorite, epidote, quartz and sulfides, and minor albite and muscovite
Notes: Main mineral components are shown in upper case; minor mineral components in lower case. Six-figure numbers are GSWA sample numbers. Fv is volume factor (Gresens, 1967). SG is specific gravity

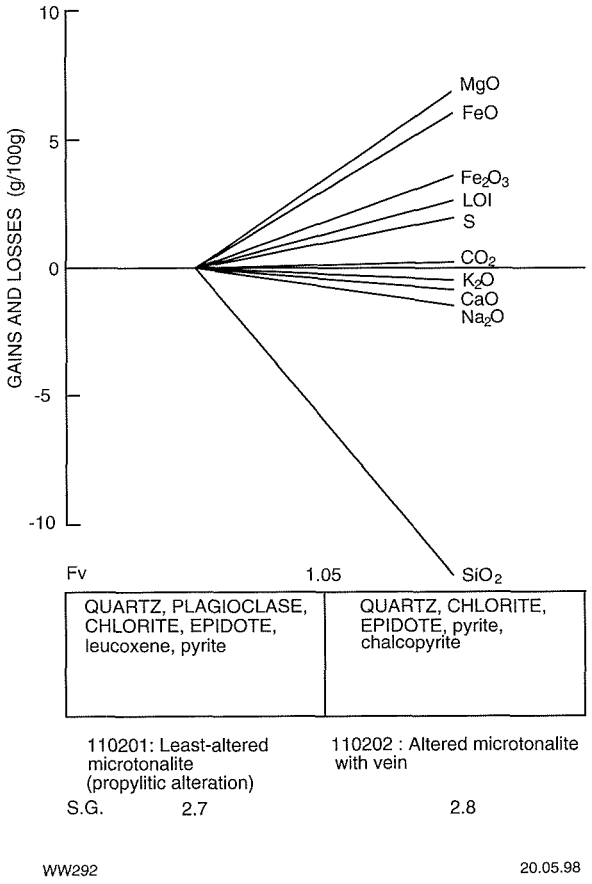

Figure 4.6. Mass balance diagram showing gains and losses associated with alteration and mineralization, Beryl mine, BD–13, 165 m. Alteration associated with mineralized shear, including weakly banded quartz–epidote–chlorite–epidote–chlorite–chalcopyrite–pyrite vein with minor albite and carbonate. See notes for Figure 4.5

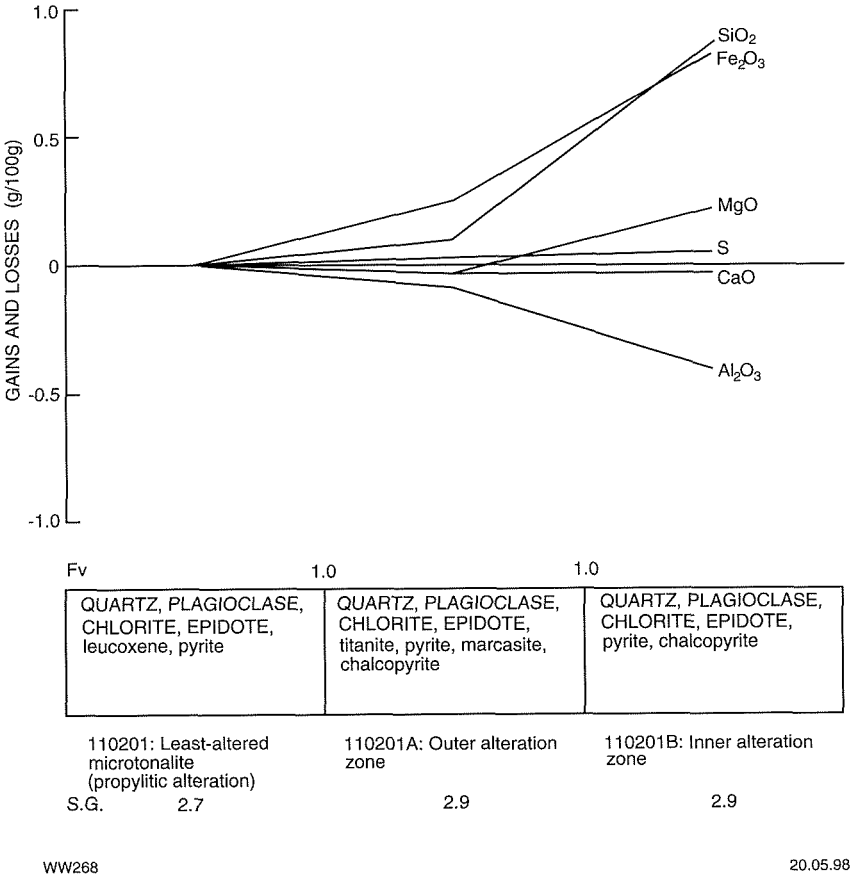

Figure 4.7. Mass balance diagram showing gains and losses associated with alteration and mineralization, Beryl mine, BD–13, 174–175 m. Alteration adjacent to weakly banded quartz–albite–chlorite–pyrite–chalcopyrite vein. See notes for Figure 4.5

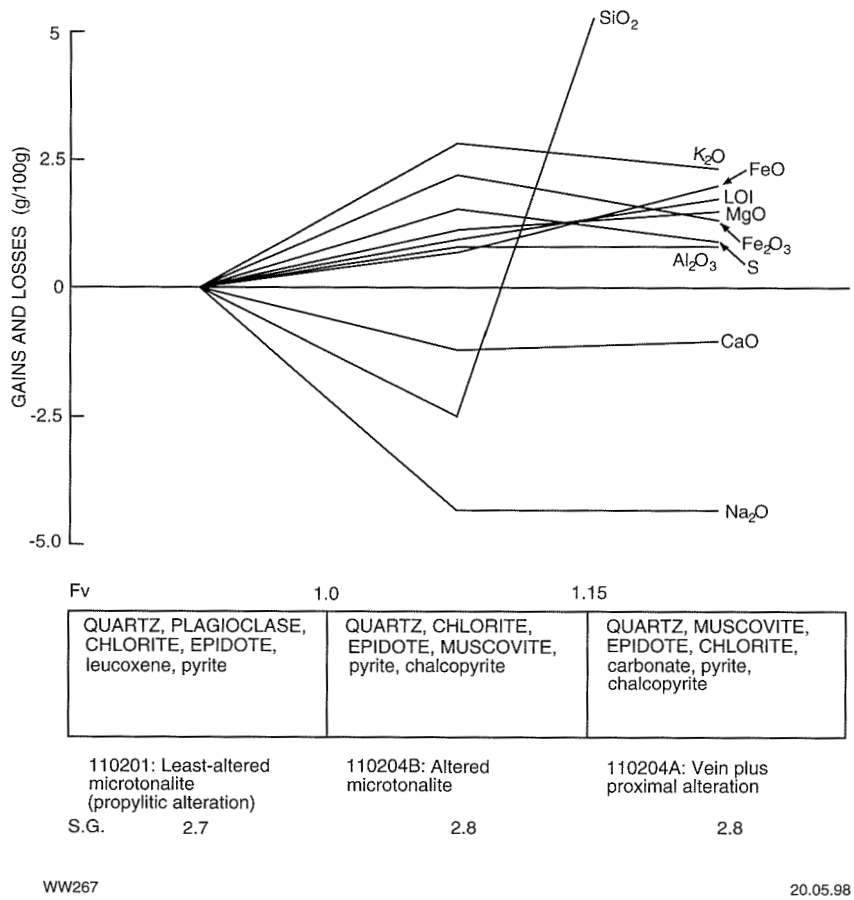

Figure 4.8. Mass balance diagram showing gains and losses associated with alteration and mineralization, Beryl mine, BD–13, 160 m. Alteration associated with quartz–chlorite–sulfide vein in microtonalite. See notes for Figure 4.5

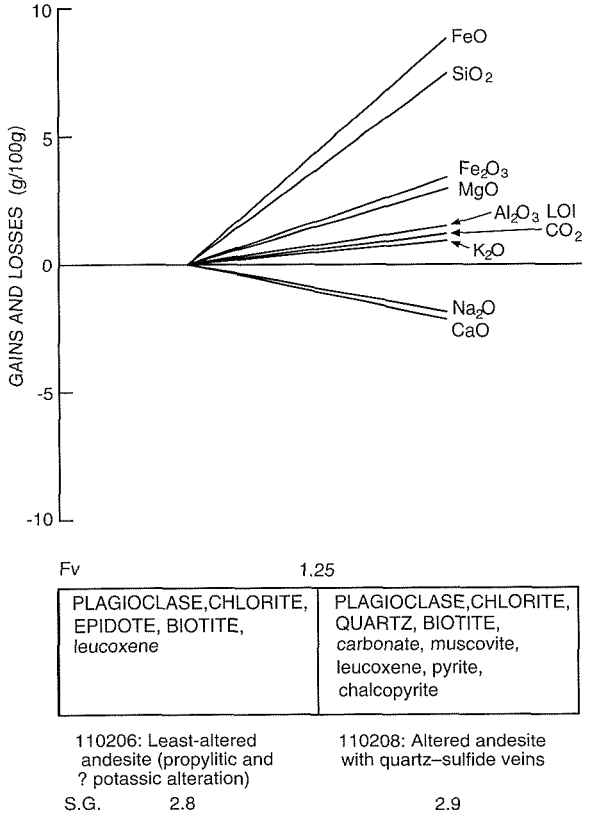

Figure 4.9. Mass balance diagram showing gains and losses associated with alteration and mineralization, Flag mine, FD–13, 194 m. Alteration associated with quartz–chlorite–carbonate–pyrite–chalcopyrite–sphalerite veins and chlorite–pyrite–chalcopyrite veins with minor quartz and carbonate. See notes for Figure 4.5

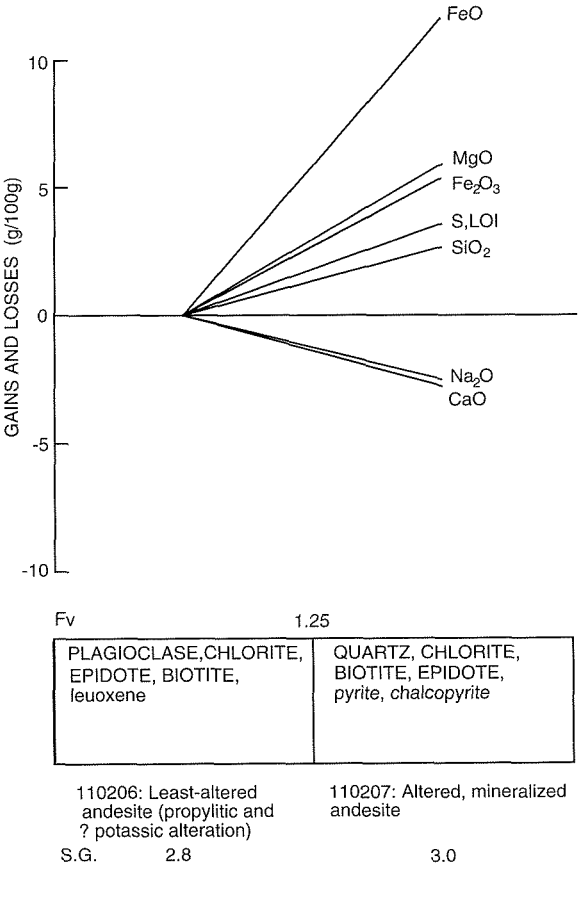

Figure 4.10. Mass balance diagram showing gains and losses associated with alteration and mineralization, Flag mine, FD–13, 230 m. Alteration associated with mineralized shear, including irregular quartz–chalcopyrite–pyrite vein with minor sphalerite, chlorite, biotite, muscovite, carbonate and gold. See notes for Figure 4.5

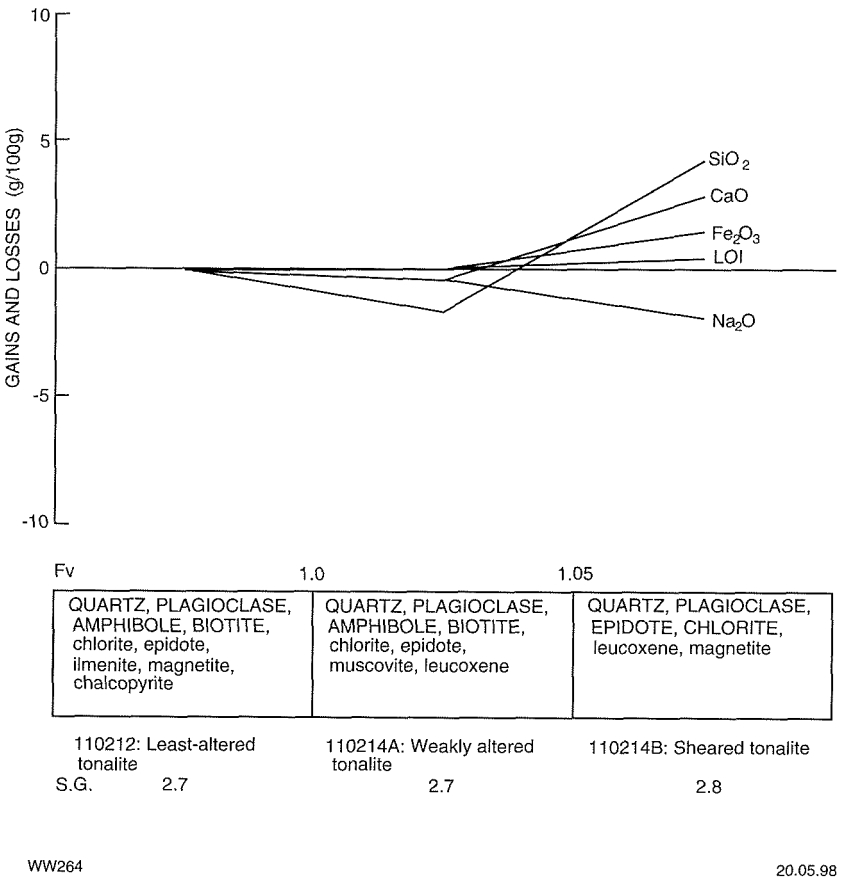

Figure 4.11. Mass balance diagram showing gains and losses associated with alteration and mineralization, Kundip, KDP–2, 119 m. Alteration associated with sheared tonalite (unmineralized). See notes for Figure 4.5

Reference

GRESENS, R. L., 1967, Composition–volume relationships of metasomatism: Chemical Geology, v. 2, p. 47–65.

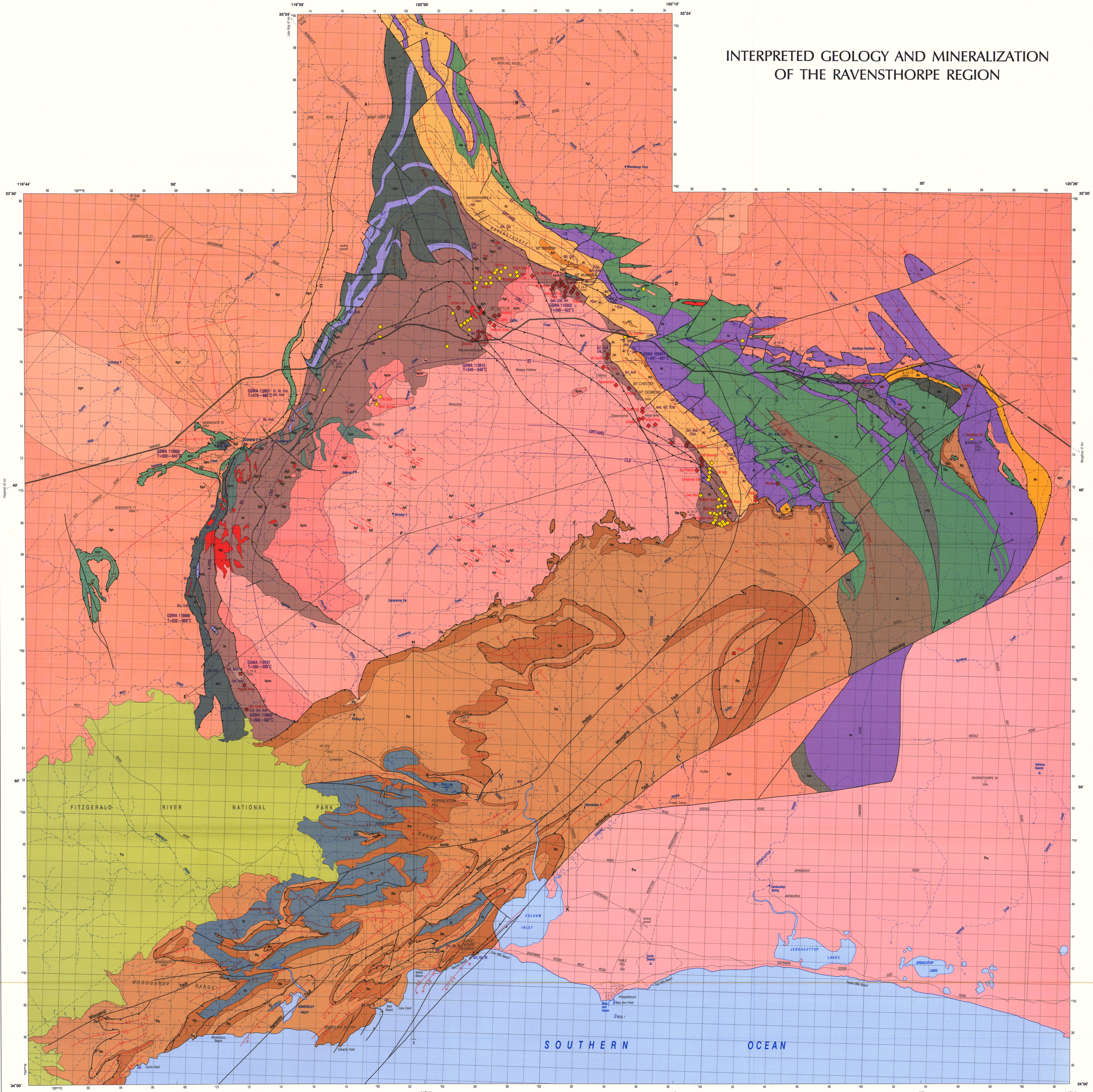

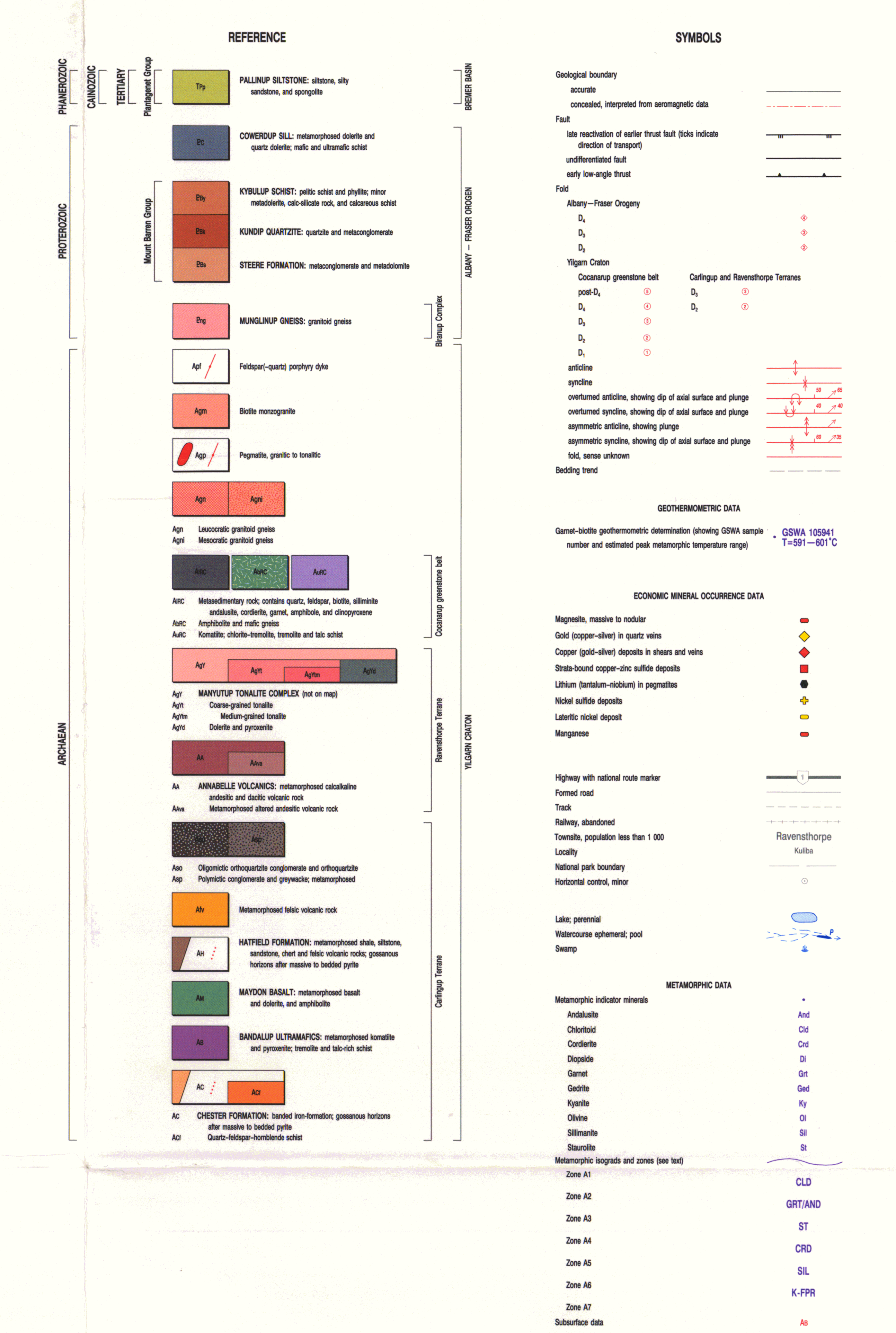

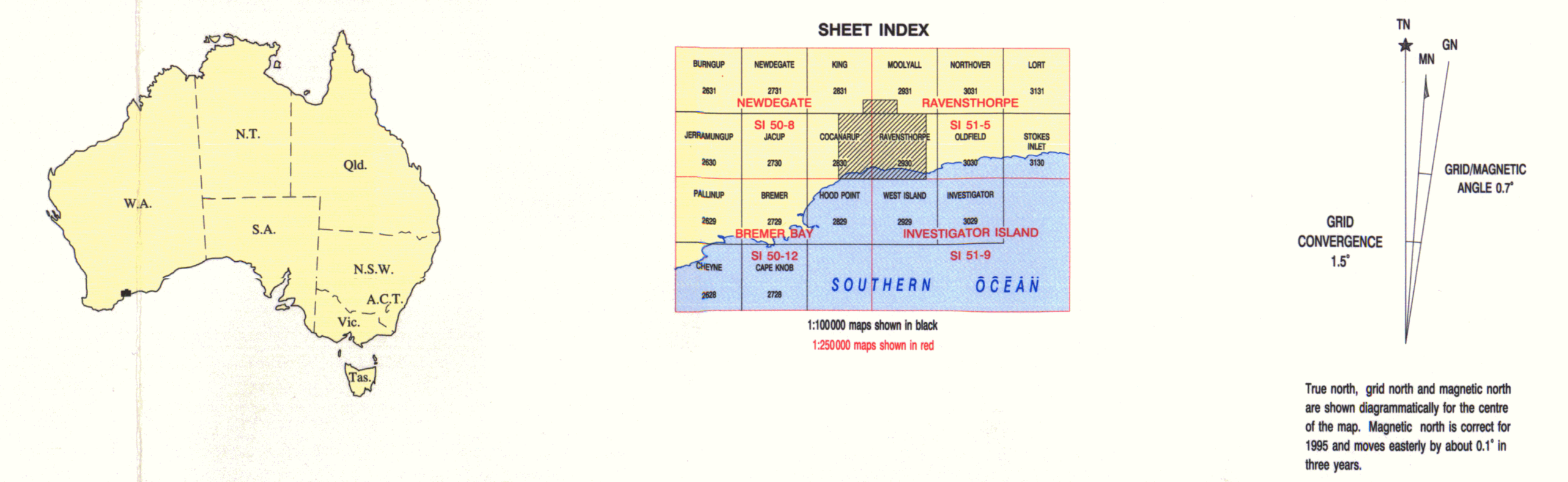

SCALE 1:100 000

TRANSVERSE MERCATOR PROJECTION
HORIZONTAL DATUM: AUSTRALIAN GEODETIC DATUM 1984
VERTICAL DATUM: AUSTRALIAN HEIGHT DATUM

Grid lines indicate 1000 metre interval of the Australian Map Grid Zone 51

Geology by W. K. Witt 1995

Edited by D. Ferdinando and G. Loan

Cartography by E. Green

Topography from the Department of Land Administration Sheets SI 51-5, 2930 and 2931, SI 50-8, 2830 and 2831, with modifications from geological field survey

Published by the Geological Survey of Western Australia. Copies available from the Information Centre, Department of Minerals and Energy, 100 Plain Street, East Perth, WA, 6004. Phone (08) 9222 3459, Fax (08) 9222 3444

This map is also available in digital form

Printed by the Sands Print Group, Western Australia

Diagrammatic sections for lines A to K shown on this map are in the accompanying report (Witt, 1998)

The recommended reference for this map is:
WITT, W. K., 1998, Interpreted geology and mineralization of the Ravensthorpe region (1:100 000 scale), *in* Mineralization and metamorphic geology of the Ravensthorpe region *by* Witt, W. K., Western Australia Geological Survey, Report 54 Plate 1

GEOLOGICAL SURVEY OF WESTERN AUSTRALIA

REPORT 54 PLATE 1

INTERPRETED GEOLOGY AND MINERALIZATION OF THE RAVENSTHORPE REGION